ELECTROMAGNETIC LIFETIMES OF NUCLEAR LEVELS
BY DOPPLER-SHIFT AND RECOIL METHODS

Thesis by

David Marshall Gordon

In Partial Fulfillment of the Requirements

For the Degree of

Doctor of Philosophy

California Institute of Technology

Pasadena, California

1973

(Submitted August 9, 1972)

ACKNOWLEDGMENTS

The author wishes to thank the entire faculty and staff of the Kellogg Radiation Laboratory for their support and assistance during the course of this work. The stimulating and pleasant atmosphere of this Laboratory have made the author's stay at Cal Tech a most memorable and enjoyable experience.

Particular thanks are given to Professor R. W. Kavanagh for his constant guidance and encouragement throughout these experiments; his suggestion of this research topic and his much-needed advice have made this thesis possible. Thanks are also given to Professor T. Lauritsen for his very helpful discussions, advice, and interest.

ABSTRACT

The Doppler-shift-attenuation (DSAM) and recoil-distance methods have been used to measure electromagnetic lifetimes of nuclear levels in ^{16}O, ^{26}Al, ^{30}P, ^{32}P, ^{33}S, ^{35}Cl, ^{37}Ar, ^{38}K and ^{40}K, and the electromagnetic transition strengths deduced from the measured lifetimes have been compared with recent nuclear-model calculations. In addition, measurements have been performed to investigate the existence and magnitude of possible systematic errors in nuclear lifetimes obtained using the gas-stopper version of the DSA technique due to localized heating of the stopping gas by the incident particle beam.

Parameters describing the rate of energy loss of heavy ions in Xe, Ar and He stopping gases have been extracted from DSAM measurements of the γ rays from the decay of the 418-keV level of ^{26}Al, whose lifetime is well known from electronic-timing measurements. In addition, the electronic stopping cross sections for ^{12}C and ^{27}Al ions slowing in He and Xe gases were measured for ion energies in the range $560 \leq E \leq 2320$ keV. Deviations from recent theoretical calculations of electronic stopping power as large as a factor of two have been observed.

TABLE OF CONTENTS

I. GENERAL INTRODUCTION

In attempting to understand nuclear structure, physicists have proposed a number of nuclear models, and have described nuclear states in terms of model wave functions deduced from these constructions. One test of the validity of a particular model is to compare the spins, parities, and energy-level positions predicted theoretically with those observed experimentally for nuclear species to which the model is presumed to apply. Frequently, the calculated energy-level positions do not depend very sensitively upon the model wave functions assumed, with the result that several different models may reasonably reproduce the observed level parameters.

A far more stringent test of model wave functions is provided by a comparison of experimentally measured electromagnetic radiative widths (for γ-ray transitions between levels in a nucleus) with those predicted from the model, since these theoretical widths are relatively sensitive to the wave functions used. In particular, one compares the predicted and observed values for the squares of the electromagnetic multipole transition matrix elements permitted by the spins and parities of the initial and final levels involved. The stringency of this test is due to the present excellent understanding of the electromagnetic interaction. The principal uncertainty in the theoretical calculation of such matrix elements originates not from an uncertainty in the interaction Hamiltonian but rather from the initial and final nuclear wave functions assumed. Thus, these matrix

elements are important because they provide a direct and sensitive test of nuclear-model wave functions.

For an excited nuclear level that is stable against particle decay, the experimental value of the electromagnetic matrix element for a transition of a particular multipole order to a particular final level is most commonly derived from three kinds of measurements. First the total radiative width Γ of the initial level is measured either directly or by a measurement of the level lifetime τ against decay (from which the width Γ can be derived from the uncertainty relation $\Gamma\tau = \hbar$). This total width Γ is the sum of the partial widths for transitions to each lower level to which the initial level decays. Thus, the second type of measurement involves the determination of the branching ratio for decay to each final level. Furthermore, the partial width for decay to a particular final level can itself be separated into a sum of partial widths associated with the various electric and magnetic multipole orders contributing to the transition. If either of the levels (initial or final) has spin zero, then the decay can proceed through only one electric or magnetic multipolarity transition (depending on the relative parity of the levels), and the sum consists of only one term. If both levels have non-zero spins, then in principle transitions of all multipolarities allowed by conservation of angular momentum could be present. In practice, due to the strong dependence of the transition probability on multipole order, only the lowest and next-to-lowest (L and L + 1) multipole transitions allowed are usually observed. For example, a very common observation is

the mixing of M1 and E2 multipole transitions. The third kind of measurement consists of the separation of the partial width for decay to a particular level into contributions from each multipole order, and usually consists of a measurement of the multipole mixing ratio δ of the $L+1$ to the L multipole transitions (where L is the smallest allowed change in angular momentum between initial and final levels). These three measurements determine the experimental value of the radiative partial width for each multipole order involved in the transition. These are compared with the theoretical radiative partial widths calculated from the squares of the electromagnetic multipole matrix elements with the appropriate multipole operators taken between the model wave functions assumed to describe the levels connected by the transition. It is this comparison that determines in part how well a nuclear model describes a nucleus.

A number of techniques are available for the measurement of nuclear lifetimes and of total or partial radiative widths. The selection of which technique to use depends on the length of the lifetime and on the transition energy. Reviews of nuclear-lifetime measurement techniques have been written by Devons (1960), Warburton (1967) and Schwarzschild and Warburton (1968), and extensive references to earlier work and reviews are contained therein. A brief summary of the most important techniques for lifetime and width measurements is given in the following paragraphs.

The measurement of nuclear lifetimes by direct electronic timing, mainly using fast electronic circuitry in a time-coincidence

mode, has proved to be one of the most precise techniques available.
The technique is limited to measurements of lifetimes of the order of
a few times 10^{-11} s and greater, and for this reason the transition
energies have been usually of the order of a few MeV or less. Never-
theless, the precision of this technique has made it an attractive
method of calibrating other less exact techniques which overlap this
method at its lower limit of applicability and which themselves are
applicable to much shorter lifetimes. This method (sometimes called
the "delayed-coincidence" technique) consists of the measurement of
the time interval between the formation of a nuclear level and its
γ-ray decay. The distribution of time intervals observed for an
ensemble of nuclei determines the lifetime of the nucleus in the
radiating state. The measurement is usually performed in one of
two modes. In the pulsed-beam mode, the incident beam from an
accelerator is pulsed at short regular time intervals and the time of
formation of the nuclear level is derived from the beam pulse. The
time of decay is deduced from pulses produced in a fast detector (such
as a fast scintillator-phototube combination) by the γ rays from the
decay. In the associated-particle mode, the time of formation of
the level is signaled by the observation of pulses produced in a fast
detector (either a solid-state particle detector or a fast scintillator-
phototube combination) by the particles or γ rays leading to the for-
mation of that level. The time of decay is signaled as before by the
observation of the γ rays from the decay in question. Thus, for a
reaction such as $(^{4}\text{He},p\gamma)$, one could observe particle-gamma

coincidences between the protons feeding the level of interest and the γ rays de-exciting it. If a radioactive source is used and if the level is fed by a cascade γ ray, one could observe the gamma-gamma coincidences between the γ rays producing the level and the γ rays de-exciting it. Because the delays in the detection system (such as transit times, decay times of optical excited states in scintillators, etc.) are difficult to calculate with precision, the usual procedure is to measure first the response of the detection system to radiations that are known to be prompt (that is, in time coincidence) but that in every other respect have nearly the same characteristics as the radiations whose time relation is to be measured. Then the time distribution of the pulses from the case in question can be compared with this prompt time distribution to obtain the lifetime of the nuclear level. The comparison between the unknown and prompt-coincidence time distributions is commonly made using either the centroid-shift or slope methods. If the lifetime is much longer than the width of the prompt distribution, then the slope of the curve of logarithm of coincidence counting rate versus time delay can be used to extract the lifetime. For shorter lifetimes near the width of the prompt coincidence distribution, the centroid shift between prompt and delayed time distributions can be used to obtain the lifetime.

The recoil of a nucleus from the reaction site can be utilized in several ways to determine nuclear lifetimes. In the recoil-distance method, the excited nuclei produced in a nuclear reaction in a thin target recoil at time $t = 0$ from the reaction site into vacuum in the

forward direction with a well defined velocity v. The distance D that the nucleus moves forward before it emits a γ ray can be utilized to establish a time scale $(t = D/v)$. With typical reactions induced by protons or heavier particles, velocities of the order of 10^8 - 10^9 cm/s are obtained. Thus, for level lifetimes of the order of 10^{-12} s or greater, the distance moved by the excited recoiling nucleus before it decays is directly measureable, and the lifetime measurement reduces to a distance measurement once the velocity is known. The technique can be applied to a wide range of γ-ray energies, from a few tens of keV to the MeV range, and is most commonly applied to lifetimes in the range 10^{-12} - 10^{-9} s. The exponential decay of the recoiling nuclei is often observed in one of two ways. A mechanical-recoil method, similar in principle to that of Thirion and Telegdi (1953), utilizes a movable absorber sufficiently thick to produce nearly complete attenuation of the decay γ rays incident upon it. One can then simply observe past the edge of this movable absorber the number of decay γ rays emitted by excited nuclei that have survived the flight past that edge. From the velocity and the exponential curve of count rate versus absorber displacement, the lifetime of the level can be deduced. For γ-ray energies of a few hundred keV and higher, the Doppler-shift recoil-distance, or "plunger," technique can be employed (Alexander and Allen, 1965). In this variation of the nuclear-recoil method, the excited nuclei recoil freely at 0° with velocity v into vacuum and travel until they strike a movable metal plate placed at a distance $D = vt$ from the target.

The γ rays produced both by nuclei that decay in flight and by nuclei that have stopped in the metal plate are observed in a high-resolution γ-ray detector (such as Ge(Li)) placed typically at 0° to the beam. The γ rays from nuclei that decay at rest in the plate have an energy E_0 while the γ rays from nuclei that decay in flight are Doppler shifted and have an energy $E = E_0(1 + (v/c)\cos\theta)$ where c = velocity of light and θ = angle between detector and recoil direction. Thus, two peaks are observed in the γ-ray spectrum. The intensity of the Doppler-shifted peak is $I_1 = I_0(1 - \exp(-D/v\tau))$, where I_0 is the total number of reaction-produced γ rays, while the intensity of the un-shifted peak is $I_2 = I_0 \exp(-D/v\tau)$. The measurement of the ratio $I_2/(I_1 + I_2) = \exp(-D/v\tau)$ as a function of D gives the lifetime τ if v is known. The velocity can be determined from the kinematics of the reaction or directly from the observed Doppler shift of the γ rays.

Another variation of the nuclear-recoil technique is the Doppler-shift-attenuation method (Devons et al. 1955), often referred to as DSAM. In this technique, the excited nuclei are permitted to recoil with an initially well defined velocity into a material stopping medium instead of into vacuum. The nuclei lose energy by various processes, and the time scale for this method is established by the rate of energy loss (the slowing-down time) for those nuclei in that material medium. Under appropriate conditions, the nuclear lifetime can be derived from a comparison of the lifetime with this slowing-down time, making use of precise measurements of the energies of the γ rays produced

in the decays. Since this method is the principal subject of this
thesis, a detailed description of the technique will be withheld until
a later chapter. The technique can be used to measure lifetimes in
the range 10^{-11} - 10^{-15} s if solids are used as the slowing-down
medium, and in the range 10^{-8} - 10^{-12} s if gases are used. It can
be applied for a wide range of γ-ray energies, from about 100 keV
to the MeV region.

Nuclear resonance fluorescence (reviewed by Metzger, 1959)
has been used to measure lifetimes in the range from 10^{-11} s to
below 10^{-15} s. Actually, the technique involves the determination of
the width of the level rather than its lifetime. The method has the
property that it does not selectively excite specific multipolarities,
in contrast with Coulomb excitation or inelastic electron scattering.
Moreover, it can be used to measure shorter lifetimes than are
attainable using either the electronic or nuclear-recoil techniques
mentioned above. It has the disadvantage that in practice it can be
used only to induce transitions from the ground states of stable
nuclei, and that it requires large fluxes of photons of the proper
energy. It can be applied for a wide range of γ-ray energies, from
100 keV to the MeV region. Pure nuclear resonance fluorescence
(for which the only decay mode of an excited nuclear level is directly
to the ground state) refers to the resonant absorption (and subsequent
re-emission) by nuclei of γ-ray photons with energies equal to the
sum of the transition energy (for the transition being excited from the
ground state) and the kinetic energy of the nuclear recoil following
absorption. The term "resonance fluorescence" is used somewhat

more loosely to include resonance absorption and resonance scatter-
ing for which the excited level has additional modes of decay, such
as cascades through intermediate levels or internal conversion.
These processes are characterized by the restriction of the absorption
or scattering to a very narrow range of γ-ray energies, as compared
with non-resonant interactions such as Compton scattering or pair
production.

When a γ ray of appropriate energy (including the effects of
nuclear recoil) is incident upon a nucleus, that nucleus may absorb
the photon and undergo an upward transition to an excited level. The
range of γ-ray energies which can excite this transition is determined
by the total width of the upper level (the lower level is the stable
ground state) and the Doppler width of the level due to thermal motions
of the nucleus as a whole. The cross section for resonance absorption
depends on the total width Γ of the upper level and on the partial
width Γ_o for excitation from the ground state (the simplest case
occurs for pure resonance fluorescence, for which $\Gamma = \Gamma_o$). The
nuclear resonance fluorescence technique involves the measurement
of the resonance absorption cross section integrated over γ-ray
energy (taking into account the Doppler broadening of the levels) by
the measurement in a suitable detector of the intensity of the γ rays
resonantly scattered or absorbed by a sample containing the nuclei of
interest; this integrated cross section depends on the total width of
the excited level. The usual approaches are through self-absorption
and scattering experiments; for each approach, the observed cross

section is related to the level width by theoretical formulations which take into account the integration of the Breit-Wigner resonance form over the Doppler broadening of the resonance line.

The principal experimental difficulty is that of providing a photon source of sufficient intensity in the narrow region of the absorption. The use of the transition to the ground state of the nuclear level under study provides γ radiation which is highly concentrated in a narrow energy interval; however, the center of this interval is displaced from the center of the absorption line because of the nuclear recoil energy lost in both emission and absorption processes. The resonance condition can be restored in several ways. If a radioactive source is used, the source can be heated, thereby increasing the Doppler width of the γ-ray emission line so as to overlap the absorption line. Mechanical motion (such as the use of an ultracentrifuge) can be used to provide the radioactive source with a velocity in the direction of the absorber, thus Doppler shifting the emission line into overlap with the absorption line. For sources produced in nuclear reactions, the Doppler shifting and broadening of the emission line due to the kinematics of the reaction for the nuclear recoil can be used to produce overlap between the emission and absorption lines. In scattering and self-absorption measurements, it is common to perform control experiments by using dummy scatterers or absorbers made with dimensions and materials as similar as possible to those used in the resonance experiments, but containing no resonance nuclei. These control experiments provide a way to subtract

the background encountered in the resonance experiments more
reliably.

Coulomb excitation can be used to measure partial lifetimes
in the range $10^{-8} - 10^{-15}$ s and for transition energies of about 1 MeV
or less. It has the disadvantage that it is limited primarily to excita-
tions of transitions from the ground states of stable nuclei, although
multiple excitations have been observed using heavy-ion beams. It
also has the property that it selectively excites E2 transitions, so
that only partial information about the electromagnetic transition
probabilities between the two levels can be obtained. The technique
consists of observations of nuclear excitation resulting from the
nearby passage of a charged particle, which can produce a transition
of the nucleus out of its ground state by inducing oscillations in the
nuclear surface through the electric interaction. The cross section
for this excitation may be used to derive the E2 radiative-transition
probability. The downward E2 electromagnetic matrix element is
related by a statistical factor involving the level spins to the upward
E2 matrix element, which is in turn related by a factor dependent on
the transition energy to the reduced matrix element B(E2). The B(E2)
matrix element is a factor in the Coulomb excitation cross section,
which is the quantity measured. The measurement of the cross section
may be made for a thin target by observing the intensity of the in-
elastic particle group corresponding to Coulomb excitation of the
state, in comparison with the intensity of the elastic particle group
whose cross section is given from the Rutherford elastic scattering

formula (assuming that the incident beam energy is kept low enough so that only Coulomb forces are important). The measurement may also be made by observing the intensity of the γ radiation produced as the excited nucleus decays back to the ground state following Coulomb excitation. The analysis for this case is complicated by the necessity of corrections for internal conversion and for γ-ray decay branches to other levels, both of which make the number of ground-state transitions smaller than the number of excited states formed.

Inelastic electron scattering by nuclei has been used to measure nuclear level lifetimes in the range $10^{-10} - 10^{-15}$ s and transition energies on the order of a few hundred keV and greater. It has the disadvantage that the extraction of the lifetime requires a rather complex theoretical analysis. It is limited to excitation of transitions from the ground states of stable nuclei, and it selectively excites electric multipole transitions. Inelastically-scattered electrons are observed to measure the magnitude and dependence on energy and angle of the scattering cross section, which in turn can be used to determine the magnitude and multipolarity of the electromagnetic matrix element.

This thesis reports the measurement of nuclear lifetimes by the Doppler-shift-attenuation method and by the mechanical recoil-distance method, although the former was employed for the bulk of the measurements. It also describes some DSAM measurements made to calibrate and check the reliability of the technique when gases are used as the stopping medium. Finally, it describes the

results of measurements of electronic stopping power for C and Al in He and Xe, pursued as required for the interpretation of the Doppler-shift results. Chapter II deals with the measurement of the lifetime of the 78-keV first excited state of ^{32}P. In Chapter III, a detailed explanation of the Doppler-shift-attenuation method is given, and the general experimental techniques used in all the DSAM measurements are outlined. This chapter also includes a discussion of the theoretical and experimental state of knowledge of the rate of energy loss for heavy ions in matter, and contains a summary of the relevant energy-loss data taken from published literature. Chapter IV deals with the method of analysis applied to the DSAM results using both solid and gaseous stopping media and sets forth the assumptions and approximations employed. It also includes the results of measurements performed to calibrate the gas DSAM using a known lifetime and to check the existence and importance of possible systematic errors due to localized heating of the stopping gas by the incident beam. Chapter V reports the results of DSAM lifetime measurements for three nuclear levels which have been previously measured by other methods and which were performed in the present work as a check on the gas-DSA technique. Chapter VI presents the level lifetime results for the nuclei studied and compares these results with the theoretical predictions of various nuclear models. Chapter VII gives the experimental details and results for the measurements of electronic stopping power for C and Al ions in He and Xe gases, and compares these results with theoretical values and those of other measurements.

II. THE LIFETIME OF THE 78-keV LEVEL OF ^{32}P
BY THE RECOIL DISTANCE METHOD

1. Introduction

A number of previous experiments have established the spins of the ground and first excited states of ^{32}P to be 1^+ and 2^+, respectively (Endt and Van der Leun, 1967). The 78-keV first excited state decays to the ground state by γ-ray emission with a mean life known to be < 40 ns at the start of this work, and from this and the decay energy, it may be inferred that the transition is principally M1 in character. In order to determine the radiative transition probability between these levels, the lifetime of the first excited state was measured by means of a mechanical-recoil method (similar in principle to that of Thirion and Telegdi, 1953) and the ^{29}Si(^{4}He,p)^{32}P reaction.

2. Experimental Procedure

To populate the first-excited state of ^{32}P, a target of ^{29}SiO$_2$, 29 μg/cm^2 thick and enriched to 95% ^{29}Si, was exposed to a beam of 4.52-MeV ^{4}He particles, produced by the ONR-CIT tandem accelerator. The ^{29}SiO$_2$ was evaporated onto a backing of 150-μg/cm^2 copper, and bombarded through the backing, with a resulting beam energy at the target of 4.46 MeV. This was the energy of the first large resonance for the production of 78-keV γ rays observed in the excitation function for the ^{29}Si(^{4}He,p)^{32}P reaction. The

target thickness was subsequently measured at the 3-MV accelerator by observing the width of the 698-keV resonance in the excitation function for the ^{29}Si$(p,\gamma)^{30}$P reaction. A plot of the observed γ-ray yield as a function of beam energy is given in Figure 1. The target thickness was obtained from these data by use of the energy-loss compilations of Whaling (1958).

The target geometry for the τ measurement is illustrated in Figure 2. The excited ^{32}P nuclei recoiled into vacuum, and if they survived past the absorber edge, the deexcitation γ rays were observed at 90° by means of a narrow Ge(Li) detector, 2 mm wide by 20 mm long and drifted to a depth of 2 mm. The maximum ^{32}P recoil angle was 16.5° at the bombarding energy used. In Figure 2, the long axis of the counter is perpendicular to the plane of the figure. The γ-ray absorber was composed of 0.19-mm wall Ta tubing surrounded by a 0.56-mm wall cast-Sn cylinder. The attenuation of 78-keV γ rays by the Ta was 93%, while that of the Ta-Sn combination was 98%.

Between successive runs, the target was held fixed and the absorber was advanced by means of a micrometer screw. Since the velocity of the recoils can be deduced, the lifetime measurement reduces to a measurement of the exponential rate of fall of γ-ray yield versus absorber position. The geometrical resolution of the apparatus, using the configuration of target, absorber, and detector as indicated in Figure 2, was 40 μm. The complete assembly is shown in Figure 3. The ^{4}He beam, typically about 0.4 μA, was collimated prior to entering the stainless-steel tube onto which the

target foil was cemented. The Ta-Sn absorber was attached to the
micrometer screw by means of a short piece of Pyrex glass tubing,
around which was painted a ring of conductive paint, held at a
potential of - 300 volts to serve as an electron suppressor. The
beam was stopped by a 0.25-mm-thick copper disk attached to the
micrometer end and maintained at a potential of + 300 volts. The
micrometer was insulated from the main apparatus by means of
lucite and epoxy to facilitate beam-current integration.

As a monitor of the target thickness and the current integra-
tion, a 7.6-cm by 7.6-cm NaI(Tl) crystal was installed at 90° and
2.5 cm from the beam axis to observe the 2.24-MeV γ rays from the
first excited state of ^{32}S, produced by the $^{29}Si(^4He,n)^{32}S$ reaction.

3. Results

Two of the ^{32}P γ-ray spectra obtained in the Ge(Li) detector
for typical absorber positions are shown in Figure 4. The FWHM
energy resolution of the detector was about 2.5 keV. In addition to
the γ-ray peak at 78 keV, there was a small contaminant peak at
74 keV, attributed to the $^{19}F(^4He,n)^{22}Na$ reaction on residual
fluorine in the Cu beam stop from prior measurements with CaF_2.
By comparison with the well-known γ rays from ^{57}Co and ^{241}Am,
the energy of the 78-keV transition was determined to be 78.2 ± 0.1
keV.

The results of one series of runs are shown in Figure 5. The
yield of 78-keV γ rays has been corrected for target deterioration
by normalizing to the NaI(Tl) monitor-counter yield. It has also

been corrected for geometrical effects (5% correction to the lifetime)
arising from the non-zero diameter of the absorber cylinder and for
its $2 \pm 1\%$ transmission. A least-squares fit with an exponential
function gives a mean recoil distance $x_m = 0.70 \pm 0.02$ mm. The
data indicated by crosses, exhibiting the position resolution of the
apparatus, were taken with a layer of copper, sufficiently thick
(600 $\mu g/cm^2$) to stop the recoils, evaporated onto the target used in
the lifetime run. The resolution of the apparatus is the mean recoil
distance in curve (a), 54 μm.

In order to convert the ^{32}P measurements into a lifetime,
the mean recoil velocity of the ^{32}P nuclei along the beam direction
must be determined. To this end, the angular distribution of the
proton group populating the 78-keV state was measured in 10° steps
from 10° to 150° using the 61-cm-radius magnetic spectrometer with
a position-sensitive detector at the focal plane. A NaI(Tl) detector
monitored the 2.24-MeV gamma radiation from ^{32}S as before. The
observed laboratory angular distribution is shown in Figure 6. From
this distribution and the reaction kinematics, the mean recoil velocity
of ^{32}P along the beam axis was calculated to be 1.82 ± 0.03 mm/ns,
which is about 1.6% less than the value calculated for an isotropic
center-of-mass proton distribution. The uncertainty in the recoil
velocity is due principally to uncertainties in the extrapolation of
the distribution to 0° and 180°.

The velocity was then corrected, using the methods of
Lindhard, Scharff, and Schiøtt (1963), for the mean energy lost by
the ^{32}P in leaving the target, amounting to about 10% of their initial

energy. The corrected mean recoil velocity for the data of Figure 5 is $\overline{v_z} = 1.73 \pm 0.04$ mm/ns.

From the above values, the mean lifetime of the 78-keV state is found to be $\tau = x_m/\overline{v_z} = 405 \pm 15$ ps. A second run with a thinner target yielded a mean distance $x_m = 0.71 \pm 0.04$ mm and a mean recoil velocity $\overline{v_z} = 1.80 \pm 0.03$ mm/ns, which lead to a lifetime $\tau = 394 \pm 24$ ps. The weighted average of these results is

$$\tau(78) = 402 \pm 13 \text{ ps}$$

in agreement with the value $\tau(78) = 365 \pm 36$ ps found by Boulter and Prestwich (1970), but in disagreement with the value $\tau(78) = 520 \pm {}^{90}_{50}$ ps found by Mendelson and Carpenter (1968). Both the above groups used the electronic-timing technique.

Assuming that the (unmeasured) E2/M1 multipole mixing ratio is zero, the measured lifetime leads to an experimental M1 transition strength of $|M(M1)|^2 = 167 \pm 5$ mW.u., where the definition of the Weisskopf unit (W.u.) is that of Skorka et al. (1966). This strength is fairly typical for transitions of this type for nuclei in the mass range $A = 20 - 40$ (Skorka et al., 1966).

Shell-model investigations into the structure of ^{32}P have been made by several authors. A recent example of such a calculation (with references therein to earlier work) is that of Wildenthal, McGrory, Halbert, and Graber (1971b). These authors have used the shell model to describe positive-parity levels in s-d shell nuclei by choosing a model space such that all $2s_{1/2}$ and $1d_{3/2}$ states and up to two holes in the $1d_{5/2}$ shell have been taken into account;

the modified-surface-delta interaction (MSDI) was used as the
effective two-body interaction. (The modified-surface-delta inter-
action and the surface-delta interaction (SDI) have been discussed
by Glaudemans et al. (1967); these authors also cite references to
earlier work related to the SDI.) The four parameters of the MSDI
and the three single-particle energies were fitted to 66 known level
energies of nuclei with A = 30 - 34, and then spins, energies, con-
figurations, static nuclear moments, and M1 and E2 transition
strengths for positive-parity levels of nuclei with A = 30 - 35 were
predicted. The M1 strengths were calculated with free-nucleon g
factors, while the E2 strengths were calculated with effective charges
for neutrons and protons. For the decay of the 78-keV level of ^{32}P,
these authors predict an M1 transition strength of $|M(M1)|^2 =$
190 mW.u., in reasonable agreement with experiment.

Glaudemans, Endt and Dieperink (1971) used the shell-model
wave functions derived by Wildenthal, McGrory, Halbert, and Graber
(1971b) for the MSDI as mentioned above, and performed a calculation
of electromagnetic transition rates and multipole moments for even-
parity levels in A = 30 - 34 nuclei. The M1 and E2 strengths were
calculated using effective g factors and charges obtained from a
least-square fit to experimentally observed magnetic dipole transi-
tion strengths and moments and electric quadrupole transition
strengths and moments. These authors predict an M1 transition
strength for this decay to be $|M(M1)|^2 = 140$ mW.u., also in
reasonable agreement with the present experimental value. Includ-
ing a small calculated E2 contribution, they calculate the lifetime

of the 78-keV state to be $\tau(78) = 490$ ps. It appears that the shell model provides an adequate description of these low-lying levels in ^{32}P.

III. THE DOPPLER-SHIFT-ATTENUATION METHOD

1. Introduction

With the advent of high resolution and high efficiency Ge(Li) γ-ray detectors, the Doppler-shift-attenuation method (DSAM) has become a widely used and powerful technique for the measurement of lifetimes of nuclear excited states which decay by γ-ray emission. This technique, originated in its modern form by Devons et al. (1955), has been employed by a number of authors (Litherland et al. 1963, Warburton et al. 1963, 1966, 1967) to measure lifetimes in the range $5 \times 10^{-15} - 5 \times 10^{-12}$ seconds. In the most commonly used version of this technique, the levels of interest are populated by means of nuclear reactions induced in a target by an incident beam of particles from an accelerator, and the excited nuclei recoil from the reaction site with a well defined velocity. The excited nuclei are allowed to slow down via energy-loss processes in some material medium, usually either the target material itself or in the target backing, and the observed energy of the γ rays emitted depends on the instantaneous velocity of the nucleus at the time of γ-ray emission. If the slowing-down time of the nucleus in that stopping medium is known, either from theory or from energy-loss experiments, and is comparable in magnitude to the lifetime, then the lifetime of the γ-ray emitting level can be deduced from a comparison of the mean Doppler shift with the slowing-down time.

In short, the rate of energy loss of the nucleus is used as a clock to measure the lifetime of the excited level.

To be more specific, consider the idealized DSAM experiment diagrammed in Figure 7. The incident beam strikes a thin (typically a few tens of $\mu g/cm^2$ thick) target from the left and the excited nuclei of interest recoil with minimal energy loss out of the target at 0° relative to the beam direction and with a well defined velocity $v(0)$. If these nuclei recoil into vacuum, then all γ rays emitted during the decay of the nuclear excited levels will be emitted from a source moving with velocity $v(0)$. If these emitted γ rays are observed with an appropriate detector (such as a Ge(Li) detector) at an angle θ relative to the recoil direction, then the γ-ray energy is given by the first-order Doppler-shift formula,

$$E_{\gamma} = E_{\gamma_0} (1 + (v(0)/c) \cos \theta) \tag{1}$$

where

E_{γ} is the observed γ-ray energy

E_{γ_0} is the γ-ray energy from a nucleus decaying at rest

θ is the angle of observation relative to the recoil direction

c is the velocity of light.

It suffices to consider the first-order formula, since $v(0)/c$ is typically of the order of a few per cent or less.

If now a material medium is introduced behind the target, the recoil nuclei lose energy by processes described below, and the velocity of the recoils is reduced, or attenuated. The energy of a single γ ray is given by $E_{\gamma} = E_{\gamma_0} (1 + (v(t)/c) \cos \theta)$ where $v(t)$

is the velocity at the instant of decay. For a collection of decaying nuclei, the mean energy of the γ rays produced by the ensemble is

$$\overline{E_\gamma} = E_{\gamma_0} (1 + (\overline{v(t)}/c) \cos \theta) \tag{2}$$

where

$\overline{E_\gamma}$ is the observed mean γ-ray energy

$\overline{v(t)}$ is the mean velocity at which the decays occur.

The Doppler-shift-attenuation factor F is defined by the relation

$$\overline{E_\gamma} = E_{\gamma_0} (1 + F(v(0)/c) \cos \theta) \tag{3}$$

so that

$$F = \overline{v(t)}/v(0) . \tag{4}$$

One can obtain an experimental measure of F by observing the centroids of the γ-ray lines produced in a suitable detector placed at 90° and at 0° from the initial recoil direction when the recoils are slowed in the stopping medium and when they are allowed to recoil freely into vacuum. From the equations above, it is seen that

$$F = \frac{\overline{E_\gamma}(0^\circ, \text{ stopper}) - \overline{E_\gamma}(90^\circ)}{\overline{E_\gamma}(0^\circ, \text{ vacuum}) - \overline{E_\gamma}(90^\circ)} \tag{5}$$

where

$\overline{E_\gamma}(0^\circ, \text{ stopper})$ is the centroid of the γ-ray line observed at

0° for recoil into the stopping medium

$\overline{E_\gamma}(0^\circ, \text{ vacuum})$ is the centroid observed at 0° for recoil into

vacuum

$\overline{E}_\gamma(90^\circ)$ is the centroid observed at 90° for recoil into either vacuum or the stopping medium.

The lifetime of the level of interest is obtained by comparing the experimental value of F obtained from Equation 5 with a theoretical F value obtained by a calculation which incorporates present theoretical formulations of the slowing-down process, modified as necessary by relevant experimental energy-loss measurements, and which depends on the lifetime of the level.

$$F = \overline{v(t)}/v(0) = (\tau v(0))^{-1} \int_0^\infty v(t) \exp(-t/\tau)\, dt \qquad (6)$$

where

v(t) is the recoil velocity as a function of time

τ is the lifetime of the nuclear level.

If the rate of energy loss for the recoil nucleus is known, either from theory or experiment, then the integral can be evaluated and the result will depend on the lifetime of the nuclear level.

As an example of such a calculation, consider the approximation in which the rate of energy loss of a recoil nucleus is proportional to its velocity. That is,

$$NS_e \equiv -dE/dx = Bv \qquad (7)$$

where

N = number of atoms/cm^3 for the stopping medium

E = energy of the recoil nucleus

x = distance traversed by the recoil nucleus

S_e = electronic stopping cross section in ev-cm^2/atom

B = constant of proportionality

v = velocity of the recoil nucleus.

This approximation describes reasonably well the rate of energy loss due to electronic excitation and ionization for heavy ions in solids with velocity

$$v \lesssim v_o Z_1^{2/3}$$

where

$v_o = e^2/\hbar = c/137 =$ velocity of electron in the first Bohr orbit of hydrogen

$Z_1 =$ atomic number of recoil nucleus.

Using this approximation, it follows that the velocity of the ions falls exponentially with a time constant α, known as the slowing-down time.

$$v(t) = v(0) \exp(-t/\alpha) \quad \text{with} \quad \alpha = B/m \tag{8}$$

Inserting this functional dependence for the velocity into the equation for F, it follows that in this approximation

$$F = \alpha/(\alpha + \tau) \tag{9}$$

A plot of Equation 9 in which F is plotted as a function of τ/α is shown in Figure 8. From this graph, it is clear that a given absolute precision in the experimental value of F will lead to the greatest relative precision in the deduced value of τ if $F = 1/2$ ($\tau = \alpha$ in this approximation). Because the relative uncertainty in the derived lifetime is large when τ is not comparable to α, the limits of applicability of the DSAM occur roughly for lifetimes in the

range $0.1\alpha \leq \tau \leq 10\alpha$. In reality, the slowing-down process is more complicated than indicated in Equation 7 and the dependence of F on τ and α is more complicated than indicated in Equation 9. These complications will be dealt with more thoroughly in Section 3 of this chapter. However, the essential features are presented in Figure 8.

The slowing-down time α for low-energy heavy ions with atomic masses A = 30 - 40 in a solid such as carbon or aluminum is about 0.5 ps. While there is some variability in α for various solids (within about a factor of 2), the Doppler-shift-attenuation method in solid media is limited to the measurement of nuclear lifetimes in about the range 0.05 - 5.0 ps. It is with solid media that the DSAM has been most widely applied. The range of applicability of the DSAM can be extended toward longer lifetimes by the use of a gas as the stopping medium. In this modification of the Doppler-shift technique, the slowing-down time can be changed simply by changing the gas pressure. For example, the slowing-down time for low-energy ^{30}P ions in Xe gas is 52 ps at 20 atm pressure and is 1045 ps at 1 atm pressure. Lifetimes in ^{30}P as low as 5 ps could be measured using Xe gas at 20 atm pressure as the stopping gas, while there is no upper limit since the gas can be made as tenuous as is desired. Thus, the gas-stopper DSAM can be used to bridge the lifetime region between the solid-stopper DSAM at one end and the delayed-coincidence technique at the other. The gas-absorber technique has been recently applied to lifetime measurements by Kavanagh (1967), Blaugrund, Fisher, and

Schwarzschild (1968), Brandolini and Signorini (1969), Kavanagh, Merdinger, and Schulz (1970), Champlin, Howard, and Olness (1971), and Donahue and Hershberger (1971). The gas-stopper version of the DSAM has been used less frequently than the solid-stopper version, partly because of possible systematic errors due to localized heating of the stopping gas by the incident beam and because fewer experimental data exist for the slowing of heavy ions in gases than in solids. One purpose of this work was to investigate these effects and to make the gas DSAM into a reliable technique for nuclear-lifetime measurements. It should be noted that for both gaseous and solid media, the principal uncertainty in the derived lifetime arises from the lack of precise knowledge of the rate of energy loss of low-energy heavy ions in matter.

2. General experimental procedure

All of the DSAM experiments discussed in the following chapters have several experimental techniques in common. In all these experiments, nuclear levels were populated by endoergic $(^4He,n)$ or $(^4He,p)$ reactions using ^4He-particle beams produced by the 6-MV ONR-CIT tandem Van de Graaff accelerator. Excitation functions for the γ rays of interest were measured and the experiments were performed as close to threshold for the reaction as possible, consistent with an adequate yield from the reaction. This usually meant that the bombarding energy was about 0.5 - 1.0 MeV above threshold. The recoiling nuclei were kinematically confined to a narrow forward cone, usually within about 10° of the beam axis.

The targets were thin, usually about 30 $\mu g/cm^2$ thick, and were prepared by vacuum evaporation in a bell jar at an ambient pressure of 1×10^{-6} Torr.

The experimental arrangement employed when gases were used as the stopping medium is illustrated in Figure 9. The beam entered from the left and was collimated by two Ta apertures 1.0 mm in diameter. The target was evaporated onto the down-beam side of a gas-retaining foil consisting of 5.7, 7.2, 11.4 or 12.9 mg/cm^2 Pt, and was bombarded through the foil. With the thicker foils, stopping-gas pressures of up to 22 atm were successfully retained in the gas cell. The foil was epoxied over the end of a Zr foil holder which had a beam-entrance hole 1.32 mm in diameter. The alignment of the Ta collimator and the aperture in the Zr foil holder was checked and adjusted before each run so that they were coaxial to within about 0.1 mm. The beam was stopped at the back of the gas cell by a 0.15-mm-thick Ta disk; the sides of the gas cell were lined with 0.08-mm-thick Ta foil to prevent background radiation induced by scattered beam particles striking the walls of the gas cell, which were constructed of 0.69-mm Al. At pressures greater than 1 atm the gas cell was clamped in place with set screws. The excited nuclei recoiled out of the target into the cell and were allowed to decay either in vacuum or in a stopping gas. The stopping gases used during these measurements were xenon, argon, and helium. Xenon was the gas used most often, since it had a lower slowing-down time α for a given presure than did Ar or He, and since interfering background γ radiation due to reactions on the stopping gas was

less troublesome for xenon than for argon. The γ rays from the de-excitation of the level of interest were observed with a 55-cm^3 Ge(Li) detector at 0° and 90° from the beam direction as the nuclei recoiled into vacuum and as they slowed down in the stopping gas. Several runs were taken at both detector angles and at each gas pressure, and the detector angle was alternated regularly to help eliminate systematic errors due to drifts in the pulse-analysis system. The detector was typically located between 4 and 8 cm from the target. Whenever possible, the gas pressure was adjusted so that the measured F value was near F = 0.5 in order to improve the relative precision of the extracted lifetime. The precision of the measurement of the F value was usually about ± 5%. The gases used had the following purities: Xe, 99.995%; Ar, 99.99%; He, 99.99%. The gas pressure was measured with two different Wallace and Tiernan pressure gauges, covering different pressure ranges. The Wallace and Tiernan FA233 covered the pressure range 0 - 500 pounds per square inch absolute (psia) with an accuracy of ± 0.5 psia, while the Wallace and Tiernan FA145 covered the pressure range 0 - 15 psia with an accuracy of ± 0.015 psia. When xenon was used as the stopping gas, it was recovered by freezing it in its storage bottle with liquid nitrogen; argon and helium were merely pumped away.

The experimental arrangement employed when a solid was used as the stopping medium is illustrated in a top view of Figure 10. The beam entered from the left after being collimated by a single 3.2-mm-diameter aperture in a 0.25-mm-thick Ta disk.

The target chamber was made of glass in the form of a tee. The target material was evaporated onto a 200-μg/cm^2-thick carbon foil and mounted with epoxy over an 8.9-mm-diameter hole in a 0.25-mm Ta sheet. After passing through the target layer and the carbon foil, which served as the stopping medium for the recoils and which was placed at 45° from the beam direction, the beam was stopped by a 0.25-mm-thick cylindrical sheet of Ta which lined the glass chamber and which had a 1-cm diameter beam-entrance hole punched in it. Placing the foil so that the target material was down-beam from the carbon permitted the excited nuclei to recoil into vacuum; by simply rotating the foil by 180°, the recoiling nuclei were permitted to stop in the carbon foil backing. The beam energy was adjusted so that the beam energy at the target layer was the same in both cases. As in the case of the DSAM in gases, the γ rays from the decay of the excited recoiling nuclei were observed at 0° and 90° from the beam direction in the 55-cm^3 Ge(Li) detector as the nuclei recoiled into the carbon and into vacuum. Again, several runs were taken at both detector angles and both target orientations, and the detector angle was alternated to eliminate systematic drifts.

The signals from the Ge(Li) detector were amplified and analyzed by a standard pulse-height analysis system (see Figure 11). The amplifier shaping time constants necessary for the best γ-ray energy resolution were found by experimentation for the particular combination of detector, preamplifier, amplifier, and experimental pulse rate used during a given measurement. The shaping time

constants employed were typically 1.6 μs or 3.2 μs, the shorter
time constants being used to reduce pulse pile-up when the pulse
rate from the detector for γ rays with energy greater than about
100 keV was more than about 1500 s^{-1}. In order to reduce the rate
of resolution-degrading low-energy γ rays from the target, usually
due to x-rays and to Coulomb excitation of nuclei in the Ta beam
stop or the Pt gas-retaining foil, various thicknesses of Pb were
interposed between target and detector; if the γ ray of interest had
an energy less than about 1 MeV, then about 1.5 mm of Pb was used
as the absorber, while for higher energy γ rays of interest, up to
5 mm of Pb was used. In order to prevent pulse-amplitude changes
due to varying pulse rates, the beam intensity was maintained as
constant as possible during a given run and held at the same value
from one run to the next. The beam intensity was typically 0.1 μA.
The run length varied, depending on the yield of the γ ray being
studied, from about 1/2 hour to as long as 8 hours. Because of the
length of the runs and because of the small shifts in γ-ray energy
being measured ($\Delta E_\gamma / E_\gamma = v/c < 1\%$ for these measurements), the
analysis system was digitally stabilized against gain drifts in the
preamplifier-amplifier system and against threshold drifts in the
pulse-height analyzer. The gain was stabilized by use of a Canberra
Industries Model 1495 Digital Spectrum Stabilizer. The reference
spectral line used for gain stabilization was provided by exposing the
Ge(Li) detector to a radioactive source positioned near the gas cell
or glass target chamber. The particular source used was chosen so
as to provide a γ ray of similar energy to the γ ray of interest

but to interfere with it as little as possible. Ideally this would imply a source γ ray well resolved from and slightly lower in energy than the γ ray under investigation. The threshold level of the multi-channel analyzer was stabilized by means of a Canberra Industries Model 1496 Zero Level Stabilizer. The reference spectral line used for zero stabilization was provided by a stable precision electronic pulser and was placed in a low channel of the pulse-height analyzer. Both the 4096-channel Nuclear Data Model ND2200 and the 400-channel Radiation Instruments Development Laboratory Model 34-27 pulse-height analyzers were used during the course of these measurements. In addition, other well-known γ-ray lines from radioactive sources were introduced into the spectrum to serve as a check on the stability of the system and to serve as calibration lines for γ-ray energy measurements.

In order to be able to correct the initial recoil energy for the energy lost as the nucleus left the target layer, the thicknesses of all targets used in the DSAM experiments were measured. This was accomplished by observing the energy of elastically scattered 5.00-MeV ^{4}He particles from the Pt and/or Ta backings, both directly and through the target material, in the 61-cm-radius magnetic spectrometer at 90° in the laboratory. The targets were placed at 45° to both the incident beam and the spectrometer. An example of the observed yields is shown in Figure 12. The observed frequency shift of the front step of the elastic-scattering profile for ^{4}He from the backing, directly and through the target layer, was converted to a shift in energy, corresponding to the energy lost by

the ^{4}He in traversing in this geometry a thickness 2.8 times the perpendicular thickness of the layer. The target thickness is obtained by comparison with the energy-loss tabulations of Whaling (1958).

The initial mean recoil velocity along the beam direction for the nuclei under investigation was calculated from the kinematics of the reaction, assuming that the outgoing proton or neutron angular distribution was isotropic in the center-of-mass system. The recoil energy was corrected for the energy lost in the target layer using the methods of Lindhard, Scharff, and Schiøtt (1963). It was assumed that the reaction took place uniformly throughout the target layer. The mean initial recoil velocity as calculated from kinematics and the energy loss in the target layer was compared with that obtained from an observation of the full Doppler shift. The calculated velocity was usually in reasonable agreement with the observed velocity.

3. The rate of energy loss of heavy ions in matter

a. Theoretical

It is clear from Section 1 of this chapter that in order to extract lifetimes of nuclear states from the observed Doppler shifts, one must know the velocity of the recoil nuclei as a function of time; that is, one must know the rate with which a nucleus loses energy as it traverses a material medium.

In general, energetic ions lose energy in matter by two kinds of collisions: (i) inelastic collisions with the atomic electrons of the material medium, leading to excitation and ionization of that medium,

as well as electron capture and loss by the ion, and (ii) elastic collisions with the atoms of the medium. Energy loss due to collisions of type (i) is termed the electronic energy loss while that due to collisions of type (ii) is termed the nuclear energy loss. The loss of energy to electronic collisions occurs in many small increments, and leaves the incident ion essentially undeflected from its initial direction. The loss of energy in a nuclear collision, however, can remove a large fraction of the initial energy, and can also deflect the ion by a large angle from its initial direction. This scattering of the incident ion from its original direction through the scattering angle ϕ changes the observed γ-ray Doppler shift by an amount $\cos \phi$, and in some cases the nuclear scattering can be more important than the nuclear energy loss in the calculation of the Doppler-shift-attenuation factor F.

The present theoretical framework for the energy loss of ions penetrating matter is based on work of Lindhard and Scharff (1961), herein referred to as LS, and on the theory of atomic collisions as developed by Lindhard, Scharff, and Schiøtt (1963), herein referred to as LSS.

Lindhard and Scharff (1961) have treated the electronic stopping of low-velocity ions on the basis of the Thomas-Fermi statistical model of the atom, and they have calculated the electronic stopping power S_e valid for ion velocities less than $v = v_o Z_1^{2/3}$ to be

$$-(1/N)\ dE/dx \equiv S_e = \xi_e 8\pi e^2 a_o Z_1 Z_2 (Z_1^{2/3} + Z_2^{2/3})^{-3/2} (v/v_o) \quad (10)$$

where

a_o = Bohr radius = 0.529×10^{-8} cm

v_o = Bohr velocity = $e^2/\hbar$ = $c/137$

e = electron charge

Z_1 = atomic number of projectile (ion)

Z_2 = atomic number of target

v = ion velocity

ξ_e = a constant of the order 1-2, which may vary as $Z_1^{1/6}$.

Hence, the electronic stopping cross section is a monotonically increasing function of the projectile velocity and atomic number (Z_1).

Lindhard, Scharff, and Schiøtt (1963) have developed a universal theory of nuclear stopping, applicable to all ions and absorbers, in terms of two dimensionless parameters ϵ and ρ, proportional to the energy of and path length traversed by the incident ion. In the same manner, they write the total stopping power in the dimensionless form $d\epsilon/d\rho$. They define the variables ϵ and ρ as

$$\epsilon = \frac{aM_2}{Z_1 Z_2 e^2 (M_1 + M_2)} E \qquad (11)$$

$$\rho = \frac{4\pi a^2 N M_1 M_2}{(M_1 + M_2)^2} x \qquad (12)$$

where the subscripts 1 and 2 refer to the moving atom and to the atoms of the stopping medium, respectively, and where

$a = 0.8853 \, a_o (Z_1^{2/3} + Z_2^{2/3})^{-1/2}$

e = electronic charge

Z = atomic number

M = atomic mass

N = number of scattering atoms per unit volume

E = kinetic energy of the moving ion

x = distance traveled along the ion path

They then write the total rate of energy loss $(d\epsilon/d\rho)$ as a sum of two terms

$$(d\epsilon/d\rho) = (d\epsilon/d\rho)_e + (d\epsilon/d\rho)_n \tag{13}$$

where $(d\epsilon/d\rho)_e$ and $(d\epsilon/d\rho)_n$ are the electronic and nuclear rate of energy loss in dimensionless units.

The expression for $(d\epsilon/d\rho)_e$ is derived from the expression (Equation 10) found by LS for the energy loss due to collisions with electrons. In this formulation, it becomes

$$-(d\epsilon/d\rho)_e = k\epsilon^{1/2} \tag{14}$$

where

$$k = \xi_e \frac{0.0793 \, Z_1^{1/2} Z_2^{1/2} (M_1 + M_2)^{3/2}}{(Z_1^{2/3} + Z_2^{2/3})^{3/4} M_1^{3/2} M_2^{1/2}} \tag{15}$$

and

$$1 < \xi_e < 2 \quad \text{and} \quad \xi_e \text{ may vary as } Z_1^{1/6}$$

This expression is again applicable for ion velocities $v \lesssim v_o Z_1^{2/3}$. As examples of the values of k and ϵ encountered in this thesis, for 690-keV ^{26}Al recoils in Ar, $k = 0.13$ and $\epsilon = 16.7$, while for the same energy ^{26}Al in Xe, $k = 0.32$ and $\epsilon = 6.1$.

LSS then formulated the theoretical nuclear energy loss $(d\epsilon/d\rho)_n$ by representing the ion-atom interaction as a screened

potential of the Thomas-Fermi type, of the form

$$V(r) = \frac{Z_1 Z_2 e^2}{r} \phi_o(r/a) \tag{16}$$

where $\phi_o(r/a)$ is the Fermi function. Using this screened potential, LSS arrived at a universal differential atomic scattering cross section, applicable to all ion-atom combinations, of the form

$$d\sigma(\theta) = \frac{\pi a^2 f(t^{1/2}) \, dt}{2t^{3/2}} \tag{17}$$

where

$$t^{1/2} = \epsilon \sin(\theta/2)$$

θ = deflection angle in the center-of-mass system

The function $f(t^{1/2})$ was numerically calculated by LSS and is given in Table 2a of the paper by Lindhard, Nielsen, and Scharff (1968). Using this cross section, it can be shown that

$$-(d\epsilon/d\rho)_n = \epsilon^{-1} \int_0^\epsilon f(t^{1/2}) \, d(t^{1/2}) \tag{18}$$

The values of $(d\epsilon/d\rho)_n$ as a function of ϵ are given in Table 2b of the paper by Lindhard, Nielsen, and Scharff (1968). The nuclear energy loss $(d\epsilon/d\rho)_n$ can be fairly well approximated by a set of analytic functions for various regions of ϵ. As one example,

$$(d\epsilon/d\rho)_n \approx 0.4 \, \epsilon^{-1/2} \qquad 1.2 \lesssim \epsilon \lesssim 21 \tag{19}$$

$$(d\epsilon/d\rho)_n \approx 0.38 \qquad 0.01 \lesssim \epsilon \lesssim 1.2 \tag{20}$$

The LSS numerical curve for $(d\epsilon/d\rho)_n$ as well as the approximations above are shown in Figure 13.

As was mentioned in Section 1, the observed Doppler shift
of γ rays emitted from a recoiling nucleus depends not only on
the nuclear and electronic rates of energy loss, but also on the
laboratory angle ϕ through which an initially parallel beam of
recoils (travelling in the direction of the detector at 0°) is scattered
by nuclear collisions. Blaugrund (1966) has explicitly included this
scattering, as well as the electronic and nuclear energy loss, in his
formulation of the theoretical Doppler-shift-attenuation factor F
by calculating the average value of $\cos \phi$ as a function of time.
Using the theoretical expressions for the nuclear and electronic
energy loss as formulated by LSS and incorporating the dimension-
less variables ϵ and ρ, Blaugrund defines two additional dimension-
less variables ϑ and Θ. He lets $\vartheta = (\hbar c/e^2)(v/c) = v/v_0$ be a
dimensionless variable corresponding to the velocity of the moving
ion and lets Θ be a dimensionless variable corresponding to the
time such that $\vartheta = d\rho/d\Theta$. It can be shown that $\Theta = t/T$, where t
is the time and $T = \hbar(M_1 + M_2)^2/(e^2 4\pi a^2 N M_1 M_2)$. He then considers
a point detector detecting γ rays emitted along the initial direction
of motion of the recoiling excited nuclei which are slowing down in
a stopping medium, and lets ϕ be the instantaneous laboratory angle
through which the nuclei have been scattered. Then the Doppler-
shift-attenuation factor F is given by

$$F = (T/\tau)\int_0^\infty \exp{(-\Theta T/\tau)}(\vartheta/\vartheta_0)\, \overline{\cos \phi}\, d\Theta \qquad (21)$$

$(\vartheta_0 = \text{initial value of } \vartheta)$

and he develops relations for the value of $\overline{\cos \phi}$ and for ϑ as functions of time. In particular, he lets m be defined by the equation

$$\epsilon = \frac{1}{2} \mathrm{m} \vartheta^2 \tag{22}$$

from which it follows that

$$\mathrm{m} = \frac{(1.63)(10^3) M_1 M_2}{Z_1 Z_2 M_1 M_2 (Z_1^{2/3} + Z_2^{2/3})^{1/2}} \tag{23}$$

The energy and hence the velocity of an ion passing through the stopping medium can be calculated as a function of time from the expression

$$\Theta = (\mathrm{m}/2)^{1/2} \int_\epsilon^{\epsilon_0} \frac{d\epsilon}{\epsilon^{1/2}(d\epsilon/d\rho)} \tag{24}$$

where ϵ_0 is the dimensionless ion energy at $\Theta = 0$ and

$$(d\epsilon/d\rho) = (d\epsilon/d\rho)_n + /(d\epsilon/d\rho)_e .$$

The integral of Equation 24 can be evaluated numerically to obtain ϵ and hence ϑ as a function of Θ.

In order to calculate the value of $\overline{\cos \phi}$ as a function of time, Blaugrund begins with the multiple-scattering theory developed by Goudsmit and Saunderson (1940a, 1940b) and extended by Lewis (1950), but extends its applicability to the case where the ion and atom have comparable masses. He makes use of the center-of-mass atomic scattering cross section derived by LSS (Equation 17) and after translating the multiple-scattering equations into the laboratory system, he obtains the relation

$$\overline{\cos \phi} = \exp [- (1/2)(M_2/M_1) G(r) I] \tag{25}$$

where

$$I = \int_{\epsilon}^{\epsilon_o} \frac{(d\epsilon/d\rho)_n}{\epsilon(d\epsilon/d\rho)} \, d\epsilon \qquad (26)$$

and

$$G(r) = \begin{cases} 1 + 2/3 \, r - 7/15 \, r^2 + 8 \sum_{n=3}^{\infty} \frac{(-r)^n}{(2n+1)(2n-1)(2n-3)} & , \; r < 1 \\ \\ 2/3 + 8/15 \, r^{-1} - 8 \sum_{n=3}^{\infty} \frac{(-1/r)^{n-1}}{(2n+1)(2n-1)(2n-3)} & , \; r > 1 \end{cases} \qquad (27)$$

and

$$r = M_1/M_2$$

The sums in the expression for $G(r)$ can usually be neglected. One can numerically integrate the expression for F in Equation 21 once $\overline{\cos \phi}$ and ϑ/ϑ_o are known as functions of the time Θ.

b. <u>Experimental</u>

In the last decade, a number of experimental studies of the rate of energy loss of heavy ions in matter have been performed to check the theoretical predictions of Lindhard and Scharff (1961) and of Lindhard, Scharff, and Schiøtt (1963). Most of these studies have dealt with the rate of energy loss in amorphous and crystalline solids; recently, a few studies have been made of energy losses for heavy ions in gases. The most relevant of these dE/dx studies will be reviewed here.

The electronic part of the total stopping power is more readily accessible to direct measurement than is the nuclear part, mainly due to the energy range and geometrical arrangement of the most commonly-used laboratory apparatus and techniques for energy-loss

measurements. For example, the rate of energy loss of a beam of
heavy ions is commonly determined by measuring the energy of that
beam in a suitable detector or analyzer system both directly in
vacuum and when the beam has passed through a thin layer of known
thickness of the stopping material. From the change in beam energy
and the absorber thickness, one can calculate the rate of energy loss
dE/dx. Because this arrangement usually employs collimators in
front of the detector or analyzer system, large-angle scattering (due
to nuclear collisions) away from the incident beam direction is dis-
criminated against geometrically. Only that part of the nuclear
scattering remains which is due to scattering into the forward
direction and within the solid angle subtended by the detection
system collimators. Moreover, nuclear stopping becomes important
only at very low ion energies (on the order of 100 - 200 keV or less;
cf. Figure 13). If the energy is sufficiently low that nuclear stopping
is significant in an electronic energy-loss measurement, a correction
for the contribution to the observed energy loss due to forward
nuclear scattering is usually made based upon the theoretical formu-
lations of LSS.

The nuclear stopping power is not generally measured directly
in energy-loss determinations but rather is inferred from range
measurements. Since the ion range depends on nuclear and electronic
stopping powers, and since the electronic part can be measured inde-
pendently (corrected slightly if necessary for nuclear stopping), the
nuclear part of the stopping can be extracted. For very low energy,
very heavy particles in medium-to-heavy absorbers (such as 97-keV

^{224}Ra in Kr or Xe), the range distribution depends almost entirely on the nuclear stopping power, and thus serves as a nearly direct check of the LSS formulation of $(d\epsilon/d\rho)_n$.

The electronic stopping cross section S_e (defined in Equation 7) for heavy ions in solids has become the subject of a number of experimental studies in the last 10 years, mostly because of the observation of phenomena not predicted by the LS formulation (Equation 10). In particular, while the LS theory predicts a smooth, monotonically increasing dependence of S_e on Z_1, the experimental data show oscillations of S_e with Z_1 about the predicted curve. Teplova et al. (1962) first observed this non-monotonic dependence of S_e in their studies of range and energy loss of various heavy ions with $2 \leq Z_1 \leq 36$ and with velocities between 2.6 and 11.8 $\times 10^8$ cm/s slowing down in H, He, methane, benzene, air, Ar, celluloid, Al, Ni, Ag, and Au. However, the first systematic investigation into this phenomenon was performed by Ormrod and Duckworth (1963) and Ormrod, Macdonald, and Duckworth (1965). They measured the electronic stopping cross section S_e for ions with $1 \leq Z_1 \leq 19$ and energies $E < 150$ keV in carbon, and for ions with $1 \leq Z_1 \leq 11$ in a similar energy range in aluminum. Their results for ions in carbon and aluminum, plotted at a constant ion velocity $v = 0.41 v_o$, indicate that the LS formulation with $\xi_e = Z_1^{1/6}$ accurately describes the average behavior of S_e, and that the measured S_e lie essentially within the limits on ξ_e suggested by LS, namely $1 \leq \xi_e \leq 2$. However, the Z_1 oscillations observed experimentally

are not predicted by this formulation, which is based on the statistical Thomas-Fermi model of the atom. Based on their results, Ormrod et al. (1965) conclude that the amplitude and position of the maxima and minima of the oscillations are essentially independent of the stopping medium, and depend on the incident ion. In addition, they fit their data to the functional form $S_e = KE^p$ and derived the coefficient K and the exponent p. They find that the experimental value of p varies from 0.40 up to 0.58, in comparison with the LS theoretical value of $p = 0.5$.

Fastrup, Hvelplund, and Sautter (1966) and Hvelplund and Fastrup (1968) measured the electronic stopping cross section S_e for ions with $6 \leq Z_1 \leq 39$ and energies in the range $0.1 \leq E \leq 1.5$ MeV in carbon. In Figure 6 of their 1968 publication, Hvelplund and Fastrup plot the observed S_e in carbon as a function of Z_1 for three different ion velocities $v = 0.41 \, v_o$, $0.63 \, v_o$, and $0.91 \, v_o$, as well as some measurements made by Eriksson et al. (1967) in an oriented tungsten monocrystal. At a constant ion velocity, they also observe the periodic dependence of S_e on Z_1 over an extended Z_1 range; however, the amplitude of the oscillations decreases with increasing ion velocity. In addition, they observe that the "wavelength" of the oscillations increases with increasing Z_1. Again, the theoretical curve of LS with $\xi_e = Z_1^{1/6}$ represents a good mean value for the experimental data for all Z_1. The results of Eriksson et al. (1967), presented by Hvelplund and Fastrup (1968), indicate that the oscillations are a general phenomenon and that they are even more pronounced for particles channeled in an oriented tungsten

monocrystal than in amorphous solids. On the basis of their data,
Hvelplund and Fastrup (1968) conclude that the positions of maxima
and minima are insensitive both to Z_2 and to the degree of channel-
ing, and that the amplitude of the oscillations appears to be correlated
with the degree of interpenetration of atomic shells during collisions.
They also fit their data to the functional form $S_e = KE^p$, and find
values of p in the range 0.40 - 0.71 for $Z_1 \leq 20$.

Results showing similar oscillations of S_e with Z_1 have
been reported for ions in boron (Macdonald, Ormrod, and Duckworth
(1966)) and in nickel (Ormrod, Macdonald, and Duckworth in a private
communication to Hvelplund and Fastrup (1968)). The literature
pertaining to range and energy-loss studies for heavy ions in solids
is voluminous, and no attempt will be made to review it here.
Reviews of experimental results for the range and electronic stopping
power of heavy ions in various solids and gases have been written by
Northcliffe and Schilling (1970) and by Bergström and Domeij (1966).
If absorbers other than C or Al are used, the literature may be
consulted for data relevant to the ion-absorber combination being
employed.

Far fewer experimental data exist for the rate of electronic
energy loss of heavy ions in gases than in solids, at least for ions
with $Z_1 \leq 20$ and energy $E < 1.5$ MeV. Ormrod (1968) measured
the electronic stopping cross section S_e for heavy ions with
$Z_1 \leq 10$ and $E < 200$ keV in nitrogen and argon. He found that the
periodic dependence of S_e on Z_1 at a constant ion velocity
$v = 0.41 \, v_o$, observed previously for solid targets, also occurs for

low-pressure gas targets. Thus, this Z_1 dependence does not depend on the collision frequency, since the frequency of collision in this low pressure (~ 0.01 Torr) gas measurement is eight orders of magnitude below that in solids. However, in contrast to the results in solids, it is clear from Ormrod's data that the LS theoretical formulation with $\xi_e = Z_1^{1/6}$ is not a reasonable average to the experimental data, particularly for Ar, but rather the experimental data fall on the average below the theoretical prediction. It appears that a reasonable average to the experimental data can be formed by using the LS theoretical prediction but with the factor ξ_e simply scaled down from the theoretical $\xi_e = Z_1^{1/6}$ by a multiplicative factor. In Figure 14, Ormrod's results for S_e versus Z_1 for ions with $v = 0.41\ v_o$ slowing in Ar are shown along with three examples of the LS theory for ions in **Ar** scaled down by using $\xi_e = 0.4\ Z_1^{1/6}$, $0.5\ Z_1^{1/6}$, and $0.7\ Z_1^{1/6}$. While these data are not complete enough ($Z_1 \lesssim 10$) to determine the scaling-down factor unambiguously, it appears that the curve with the same shape as the LS theoretical curve and which is a reasonable average to the experimental data lies roughly 50% lower than the LS prediction with $\xi_e = Z_1^{1/6}$. However, it appears that the oscillations are the same in amplitude and position as in solids.

Fastrup, Borup, and Hvelplund (1968) measured the electronic stopping cross section for ions with $6 \le Z_1 \le 24$ and energies in the range $0.2 \le E \le 0.5$ MeV in atmospheric air. They plotted S_e as a function of Z_1 for a constant ion velocity $v = 0.63\ v_o$, and found oscillations of S_e with Z_1 with amplitude and position in agreement

with those observed in carbon. In agreement with Ormrod (1968), they find that the experimental data lie below the LS prediction with $\xi_e = Z_1^{1/6}$. A smooth mean curve drawn through the experimental data lies approximately 35% below the LS prediction, consistent with the observation of Ormrod (1968) who found that the best mean curve for heavy ions in nitrogen lies about 40% below the LS theoretical prediction. The exponents p found from fitting the observed S_e to the function form $S_e = KE^p$ fell in the range $0.44 \leq p \leq 0.78$ for $6 \leq Z_1 \leq 24$.

Hvelplund (1971) measured the electronic stopping cross section for ions with $2 \leq Z_1 \leq 12$ in the energy range $100 \leq E \leq 500$ keV in helium, air, and neon. For ions with a constant velocity $v = 0.9\, v_o$, he observed oscillations of S_e with Z_1 possessing amplitude and position of maxima and minima consistent with those found in C and Al. In all three gases, the experimental data lie below the LS theoretical prediction with $\xi_e = Z_1^{1/6}$. For heavy ions in He, the best average curve through the experimental data is about 50% lower than the LS prediction, while for heavy ions in Ne and air, the best average curve is about 40% lower than the LS theory. The exponents p found from fitting the data to the form $S_e = KE^p$ lie in the range $0.33 \leq p \leq 0.70$, with one case (^{7}Li in He) having $p = 0.77$.

The nuclear part of the stopping power has been investigated primarily through range studies rather than dE/dx measurements. Numerous measurements have been made of the ranges of low-energy heavy ions in both light and heavy gaseous and solid absorbers. These

studies indicate that the LSS theory of nuclear energy loss is essentially correct, but that deviations of the order of 20 - 25% can occur. Several of the range studies such as that of Leon and Steiger-Shafrir (1971) indicate that the experimental ranges can exceed the LSS predicted range by as much as 25%, indicating that the LSS theory can overestimate the nuclear stopping power by the same amount.

IV. ANALYSIS OF THE DSAM DATA

1. Introduction

For the extraction of nuclear excited-state lifetimes from the DSAM data of this work, the electronic and nuclear stopping-power theories of Lindhard and Scharff (1961) and of Lindhard, Scharff, and Schiøtt (1963) are assumed to be essentially correct descriptions of the rate of energy loss of heavy ions in matter. Corrections to these theoretical formulations are based upon the experimental energy-loss studies mentioned in Chapter III and upon indirect studies of the energy-loss mechanism employing DSAM measurements of known lifetimes to be described below. In addition, the theoretical formulation of $\overline{\cos \phi}$ as a function of time put forth by Blaugrund (1966) is assumed to be adequate for the attenuation of the γ-ray Doppler shift due to nuclear scattering.

For the DSAM measurements which employed solids as the stopping media, the corrections to the theoretical formulations are taken directly from published experimental dE/dx studies for the nuclei of interest in the stopping medium used or from reasonable extrapolations and interpolations of such studies. This is possible because of the existence of a relatively large quantity of experimental stopping-power data for heavy ions in solids and particularly in carbon, the material used for the present solid-DSAM measurements.

For the lifetime experiments which employed gases as the absorbing media, the corrections to the theoretical formulations for each gas are derived from DSAM measurements for a case in which

the lifetime is well known from other techniques. From the observed Doppler-shift-attenuation data and from the known lifetime for this case, one can extract information concerning the rate of energy loss for this atom in the gases used, and thus calibrate the gas-DSAM technique. This approach is necessary because of the paucity of experimental stopping-power data for heavy ions in gases. For example, apart from the new data presented in Chapter VII, no experimental information exists for the rate of energy loss of ions with $8 \leq Z_1 \leq 19$ and $E < 1$ MeV in xenon, the stopping gas used in many of the lifetime measurements of this work. Moreover, as noted in Chapter III, only very limited experimental information is available for the stopping power of ions in He and Ar, the other stopping gases used. However, the available information is used to guide the application of the stopping-power parameters derived from known lifetimes to the deduction of unknown lifetimes.

2. Analysis for Solid Stopping Media

The total universal nuclear stopping power in reduced units $(d\epsilon/d\rho)_n$ used in this analysis of DSAM experiments employing solid media is related to that formulated by LSS theory $(d\epsilon/d\rho)_{n,LSS}$ by a scaling factor f_n, where f_n is a constant of the order of unity.

$$(d\epsilon/d\rho)_n = f_n(d\epsilon/d\rho)_{n,LSS}$$

The overall good agreement between ion ranges observed experimentally with those predicted theoretically by the LSS formulation

indicates that this theory is an essentially correct description of the nuclear energy-loss phenomenon. However, some of the data indicates that the observed ranges are somewhat greater (usually about 20 - 25%) than predicted by LSS, implying that this theory perhaps overestimates the nuclear stopping power. The simplest way to correct such overestimation is to merely scale down the whole $(d\epsilon/d\rho)_n$ versus ϵ curve by about 20%, that is, by setting $f_n = 0.8$. Furthermore, Bell et al. (1969) have analyzed experimental range data of Powers and Whaling (1962), Poskanzer (1963), and Davies and Sims (1961) for low-energy ^{14}N, ^{20}Ne, and ^{40}Ar in ^{12}C and for ^{14}N, ^{24}Na, and ^{42}K in ^{27}Al at velocities where the Z_1 oscillations of the electronic stopping power S_e have been studied by Ormrod et al. (1965). Including the effects of the oscillations of S_e with Z_1 and incorporating the nuclear stopping theory of LSS, they calculated the value of f_n which best fitted the published ranges. They found that the mean best value of f_n for these cases lay in the range $0.68 \leq f_n \leq 0.88$ and adopted a best value of $f_n = 0.75 \pm 0.10$ as representative of all six cases. Considering only the three cases in carbon, the mean best value is $f_n = 0.80 \pm 0.05$. The value of f_n for ions stopping in carbon adopted for the present work is $f_n = 0.8 \pm 0.2$.

In order to simplify the calculation of the DSAM factor F, the LSS numerical formulation $(d\epsilon/d\rho)_{n,LSS}$ as a function of ϵ is approximated by the two analytical forms given in Equations 19 and 20. The agreement between these analytic forms and the numerical results of the LSS theory ($f_n = 1$) are shown in Figure 13. Values of the reduced

energy $\epsilon < 0.01$ are not considered. Initial values ϵ_o of the
reduced energy for the nuclei studied in this work are typically 20
when the stopping medium is C or He, 15 when the medium is Ar,
and 5 when the medium is Xe. Thus even in the worst case
($\epsilon_o = 5$ for recoils in Xe), the ion has lost 99.8% of its energy when
the lower limit $\epsilon = 0.01$ is reached. In summary, the nuclear
stopping power $(d\epsilon/d\rho)_n$ is approximated in the present DSAM
analysis by the following relations

$$(d\epsilon/d\rho)_n = f_n \, 0.4 \, \epsilon^{-1/2} \qquad 1.2 \lesssim \epsilon \leq \epsilon_o \leq 24$$

$$(d\epsilon/d\rho)_n = f_n \, 0.38 \qquad 0.01 \lesssim \epsilon \leq 1.2$$

where $f_n = 0.8 \pm 0.2$ for ions in C.

The electronic stopping power in reduced units $(d\epsilon/d\rho)_e$ used
in the analysis of the present DSAM measurements employing solid
media is related to that formulated by the LS theory $(d\epsilon/d\rho)_{e,LS}$ by
a scaling factor f_e, where f_e is of the order of unity,

$$(d\epsilon/d\rho)_e = f_e \, (d\epsilon/d\rho)_{e,LS} = f_e k \epsilon^{1/2}$$

and where the symbols are as defined in Chapter III. In that chapter,
it is noted that the LS theory is a reasonable average to experimentally
observed stopping cross sections for ions in solids, but that significant
deviations ($\sim 35\%$) from this average are observed due to oscillations
of S_e with Z_1. Moreover, it is seen that the exponent p in the
relation $S_e = KE^p$ has values usually within 20 - 30% of the theoreti-
cally predicted exponent $p = 0.5$. It is assumed in the present

analysis for solid media that the LS electronic stopping power theory is essentially correct. It is assumed that the exponent p in the power-law dependence of S_e on E is the theoretically predicted $p = 1/2$, and that the oscillatory deviations from the LS theory of the observed electronic stopping power can be accounted for by introducing an oscillating factor $f_e(Z_1)$. It is also assumed that the Z_1 oscillations are insensitive to Z_2; that is, the magnitude and position of maxima and minima depend only on the incident ion and its velocity. It is therefore presumed that a table of values of $f_e(Z_1)$ compiled from a comparison of experimental and theoretical electronic stopping powers in carbon can be applied to these same ions stopping in other media. It was seen in Chapter III that as the ion velocity increases, the magnitude of the Z_1 oscillations decreases. Thus, the correction factor f_e will also be a function of the ion velocity, so that $f_e = f_e(Z_1, v)$. The problem then arises of what velocity to use in selecting f_e for a particular DSAM measurement. It seems reasonable to use the mean velocity at the time of nuclear decay as the velocity representative of the ensemble of recoil ions. This velocity can be determined from the measured DSAM factor F, since to first approximation, F is the ratio of the mean ion velocity at time of decay to the initial ion velocity (see Equation 4). The values of f_e as a function of Z_1 and $\overline{v(t)}/v_o = F v(0)/v_o$ (where $v_o = c/137$) used in the present analysis are given in Table I. For values of $\overline{v(t)}/v_o$ not included in the table, it seems reasonable to interpolate between those given. The values of $f_e(Z_1, \overline{v(t)}/v_o)$ quoted are

derived from a comparison of the LS prediction of S_e for heavy ions in carbon with the experimental values obtained by Ormrod and Duckworth (1963), Omrod et al. (1965), Fastrup et al. (1966), and Hvelplund and Fastrup (1968).

The theoretical formulation of $\overline{\cos \phi(t)}$ put forth by Blaugrund (1966) is assumed to be correct. Currie (1969) performed a Monte-Carlo calculation to test the validity of Blaugrund's mathematical procedure. He adopted as the general basis for his program the theoretical formalism of LSS. The electronic stopping power formulated by LS was treated as a background effect, slowing the ions continuously but not deflecting them, while the nuclear stopping and scattering was treated as a random process occurring on top of the background. Each ion was allowed to collide randomly with the atoms of the stopping medium and was followed through successive deflections. The values of $\overline{\cos \phi(t)}$ calculated in this way were in excellent agreement with the $\overline{\cos \phi(t)}$ calculated using Blaugrund's formalism.

3. Analysis for Gaseous Stopping Media

As in the case of solid absorbers, the total universal nuclear stopping power $(d\epsilon/d\rho)_n$ given by LSS theory is assumed to be essentially correct for gaseous media. The correction to the theoretical formulation is accomplished through the scaling factor f_n, again of the order of unity, so that

$$(d\epsilon/d\rho)_n = f_n (d\epsilon/d\rho)_{n,\,LSS}$$

where $(d\epsilon/d\rho)_{n,LSS}$ is approximated by the two analytic forms given in Section 2 of this chapter. It is expected that $f_n = 0.8 \pm 0.2$; however, the actual value of f_n used is determined by calibration DSAM measurements to be described in Section 5 of this chapter.

The electronic stopping power for ions slowing in gases is treated somewhat differently from the case of ions in solids. As noted in Chapter III, the observed electronic stopping cross section S_e for ions in He, air, N, Ne, and Ar shows Z_1 oscillations similar in amplitude and shape to those observed in solids. In contrast to the case for solids, however, the LS theoretical formulation is <u>not</u> a reasonable average to the observed S_e; the best average line through the experimental data falls 40 - 50% below the LS prediction. This discrepancy is presumably somehow due to the state of condensation of the stopping medium, but no satisfactory theoretical explanation for this difference has been proposed. To take account of this difference between solid and gaseous absorbers, the electronic stopping power $(d\epsilon/d\rho)_e$ used in the analysis for gases is assumed to be related to the LS formulation by

$$(d\epsilon/d\rho)_e = f_e(Z_1, \overline{v(t)}/v_o, gas)(d\epsilon/d\rho)_{e,LS} = f_e(Z_1, \overline{v(t)}/v_o, gas)k\epsilon^{1/2}$$

with k and ϵ as stated before but with f_e given by the product

$$f_e(Z_1, \overline{v(t)}/v_o, gas) = f_e(Z_1, \overline{v(t)}/v_o)f_e(gas)$$

where $f_e(Z_1, \overline{v(t)}/v_o)$ is given in Table I and where $f_e(gas)$ is of the order 0.5. As in the case for solids, it is assumed that the exponent p

in the power-law dependence of S_e on energy is that expected theoretically ($p = 0.5$), and that discrepancies between theory and experiment can be accounted for by using the scaling factor f_e. It is assumed that the Z_1 oscillations are independent of Z_2 so that the factor $f_e(Z_1, \overline{v(t)}/v_o)$ can be applied not only to the stopping gases He and Ar (for which the experimentally observed S_e are consistent with this assumption) but also to Xe, for which no equivalent measurements have been performed. Because the measurements of S_e in He and Ar were performed only for $Z_1 \leq 12$, insufficient data exist to establish unambiguously the location of the curve that is the best average through the oscillations. For that reason, even for He and Ar, the value of f_e(gas) cannot be definitely determined from published data. However, the data for He and Ar indicate that f_e(gas) should be ~ 0.5 when these two gases are used. Since no equivalent data exist for heavy ions in Xe (see, however, Chapter VII), it can only be inferred from the S_e data for He, air, N, Ne, and Ar that f_e(gas) ~ 0.5 could easily be anticipated for Xe. Therefore, a determination of f_e(gas) and of f_n was carried out for each gas used (He, Ar, and Xe) in the present DSAM lifetime measurements; these calibration measurements are described in Section 5 of this chapter. As in the case of solid stopping media and for the same reasons, it is assumed that Blaugrund's (1966) formulation of $\overline{\cos \phi}$ is correct.

4. Localized Heating of the Stopping Gas

One possible difficulty in the Doppler-shift-attenuation method when a gas is employed as the stopping medium is the local heating of that gas by the beam of incident particles. Such heating could locally reduce the number of stopping atoms in the region into which the excited nuclei recoil. In order to ascertain the existence and importance of this effect, the Doppler-shift-attenuation factor F was measured as a function of the beam intensity in amperes for two different cases in which the pressure of the stopping gas differed by a factor of thirty. It was presumed that if the incident beam does significantly heat the gas locally, then as the beam current decreases, the heating will decrease proportionately so that the number of stopping atoms per cm^3 and hence the attenuation of the recoil velocity will increase and F will decrease.

The first case investigated was the heating effect of incident ^{4}He beams in low-pressure xenon. The nuclear decay selected for study was the γ-ray decay of the 3^+ second-excited state of ^{26}Al located at 418 keV. The level diagram (Endt and Van der Leun 1967) for this nucleus is shown in Figure 15. This level decays to the 5^+ ground state with the emission of a 418-keV γ ray, and the level lifetime is well known to be $\tau(418) = 1.82 \pm 0.04$ ns from a number of direct electronic measurements (Endt and Van der Leun 1967). The level of interest was populated using the ^{23}Na$(^4$He,n$)^{27}$Al reaction. The target was a thin (50 ± 10 $\mu g/cm^2$) layer of natural NaBr evaporated onto the downbeam side of a 5.7 mg/cm^2 platinum

gas-retaining foil. This foil was epoxied over a 4.0-mm-diameter hole in a stainless steel foil holder and placed in position in the apparatus shown in Figure 9. The target was bombarded with a beam of 6.10-MeV ^{4}He particles. Including the energy loss of the recoils in a half-thickness of the target layer, the kinematically calculated mean recoil velocity immediately following the target layer was $\beta(0) = v(0)/c = (7.38 \pm 0.12) \times 10^{-3}$. Further experimental details for this calculated velocity may be found in Table II.

The 418-keV γ rays from this decay were observed with a 6-cm^3 Ge(Li) detector placed at 0° and 90° from the beam direction both in vacuum and as the ^{26}Al recoils slowed in Xe gas at a pressure of 0.52 atm and for incident beam currents from 18 to 100 nA. A second set of runs with a thicker target was taken with a Xe pressure of 0.40 atm and for beam currents from 40 to 125 nA. The pulses from the detector were amplified by an ORTEC Model 118A pre-amplifier and a Tennelec TC200 main amplifier and then analyzed in an RIDL Model 34-27 400-channel analyzer. The pulse-analysis system was stabilized against gain and threshold-level drifts as described in Chapter III using the 478-keV γ rays from a ^{7}Be source placed near the target as the reference line for gain stabilization and using pulses from a stable electronic pulser placed in a low channel of the analyzer as the reference line for zero-level stabilization. In addition, 279-keV γ rays from a ^{203}Hg source were introduced into the spectrum to check on the stability of the system. An example of the spectra obtained in the Ge(Li) detector is shown in Figure 16. The

FWHM energy resolution for this arrangement was 2.6 keV for 400-keV γ rays. The observed mean full Doppler shift for recoils into vacuum, corrected by 4.2% for the solid angle subtended by the detector, was 3.00 ± 0.09 keV, leading to an observed mean recoil velocity of $\beta(0) = (7.18 \pm 0.22) \times 10^{-3}$, in agreement with the velocity calculated from kinematics. The measured DSAM factors F as a function of beam current for both sets of runs are given in Table II and are plotted in Figure 17. These data are consistent with a beam-heating effect, as the F value decreases a total of $17 \pm 8\%$ as the beam current is decreased by a factor of 5.5. However, the variation of this effect can be kept small ($< 5\%$) if the beam current is limited to the region 100 ± 20 nA.

The second case investigated was the local heating effect of an incident ^{4}He beam in high-pressure xenon. The γ-ray decay employed in this instance is that of the $7/2^-$ fifth excited state of ^{33}S located at 2934 keV. The level diagram (Endt and Van der Leun 1967) for this nucleus is shown in Figure 18. The 2934-keV level decays with essentially equal probability to the $5/2^{(+)}$ level at 1968 keV and to the $3/2^+$ ground state. At the time this measurement was performed, two determinations of the lifetime of this level had been reported. Brandolini and Signorini (1969) obtained the value $\tau(2934) = 38 \pm 11$ ps, while Kavanagh et al. (1970) found $\tau(2934) = 36 \pm 8$ ps. It was therefore expected that a Xe pressure of greater than 10 atm would be necessary to effect a DSAM factor F of about 0.5.

The level of interest was populated using the $^{30}Si(^{4}He,n)^{33}S$ reaction. The target was a 100 ± 10 μg/cm^2 layer of elemental silicon, enriched to 95% in ^{30}Si and evaporated onto a backing of 510 ± 40 μg/cm^2 of gold. This gold backing was then epoxied at its perimeter onto the downbeam side of an 11.4 mg/cm^2 platinum gas-retaining foil and exposed to a beam of 9.70-MeV ^{4}He particles. Including the energy loss of the recoils in a half-thickness of the target layer, the kinematically calculated mean recoil velocity immediately following the target layer was $\beta(0) = (6.51 \pm 0.18) \times 10^{-3}$. Further experimental details for this calculated velocity may be found in Table III.

The 2934-keV γ rays from the decay of the 2934-keV level to the ground state were observed with a 55-cm^3 Ge(Li) detector placed at 0° and 90° from the beam direction both in vacuum and as the ^{33}S recoils slowed in Xe gas at a pressure of 13.6 atm and for incident beam currents ranging from 20 to 130 nA. The 966-keV γ rays from the decay to the 1968-keV level were observed but not analyzed due to a high background which interfered with this peak. The pulses from the detector were amplified in an ORTEC Model 120-F preamplifier and a Canberra Industries CI-1416 main amplifier and then analyzed in a 4096-channel Nuclear Data Model ND2200 pulse-height analyzer. Due to difficulties in the digital stabilizer electronics, the pulse-analysis system was operated with no digital spectrum stabilization. In order to keep track of any electronic drifts, lines from γ rays due to ^{88}Y, ^{60}Co, and ^{212}Pb sources placed near the target were introduced into the pulse spectrum.

An example of part of the spectra obtained with the Ge(Li) detector is shown in Figure 19. The FWHM energy resolution for 2615-keV γ rays is 6.2 keV. The observed mean full Doppler shift for recoils into vacuum, corrected by 1.5% for the solid angle subtended by the detector, is 18.65 ± 0.61 keV, leading to an observed mean recoil velocity of $\beta(0) = (6.35 \pm 0.21) \times 10^{-3}$, in excellent agreement with the kinematically calculated value. The measured DSAM factors F as a function of beam current are given in Table III and are plotted in Figure 20. Similar to the results with low-pressure xenon, these data are consistent with a beam-heating effect, since the F value decreases by a total of $18 \pm 12\%$ when the beam current is decreased by a factor of 6.5. As before, the variation of this effect can be kept small ($< 5\%$) if the beam current is limited to the range 100 ± 20 nA.

These results show that the effect of localized heating of the stopping gas by the incident beam is similar at both the high and low pressures used for the gas-DSAM lifetime measurements of the present work, and that the variation of this effect can be kept small ($< 5\%$) if the incident beam current is restricted to the range 100 ± 20 nA. No uncertainty in the derived lifetimes presented in Chapter VI is included from this source, since both calibration and unknown lifetime runs were performed in this beam-current interval.

5. DSAM Calibration of the Stopping Gases

a. Introduction

As is mentioned in Section 3 of this chapter, there are insufficient experimental data to permit an assignment of the stopping parameters f_n and $f_e(gas)$ for the stopping gases employed in the present work, based on published energy-loss results. Using the existing energy-loss data as a guide, these parameters have been determined from measurements in which the Doppler-shift attenuation of the γ rays from a nuclear level with a well known lifetime is used to calibrate the slowing-down mechanism of that nucleus in Xe, Ar, and He. The most suitable case for this study from the standpoint of length of lifetime, precision with which that lifetime is known, γ-ray energy, and reaction type ((^{4}He, n or p)) is the decay of the 418-keV level of ^{26}Al, whose lifetime ($\tau = 1.82 \pm 0.04$ ns) has been determined in a number of direct electronic timing measurements (Endt and Van der Leun 1967). This decay was mentioned in Section 4 of this chapter.

The determination of f_n, $f_e(gas)$ for a particular stopping gas is accomplished by measuring the DSAM factor F as the excited ^{26}Al recoils slow down and decay in that gas, and then determining the values of f_n, $f_e(gas)$ necessary to reproduce the known lifetime. The parameter $f_e(Z_1, \overline{v}/v_o)$ is determined from the measured DSAM factor F and the initial recoil velocity, and is obtained from Table I. Since only the lifetime is known, the parameters f_n and $f_e(gas)$ are not both determined independently. All that can be deduced (if only a

centroid analysis of the γ-ray peak is performed) are pairs of f_n, f_e(gas) that reproduce the lifetime. However, as will be demonstrated in Chapter V, when these different f_n, f_e(gas) pairs are applied to the measurement of an unknown lifetime, they all lead to nearly the same value for that lifetime. Thus, the particular set of f_n, f_e(gas) deduced is not unique, and the decision of which set is to be used is based on plausibility or convenience. From the dE/dx evidence considered above, it is plausible that f_n should be in the range $f_n = 0.8 \pm 0.2$ and that f_e(gas) should be on the order of f_e(gas) ~ 0.5. Given the mean lifetime τ and the measured DSAM factor F for the ^{26}Al decay in a particular stopping gas, one finds the f_e(gas) necessary to reproduce that lifetime for each of the three values $f_n = 0.6$, 0.8, and 1.0. The best value of f_e(gas) for each f_n is that which reproduces $\tau = 1.82$ ns using the best value of the measured DSAM factor F, while the error limits for f_e(gas) are obtained from those values of f_e(gas) necessary to reproduce $\tau = 1.82$ ns when F is assigned its error-limit values. This procedure is followed for the stopping gases Xe, Ar, and He. Since most of the experimental details for the DSAM measurement of the ^{26}Al decay were outlined in Section 4 of this chapter, only the particulars for each stopping gas will be mentioned.

b. Xenon

The experimental arrangement used in the determination of the stopping parameters for ^{26}Al in Xe has already been presented in Section 4. The beam intensity was maintained at 100 ± 5 nA for all

runs. An example of the spectra obtained with the 6-cm^3 Ge(Li) detector is shown in Fig. 16. In this figure, the 418-keV γ-ray line from ^{26}Al recoils at 0° in vacuum exhibits a smaller shoulder on the low-energy side of the peak. This shoulder arises from the 9.5% of the nuclei that strike the end of the gas cell before decaying, and was subtracted before calculation of the centroid of the fully-Doppler-shifted line. The density of Xe at 1 atm pressure and 23°C is taken as 5.42×10^{-3} g/cm^3.

The observed DSAM factor F for the Xe pressure of 0.52 atm was $F = 0.41 \pm 0.03$. From this F value and the mean initial recoil velocity (taken as the average of the observed and calculated velocities), one obtains $f_e(Z_1, \bar{v}/v_o) = 0.68$ (see Table I). An example of the determination of f_e(gas) for $f_n = 0.8$ from the measured F value is given in Figure 21. The stopping parameters f_e(gas) deduced from the present measurements for each f_n are summarized in Table IV.

2. Argon

The stopping parameters f_n, f_e(gas) were determined for argon principally as a consistency check, since the electronic stopping cross section measurements of Ormrod (1968) indicate that the S_e for heavy ions with $Z_1 \leq 10$ in argon is on the average about 50% of that predicted by LS theory, implying that f_e(gas) should be about 0.5. The experiment was performed in a similar fashion to that described in Section 4 of this chapter except that Ar was used as the stopping gas. The beam intensity was maintained at 105 ± 5 nA for all runs.

The density of Ar at 1 atm pressure and 23° C is taken to be 1.64×10^{-3} g/cm^3. The spectra obtained in the 6-cm^3 Ge(Li) detector were similar to those obtained using Xe as the stopping gas, and will not be repeated. The observed full Doppler shift for recoils into vacuum, corrected for the finite solid angle subtended by the detector, was 2.96 ± 0.10 keV, leading to an observed mean recoil velocity of $\beta(0) = (7.09 \pm 0.25) \times 10^{-3}$, in reasonable agreement with the kinematically calculated value. The initial recoil velocity assumed in the analysis is the average of the observed and calculated values.

The Doppler-shift-attenuation factor F was measured as the ^{26}Al recoils slowed and decayed in Ar gas at three pressures from 0.34 to 1.01 atm. The measured F values as well as the stopping parameters f_e(gas) deduced for each f_n are presented in Table V.

d. Helium

The stopping parameters for ^{26}Al in He were determined using a longer gas cell to avoid having a significant number of recoils strike the end wall of the cell before decaying. In addition, the 55-cm^3 Ge(Li) detector was employed instead of the 6-cm^3 detector. A new target of natural NaBr with thickness 32 ± 3 μg/cm^2 was evaporated onto the downbeam side of a 5.7 mg/cm^2 Pt foil and exposed to a beam of 6.10-MeV ^{4}He particles as in the case of the Xe and Ar measurements. The beam current was maintained at 100 ± 10 nA for all runs. Taking into account the various energy losses mentioned

previously, the kinematically calculated mean initial recoil velocity was $\beta(0) = (7.50 \pm 0.10) \times 10^{-3}$. The observed full Doppler shift for recoil into vacuum, corrected by 3% for the finite solid angle subtended by the detector, was 2.55 ± 0.10 keV, leading to an observed velocity of $\beta(0) = (6.11 \pm 0.21) \times 10^{-3}$, in unexplained disagreement with the calculated value. The observed velocity was used in the analysis of the DSAM data. The density of He at 1 atm pressure and 23° C is taken as 1.65×10^{-4} g/cm^3.

An example of the spectra obtained with the 55-cm^3 Ge(Li) detector is shown in Figure 22. The energy of the γ ray from the decay of the 418-keV level was determined from Ge(Li) detector spectra taken at 90° relative to the beam direction in conjunction with the well known energies of the γ rays from ^{7}Be and ^{203}Hg sources placed near the target. The γ ray energy is determined to be

$$E_\gamma = 417.3 \pm 0.2 \text{ keV}.$$

The DSAM factor F was measured as the ^{26}Al recoils slowed and decayed in He gas at pressures of 3.7 and 5.4 atm. The measured F values as well as the stopping parameters f_e(gas) deduced for each f_n are presented in Table VI.

V. MEASUREMENTS TO CHECK THE DSAM TECHNIQUE

1. Introduction

In order to check the reliability of the gas-stopper version of the DSA method as described in Chapters III and IV, lifetime measurements have been performed for nuclear levels whose mean-lives have been determined with other techniques. The lifetimes of the 3^- level of ^{16}O at 6131 keV and of the $7/2^-$ level of ^{37}Ar at 1611 keV have been measured in the present work. In addition, the meanlife of the 5^- level of ^{38}Ar at 4585 keV has been determined by Lindskog, Gordon and Kavanagh (1972) using the "plunger" technique and using the DSAM with Xe gas as the stopping medium in conjunction with the analysis described in Chapter IV.

2. The Lifetime of the 6131-keV Level of ^{16}O

a. Introduction

The 6131-keV level of ^{16}O has a spin and parity known to be 3^- from previous work (Ajzenberg-Selove 1971), and decays to the 0^+ ground state via the emission of pure E3 γ radiation. The relevant portion of the level diagram for ^{16}O is illustrated in Figure 23. Devons et al. (1955) placed an upper limit of $\tau(6131) \leq 10$ ps on this lifetime by using a mechanical-recoil technique, and placed a lower limit $\tau(6131) \geq 5$ ps using the DSAM with solid stopping media. Kohler and Hilton (1958) measured the lifetime to be $\tau(6131) = 12 \pm 6$ ps by applying a mechanical-recoil method similar to that of Devons et al. (1955). Alexander and Allen (1965) made use of the Doppler-

shift recoil-distance, or "plunger," technique along with a beam of ^{19}F particles and the then newly developed Ge(Li) detectors to obtain the value $\tau(6131) = 25 \pm 2$ ps. Nickles (1969) has also employed the "plunger" technique and found $\tau(6131) = 21 ^{+1}_{-7}$ ps. This lifetime has been measured in the present work by using the DSAM with Xe gas as the stopping medium, and employs the assumptions of Chapter IV in the analysis of the experimental result.

b. Experimental Procedure

The 6131-keV level of ^{16}O was populated by using the $^{13}C(^4He,n)^{16}O$ reaction. A target of ^{13}C was produced by admitting $^{13}C_2H_2$ gas, enriched to 63.8% in ^{13}C, into the gas cell shown in Figure 9 and bombarding it with a beam of 8-MeV ^4He particles. The C_2H_2 gas pressure was 0.05 atm and the gas-retaining foil was 5.1-mg/cm^2 Havar (stainless steel). The C_2H_2 was "cracked" by the beam onto the down-beam side of the Havar target foil and onto the Ta beam stop; the beam stop was subsequently removed and replaced with a clean piece of Ta. The target was then bombarded with a beam of 7.92-MeV ^4He particles. Not including the energy loss of the recoils in the carbon target layer, the kinematically calculated mean initial recoil velocity was $\beta(0) = (1.35 \pm 0.02) \times 10^{-2}$. However, because of the manner in which the target was produced, the carbon thickness was unknown and hence the recoil velocity could not be corrected for the energy lost in this layer. For this reason, the observed mean initial recoil velocity, determined from the full Doppler shift for recoils into vacuum, was used in the

analysis of the data. The 6131-keV γ rays from the decay of this level were observed in a 40-cm^3 Ge(Li) detector placed at 0° and 90° from the beam direction both in vacuum and as the ^{16}O recoils slowed in Xe gas at a pressure of 21.1 atm. The beam current was maintained at 100 ± 5 nA for the Doppler-shift runs with Xe in the cell. The pulse-analysis system was similar to that described in Chapter III except that digital stabilization was not employed. This was due to the unavailability of a radioactive source with a γ ray of sufficiently high energy. The photopeak, single-escape and double-escape lines from the 6131-keV γ ray were used in the derivation of the DSAM factor F for this decay. An example of the spectra obtained in the 40-cm^3 Ge(Li) detector is shown in Figure 24. The FWHM energy resolution for non-Doppler-broadened 6-MeV γ rays was 11 keV. This was determined during the target production run from an observation at 0° of the γ rays from reactions on ^{13}C deposited on the beam stop; these ^{16}O nuclei stopped in the Ta backing before decaying, and thus produced γ rays with no Doppler broadening. The energy calibration of the pulse-analysis system was provided internally by the 511-keV separation between the observed photopeak, single-escape and double-escape lines. The observed full Doppler shift for recoils into vacuum, corrected by 1% for the solid angle subtended by the Ge(Li) detector, was 74.0 ± 0.4 keV, leading to an observed mean initial recoil velocity of $\beta(0) = (1.21 \pm 0.01) \times 10^{-2}$.

c. Results

At a Xe pressure of 21.1 atm, the average measured DSAM factor F from the photopeak, single-escape, and double-escape lines was F = 0.59 ± 0.02. From this F value and the observed initial recoil velocity above, one obtains the parameter $f_e(Z_1, \bar{v}/v_o) = 1.15$ (see Table I). This measured F value has been analyzed using the three sets of stopping parameters derived for Xe as listed in Table IV. The lifetime results from this analysis are presented in Table VII and an example of the analysis is illustrated in Figure 25. The uncertainty in the lifetime quoted in Table VII for each f_n is the rms sum of two contributions: (1) the uncertainty in the lifetime due to the uncertainty in the measured F, computed using the best value of f_e(gas) and (ii) the uncertainty in the lifetime due to the uncertainty in f_e(gas), computed using the best value of the measured F. This method of calculating the uncertainty in the derived lifetime is employed in all subsequent meanlife determinations.

The lifetime of the 6131-keV level of ^{16}O obtained from the present measurements is

$$\tau(6131) = 29 \pm 5 \text{ ps} .$$

This is the weighted average of the three results of Table VII; the uncertainty has not been reduced since these are not independent determinations. This result is in reasonable agreement with the value $\tau(6131) = 24 \pm 2$ ps quoted in the recent compilation by Ajzenberg-Selove (1971).

While in this case there appears to be a trend toward shorter lifetimes as f_n decreases, nevertheless, the lifetimes derived from the three sets of stopping parameters agree within the experimental errors. Moreover, it appears that the lifetime derived with $f_n = 0.8$ and $f_e(gas) = 0.50 \pm 0.15$ represents a reasonable average to all three results. Therefore, the DSAM lifetime measurements using Xe gas to be presented in Chapter VI will be analyzed using the above pair of stopping parameters.

3. The Lifetime of the 1611-keV Level of ^{37}Ar

a. Introduction

The 1611-keV level of ^{37}Ar has a spin and parity known to be $7/2^-$ from previous measurements (Endt and Van der Leun 1967), and decays to the $3/2^+$ ground state via the emission of mixed M2-E3 radiation. The relevant portion of the level diagram for this nucleus is shown in Figure 26. Goosman and Kavanagh (1967) used the Doppler-shift recoil-distance technique to measure the lifetime of this level, with the result $\tau(1611) = 7.4 \pm 1.0$ ns. Ragan et al. (1971) employed the same method and obtained the value $\tau(1611) = 6.02 \pm 0.29$ ns, while Randolph et al. (1971) applied an electronic-timing technique to obtain $\tau(1611) = 6.49 \pm 0.29$ ns. This lifetime has been remeasured in the present work using the DSAM with Xe gas as the stopping medium. The analysis of the experimental data leading to the lifetime is carried out in the manner described in Chapter IV.

b. Experimental Procedure

The 1611-keV level of ^{37}Ar was populated using the ^{34}S(^{4}He,n)^{37}Ar reaction. The target was a thin (40 ± 15 µg/cm^2) layer of CdS, enriched to 85% in ^{34}S and evaporated onto the down-beam side of a 5.7 mg/cm^2 platinum gas-retaining foil. The foil was epoxied over a 4.0-mm-diameter hole in a stainless-steel foil holder and placed in position in the apparatus shown in Figure 9. However, the gas-cell length was increased to 2.7 cm to decrease the number of recoils which survived the flight undecayed before striking the end of the gas cell. The target was bombarded with a beam of 9.40-MeV ^{4}He particles. Including the energy loss of the recoils in a half-thickness of the target layer, the kinematically calculated mean recoil velocity immediately following the target layer was $\beta(0) = (7.0 \pm 0.1) \times 10^{-3}$. Further experimental details for this calculated velocity may be found in Table VIII. However, since this reaction took place relatively far above threshold, it is possible that anisotropy in the outgoing neutron center-of-mass angular distribution could significantly alter the recoil velocity from that calculated above.

The 1611-keV γ rays were observed with the 55-cm^3 Ge(Li) detector placed at 0° and 90° from the beam direction both in vacuum and as the ^{37}Ar recoils slowed in Xe gas at a pressure of 0.108 atm. The beam current was maintained at 100 ± 5 nA during the Xe gas runs. Digital stabilization of the pulse-analysis system (see Figure 11) was accomplished using the 1333-keV γ rays from a ^{60}Co source as the reference line for gain stabilization and using

pulses from a stable electronic pulser placed in a low channel of the 1024-channel pulse-height analyzer as the reference line for zero-level stabilization. An example of the spectra obtained with the 55-cm^3 Ge(Li) detector is shown in Figure 27. The FWHM energy resolution for 1333-keV γ rays was 4.5 keV. The observed full Doppler shift for recoils into vacuum, corrected by 2.4% for the solid angle subtended by the detector, was 10.00 ± 0.15 keV, leading to an observed mean initial recoil velocity of $\beta(0) = (6.2 \pm 0.1) \times 10^{-3}$. This measured velocity was used in the analysis of the DSAM results in view of the uncertainty in the kinematically calculated value as previously mentioned.

Since the lifetime of this level is about 6.5 ns and the velocity is 1.86 mm/ns, the distance travelled in vacuum during one mean-life is about 1.2 cm. Since this distance is not negligible in comparison with the distance from the target to the detector (7.4 cm), the detection efficiency varies for γ rays emitted from nuclei decaying at various positions along the flight path. In order to be able to take into account this effect, the detector photopeak efficiency was measured as a function of distance from the Ge(Li) detector for the 1333-keV and 1836-keV γ rays from ^{60}Co and ^{88}Y sources, respectively. At the detector-to-target distance used in the DSAM experiment (7.4 cm), the photopeak efficiency for 1611-keV γ rays varied by 23% per cm. This variation was included in the centroid-shift calculations.

c. Results

At a Xe pressure of 0.108 atm, the measured DSAM factor F was F = 0.30 ± 0.02. From this F value and the observed initial recoil velocity above, one obtains the parameter $f_e(Z_1, \overline{v}/v_o) = 1.34$ (see Table I). This measured F value has been analyzed using the three sets of stopping parameters derived for Xe as listed in Table IV. The lifetime results from this analysis are presented in Table VIII and an example of the analysis is illustrated in Figure 28. The analysis takes into account the varying detector efficiency with distance as mentioned above.

The lifetime of the 1611-keV level of ^{37}Ar obtained from the present measurements is

$$\tau(1611) = 8.2 \pm 1.3 \text{ ns} .$$

This is the weighted average of the three results of Table VIII; the uncertainty has not been reduced since these are not independent determinations. This result is in slight disagreement with those obtained with other methods as mentioned above.

The lifetimes for this level derived in the present measurements from the three sets of stopping parameters agree within the experimental uncertainties. Moreover, it appears that the lifetime obtained with $f_n = 0.8$ and $f_e(\text{gas}) = 0.50 \pm 0.15$ represents a reasonable average to all three results. This is consistent with the conclusion of the previous section, and hence the DSAM lifetime measurements using Xe gas to be presented in Chapter VI will be analyzed using the above pair of stopping parameters.

4. The Lifetime of the 4585-keV Level of ^{38}Ar

The 4585-keV level of ^{38}Ar has a spin and parity known to be 5⁻ from previous measurements (Endt and Van der Leun 1967). This level decays through a 90% branch to the 4480-keV level and through a 10% branch to the 3810-keV level. The lifetime of the 4585-keV level has been measured by Lindskog, Gordon and Kavanagh (1972) by applying the Doppler-shift recoil-distance technique and by the Doppler-shift-attenuation method using Xe gas as the stopping medium. The "plunger" measurement yielded a lifetime $\tau(4585) = 226 \pm 21$ ps. The DSAM measurement, using the stopping parameters $f_n = 0.8$, $f_e(gas) = 0.51 \pm 0.14$ and $f_e(Z_1, \bar{v}/v_o) = 1.35$, yielded the value $\tau(4585) = 234 \pm 40$ ps, in good agreement with the plunger result. This lifetime has also been measured by Ball et al. (1972), who obtained $\tau = 196 \pm 10$ ps, by Engelbertink et al. (1970), who obtained $\tau = 181 \pm 13$ ps, and by Kern and Bond (1972), who obtained $\tau = 172 \pm 8$ ps. These authors all used the Doppler-shift recoil-distance method. A more recent value, $\tau = 214 \pm 15$ ps, is in better agreement with the present work (J. C. Merdinger, 1972, private communication). The weighted average of all five recoil-distance measurements is $\tau(4585) = 188 \pm 6$ ps. The agreement of the gas-DSAM measurement and the "plunger" measurements provides support for the method of analysis and the derived stopping parameters f_n, f_e adopted for the present work.

VI. LIFETIMES OF NUCLEAR LEVELS BY THE DOPPLER-SHIFT-ATTENUATION METHOD

1. The Lifetime of the 709-keV Level of ^{30}P

a. Introduction

The odd Z-odd N self-conjugate nucleus ^{30}P has been the subject of a number of experimental and theoretical investigations since 1967. The sparse experimental information available at that time is summarized by Endt and Van der Leun (1967) and is illustrated in part in Figure 29. While the spins and parities of a number of levels, including the ground state and the first five excited states, were known, virtually no information was available for electromagnetic transition rates between levels. In fact, only the lifetime of the 0^+ first-excited state at 678 keV had been measured, and only a lower limit of $\tau \geq 3.0$ ps (Kennedy et al. 1967) had been placed on the lifetime of the 1^+ second-excited state at 709 keV. Since then, a great deal of experimental work has been performed to measure spins, parities, lifetimes, branching ratios and multipole mixing ratios for transitions between levels in ^{30}P up to about 5 MeV excitation. Extensive references to this work may be found in the papers by Sharpey-Schafer et al. (1971) and by Bini et al. (1971). In addition, several theoretical investigations of the structure of ^{30}P have been made; a discussion of these calculations will be deferred until the present experimental measurements have been discussed.

When this work was begun, only the lower limit of $\tau(709) \geq 3.0$ ps (Kennedy et al. 1967) had been established for the decay of the 709-keV level of ^{30}P. After the present work was completed, two other measurements became available. Pixley and Poletti (1969) obtained the value $\tau(709) = 22 \pm 5$ ps using the ^{27}Al(^{4}He,n)^{30}P reaction and the DSA method employing carbon dioxide gas at a pressure of 5.0 atm as the stopping medium, while Haas et al. (1970) found $\tau(709) = 55 \pm 7$ ps using the same reaction and the recoil-distance technique. The present measurement was performed using the DSA method with Xe gas as the absorber.

b. Experimental Procedure

The 1^+ level of ^{30}P at 709 keV was populated using the ^{27}Al(^{4}He,n)^{30}P reaction. The target was a thin (36.5 ± 3.0 $\mu g/cm^2$) layer of natural Al, evaporated onto the downbeam side of a 7.2 mg/cm^2 platinum gas-retaining foil. This foil was epoxied over a 1.3-mm-diameter hole in a Zr foil holder and placed in position in the apparatus shown in Figure 9. The target was bombarded with a beam of 6.50-MeV ^{4}He particles. Including the energy loss of the recoils in a half-thickness of the target layer, the kinematically calculated recoil velocity immediately following the target layer was $\beta(0) = (6.39 \pm 0.13) \times 10^{-3}$. Further experimental details for this calculated velocity may be found in Table IX.

The 709-keV γ rays from the decay of the 709-keV level to the ground state were observed in a 55-cm^3 Ge(Li) detector placed at 0° and 90° from the beam direction both in vacuum and as the ^{30}P

recoils slowed in Xe gas at pressures ranging from 3.4 to 9.9 atm. The detector was placed 4 cm from the target. Digital stabilization of the pulse-analysis system (see Figure 11) was accomplished using the 662-keV γ rays from a ^{137}Cs source as the reference line for gain stabilization and using pulses from a stable electronic pulser placed in a low channel of the 400-channel pulse-height analyzer as the reference line for zero-level stabilization. In addition, the 478-keV γ-ray line from a ^{7}Be source placed near the target and the 511-keV line from electron-positron annihilation at the target were used to check the stability of the pulse-analysis system. The FWHM energy resolution for 662-keV γ rays was 3.1 keV. The observed full Doppler shift for recoils into vacuum, corrected by 5% for the solid angle subtended by the detector and by 4% for the differential absorption of the 709-keV γ rays by the Zr foil holder, leads to an observed mean initial recoil velocity of $\beta(0) = (6.0 \pm 0.3) \times 10^{-3}$. The average of the observed and calculated velocities $\beta(0) = (6.2 \pm 0.2) \times 10^{-3}$ was used in the analysis of the DSAM data. An example of the spectra obtained in the 55-cm^3 Ge(Li) detector is illustrated in Figure 30.

c. Results and Discussion

The observed DSAM factors F as a function of the Xe stopping gas pressure are given in Table IX. These F values and the observed mean initial recoil velocity lead to the values of $f_e(Z_1, \overline{v}/v_0)$ quoted in Table IX (see Table I). These F values have

been analyzed using the procedure presented in Chapter IV and incorporating the representative stopping parameters derived experimentally for heavy ions in Xe; namely, $f_n = 0.8$ and $f_e(gas) = 0.50 \pm 0.15$. In Chapter V, it was seen that the lifetimes obtained with $f_n = 0.8$ are also reasonably representative of the lifetimes found with $f_n = 0.6$ and $f_n = 1.0$. The results of the analysis are presented in Table IX, and an example of the analysis is shown in Figure 31. Including a 12% uncertainty in the rate of energy loss assumed in the analysis, the lifetime of the 709-keV level of ^{30}P derived from the present measurements is

$$\tau(709) = 43 \pm 6 \text{ ps}.$$

This is in agreement with the result of Haas et al. (1970), who obtained the value $\tau(709) = 55 \pm 7$ ps, but is in disagreement with the result of Pixley and Poletti (1969), who obtained the value $\tau(709) = 22 \pm 5$ ps.

Several authors have investigated the decay properties of the 709-keV level, which decays (Endt and Van der Leun 1967) to the ground state via the emission of mixed M1/E2 γ radiation. The results of lifetime and mixing-ratio measurements for this decay are summarized in Table X, along with the electromagnetic transition strengths in Weisskopf units (W.u.) calculated from these quantities. The definitions for the Weisskopf units have been taken from Skorka, Hertel and Retz-Schmidt (1966). In this table, the adopted value for the lifetime of the 709-keV level is taken as the weighted average of the present work and that of Haas et al. (1970); the result of Pixley and Poletti (1969) is neglected pending its publication in final form.

The multipole mixing ratio for this decay is taken as the weighted average of the works of Vermette et al. (1968) and of Harris et al. (1969), whose work with superior instrumentation supersedes their earlier result (Harris and Hyder 1966). For self-conjugate nuclei with $A = 20 - 40$, the average $M1$, $\Delta T = 0$ transition strength is hindered by a factor of about 20 compared with the average $M1$, $\Delta T = 1$ strength (Skorka et al. 1966). The smaller and larger values of $E2/M1$ mixing ratio lead to hindrances for this $M1$, $\Delta T = 0$ transition of about 110 and 2300, respectively, compared with the average $\Delta T = 1$ transition; hence, the smaller value for this mixing ratio is the more probable.

Theoretical investigations of the structure of ^{30}P have been carried out using several different nuclear models. Glaudemans, Wiechers and Brussaard (1964a, 1964b) used the shell model to obtain positive-parity energy-level spectra for s - d shell nuclei in the range ^{29}Si-^{40}Ca. They assumed an inert ^{28}Si core and considered two-particle interactions between the A-28 nucleons placed in the $2s_{1/2}$ and $1d_{3/2}$ shells. They obtained the parameters of the interaction matrix elements from a fit to the energies of 50 known nuclear levels, and then predicted the spins, energies and configurations of 400 nuclear levels for nuclei in the range mentioned above. In this model, ^{30}P is described as an inert ^{28}Si core with the odd neutron and odd proton placed in the $2s_{1/2}$-$1d_{3/2}$ shells. Wiechers and Brussaard (1965) used the shell-model wave functions of Glaudemans et al. (1964a, 1964b) to predict the M1 transition strength for the

709-keV to ground-state transition in ^{30}P, using both single-particle and effective g factors. The theoretical predictions of this model are given in Table X; it is seen that even incorporating effective g factors, the theoretical prediction exceeds the experimentally observed M1 transition strength by a factor of 8.

Subsequent to the early shell-model calculations of Glaudemans et al. (1964a, 1964b), a comprehensive and continuing investigation into the shell-model description of s-d shell nuclei has been undertaken by several authors. These studies have made use of several different effective Hamiltonians and have included more complete sets of basis states, up to and including the full space ($1d_{5/2}$, $2s_{1/2}$, $1d_{3/2}$) of s-d shell model wave functions. These investigations include the work of Glaudemans and collaborators (1967, 1969, 1971), Dieperink and collaborators (1968, 1969a, 1969b), and Wildenthal and collaborators (1968a, 1968b, 1970, 1971a, 1971b). Wildenthal, McGrory, Halbert and Graber (1971b) have used the shell model to describe positive-parity levels in s-d shell nuclei by choosing a model space such that all $2s_{1/2}$ and $1d_{3/2}$ states and up to two holes in the $1d_{5/2}$ shell have been taken into account; the modified-surface-delta interaction (MSDI) was used as the effective two-body interaction. (The modified-surface-delta interaction and the surface-delta interaction (SDI) have been discussed by Glaudemans et al. (1967); these authors also give references to earlier work related to the SDI.) The four parameters of the MSDI and the three single-particle energies were fitted to 66 known levels of nuclei with A = 30 - 34, and then spins, energies, configurations, static nuclear moments

and M1 and E2 transition strengths for positive-parity levels of nuclei with A = 30 - 35 were predicted. The M1 strengths were calculated with free-nucleon g factors, while the E2 strengths were calculated with effective charges for neutrons and protons. In addition, a second effective Hamiltonian was investigated in which the two-body matrix elements which did not involve the $d_{5/2}$ orbit were treated as independent free parameters in a least-squares search to fit the above experimental level energies. This procedure was labeled the free-parameter surface delta interaction (FPSDI), and the various observables mentioned above were calculated with this model, again with free nucleon g factors and effective charges. The M1 and E2 transition strengths for the decay of the 709-keV level of ^{30}P predicted using these two approaches are given in Table X, and are in fair agreement with the experimentally measured strengths. However, the predictions of this model are in relatively poor agreement with transition strengths for other levels in ^{30}P, particularly the E2 transitions from the 3^+ states. For these levels, the disagreement is a factor of 10 or more. These authors suggest that these discrepancies may be due to the assumption of a truncated $1d_{5/2}$ configuration space.

Glaudemans, Endt and Dieperink (1971) used the shell-model wave functions derived by Wildenthal, McGrory, Halbert and Graber (1971b) for the modified-surface-delta interaction as mentioned above, and performed an independent calculation of electromagnetic rates and multipole moments for positive-parity levels in A = 30 - 34 nuclei. Transition strengths were calculated for three cases.

First the M1 and E2 transition strengths were calculated using bare-nucleon g factors and charges. Then the M1 and E2 strengths were calculated using effective g factors and charges obtained from a least-squares fit to experimentally observed magnetic dipole transition strengths and moments and electric quadrupole transition strengths and moments. Finally, the M1 transition strengths were calculated using a set of effective single-particle M1 matrix elements obtained from a least-squares fit to the experimentally measured M1 strengths and moments mentioned above. The results of these calculations for the decay of the 709-keV level of ^{30}P are given in Table X, and also are in agreement with the experimentally measured rates. As mentioned above, the most marked disagreements for transition strengths for other ^{30}P levels involve the E2 transitions.

Wasielewski and Malik (1971) applied the unified model with Coriolis coupling to the doubly-odd nuclei ^{22}Na, ^{26}Al and ^{30}P. They assumed that the odd neutron and odd proton are placed in Nilsson orbitals generated by an axially symmetric deformed rotating core. They employed a Hamiltonian composed of the collective rotational energy, including the Coriolis terms, the single-particle Nilsson energies, and a residual interaction between the last odd neutron and proton. Using this model, they calculated the M1 and E2 transition strengths, as well as energy-level spectra and wavefunctions, for these nuclei. The results of their calculations for the decay of the 709-keV level of ^{30}P are shown in Table X, and are in only fair agreement with the experimentally observed transition strengths. While the calculated M1 strengths for other levels are in general agreement with

experiment, the E2 strengths generally disagree by a factor of 10 or more.

Several other authors have made theoretical investigations of the structure of ^{30}P but have not made predictions of electromagnetic transition strengths. Ascuitto, Bell and Davidson (1968) considered a model for odd-odd nuclei in which the odd neutron and odd proton are coupled to a symmetric rotating core, assumed to be inert to vibration. Using this model, they calculated energy-level spectra and static magnetic dipole and electric quadrupole moments. Bouten, Elliott and Pullen (1967) performed an intermediate-coupling shell-model calculation to obtain energy-level spectra for nuclei in the mass region A = 18 - 38. Picard and De Pinho (1966) used a rotational Nilsson model to calculate energy-level spectra for ^{30}P, but could obtain a satisfactory prediction of level energies for only the first two excited states.

2. The Lifetime of the 3163-keV Level of ^{35}Cl

a. Introduction

The nucleus ^{35}Cl has been the subject of extensive recent experimental and theoretical investigations. The experimental information available in 1967 is summarized by Endt and Van der Leun (1967) and is illustrated in part in Figure 32. In addition to the spins, parities and branching ratios for γ-ray transitions indicated in this figure, lifetimes had been measured for only the 1220-, 1763- and 3163-keV excited states, and the multipole mixing ratios had been measured for only the ground-state transitions from the 1763- and

3163-keV levels. Since 1967, numerous experimental measurements of spins, parities, lifetimes, branching ratios and mixing ratios have been performed for levels in ^{35}Cl up to about 6-MeV excitation. Extensive references to these studies may be found in the papers by Prosser and Harris (1971) and by Wiesehahn (1971a, 1971b). In addition to these experimental studies, several theoretical investigations have been made. These will be discussed after the presentation of the results of this work.

The lifetime of the $7/2^-$ level of ^{35}Cl at 3163 keV was first measured by Azuma, Anyas-Weiss and Charlesworth (1968), who employed the ^{34}S$(p, \gamma\gamma)^{35}$Cl reaction and the delayed-coincidence technique to obtain the value $\tau(3163) = 140 \pm 40$ ps; a preliminary value for their measurement was quoted in an earlier publication by Azuma, Oleksiuk, Prentice and Taras (1966). However, Ingebretsen, Alexander, Häusser and Pelte (1969) performed a recoil-distance measurement incorporating the ^{32}S$(^4$He$,p)^{35}$Cl reaction to obtain the result $\tau(3163) = 60 \pm 7$ ps.

In an attempt to resolve this discrepancy, the lifetime of the 3163-keV level of ^{35}Cl has been measured in the present work, employing the Doppler-shift-attenuation method with Xe gas as the stopping medium. After the completion of this work, another measurement of this meanlife became available. Barton, Wadden, Carter and Pai (1971) reported the value $\tau(3163) = 37 \pm 4$ ps obtained from an experiment employing the ^{34}S$(p, \gamma\gamma)^{35}$Cl reaction and the delayed-coincidence technique.

b. <u>Experimental Procedure</u>

The $7/2^-$ level of ^{35}Cl at 3163 keV was populated using the ^{32}S$(^4$He,p$)^{35}$Cl reaction. The target was a thin $(85 \pm 7 \; \mu g/cm^2)$ layer of natural CdS, evaporated onto the downbeam side of a 5.7 mg/cm^2 platinum gas-retaining foil. This foil was epoxied over a 1.3-mm-diameter hole in a Zr foil holder and placed in position in the apparatus shown in Figure 9. The target was bombarded with a beam of 9.34-MeV ^{4}He particles. Including the energy loss of the recoils in a half-thickness of the target layer, the kinematically calculated recoil velocity immediately following the target layer was $\beta(0) = (7.22 \pm 0.06) \times 10^{-3}$. Further experimental details for this calculated velocity may be found in Table XI. However, since this reaction took place relatively far above threshold, it is possible that anisotropy in the outgoing proton angular distribution could significantly alter the mean recoil velocity from that calculated above.

The 3163-keV γ rays from the decay of the 3163-keV level to the ground state were observed in a 55-cm^3 Ge(Li) detector at 0° and 90° from the beam direction both in vacuum and as the ^{35}Cl recoils slowed in Xe gas at pressures of 5.4 and 8.2 atm. The 518-keV γ rays from the decay to the 2645-keV level were not utilized in this measurement due to interference from 511-keV annihilation radiation. The detector was placed 6 cm from the target. The beam current was maintained at 105 ± 5 nA for all the runs. Digital stabilization of the pulse-analysis system (see Figure 11) was accomplished using the 2754-keV γ rays from a ^{24}Na source as the

reference line for gain stabilization and using pulses from a precision stable electronic pulser placed in a low channel of the Nuclear Data 1024-channel pulse-height analyzer as the reference line for zero-level stabilization. In addition, the 1369-keV, 898-keV and 1836-keV γ-ray lines from ^{24}Na and ^{88}Y sources placed near the target were introduced into the spectrum to check on the stability of the pulse-analysis system. The FWHM energy resolution for 2754-keV γ rays was 6.7 keV. The observed full Doppler shift from recoils into vacuum for the 3163-keV, corrected by 3.0% for the solid angle subtended by the Ge(Li) detector, was 20.6 ± 0.3 keV, leading to an observed mean initial recoil velocity of $\beta(0) = (6.5 \pm 0.1) \times 10^{-3}$. This measured velocity was used in the analysis of the DSAM results in view of the uncertainty in the kinematically calculated velocity previously mentioned. An example of the spectra obtained in the 55-cm^3 Ge(Li) detector is illustrated in Figure 33.

c. Results and Discussion

The observed DSAM factors F for the two values of Xe stopping-gas pressure are given in Table XI. From these F values and the measured mean initial velocity, one obtains $f_e(Z_1, \overline{v}/v_o) = 1.24$ (see Table I). These two F values have been analyzed using the procedure presented in Chapter IV and incorporating the stopping parameters derived experimentally for heavy ions in Xe, namely, $f_n = 0.8$ and $f_e(gas) = 0.50 \pm 0.15$. In Chapter V, it was seen that the lifetimes obtained with $f_n = 0.8$ are also reasonably representative

of the lifetimes found with $f_n = 0.6$ and $f_n = 1.0$. The results of
the analysis are presented in Table XI, and an example of the analysis
is illustrated in Figure 34. Including a 12% uncertainty in the rate
of energy loss assumed in the analysis, the lifetime of the 3163-keV
level of ^{35}Cl derived from the present measurements is

$$\tau(3163) = 55 \pm 8 \text{ ps.}$$

This is in excellent agreement with the result of Ingebretsen et al.
(1969), who obtained the value $\tau(3163) = 60 \pm 7$ ps, but is in disagree-
ment with the results of Azuma et al. (1968) and of Barton et al.
(1971), who obtained $\tau(3163) = 140 \pm 40$ ps and $\tau(3163) = 37 \pm 4$ ps,
respectively, using the delayed-coincidence technique.

Several authors have investigated the decay properties of the
3163-keV level. The branching ratios for the decay of this level are
now well determined, while only the multipole mixing ratios for the
transitions to the ground state and to the 1763-keV level have been
measured. These properties are summarized in Table XII; they
were not determined in the present work. The adopted value for the
lifetime of this level in the table is taken as the weighted average of
the present work and that of Ingebretsen et al. (1969); the two results
obtained with the delayed-coincidence technique are excluded from
this average, as this lifetime is near the limit of applicability of
that method.

Using the adopted experimental decay properties from
Table XII, the transition strengths in Weisskopf units (Skorka et al.
1966) for the decay of the 3163-keV level of ^{35}Cl are given in

Table XIII. The mixed M2/E3 decay to the ground state has an M2 component with a strength of $|M(M2)|^2 = 0.20 \pm 0.02$ W.u. and an E3 component with a strength of $|M(E3)|^2 = 2.9 \pm 0.4$ W.u. These are in the range commonly found (Skorka et al. 1966) for similar transitions in the s-d shell. On the other hand, the mixed M2/E1 transition to the 1763-keV $5/2^+$ level has an E1 component inhibited by the remarkably large factor of 10^8 compared with the single-particle estimate, and is inhibited by a factor of 10^5 compared with similar E1 transitions in the s-d shell.

The structure of ^{35}Cl has been discussed in the light of several theoretical frameworks. However, most of these calculations have been concerned with positive-parity levels in this nucleus. Erné (1966) used the shell model to investigate negative-parity levels of nuclei in the range ^{33}S - ^{41}Ca by assuming an inert ^{32}S core with a residual two-particle interaction for the outer nucleons. Only one nucleon was considered to be in the $f_{7/2}$ shell, while the others were in the $d_{3/2}$ shell. The interaction matrix elements were determined from a fit to the energies of 50 known levels. The energy-level spectra obtained with this model are in reasonable agreement with experiment, but no transition strengths were predicted. Watson and Lee (1967) used a simplified shell model to explain $7/2^-$ and $3/2^-$ levels of s-d shell nuclei from ^{33}S to ^{41}Sc. They assumed a $J = 0$ core coupled to a single $1f_{7/2}$ or $2p_{3/2}$ nucleon, and adjusted parameters to obtain agreement with observed level energies. In this way, they describe the $7/2^-$ level of ^{35}Cl at 3163 keV as a pure $1f_{7/2}$ single-particle configuration. However, they did not calculate

transition strengths for its decay. Maripuu and Hokken (1970) performed shell-model calculations for negative-parity levels in A = 35, 37 and 39 nuclei by assuming an inert ^{32}S core with the residual interaction taking place within the $1d_{3/2}^n 1f_{7/2}$ and $1d_{3/2}^n 2p_{3/2}$ configurations (with n = 2, 4, or 6). The modified-surface-delta interaction was used as the effective two-body interaction, and the interaction parameters were determined from a fit to known level energies in A = 35, 37 and 39 nuclei. Within this framework, they calculated energy-level spectra and, using free-nucleon g factors and effective charges, they calculated M1 and E2 transition strengths for the decay levels in ^{35,37}Cl, ^{39}K and ^{39}Ar. The calculated level positions for ^{35}Cl are in good agreement with the experimental values. Unfortunately, they did not calculate transition strengths for the decay of the 3163-keV level. In their model, the dominant configuration for this level is $1d_{3/2}^2 1f_{7/2}$.

Harris and Perrizo (1970) and Prosser and Harris (1971) have calculated the lifetime of the 3163-keV level using the shell-model wave functions of Maripuu (1969) and Maripuu and Hokken (1970). Using free-nucleon g factors and effective charges, they obtain the value $\tau(3163) = 4$ ps. The use of pure $1d_{3/2}^2 1f_{7/2}$ configurations leads to the calculated lifetime $\tau(3163) = 8$ ps. In addition, they calculated the M2 transition strength for the ground-state transition of this level employing the two sets of wave functions; the results may be found in Table XIII. Apparently these shell-model configurations do not provide an adequate description of this level in ^{35}Cl. These authors then performed a shell-model calculation for

the $A = 35$ system using an inert ^{32}S core with two nucleons in the $1d_{3/2}$ shell and one nucleon in the $1f_{7/2}$ shell, and allowed re-coupling of the two $d_{3/2}$ nucleons. By making use of experimentally observed lifetimes, branching ratios and multipole mixing ratios, they derived, among other quantities, the wave function for the 3163-keV level. Employing this derived wave function, they calculated the M2 transition strength for the decay to the $5/2^+$ 1763-keV level, a transition not utilized in the derivation of the wave function. The result is included in Table XIII and is in excellent agreement with the observed value.

Wiesehahn (1971b) proposed a model for ^{35}Cl in which he considered a vibrating ^{34}S core coupled to the additional proton. In this model, he assumed that the proton is in the $1d_{3/2}$ shell and that the ^{34}S core is in the 2^+ vibrational first excited state. The interaction between nucleon and core splits the degeneracy to form the low-lying quadruplet of even-parity levels $1/2^+$, $3/2^+$, $5/2^+$, and $7/2^+$, whose center of gravity should nearly coincide with that of the first-excited state of ^{34}S. This is in agreement with the experimental results. Since the $7/2^-$ level at 3163-keV appears to be a fairly pure single-particle $f_{7/2}$ state, he asserts that one would expect transitions from this level to the members of the quartet to be weak. The great inhibitions of the E1 transitions from the $7/2^-$ level to the $5/2^+$ level at 1763 keV and to the $7/2^+$ level at 2645 keV support his assumptions.

Taras (1966) used the unified model to study positive- and negative-parity levels in ^{35}Cl. He describes the 3163-keV $7/2^-$ level as the result of the promotion of the single proton from the

Nilsson orbit 8 (the ^{35}Cl ground state) to the Nilsson orbit 10; the level at 3163-keV would then be the first member of the K = 7/2 band. He described the 3/2$^+$ ground state and the 5/2$^+$, 1763-keV state as the first and second members of the K = 3/2 band. On the basis of this model, the E1 transition from the 7/2$^-$ 3163-keV level to the 5/2$^+$ 1763-keV level is inhibited by a factor of 100 compared with the single-particle estimate, as it has one degree of K-forbidden-ness. However, this still does not explain the extremely large observed E1 inhibition.

The other theoretical investigations of ^{35}Cl have been con-cerned with the even-parity states. References to the studies may be found in the works of Wiesehahn (1971b) and of Wildenthal and collaborators (1970, 1971a, 1971b).

3. The Lifetime of the 2934-keV Level of ^{33}S

   a. Introduction

     The experimental information available in 1967 for the nucleus ^{33}S is summarized by Endt and Van der Leun (1967) and is illustrated in part in Figure 18. Most of this information was obtained from (d,p) and (n,γ) reactions on ^{32}S, and very little was known concerning the transition rates between levels, viz., only upper limits had been placed on six low-lying states. Following the advent of Ge(Li) detectors, much more information was reported regarding spins, parities and decay properties of this nucleus. Much of this work is cited in the references compiled in Table XIV.

The lifetime of the $7/2^-$ level of ^{33}S at 2934 keV was first measured by Brandolini and Signorini (1969), who employed the ^{30}Si$(^4$He,n$)^{33}$S reaction and the DSA technique with Kr gas as the stopping medium to obtain the value $\tau(2934) = 38 \pm 11$ ps. Kavanagh, Merdinger and Schulz (1970) used the same reaction and technique with Xe gas to obtain the value $\tau(2934) = 36 \pm 8$ ps. This meanlife was also measured in the present work by making use of the Xe-gas DSA method. Subsequently, the present author became aware of two other measurements. Ragan et al. (1970) obtained the value $\tau(2934) = 40.5 \pm 2.0$ ps while Brandolini et al. (1971) found $\tau(2934) = 44 \pm 4$ ps, both of whom used the above reaction and the recoil-distance method.

b. Experimental Procedure

The $7/2^-$ level of ^{33}S at 2934 keV was populated using the ^{30}Si$(^4$He,n$)^{33}$S reaction. The principal experimental details have been presented in Section 4 of Chapter IV. As noted therein, the observed mean initial recoil velocity as determined from the γ-ray full Doppler shift was $\beta(0) = (6.35 \pm 0.21) \times 10^{-3}$. The F value used in the determination of the lifetime for this level is the mean of the values found for beam currents of 100 and 130 nA: $F = 0.44 \pm 0.02$ at a Xe pressure of 13.6 atm. An example of the spectra obtained in the 55-cm^3 Ge(Li) detector is shown in Figure 19.

c. <u>Results and Discussion</u>

From the observed DSA factor F and the measured mean initial recoil velocity, one obtains $f_e(Z_1, \overline{v}/v_o) = 1.17$ (see Table I). This F value has been analyzed using the procedure presented in Chapter IV and incorporating the stopping parameters derived experimentally for heavy ions in Xe, namely, $f_n = 0.8$ and $f_e(gas) = 0.50 \pm 0.15$. An example of this analysis is illustrated in Figure 35. Including a 10% uncertainty for the rate of energy loss assumed in the analysis, the lifetime of the 2934-keV level of ^{33}S derived from the present measurement is

$$\tau(2934) = 43 \pm 7 \text{ ps.}$$

This is in excellent agreement with the other recoil-distance and Doppler-shift-attenuation measurements. The energy of the γ ray from this decay is measured to be

$$E_\gamma = 2933.7 \pm 1.0 \text{ keV}$$

by a comparison with γ-ray lines of well-known energy from ^{212}Pb and ^{88}Y sources.

Several authors have investigated the decay properties of the 2934-keV level. A summary of the lifetime, branching ratio and multipole mixing ratio measurements for this decay is presented along with the derived transition strengths in Table XIV. As is noted therein, the 51% branch to the $5/2^+$ level at 1966 keV proceeds via the emission of essentially pure E1 γ radiation with a strength $|M(E1)|^2 = 1.3 \times 10^{-5}$ W.u., and thus is inhibited by a factor of 100

compared with the typical transition of this type in A = 20 - 40

nuclei (Skorka et al. 1966). The two measurements of the mixing

ratio for the mixed E3/M2 decay branch (49%) to the $3/2^+$ ground

state are in poor agreement. However, the higher values for this

mixing ratio as reported by both authors can probably be excluded,

since they lead to an E3 transition strength $|M(E3)|^2 \geq 100$ W.u.,

in comparison with the mean value of $|M(E3)|^2 = 6.3$ W.u. found

for transitions of this type (Skorka et al. 1966) in this mass region.

Several theoretical investigations of the structure of ^{33}S

have been carried out, but most of them have dealt with the even-

parity levels. Erné (1966) used the shell model to describe the

negative-parity levels of nuclei in the range ^{33}S - ^{41}Ca by assuming

an inert ^{32}S core with a residual two-particle interaction between

the outer nucleons, placed in the $1f_{7/2}$ and $1d_{3/2}$ shells; his work

has been mentioned previously in Section 2c of this chapter. In this

model, the $7/2^-$ level is described as an odd neutron in the $1f_{7/2}$

shell outside the inert core, while the $3/2^+$ ground state is formed

with the neutron in the $1d_{3/2}$ shell. However, Erné did not predict

transition strengths, and predicted only the position of the $7/2^-$

level for ^{33}S, in agreement with experiment.

Watson and Lee (1967) used a simplified shell model to

explain $7/2^-$ and $3/2^-$ levels of s-d shell nuclei from ^{33}S to ^{41}Sc

by assuming a J = 0 ^{32}S core coupled to a single $1f_{7/2}$ or $2p_{3/2}$

nucleon. They thus describe the $7/2^-$ level of ^{33}S in the same manner

as Erné (1966). They also obtain good agreement with experiment for

their predicted level energies, but did not calculate transition

strengths.

Harris (1969) has computed the lifetime of the $7/2^-$ level using wave functions derived from a least-squares fit to known transition strengths and mixing-ratio values for nuclei in the range $A = 33 - 41$. In this manner he obtains $\tau(2934) = 161$ ps, in disagreement with the observed value.

Kavanagh et al. (1970) have pointed out that the inhibition of the E1 transition to the $5/2^+$ level at 1966 keV can be understood in terms of the shell-model wave functions derived for ^{33}S by Glaudemans et al. (1964a, 1964b). The dominant configuration for the $5/2^+$ level is $1s^3_{1/2} 1d^2_{3/2}$ and if it be assumed that the configuration for the $7/2^-$ level is $1s^4_{1/2} 1f_{7/2}$, then an E1 transition between these two configurations is forbidden, since this would involve a change in orbits of two particles.

The other theoretical studies of ^{33}S have dealt with the positive-parity levels. Wildenthal et al. (1971b) have used the shell model and two forms of the modified-surface-delta interaction to calculate energy-level spectra and transition rates that are in good agreement with experiment for even-parity levels of ^{33}S. Glaudemans, Endt and Dieperink (1971) have used the shell-model wave functions of Wildenthal et al. (1971b) to calculate M1 and E2 transition strengths for positive-parity levels in ^{33}S that also agree well with observed strengths.

Bailey and Choudhury (1970) have investigated the effects of vibration-particle coupling on the properties of low-lying levels in several odd-mass light nuclei. They assume that the last odd nucleon

has the $1d_{3/2}$ and $2s_{1/2}$ states available to it and is coupled to the quadrupole surface vibrations of the doubly-even core of the nucleus. Using this model they have calculated energy-level spectra and lifetimes for positive-parity levels in ^{33}S. The predicted level spectra are in fair agreement with experiment. Of the two predicted lifetimes that can be associated with observed levels, the lifetime of the 1.97-MeV $5/2^+$ level agrees reasonably well with the measured value, but the lifetime of the 0.84-MeV $3/2^+$ level disagrees by a factor of 18. Overall, it appears that this model is not as successful as the shell model mentioned above as a description of the positive-parity levels of ^{33}S.

4. The Lifetime of the 451-keV Level of ^{38}K

a. Introduction

The ^{38}K nucleus is one of the odd-odd self-conjugate nuclei in the s-d shell. The sparse experimental information available for this nucleus in 1967 is summarized by Endt and Van der Leun (1967) and is illustrated in part in Figure 36. At that time, spins and/or parities had been determined for only the ground state and the first four excited states, the lifetime of only the 0^+ first-excited level had been established, and no branching ratios or multipolarity mixing ratios for γ-ray decays had been measured.

When this study was begun, no value for the meanlife of the 451-keV level had been published. A preliminary Doppler-shift-attenuation method measurement employing a carbon backing established a lower limit for this lifetime of $\tau(451) > 5$ ps, and thus

indicated that the DSA technique with a gaseous stopping medium might be successfully applied to this case. After the present work was completed, Engmann et al. (1971) measured the lifetime of this level to be $\tau(451) = 740 \pm 160$ ps with the recoil-distance technique.

b. Experimental Procedure

The positive-parity level of ^{38}K at 451 keV was populated using the ^{35}Cl(^{4}He,n)^{38}K reaction. The target was a thin $(19.8 \pm 2.0 \ \mu g/cm^2)$ layer of $BaCl_2$, enriched to 99% in ^{35}Cl and evaporated onto the downbeam side of a 9.7-mg/cm^2 Ta gas-retaining foil. Tantalum was used for this experiment since Coulomb excitation of platinum isotopes in the foil normally used produced γ-ray lines that interfered with the γ ray under investigation. This foil was epoxied over a 1.3-mm-diameter hole in a Zr foil holder and placed in position in the apparatus shown in Figure 9. The target was bombarded with a beam of 9.56-MeV ^{4}He particles. Allowing for the energy loss of the recoils in a half-thickness of the target layer, the kinematically calculated mean recoil velocity immediately following the target layer was $\beta(0) = (6.56 \pm 0.10) \times 10^{-3}$. Further experimental details for this calculated velocity may be found in Table XV.

The 324-keV γ rays from the decay of the 451-keV level to the 127-keV first-excited state were observed in a 55-cm^3 Ge(Li) detector placed at 0° and 90° from the beam direction both in vacuum and as the ^{38}K recoils slowed in He gas at a pressure of 13.6 atm.

Helium was used as the stopping gas in this experiment since Coulomb excitation of Xe isotopes in the gas normally used produced interfering γ-ray lines. The detector was placed 1.2 cm from the target and the beam current was maintained at 70 ± 10 nA. The beam current was limited due to counting-rate considerations. Digital stabilization of the pulse-analysis system (see Figure 11) was accomplished using the 511-keV γ rays from the annihilation of positrons produced in the decay of ^{38}K as the reference line for gain stabilization and using pulses from a stable electronic pulser placed in a low channel of the 400-channel pulse-height analyzer as the reference line for zero-level stabilization. In addition, the 279-keV γ-ray line from a ^{203}Hg source placed near the target and the 301-keV line from Coulomb excitation of ^{181}Ta nuclei of the gas-retaining foil were employed to check the stability of the pulse-analysis system. The FWHM energy resolution for 279-keV γ rays was 2.7 keV. The observed full Doppler shift for recoils into vacuum, corrected by 10% for the solid angle subtended by the detector and by 9% for the differential absorption of the 324-keV γ rays by the Zr foil holder, leads to an observed mean initial recoil velocity of $\beta(0) = (5.8 \pm 1.0) \times 10^{-3}$.

In order to reduce the uncertainty in the full Doppler shift and in the initial velocity, the full shift was measured in a separate experiment which permitted a more favorable peak-to-background ratio for the 324-keV line. An enriched $Ba^{35}Cl_2$ target of the thickness mentioned above was evaporated onto a 10 μg/cm^2 carbon foil and placed in the apparatus shown in Figure 10. This target was then

bombarded with a beam of 7.70-MeV ^{4}He particles. (This was the energy of a prominent resonance seen in the excitation function for the production of 324-keV γ rays from the ^{35}Cl(^{4}He,n)^{38}K reaction.) The γ rays were observed with the Ge(Li) detector placed 3.3 cm from the target and at 0° and 90° from the beam direction as the ^{38}K nuclei recoiled into vacuum. Including a 6% correction for the solid angle subtended by the detector, the observed full Doppler shift was 2.14 ± 0.11 keV, leading to an observed mean initial recoil velocity of $\beta(0) = (6.51 \pm 0.33) \times 10^{-3}$, in agreement with the gas-cell measurement and with the kinematically calculated value. This measured velocity was used in the analysis of the DSAM data. An example of the spectra obtained with the Ge(Li) detector for the carbon-backed target is illustrated in Figure 37. The energy of the γ ray from the decay of the 451-keV level of ^{38}K is measured from these data to be

$$E_\gamma = 328.7 \pm 0.5 \text{ keV}$$

by a comparison with the γ-ray lines of well known energy from a ^{203}Hg source and from positron annihilation. An example of the spectra obtained with the Ge(Li) detector for the gas-cell DSAM data is illustrated in Figure 38.

c. Results and Discussions

The observed DSAM factor F for the He pressure of 13.6 atm is F = 0.78 ± 0.11. From this F value and the measured mean initial recoil velocity, one obtains $f_e(Z_1, \overline{v}/v_o) = 1.25$ (see Table I).

This F value has been analyzed using the procedure presented in Chapter IV and incorporating the three sets of stopping parameters derived experimentally for heavy ions stopping in He gas. The results of this analysis may be found in Table XV and an example of the analysis is shown in Figure 39. Including a 12% uncertainty for the rate of energy loss assumed in the analysis, the lifetime of the 451-keV level of ^{38}K derived from the present measurements is

$$\tau(451) = 155 \pm 90 \text{ ps.}$$

This is in disagreement with the result of Engmann et al. (1971), who obtained the value $\tau(451) = 740 \pm 160$ ps from a recoil-distance measurement.

Very little experimental work has been carried out on the decay properties of the 451-keV level. The parity of this level is known to be positive (Endt and Van der Leun 1967); in fact, Jänecke (1963) had measured the spin of this level to be 1^+ from an analysis of the ^{4}He angular distribution observed in the ^{40}Ca(d, ^{4}He)^{38}K reaction. Recently, Hasper and Smith (1971) also found the spin of this level to be 1^+, and measured the branching ratio to the 127-keV 0^+ level to be 100%, placing an upper limit of 1% on the ground-state transition. The lifetime determined in the present work confirms the spin assignment $J^\pi(451) = 1^+$, since the assumption of $J^\pi = 2^+$ would lead to a $\Delta T = 1$, E2 transition strength of $180 ^{+250}_{-66}$ W.u., in comparison with the strength of 0.44 W.u. found for similar transitions for self-conjugate nuclei in this mass region (Skorka et al. 1966). Higher values for the spin of this level are even less probable.

The transition strengths for the decay of the 451-keV level have been calculated from the spin and branching ratios mentioned above using the present lifetime result; the values are given in Table XVI. The M1 transition strength for the decay to the first excited state is $|M(M1)|^2 = \left(5.8 \begin{smallmatrix} +8.0 \\ -2.1 \end{smallmatrix}\right) \times 10^{-3}$ W.u. and thus is hindered by about a factor of 30 compared with similar transitions in A = 20 - 40 nuclei (Skorka et al. 1966).

Recently, several authors have carried out many-particle shell-model investigations of the structure of ^{38}K. Engelbertink and Glaudemans (1969) used the shell model to investigate the properties of positive- and negative-parity levels in A = 38 nuclei by assuming an inert ^{28}Si core with a residual two-particle interaction between the outer nucleons. The negative-parity states were described by a closed $2s_{1/2}$ shell, five nucleons in the $1d_{3/2}$ shell, and one nucleon in the $1f_{7/2}$ or $2p_{3/2}$ shell. For the positive-parity states, all configurations in the $2s_{1/2}$ and $1d_{3/2}$ shell were taken into account. The effective two-particle interaction chosen was the modified-surface-delta interaction. Within the framework of this model, they calculated energy-level spectra but no transition strengths for ^{38}K. The calculated level energies were in poor agreement with experiment and the ordering of the 3^+ ground state and the 1^+ second-excited state was inverted.

Dieperink and Glaudemans (1969b) studied the structure of ^{38}K with a shell-model calculation by assuming that the low-lying even-parity levels of that nucleus can be described as two holes distributed over the $1d_{5/2}$, $1d_{3/2}$ and $2s_{1/2}$ single-particle orbits.

Two different types of residual shell-model interaction were used, the phenomenological modified-surface-delta interaction (MSDI) and a modification of the "realistic" Tabakin interaction (Tabakin 1964). The parameters of the MSDI were obtained from a fit to known level energies of nuclei with A = 36 - 39. The Tabakin interaction is a sum of separable potentials which fit the S-, P- and D-wave phase shifts for free nucleon-nucleon scattering, and which can be converted into an effective shell-model interaction by applying an appropriate set of corrections (Clement and Baranger 1968). They obtained wave functions and level energies for the ground state and first four excited states, and calculated lifetimes and branching ratios for its γ-ray transitions. The decay properties for this nucleus generally appear to depend sensitively upon the interaction assumed, although this is not reflected in the decay of the 451-keV level. The lifetime of this level calculated for each of these interactions may be found in Table XVI, and are in agreement with the results of the present experiment. On the other hand, the position of the 0^+ first-excited state and the 3^+ ground state are inverted with the MSDI calculation, while they are ordered correctly with the Tabakin interaction. Overall, it is found that the Tabakin interaction reproduces the experimentally observed transition rates for this nucleus much better than does the modified-surface-delta interaction.

Evers and Stocker (1970) have used the shell model to study the properties of even-parity levels of ^{38}K by assuming an inert ^{28}Si core and a model space that includes the $1d_{3/2}$ and $2s_{1/2}$ orbits, plus 0 or 2 particles in the $1f_{7/2}$ shell, with three forms of the

modified-surface-delta interaction considered as the two-particle interaction between the outer nucleons. In each case, the parameters of the interaction were obtained from a fit to 28 known level energies in the mass region A = 34 - 39. They performed calculations with the standard modified-surface-delta interaction (MSDI), with a tensor force added to the modified-surface-delta interaction (MSDIT), and with one of the parameters of this tensor force held constant (MSDIT C). Using these approaches, they calculated wave functions, energy-level spectra and transition rates for even-parity levels in ^{38}K. The lifetimes for the 451-keV level predicted with the three interactions are given in Table XVI. As in earlier work, these authors also found that the MSDI predicted an inverted ordering of the ground and first-excited states; however, this is remedied by the addition of the tensor force. The MSDIT C interaction produced the best agreement with experimental lifetimes and leads to energy-level spectra in reasonable agreement with observation.

Wildenthal, Halbert, McGrory and Kuo (1971a) performed a shell-model calculation to investigate the properties of positive-parity states of nuclei with masses in the range A = 34 - 38. They assumed a model space defined by a complete set of many-particle basis states for A - 16 nucleons distributed among the three single-particle orbits $1d_{5/2}$, $2s_{1/2}$ and $1d_{3/2}$. The model core was ^{16}O. They employed several different effective Hamiltonians for the two-particle interaction. With this model, they calculated energy-level spectra, static nuclear moments, and M1 and E2 transition strengths. For the calculation of these transition strengths, they employed

effective charges and free-nucleon g factors. For ^{38}K, the calcu-
lated energy-level spectra are in reasonable agreement with experi-
ment, with the 3$^+$ ground state and the 1$^+$ excited states in the correct
order. However, the 451-keV level is placed about 800 keV too high
in excitation. The predicted M1 transition strength for the decay of
the 1$^+$ 451-keV level to the 0$^+$ 127-keV level is given in Table XVI
and is in good agreement with the result of the present work. The
predictions of this model for the transition strengths of other low-
lying levels in ^{38}K are also in reasonable agreement with experiment
(Engmann et al. 1971); it thus appears that this model provides a
reasonably adequate description of these levels.

5. The Lifetime of the 1760-keV Level of ^{26}Al

   a. Introduction

   The experimental information available in 1967 for the odd-odd
self-conjugate nucleus ^{26}Al is summarized by Endt and Van der Leun
(1967) and is illustrated in part in Figure 15. While the spins and
parities of the ground state and 15 excited states up to an excitation
of about 4 MeV had been determined, very little information was
available for electromagnetic transition rates between levels. In
fact, only the lifetimes of the first two excited states had been
measured. Since then, measurements of lifetimes, branching
ratios and multipole mixing ratios have been reported for levels up
to about 4-MeV excitation. References to much of this work may be
found in the publication of Bissinger et al. (1969).

When this work was begun, only a lower limit of $\tau(1760) > 3.4$ ps had been placed on this lifetime by Häusser, Alexander and Broude (1968). During the course of these experiments, a preliminary value of $\tau(1760) = 6.5 \pm 2.0$ ps was reported by Marmor et al. (1969), who employed the ^{23}Na(^{4}He,n)^{26}Al and the recoil-distance method. The present measurement was performed using the DSA method with carbon as the stopping medium.

b. Experimental Procedure

The 2^+ level of ^{26}Al at 1760 keV was populated using the ^{23}Na(^{4}He,n)^{26}Al reaction. The target was a thin (54 ± 10 μg/cm^2) layer of natural NaBr, evaporated onto a thick (0.7 g/cm^2) carbon block. This target was placed at an angle of 45° from the beam direction in the target chamber shown in Figure 10 and bombarded with a beam of 6.06-MeV ^{4}He particles. Allowing for the energy loss of the recoils in a half-thickness of the target layer, the kinematically calculated recoil velocity immediately following the target layer was $\beta(0) = 8.0 \times 10^{-3}$. Further experimental details for this calculated velocity may be found in Table XVII.

The 1342-keV γ rays from the decay of the 1760-keV level to the 418-keV state were observed in a 55-cm^3 Ge(Li) detector placed at 0° and 90° from the beam direction as the recoils slowed in the carbon backing. The detector was placed at 3.5 cm from the target. Digital stabilization of the pulse-analysis system (see Figure 11) was accomplished using the the 1275-keV γ rays from a ^{22}Na source as the reference line for gain stabilization and using

pulses from a stable electronic pulser as the reference line for zero-level stabilization. In addition, the 835-keV line from a ^{54}Mn source placed near the target served as a check on the stability of the system. The FWHM energy resolution for 1275-keV γ rays was 4.6 keV.

A separate experiment was performed to measure the full γ-ray Doppler shift and initial recoil velocity. In order to accomplish this, a NaBr target of the thickness mentioned above was evaporated onto the downbeam side of a 208 μg/cm^2 carbon foil and placed at 45° from the beam direction in the apparatus shown in Figure 10. The beam energy was raised by 200 keV to compensate for the energy loss in the carbon foil, and the γ rays from the reaction were observed in the Ge(Li) detector placed at 0° and 90° from the beam direction as the ^{26}Al nuclei recoiled into vacuum. The gain and zero stabilization of the pulse-analysis system was maintained as described above. The observed full Doppler shift, corrected by 4.5% for the solid angle subtended by the detector, was 9.49 ± 0.15 keV, leading to an observed mean initial recoil velocity of $\beta(0) = (7.06 \pm 0.13) \times 10^{-3}$. This is in unexplained disagreement (12%) with that calculated from kinematics; the observed velocity was used in the DSAM analysis. An example of the spectra obtained in the Ge(Li) detector for both targets is shown in Figure 40. The energy of the γ ray from the decay of the 1760-keV level of ^{26}Al is measured from the present data to be

$$E_{\gamma} = 1341 \pm 1 \text{ keV}$$

by a comparison with the γ-ray lines of well known energy from ^{54}Mn and ^{22}Na sources placed near the target.

c. Results and Discussion

The observed DSAM factor F for the thick carbon block was $F = 0.11 \pm 0.03$. From this F value and the observed mean initial recoil velocity, one obtains $f_e(Z_1, \bar{v}/v_o) = 0.66$ (see Table I). This F value has been analyzed using the procedure presented in Chapter IV for solid backings, with $f_n = 0.8 \pm 0.2$. In addition to this uncertainty in the nuclear stopping parameter, two other uncertainties were included in the analysis of this observed F value. The uncertainty in the initial recoil velocity was taken as the difference between the observed and calculated values. In addition, the density of the thick carbon block was taken as $1.70 \, ^{+0.20}_{-0.10} \, g/cm^3$. The measured bulk density of the carbon used was $1.58 \pm 0.01 \, g/cm^3$. However, the density of amorphous carbon is generally considered to lie in the range $1.8 - 2.1 \, g/cm^3$ (CRC Handbook of Chemistry and Physics, 1968); in addition, the density of carbon evaporated onto a cold substrate has been measured by Kennedy et al. (1967) to be $1.82 \pm 0.10 \, g/cm^3$. The assumed density above was taken as a reasonable approximation for the density of the block. The results of the analysis may be found in Table XVII, and an example of the analysis is illustrated in Figure 41. The lifetime of the 1760-keV level derived from the present measurements is

$$\tau(1760) = 5.0 \, ^{+2.2}_{-1.4} \, ps.$$

This is in agrement with the result of Marmor et al. (1969) who found $\tau(1760) = 6.5 \pm 2.0$ ps.

It should perhaps be noted that the F value obtained when the ^{26}Al nuclei recoiled into the 208-μg/cm^2 foil (F = 0.18 ± 0.03) was somewhat larger than that obtained with the thick carbon block. The larger value is discarded as spurious, on the grounds that it arises from undecayed ^{26}Al recoils not completely stopped in the thin C foil. The range of 780-keV ^{26}Al (the calculated mean initial recoil energy) in carbon is given by Northcliffe and Schilling (1970) to be 180 μg/cm^2, while the thickness of the foil at 45° is 294 μg/cm^2. However, the range of the most energetic ^{26}Al recoils (E = 1120 keV) is 234 μg/cm^2, and if the foil were not at 45° (due to observed warping of the foil exposed to the beam), then the recoils could escape from the backing with a finite velocity.

Little information exists for the decay properties of the 2^+ level at 1760 keV. The branching ratio for the decay to the 3^+ 418-keV level has been measured by Bissinger et al. (1968) to be 100% with an uncertainty of 20%, while Häusser et al. (1968) have established a lower limit of 90% for this branch. The multipole mixing ratio for this decay has not been measured. The electromagnetic transition strengths have been calculated and are given in Table XVIII, along with a summary of the experimental data available for the decay of this level. Assuming that the decay proceeds only by the probable lowest multipole, the M1 transition strength is $$|M(M1)|^2 = \left(2.3 \,^{+0.5}_{-0.6}\right) \times 10^{-3} \text{ W.u.}$$ Such an inhibition is expected for $\Delta T = 0$, M1 transitions in self-conjugate nuclei in this mass

region (Warburton and Weneser 1969); the average M1 strength for transitions of this type for nuclei with A = 20 - 40 is 8.8×10^{-3} W.u. (Skorka et al. 1966).

Very few theoretical investigations into the structure of ^{26}Al have been carried out. A simple shell model assuming a pure $1d_{5/2}^{-2}$ configuration predicts three T = 0 levels (1^+, 3^+, and 5^+) and three T = 1 levels (0^+, 2^+, and 4^+). These might be identified with the levels at 1059, 418, 0, 229 and 2070 keV, respectively, with the 4^+ level as yet unobserved. States above 1.5 MeV excitation might be explained if the promotion of one or more particles from the $1d_{5/2}$ shell to the $2s_{1/2}$ or $1d_{3/2}$ orbits were considered.

Bouten, Elliott and Pullen (1967) used the shell model in an intermediate-coupling approach to calculate energy-level spectra for nuclei in the mass region A = 18 - 38. The calculated energies for the lowest five levels in ^{26}Al are in reasonable agreement with experiment, but these authors calculated no transition strengths from their model.

Wasielewski and Malik (1971) applied the unified model to the odd-odd s-d shell nuclei ^{22}Na, ^{26}Al, and ^{30}P. They assumed that the odd neutron and odd proton are placed in Nilsson orbitals generated by an axially symmetric rotating deformed core, and then calculated positive-parity energy-level spectra, static nuclear moments, and M1 and E2 transition strengths. The level spectra calculated for the low-lying states of ^{26}Al were in general agreement with experiment except for discrepancies of about 500 keV in the positions of the first spin 0 and the spin 1 states. The calculated

M1 and E2 transition strengths for the decay of the 1760-keV level to the 418-keV level are given in Table XVIII and are consistent with the experimental result of the present work (since the multipole mixing ratio has not been measured). However, the predicted strengths for decays of other levels are in disagreement with observation, particularly transitions into and from the 418-keV level, where the model underestimates the transition strength by a factor of more than 10^4. The authors conclude that their present model does not adequately describe the ^{26}Al nucleus, and suggest that an axially asymmetric rotator model might remedy the discrepancies.

6. The Lifetimes of the 800- and 890-keV Levels of ^{40}K

a. Introduction

In the j-j coupling shell model, the low-lying states of ^{40}K are described as a $1d_{3/2}$ proton hole coupled to a $1f_{7/2}$ neutron. The facts that the ground state and the first three excited states (see Figure 42) have the predicted spins (4$^-$, 3$^-$, 2$^-$, 5$^-$) and that the model can be used to predict the level energies with reasonable accuracy (Erné 1966; Dieperink and Brussaard 1968) provide further support for this viewpoint. De-Shalit (1965) has pointed out the need to test this model by measurements of static nuclear moments and M1 rates in ^{40}K, in particular, the 2$^-$ $\rightarrow$ 3$^-$ and the 5$^-$ $\rightarrow$ 4$^-$ transitions from the 800-keV and 890-keV levels, respectively.

The experimental information available for this nucleus in 1967 is summarized by Endt and Van der Leun (1967) and is illustrated

in part in Figure 42. Since then, several experimental investigations have provided new information concerning spins, parities, lifetimes, branching ratios and multipolarity mixing ratios for levels up to about 4-MeV excitation. References to much of this work may be found in the papers by James et al. (1971) and Wechsung et al. (1971).

When this work was begun, the lifetimes of the 2^- 800-keV and the 5^- 890-keV levels had been measured by Merdinger (1969), who obtained $\tau(800) = 0.33 \, ^{+0.10}_{-0.08}$ ps and $\tau(890) = 0.91 \, ^{+0.55}_{-0.25}$ ps, and by Segel et al. (1970), who obtained preliminary values of $\tau(800) = 2 \pm 1$ ps and $\tau(890) = 4.5 \pm 1.5$ ps. In order to resolve this discrepancy, the lifetimes of these levels were measured in the present work using the Doppler-shift-attenuation method with carbon as the stopping medium. After these experiments were completed, other measurements of these lifetimes became available, including the final values of Segel et al. (1970) and those of Bass and Wechsung (1970) and James et al. (1971). These results are collected in Table XX.

b. Experimental Procedure

The 2^- and 5^- levels of ^{40}K were populated using the ^{37}Cl(^{4}He,n)^{40}K reaction. The target was a thin ($38 \pm 10 \, \mu g/cm^2$) layer of NaCl, enriched to 99.3% in ^{37}Cl and evaporated onto a 180 $\mu g/cm^2$ carbon backing. This target was placed at an angle of 45° from the beam direction in the target chamber shown in Figure 10 and then bombarded with a beam of 5.90-MeV ^{4}He particles. Including the energy loss of the recoils in a half-thickness of the target

layer, the kinematically calculated recoil velocity immediately follow-
ing the target layer was $\beta(0) = (5.0 \pm 0.2) \times 10^{-3}$. Further experi-
mental details for this calculated velocity may be found in Table XIX.

The 890-keV and 770-keV γ rays from the decay of these two
levels were observed in a 55-cm^3 Ge(Li) detector placed at 0° and
90° from the beam direction as the recoils slowed in the carbon backing
and in vacuum. The detector was placed 4.5 cm from the target.
Digital stabilization of the zero level of the pulse-analysis system
was accomplished using a stable electronic pulser to provide a
reference line in a low channel of the 400-channel analyzer. In
addition, the 662-keV line from a ^{137}Cs source placed near the target
served as a check on the stability of the pulse-analysis system. The
FWHM energy resolution for 662-keV γ rays was 3.2 keV. The
observed full Doppler shift for recoils into vacuum, corrected by
4% for the solid angle subtended by the detector, leads to an observed
mean initial recoil velocity of $\beta(0) = (4.4 \pm 0.2) \times 10^{-3}$, somewhat in
disagreement (12%) with the kinematically calculated velocity. The
observed recoil velocity was used in the analysis of the DSAM data.
An example of the spectra obtained in the Ge(Li) detector is illus-
trated in Figure 43. The experiment was repeated with another
target believed to be similar to the one described above; in this case,
the observed full Doppler shift, corrected by 3.1% for the solid angle
subtended by the detector, led to an observed recoil velocity of
$\beta(0) = (5.2 \pm 0.2) \times 10^{-3}$, in good agreement with the calculated
velocity, and this velocity was used to analyze the DSAM data ob-
tained on that day.

c. Results and Discussion

The observed DSAM factors F for these two levels are given in Table XIX. The reason for the discrepancy in the observed F values and in the measured recoil velocities for the two runs is not understood. These F values have been analyzed using the procedure presented in Chapter IV for solid backings, with $f_n = 0.8 \pm 0.2$. For these cases, one obtains $f_e(Z_1, \overline{v}/v_o) = 1.28$ from Table I. The density of the carbon backing has been taken as $D = 1.82 \pm 0.10$ g/cm^3, the value found by Kennedy et al. (1967) for the density of amorphous carbon evaporated onto a cold substrate. The lifetimes derived from the present measurements are the weighted averages of the two runs; the uncertainties in the derived results include statistical uncertainties in the measured F, incertitudes in the density and in the nuclear stopping parameter, and a 10% uncertainty in the electronic stopping power for ^{40}K in carbon. The results of the analysis may be found in Table XIX, and an example of the analysis is illustrated in Figure 44. It should perhaps be noted that in this case, the most energetic ^{40}K recoil (768 keV) has a range in carbon of only 135 $\mu g/cm^2$ (Northcliffe and Schilling 1970), thus precluding the escape of recoils from the carbon backing. The lifetimes of the 800-keV and 890-keV levels of ^{40}K derived from the present measurements are

$$\tau(800) = 0.35 \pm 0.07 \text{ ps}$$

$$\tau(890) = 1.17 \pm 0.31 \text{ ps}$$

in reasonable agreement with other recent measurements of these

lifetimes (see Table XX).

The 2^- 800-keV level decays by a pure M1 100% branch to the 3^- 30-keV level, while the 5^- 890-keV level decays by a mixed E2/M1 100% branch to the 4^- ground state. The calculated experimental transition strengths for these decays and the presently available decay properties may be found in Table XX. The M1 transition strengths are fairly typical for transitions of this type in nuclei with A = 20 - 40 (Skorka et al. 1966).

Early shell-model calculations of the structure of ^{40}K were performed by Goldstein and Talmi (1956) and by Pandya (1956), who interpreted the low-lying levels of this nucleus as pure j-j coupling configurations with one proton hole in the $1d_{3/2}$ shell and one neutron in the $1f_{7/2}$ shell. Erné (1966) extended this j-j coupling calculation to include all possible configurations with an arbitrary number of nucleons in the $1d_{3/2}$ shell. All inner shells were considered to be an inert ^{32}S core, and a residual two-particle interaction was assumed for the outer nucleons. The parameters of this interaction were determined from a fit to known level energies, and then the model was used to predict negative-parity energy-level spectra for nuclei in the range ^{33}S to ^{41}Ca. He obtained agreement with experiment for the low-lying quartet of odd-parity levels in ^{40}K, but did not calculate electromagnetic transition strengths.

Dieperink, Leenhouts and Brussaard (1968) used the shell model to calculate the lifetimes of seven low-lying negative-parity levels in ^{40}K. They included the complete s-d shell for the proton hole and the complete f-p shell for the neutron in their configuration

space, and used both the Tabakin interaction and two forms of the

modified-surface-delta interaction (MSDI) as the residual two-body

potential. The predicted lifetimes for the 2^- and 5^- levels may be

found in Table XX, and are in reasonable agreement with the experi-

mental lifetimes determined in the present work. The principal con-

figuration present in the wave functions for the four lowest-lying

levels (4^-, 3^-, 2^- and 5^-) was $1f_{7/2} 1d_{3/2}^{-1}$, with small admixtures

of $2p_{3/2} 1d_{3/2}^{-1}$ and $1f_{7/2} 2s_{1/2}^{-1}$ configurations. It appears from

this work that the first four levels of this nucleus are fairly well

described by the shell model.

Wechsung, Strassheim and Bass (1971) have performed a

shell-model calculation to predict M1 and E2 electromagnetic

transition rates for levels in ^{40}K up to 2.6-MeV excitation. They

have described the first eight odd-parity states as mixtures of the con-

figurations $1f_{7/2} 1d_{3/2}^{-1}$, $2p_{3/2} 1d_{3/2}^{-1}$ and $1f_{7/2} 2s_{1/2}^{-1}$, and

incorporated effective g factors and charges in their transition-

strength calculations. Their results for the 2^- and 5^- levels at

800 keV and 890 keV, respectively, may be found in Table XX, and

are in fair agreement with experiment; however, the M1 transition

from the 890-keV level is predicted to be about twice as fast as ob-

served. These authors state that the transition strengths for the

four lowest-lying levels can be brought into complete agreement with

experiment if small admixtures (1.3%) of the $1f_{7/2} 1d_{5/2}^{-1}$ configura-

tion are included in the wave functions for the 2^- and 5^- states. This

was also pointed out by Becker and Warburton (1971).

Becker and Warburton (1971) used the shell-model wave

functions of Perez (1969) and free-nucleon g factors to calculate the M1 transition strengths among the four lowest-lying odd-parity levels in this nucleus. Their results may be found in part in Table XX, and are also in fair agreement with experiment.

VII. MEASUREMENTS OF ELECTRONIC STOPPING POWERS IN GASES

1. Introduction

As is mentioned in Chapter III, the principal source of uncertainty in lifetime measurements by the Doppler-shift-attenuation method is the imprecise knowledge of the rate of energy loss for the recoiling ion in the stopping medium. This is particularly true for gaseous media, since far fewer experimental data exist for this case than when solids (such as carbon or aluminum) are used. The experimental studies of electronic stopping power for low-energy heavy ions are summarized in Chapter III. None of those studies deals with the specific case of the electronic energy loss of ions with $8 \leq Z_1 \leq 18$ in the energy range $E < 800$ keV slowing in xenon gas, the case relevant to the lifetime measurements of this work. In an attempt to increase the precision of the lifetimes deduced from the DSAM experiments and in order to provide new experimental data for combinations of ion, ion energy, and absorber where little work has been previously done, the electronic stopping cross section S_e for ^{27}Al and ^{12}C in He and Xe was measured over as large an energy interval as feasible. The measurement of S_e for C in He was performed as a check of the experimental technique, since a comparison was available with the recent work of Hvelplund (1971) who measured, among other combinations, the S_e for C in He in the energy range $200 \leq E \leq 500$ keV. The measurement of S_e for C in Xe was performed to determine if the exponent p in the power-law

dependence $S_e = KE^p$ is the same in low- and high-mass absorbers; equality of the exponent in these two cases would suggest that p depends on the properties of the incident ion and not on those of the stopping atom. The S_e for Al in Xe was measured to check the assumptions made in the analysis of the DSAM lifetime measurements: namely, that the S_e for Al in Xe and $E < 700$ keV is approximately 50% of that predicted by the LSS theory as modified by the Z_1 oscillations observed by Ormrod and Duckworth (1963), Ormrod, Macdonald, and Duckworth (1965), Ormrod (1968), Fastrup, Hvelplund, and Sautter (1966), Hvelplund and Fastrup (1968), and Hvelplund (1971); and that the power-law dependence on the ion energy is $S_e \propto E^{1/2}$. The S_e for Al in He was measured to determine again if the exponent p in the relation $S_e = KE^p$ is the same in low- and high-mass absorbers. The goals of the experiment were only partially achieved; for experimental reasons that will be outlined in the next section, the lowest energy at which S_e could be measured for Al in Xe and He was 790 keV. Thus, there is still no direct evidence on the rate of electronic energy loss at an ion energy as low as 175 keV, which is the approximate mean energy at the time of decay of an excited Al nucleus whose initial energy is 700 keV and for which the measured DSA factor is $F = 1/2$.

2. Experimental Procedure

The energy loss of the C and Al ions was measured by observing the energy of C and Al recoils, elastically scattered out of thin self-supporting targets by an incident beam of ^{4}He particles, in

a silicon surface-barrier detector when the recoils were permitted to reach the detector both through vacuum and through the stopping gas (He or Xe) at known pressure. The experimental apparatus is illustrated schematically in Figure 45. The target chamber is the 12-inch gas scattering chamber designed by Senhouse (1964), modified somewhat for this application. In Figure 45, an incident beam of ^{4}He particles, produced by the ONR-CIT tandem Van de Graaff accelerator, enters the apparatus from the left; the beam energies used varied from 2.4 - 9.6 MeV, and beam intensities were typically limited to 0.1 μA, mainly dictated by counting-rate considerations. The beam was collimated in vacuum by circular apertures, 1.27 mm in diameter, in two Ta disks separated by 17.6 cm. After collimation, the beam passed through an entrance window of (nominally) 5000Å-Ni foil, which separated the high vacuum of the beam-transport system from the gas in the target chamber during the energy-loss measurements. The Ni entrance foil was epoxied over a 2.54-mm hole in a removable stainless-steel foil holder of standard design in this laboratory, in order to facilitate replacement of the foil in case of breakage. The mounted foil was carefully inspected using a bright light in a darkened room and was found to be free of visible pinholes. After passing through the entrance foil, the beam traversed a distance of 1.52 ± 0.03 cm and then struck a thin self-supporting target of C or Al, mounted over an 8.9-mm hole in a Ta target frame. The distance from entrance foil to target was chosen by weighing two considerations: (1) it was desired to keep the distance as small as possible in order to minimize the effect of the divergence of the beam due to scattering

in the entrance foil, and to minimize the scattering and energy loss of the beam in traversing the gas during the energy-loss runs; (2) it was desired to have the distance sufficiently large so that the detector was not exposed to beam particles scattered through large angles by the entrance foil. The distance chosen satisfies the second criterion while leading to a beam energy loss in the gas of only a few keV. As an example, for 4.0-MeV ^{4}He particles, the energy lost by the beam in traversing this distance through Xe gas at 2.2 Torr pressure is only 8 keV; for Al recoils, this changes the recoil energy by only 3 keV. The option of maintaining the original design (Senhouse 1964), wherein the entrance foil was external to the scattering chamber with the beam being collimated in the gas, was rejected due to the large beam energy loss, with its attendant uncertainty, incurred during the traversal of the long path length in gas.

The Al targets were prepared by vacuum evaporation and were nominally 20-μg/cm^2 thick as measured by a quartz-crystal evaporation thickness monitor. This was the thinnest layer that could be easily floated and mounted over the Ta frame. The C targets were purchased commercially[*] with a thickness of 10 ± 4 μg/cm^2 as stated by the manufacturer. The target thicknesses were measured subsequently in separate experiments; typical measured thicknesses were 22.2 ± 2.0 μg/cm^2 for the Al and 14.4 ± 1.4 μg/cm^2 for the C targets. These thicknesses were measured by observing the energy of ^{4}He particles, elastically scattered from thick Ta backings, both directly and through the target material, in the 61-cm-radius magnetic

---

[*] Obtained from Yissum Research Development Corporation, Jerusalem, Israel.

spectrometer at 90° to the beam in the laboratory. The incident beam energy was 5.00 MeV and the targets were placed at 45° to both the beam and the spectrometer in a reflection geometry. The observed energy shift of the step in the yield of elastically-scattered ^{4}He particles, directly and through the target layer, was converted to a thickness in $\mu g/cm^2$ using the energy-loss tabulations of Northcliffe and Schilling (1970). An example of the observed yields of the elastically scattered ^{4}He is shown in Figure 46.

The Ta target frame was mounted on a target rod attached to an angle protractor; it is estimated that the angle of the target relative to the incident beam could be set to within $\pm 1^{\circ}$. The target angle in each run was set equal to the detector angle so that the recoils reaching the detector left the target normal to its surface.

After leaving the target, the beam was stopped in a Faraday cup attached to a port in the opposite wall of the scattering chamber, and the beam current was sent directly to the current integration system. The Faraday cup was shielded from electrons by an insulated Ta disk, maintained at a potential of - 600 V, and containing a 1.3-cm-diameter hole through which the beam passed.

The C and Al recoils were observed in a silicon surface-barrier detector obtained from ORTEC[*], with a depletion depth of 100 μm, an active area of 200 mm^2, and biased at + 50 volts. The front face of the detector was measured to be 8.92 ± 0.04 cm from the center of the target. The angle subtended by the detector was

---

[*]Oak Ridge Technical Enterprises Corporation, Oak Ridge, Tennessee.

defined by a rectangular aperture, 7.94 mm high and 1.19 mm wide, placed in front of the detector at a distance of 8.4 cm from the center of the target. Thus, the angle $\Delta\theta$ subtended by the collimator and detector was 0.80° while the azimuthal angle $\Delta\phi$ was 5.5°. At 30°, the $\Delta\theta$ due to this $\Delta\phi$ was 0.45°; at 55°, it was 0.18°. A second aperture of the same dimensions was placed 3.9 cm from the center of the target and served to limit the region of the target exposed to the detector. The angle subtended at the detector by this aperture was 1.5°; thus, the width of the area observed on the target was approximately 2.5 mm, or twice the beam diameter. The collimator-detector assembly was mounted on an arm and rotated about the axis of the cylindrical target chamber. An angle protractor and vernier with 0.1° divisions were attached to the arm for the measurement of the detector angle relative to the direction of the beam.

The instrument was aligned optically with a telescope. After levelling and aligning the telescope with beam-defining slits in the existing beam-transport system, the position of the scattering chamber was adjusted until the beam-defining collimator was coaxial with the optical axis of the telescope. This then defined 0° for the system, that is, the beam direction. The detector-collimator assembly with the detector removed was then placed in position and rotated until the axis of the detector collimator lay along the optical axis of the telescope such that one could sight through both sets of collimators. The angle on the detector protractor in this position was then the 0° for the detector, and detector angles were measured relative to this angle. The alignment was checked a number of times

during the course of these experiments and was found to remain constant to within about $1/6^{\circ}$. It is estimated that the detector angle is uncertain by no more than $\pm 1/2^{\circ}$. The detector angles used during these experiments were $31.0 \pm 0.5^{\circ}$ and $55.0 \pm 0.5^{\circ}$.

The vacuum in the target chamber was maintained with a liquid-nitrogen trap and diffusion pump; when gas was introduced into the chamber for an energy-loss run, the chamber was isolated from the pump by a valve. The vacuum in the system during the vacuum runs was measured by an ion gauge mounted directly at the base of the chamber; outgassing of the chamber limited the typical vacuum obtained to $\sim 5 \times 10^{-5}$ Torr. The pressures of the stopping gases Xe and He were measured with a Wallace and Tiernan FA-160 pressure gauge. This gauge measures pressures in the range 0 - 20 Torr with divisions of 0.1 Torr; the manufacturer's stated accuracy is 0.33% of full scale, or about 0.07 Torr. This mechanical gauge was calibrated against a McLeod-type mercury manometer and also against another Wallace and Tiernan mechanical gauge, the FA-141. Both calibrations agreed to within 0.03 Torr from 0 - 20 Torr, within the stated accuracy. The gas pressures used during energy-loss runs were typically 1.5 Torr for Xe and 15 Torr for He. The temperature of the chamber was measured by placing a thermometer in thermal contact with the walls of the chamber; it was assumed that the gas was in thermal equilibrium with the chamber and that this was the gas temperature. The temperature for all runs was $22.5 \pm 1.0^{\circ}$ C.

The initial recoil energy was calculated from the kinematics

of the elastic scattering and was corrected for the various energy losses incurred by the incident beam and by the outgoing recoils as they left the target. The incident beam energy was first corrected for the energy lost in traversing the known thickness of the Ni entrance foil, using the energy-loss tabulations of Whaling (1958); for a 5500Å Ni foil and a beam energy of 4.00 MeV, this amounted to about 250 keV. The beam energy was then corrected for the energy lost in traversing the gas (during the energy-loss runs) between the entrance foil and the target; for an initial incident beam energy of 4.00 MeV and Xe gas at a pressure of 2.2 Torr, this amounted to about 8 keV. The energy of the recoil was then calculated from the kinematics of the reaction for the detector angle being used. In the above example, the recoil energy is 2070 keV for C recoils at 31°. It was assumed that the reaction took place uniformly throughout the target.

The recoil energy was then corrected by the methods of Lindhard, Scharff, and Schiøtt (1963) for the electronic and nuclear energy loss incurred as the recoils left the target, and was computed for penetration of a half-thickness of the target layer. As an example, for a C target with a full thickness of 14.4 $\mu g/cm^2$ and the other conditions as stated previously, this loss amounted to 52 keV.

In order to know the recoil energy accurately, the thickness of the Ni entrance foil must be known accurately. One problem encountered during the course of these experiments was the continual deposition of carbon on the entrance foil due to the cracking of hydrocarbons present in the relatively poor vacuum mentioned previously. For this reason, the energy loss of the beam in the foil and hence its

thickness was measured at the beginning and end of each running period. This was accomplished by measuring the shift in the position of the 4241 ± 25 keV resonance (Ajzenberg-Selove 1971) in the $^{12}C(^{4}He,^{4}He)^{12}C$ reaction, both with the beam directly on a 14.4 μg/cm^2 carbon target and after passing through the Ni foil. For the purpose of this determination, the position of the resonance was taken to be the energy of the maximum of the yield curve. In Figure 47 is shown an example of yield curves taken directly (b) and through the Ni foil (a). The energy shift in this example is 218 ± 6 keV. Using the energy-loss tabulations of Whaling (1958), this corresponds to a Ni thickness of 5260 ± 450 Å. While the energy loss at this beam energy is known to ± 3%, an uncertainty in the foil thickness of ± 8% (the uncertainty quoted in the Whaling compilation) is quoted for use at other beam energies. As an example of the rate of carbon deposition, the energy shift increased by 14 keV (6% of the initial energy shift) over one running period of 120 hours.

The signals from the Si detector were amplified by a Tennelec Model 100A preamplifier and a Tennelec TC200 linear amplifier and were then analyzed by a Nuclear Data ND2200 pulse-height analyzer employing 1024 channels.

Because of the pulse-height defect of heavy ions in solid-state detectors, the pulse-height-analysis system could not be calibrated with light particles such as ^{4}He or protons but rather had to be calibrated with the heavy ions themselves. The calibration of pulse height versus recoil energy was accomplished by observing the centroid of

the recoil-particle peak in vacuum as the beam energy was varied for a fixed detector angle. The recoil energy corresponding to each incident beam energy was calculated as mentioned above. Usually two or three calibration points were taken. The stopping gas was then admitted into the chamber at an appropriate pressure and the centroid of the recoil-particle peak was again measured, the recoils having passed through a known number of stopping atoms per cm^2. The gas was pumped out and the calibration runs were repeated. The second calibration was performed to correct for carbon deposited on the target foil during the energy-loss run. The energy loss ΔE_o of the recoils was calculated from the centroids of the calibration and energy-loss runs and usually amounted to 15 - 20% of the initial recoil energy. In order to minimize the effect of carbon deposition, each of the runs was limited to about 15 minutes, and after each sequence of calibration, energy-loss, and calibration runs, the target position was changed by a distance equal to the beam diameter so as to expose a fresh target area to the beam. Samples of the spectra obtained in the Si detector for two vacuum calibration runs and the corresponding energy-loss run for C recoils in He are shown in Figure 48.

The lowest recoil energy attainable for Al in Xe in the present experiment was 790 keV. At lower Al recoil energies, the recoil peak was obscured by a sharply rising background. Similar conditions were found for the other ion-absorber combinations. This background was not electronic in origin, as it existed only when the ^{4}He beam was on target. It presumably was due to ^{4}He particles being scattered into the detector after being multiply scattered in the

target chamber. An example of some of the spectra obtained for Al
ions in He gas and in vacuum at a recoil energy near the lowest
measured is shown in Figure 49. The high-energy limit occurred
when interference with other peaks (thought to be due to inelastic
scattering or other reactions) became too severe.

Because of the relatively high energy of the recoils (all recoil
energies were above 560 keV) and because of the geometry of the
experiment (favoring only small-angle scattering from the original
recoil direction), the observed stopping cross section S_o is assumed
to be the electronic stopping cross section S_e. As an example, for
700-keV C ions in Xe, the LSS theory predicts that
$(d\epsilon/d\rho)_n/(d\epsilon/d\rho)_e = 0.03$, where $(d\epsilon/d\rho)_n$ is the total nuclear stopping
power for scattering into all angles.

The observed stopping cross-section S_o is defined to be

$$S_e = S_o \equiv \frac{\Delta E_o}{N\Delta R} \quad \text{at the average energy} \quad E = E_i - \frac{\Delta E_o}{2}$$

where

ΔE_o = energy lost by recoils of initial energy E_i

and

$$N\Delta R = AL \; \frac{273}{T + 273} \; \frac{P}{760}$$

with

$A = 2.687 \times 10^{19}$ atoms/atm-cm^3 (for monatomic gases)

L = ion path length in the stopping gas = 8.92 ± 0.04 cm

T = gas temperature in $^\circ$C = 22.5 ± 1.0 $^\circ$C

P = gas pressure in Torr

The principal components of the uncertainty in the recoil energy to which an S_e is assigned are the $\pm 1/2^O$ uncertainty in detector angle and the 8% uncertainty in the Ni entrance foil thickness; the total uncertainty in recoil energy is the rms sum of the partial uncertainties in recoil energy due to uncertainties in detector angle, Ni entrance foil thickness, and target thickness. No uncertainty was included from making the approximation that the average energy $E = E_i - \Delta E_o/2$ be assigned to S_e, since usually $\Delta E_o/E_i = 0.15$-0.20.

The principal component of the uncertainty in S_e usually arose from the change in pulse-height calibration between the first and second calibration runs, due to carbon build-up on the target. The $\Delta E_o(1)$ computed using the recoil-peak centroids from the energy-loss and first calibration runs was averaged with the $\Delta E_o(2)$ computed from the energy-loss and second calibration runs to form the average ΔE_o quoted in Tables XXI - XXIV. The uncertainty in ΔE_o was the rms sum of the deviation of $\Delta E_o(1)$ from ΔE_o and the uncertainty in $\Delta E_o(1)$ arising from uncertainties in the centroids of the peaks.

3. Results

The measured electronic stopping cross sections for ^{12}C and ^{27}Al in He and Xe are given in Tables XXI - XXIV and are illustrated in Figures 50 - 52. These tables also include some measured quantities relevant to the calculation of S_e. Table XXV includes the values of the exponent p and coefficient K found from a least-squares fit of the present data to a function of the form $S_e = KE^p$, along with

the values obtained theoretically by Lindhard and Scharff (1961). In all cases, the ion velocity v satisfies the relation $v \leq v_o Z_1^{2/3}$ (where Z_1 is the ion atomic number and $v_o = c/137$) and thus the LS theory given by Equation 10 of Chapter III is expected to apply. This theory predicts that S_e varies as the square root of the ion energy.

4. Comparison with Other Measurements

Hvelplund (1971) measured the electronic stopping cross section S_e for ^{12}C in ^4He in the energy interval 200 - 500 keV. He presents his experimental results as the function $S_e = 1.30 \times 10^{-15} [E(keV)]^{0.50}$ ev-cm^2/atom, corresponding to the best fit through his experimental data points, and estimates that the correct stopping cross section lies within 5% of that relation. As can be seen from Figure 50, the present data are in excellent agreement with his results, the agreement being within 5% in the region where the data (nearly) overlap.

The only other results with which to compare the present data are those of Northcliffe and Schilling (1970). The electronic stopping powers quoted by those authors are not experimentally measured data but are rather the result of a calculation incorporating extrapolations of smoothed stopping-power data from other combinations of ion, absorber, and ion energy and guided by simple theoretical expectations. These calculated results are also plotted in Figures 50 - 52.

5. Discussion

For C in He and Xe, the exponents p are 0.47 and 0.49, respectively, while for Al, the exponents p are 0.97 and 1.05, respectively. It thus appears from these data that the exponent in this energy range depends on the incident ion and not on the absorber. This same general trend can be found in the work of Hvelplund (1971), who measured S_e for ions with $2 \leq Z_1 \leq 12$ in He, air, and Ne, and in the combined work of Hvelplund and Fastrup (1968) and Fastrup, Hvelplund, and Sautter (1966), who measured S_e for ions with $6 \leq Z_1 \leq 39$ and energies $0.1 \leq E \leq 1.5$ MeV in carbon. In Figure 5 of their paper, Hvelplund and Fastrup (1968) show oscillations of the exponent p as a function of Z_1 about the LS value of $p = 0.5$.

While the exponent p for C in He and Xe agrees with the LS theory, the exponent p for Al in He and Xe disagrees with this theory by a factor of 2. Absolute deviations of S_e from the theory vary from 0 to as much as a factor of 2 in the case of Al in He.

Because the results of this experiment do not extend below 800 keV, no definite statements can be made about the rate of energy loss of Al in Xe at energies of a few hundred keV, which is the case of greatest relevance to the present DSAM measurements. For this reason, no change in the DSAM analysis will be made on the basis of these data. However, it must be noted that to some extent, the assumptions made in the DSAM analysis have not been verified.

The first assumption made is that S_e varies as $E^{1/2}$ for all ions in all gases, and in particular, for Al in Xe. This assumption is clearly not justified in this energy range for Al in Xe and

He, where S_e varies more nearly as E^1, but it is verified for C ions in these gases. The effect of an essentially linear variation of S_e with ion energy upon the lifetimes derived from measured DSAM factors F is investigated in Appendix B for the case of ^{26}Al slowing in Xe gas.

The second assumption is that the observed oscillations of S_e as a function of Z_1 do not depend on the absorber, and that these oscillations can be accounted for by appropriately adjusting the coefficient K in the relation $S_e = KE^{1/2}$. (In Chapter IV, the scaling factor $f_e(Z_1, \overline{v}/v_o)$ for Al due to the Z_1 oscillations was taken to be 0.68.) The present experimental results do not directly affirm or deny the validity of this assumption. They do suggest that the exponent p in the relation $S_e = KE^P$ is independent of the absorber.

The third assumption is that S_e for heavy ions in gases is systematically less than the prediction of LS theory, due presumably in some fashion to the gaseous state of the absorber. This deviation from theory amounts experimentally to as much as 40 - 50% in He, air, N and Ar. For Al in Xe, the reduction was taken to be about 50%. Combining the two reduction factors above, it was expected that S_e for Al in Xe would be about 35% of the LS predicted value at ion energies of a few hundred keV. While this assumption is not verified at higher energies (indeed, from this work S_e for Al ions slowing in Xe gas is greater than the LS prediction at energies above 800 keV), an extrapolation of the observed S_e-versus-E curve to energies E < 250 keV suggests that below this energy, S_e may be of roughly the right magnitude to be consistent with this third

assumption. For example, at $E = 250$ keV, $S_e = 0.54\ S_e(LS)$, while at 100 keV, $S_e = 0.35\ S_e(LS)$.

While no corrections will be made to the present DSAM analysis, it is clear that more experimental information about the rate of energy loss for the nuclei of interest in the stopping gases used is necessary before greater precision is possible in the gas-absorber version of the Doppler-shift-attenuation technique. Experimental determinations of S_e at ion energies of greatest applicability to DSAM lifetime measurements ($E \leq 500$ keV) could be carried out with apparatus similar to that of the present experiment if the ^{4}He particles involved in the scattering of the recoils from the target were measured in coincidence with those recoils; such a coincidence requirement might well eliminate the sharply rising background that interfered with the present experiments below 600 - 800 keV ion energy. Such measurements might also be accomplished by using a low-energy accelerator to accelerate directly the ion species of interest; observation of the beam energy both in vacuum and in the stopping gas of known areal density determines the stopping power directly.

APPENDIX A

PROGRAM FOR COMPUTING THE DSAM FACTOR F

A listing of the computer program used to calculate the Doppler-shift-attenuation factor F as a function of τ/α (where τ is the level lifetime and α is the slowing-down time) is given below, along with a sample of the computer output. The factor F is computed from Equations 21, 24 and 25, with the various quantities defined in Chapter III. The computer program incorporates the assumptions made in Chapter IV. That is, it is assumed that the nuclear stopping power is given by the LSS (1963) theory, as approximated by the analytic functions in Chapter IV and modified by the scaling factor f_n, so that

$$-(d\epsilon/d\rho)_n = 0.40 \, f_n \epsilon^{-1/2} \quad \text{for } 1.2 \leqq \epsilon \leqq \epsilon_o$$

$$-(d\epsilon/d\rho)_n = 0.38 \, f_n \quad \text{for } 0.01 \leqq \epsilon \leqq 1.2$$

It is further assumed that the value of $\overline{\cos \phi}$ is given by the Blaugrund (1966) formulation. Finally, it is assumed that the electronic stopping power is given by the LS (1961) formulation, modified by the scaling factor f_e, so that

$$-(d\epsilon/d\rho)_e = f_e k \epsilon^{1/2}$$

The constant k is given in Equation 15, and k is linearly dependent on ξ_e. The data necessary for the computation are provided on two cards. These are

CARD 1: Z1, A1, Z2, A2, D, BETA, TAU, DEFDX, CHI

CARD 2: B1, B2

where

Z1, A1 = atomic number, mass of nucleus undergoing decay

Z1, A2 = atomic number, mass of stopping atom

D = density of stopping medium in g/cm^3

BETA = $v(0)/c$, where $v(0)$ is the initial velocity of the nucleus

TAU = estimated level lifetime (used to calculate the effect upon F of the variation in detector efficiency with distance)

DEFDX = fractional change of detector efficiency per cm

CHI = $f_e \xi_e = f_e Z_1^{1/6}$

B1 = $0.40 f_n$

B2 = $0.38 f_n$

The output is a table of values for TAU/ALF, F(ALPHA), F(DEVONS), F1, and F1/F, where

TAU/ALF = ratio of lifetime to electronic slowing-down time

F(ALPHA) = DSAM factor F

F(DEVONS) = DSAM factor F for electronic slowing-down time

F1 = DSAM factor F corrected for variation in detector efficiency with distance

F1/F = F1/F(ALPHA) = correction for detector efficiency variation

The calculation is then repeated for a 10% increase in BETA. The computation may be performed for other cases by addition of more pairs of data cards.

```
C           R.W.KAVANAGH F(ALPHA) FOR DOPPLER SHIFT ATTENUATION
C           REF. A.E.BLAUGRUND N P 88(1966)501
C
            DIMENSION ALPHA(200),FZERO(200),   FOA(200),AOA(200),ACT(200)
            DIMENSION T1(201),T2(201) ,T3(201),T4(201)
            DIMENSION F1(200),VAR(200),F1BF(200),BET(2)
            REAL LACA(200)
            REAL K,M
   10    CONTINUE
            READ(5,100)Z1,A1,Z2,A2,D,BETA,TAU,DEFOX,CHI
  100    FORMAT(4F5.0,2F10.0,E10.0,2F10.0)
            IF(DEFOX.EQ.0.)DEFOX = 0.5
            BET(1) = BETA
            BET(2) = 1.1*BETA
         READ(5,101) B1,B2
  101    FORMAT(2F10.0 )
            Z123 = Z1**(2./3.)
            Z223 = Z2**(2./3.)
            ZZ = Z123 + Z223
            A = 4.68E-09/SQRT(Z123+Z223)
            K = 0.0793*   CHI     *SQRT(Z1*Z2)*((A1+A2)**1.5) /
     1  ((((Z123+Z223)**.75)*SQRT(A1**3)*SQRT(A2))
            M = 1630.*A1*A2/(Z1*Z2*(A1+A2)*SQRT(Z123+Z223))
            RHO = 12.5663706*A*A*D*6.02E+23*A1/((A1+A2)**2)
            TO = 4.57E-09/RHO
            ALFO = TO*SQRT(2.*M)/K
            G = 1. + 0.667*A1/A2 - .465*A1*A1/(A2*A2)
         IF(A1.GT.A2) G = 0.667 + .535*A2/A1
         N = 101
         NN = 49
            WRITE(6,200)Z1,A1,Z2,A2,D,       TAU,DEFOX           ,CHI
  200    FORMAT(55H1CALCULATIONS OF F(ALPHA) FOR DOPPLER SHIFT ATTENUATION
     1/11H WITH Z1 = F3.0, 7H, A1 = F3.0, 18H STOPPING IN Z2 = F3.0,
     2 7H, A2 = F4.0, / 1H0 5X5H100*D 7X3HTAU 4X6HDEF/DX 7X3HCHI /
     3 1H 2PF10.4,1PE10.2, 0P2F10.4)
            WRITE(6,203)A,K,M,RHO,TO,ALFO,     ZZ,G
  203    FORMAT(1H0 10X1HA 10X1HK 10X1HM 8X3HRHO / 1H 1P4E11.3, /
     1  1H0 9X2HTO 4X7HALPHA-0 9X2HZZ 10X1HG / 1H 1P4E11.3 )
            WRITE(6,204)
  204    FORMAT(32HORANGE HEREIN IS ALONG THE PATH. /63H SEE LINCHARD, SCH
     1ARFF, AND SCHIOTT (1963) FOR PROJECTED RANGE.            )
C
C
C
C           LOOP FOR BETA AND 1.1*BETA
C
            DO 6 IBETA = 1,2
            BETA = BET(IBETA)
            EPSO = M/2.*((137.*BETA)**2)
C
C
C
C           REVISION TO ADD DE/DXO AND RANGE
C           DE/DXO IS INITIAL ENERGY LOSS IN KEV PER CENTIMETER (1 ATMOS)
C           RANGE IS IN CENTIMETERS AT ONE ATMOSPHERE
C
C
            UL2 = SQRT(EPSO)
```

```
      UL1 = SQRT(1.2)
      DY1 =(UL1-0.1)/FLOAT(N-1)
      DY2 = (UL2-UL1)/FLOAT(N-1)
      Y1 = 0.1
      Y2 = UL1
      DO 20 I = 1,N
      T1(I) =Y1/(0.38 + K*Y1)
      T2(I) = Y2*Y2 / (0.4 + K*Y2*Y2)
      Y1 = Y1 + DY1
   20 Y2 = Y2 + DY2
      S1 = 0.
      S2 = 0.
      DO 21 I = 1,NN
      S1 = S1 + 4.*T1(2*I) + 2.*T1(2*I+1)
      S2 = S2 + 4.*T2(2*I) + 2.*T2(2*I+1)
   21 CONTINUE
      RI1 = DY1/3.*(S1 + 4.*T1(N-1) + T1(N)+ T1(1)          )
      RI2 = DY2/3.*(S2 + 4.*T2(N-1) + T2(N)+ T2(1)           )
      RANGE = 4.19E+08*TO*(RI1 + RI2)
      DEDXO = 2.29E-07/TO*A1/M*(K*UL2 + 0.4/UL2)
     C1=B1/(EPSO*K)
      C2 = B2/K
      WRITE(6,209)BETA,EPSO,B1,B2,DEDXO,RANGE
  209 FORMAT(1H0 2X8H100*BETA 6X5HEPS-0 9X2HB1 9X2HB2 5X6HDE/DXO
     1 6X5HRANGE / 1H 2PF10.4, 1P5E11.3 )
      NALPHA = 15
C
C     NOTE  IN ALL THIS I CALL ALPHA/TAU JUST ALPHA
C
      DO 1 I = 1,NALPHA
    1 ALPHA(I) = 1./128.*(2.**FLOAT(I-1))
      CONST = ((C1 + 1.2/EPSO)/(C1 + 1.))
      DE1 = (1.-(1.2/EPSO))/FLOAT(N-1)
      DE2 = (SQRT(1.2)-0.1    )/FLOAT(N-1)
     P2=G*A2/(2.*A1)+ 0.5
      DO 4 J = 1,NALPHA
     E1=1.2/EPSO
      E2 = 0.1
      P1 = ALPHA(J)/2.-G*A2/(2.*A1)-1.
C
C     LOOP TO COMPUTE INTEGRANDS
C
      DO 2 I = 1,N
     T1(I)=(E1+C1)**P1*E1**P2
      T2(I) = ((C2+E2)/(C2 + 1.095))**(1.+2.*P1) * E2**(2.*P2)
      T3(I) = E1**(P1+P2)
      T4(I) = (E2/1.095)**(1.+2.*P1) *E2**(2.*P2)
      E1 = E1 + DE1
      E2 = E2 + DE2
    2 CONTINUE
C
C     INTEGRATION DONE USING SIMPSON'S RULE WITH 101 POINTS
C
      S1 = 0.
      S2 = 0.
      S3 = 0.
```

```
      S4 = 0.
      DU 3 I = 1,NN
      S1 = S1 + 4.*T1(2*I) + 2.*T1(2*I+1)
      S3 = S3 + 4.*T3(2*I) + 2.*T3(2*I+1)
      S4 = S4 + 4.*T4(2*I) + 2.*T4(2*I+1)
    3 S2 = S2 + 4.*T2(2*I) + 2.*T2(2*I+1)
      FI1 = DE1/3.*(S1 + T1(1) + 4.*T1(N-1) + T1(N))   *
    1 1./((1.+C1)**(1.+P1))
      PWR = CCNST**(1.+P1)
      FI2 = DE2/3.*(S2 + T2(1) + 4.*T2(N-1) + T2(N))
    1 *(2./(EPS0**P2*(1.095 + C2))*PWR )
      FI3 = DE1/3.*(S3 + T3(1) + 4.*T3(N-1) + T3(N))
      FI4 = DE2/3.*(S4 + T4(1) + 4.*T4(N-1) + T4(N))   *
    1 (2./(EPS0**P2*1.095)*((1.2/EPS0)**(1.+P1)))
      FOA(J) = ALPHA(J)/2.*FI1 + ALPHA(J)/2.*FI2
      FZERO(J) = ALPHA(J)/2.*FI3 + ALPHA(J)/2.*FI4
      AOT(J) = ALPHA(J)*TAU
      AOA(J) =   ALF0/AOT(J)
      LAOA(J) = ALOG10(AOA(J))
      EFFK = DEFDX*BETA*3.E+10*TAU
      F1BF(J) = (1.+EFFK*FOA(J)/(2.-FOA(J)))/(1.+EFFK*FOA(J))
      F1(J) = F1BF(J)*FCA(J)
      VAR(J) = 1./ALPHA(J)
    4 CCNTINUE
      WRITE(6,202)
  202 FORMAT(1H0 3X7HTAU/ALF 4X8HF(ALPHA)2X10HF(DEVONS ) 1CX2HF1
    1 8X4HF1/F )
      WRITE(6,201)(VAR(J),FOA(J),FZERO(J),F1(J),F1BF(J),J=1,NALPHA)
  201 FCRMAT(1H 0PF10.5,1P4E12.4)
    6 CCNTINUE
      GO TO 10
      END
```

CALCULATICNS OF F(ALPHA) FCR DOPPLER SHIFT ATTENUATION
WITH Z1 = 15., A1 = 30. STOPPING IN Z2 = 54., A2 = 131.

100*D	TAU	DEF/DX	CHI
0.5400	4.50E-11	0.5000	0.8240

A	K	M	RHO
1.037E-C9	2.1C7E-01	1.088E 01	5.084E 01

TO	ALPHA-O	ZZ	G
8.989E-11	1.991E-C9	2.037E 01	1.128E C0

RANGE HEREIN IS ALCNG THE PATH.
SEE LINDHARD, SCHARFF, AND SCHIOTT (1963) FCR PROJECTED RANGE.

100*BETA	EPS-0	B1	B2	DE/DXO	RANGE
0.6200	3.926E 00	3.200E-01	3.040E-01	4.349E C3	1.289E-01

TAU/ALF	F(ALPHA)	F(DEVCNS)	F1	F1/F
128.00000	1.5493E-03	7.3619E-03	1.5493E-03	1.0J00E 00
64.C0000	3.0949E-03	1.4628E-02	3.0949E-03	9.9999E-U1
32.C0000	6.1753E-C3	2.8880E-02	6.1752E-C3	9.9999E-01
16.C0000	1.2293E-02	5.6302E-02	1.2293E-02	9.9998E-01
8.C0000	2.4358E-C2	1.C715E-01	2.4356E-02	9.9995E-U1
4.C0OC0	4.7823E-02	1.95C4E-01	4.7818E-02	9.9990E-01
2.C0000	9.2234E-02	3.2931E-01	9.2217E-02	9.9982E-J1
1.CC0C0	1.7197E-01	4.9848E-U1	1.7191E-01	9.9967E-J1
0.50C00	3.0172E-C1	6.6644E-01	3.0156E-C1	9.9948E-C1
C.25000	4.7959E-01	7.9998E-01	4.7926E-01	9.9931E-01
0.12500	6.6739E-01	8.8888E-C1	6.6652E-C1	9.9930E-U1
0.06250	8.1298E-01	9.4116E-01	8.1254E-01	9.9947E-01
0.03125	9.0160E-01	9.6966E-01	9.0130E-01	9.9966E-J1
0.01562	9.4961E-01	9.8455E-01	9.4943E-01	9.9981E-01
C.00781	9.7449E-01	9.9229E-01	9.7439E-01	9.9990E-C1

100*BETA	EPS-0	B1	B2	DE/DXO	RANGE
0.6820	4.751E 00	3.2C0E-01	3.040E-01	4.513E C3	1.535E-01

TAU/ALF	F(ALPHA)	F(DEVCNS)	F1	F1/F
128.C0CC0	1.7417E-03	7.3976E-03	1.7417E-03	1.0000E 00
64.00000	3.4788E-03	1.4658E-02	3.4788E-03	9.9999E-C1
32.C0CC0	6.9394E-03	2.9013E-02	6.9393E-03	9.9998E-U1
16.C0000	1.3807E-02	5.6545E-02	1.3806E-02	9.9997E-C1
8.C0000	2.7328E-02	1.0755E-01	2.7326E-02	9.9994E-01
4.C0CU0	5.3543E-C2	1.9560E-U1	5.3536E-02	9.9988E-01
2.C0000	1.0285E-C1	3.29E5E-C1	1.0283E-01	9.9978E-01
1.C0000	1.9033E-01	4.9875E-01	1.9025E-01	9.9961E-01
C.50000	3.2957E-C1	6.665CE-C1	3.2937E-01	9.9939E-01
C.25000	5.1349E-01	7.9998E-01	5.13C9E-01	9.9925E-01
0.12500	6.9770E-01	8.8888E-01	6.9719E-01	9.9926E-01
C.C6250	8.3310E-01	9.4115E-01	8.3265E-01	9.9945E-01
0.03125	9.1289E-01	9.6964E-U1	9.1259E-01	9.9966E-01
C.01562	9.5554E-C1	9.8452E-01	9.5536E-01	9.9981E-01
C.00781	9.7754E-01	9.9229E-01	9.7745E-01	9.9990E-01

APPENDIX B

APPLICATION OF MEASURED ELECTRONIC STOPPING POWER DATA TO COMPUTATION OF THE DSAM FACTOR F

In Chapter VII, the measurement of the electronic stopping cross section S_e as a function of ion energy for ^{12}C and ^{27}Al in He and Xe is discussed and the experimental results are compared with the Lindhard-Scharff (1961) theory and with other experimental and semiempirical data. In particular, the LS theoretical formulation predicts that the electronic stopping cross section S_e is given by the relation

$$S_e = \xi_e 8\pi e^2 a_o Z_1 Z_2 (Z_1^{2/3} + Z_2^{2/3})^{-3/2} (v/v_o) = KE^{1/2} \qquad (28)$$

where

$K =$ a constant of proportionality

$$\xi_e = Z_1^{1/6}$$

and all the other symbols are defined in Chapter III. For the case of ^{27}Al ions in Xe gas, the theoretical prediction is

$$S_e(LS) = 9.03 \times 10^{-15} [E(keV)]^{0.5} \text{ ev-cm}^2/\text{atom} \qquad (29)$$

In contrast to this theoretical value, the experimentally measured S_e has the form

$$S_e(EXP) = 0.23 \times 10^{-15} [E(keV)]^{1.05} \text{ev-cm}^2/\text{atom} \qquad (30)$$

for ^{27}Al ions in the energy range $800 \leq E \leq 2200$ keV. That is, the measured electronic stopping cross section depends nearly linearly on the energy instead of on its square root, at least over the energy

range investigated. If this linear dependence were to extend down to zero energy, the question then arises of what effect this would have on the nuclear lifetimes as measured by the Doppler-shift-attenuation method. That problem is treated in this Appendix.

Because the electronic stopping cross section has been measured for ^{27}Al ions in Xe and because Xe has been the principal stopping gas used in the DSAM lifetime measurements, the specific case that will be treated in this context is the lifetime of the 418-keV level of ^{26}Al, discussed in detail in Sections 4 and 5 of Chapter IV. The lifetime of the level is known from direct electronic timing measurements (Endt and Van der Leun 1967) to be $\tau = 1.82 \pm 0.04$ ns. In Section 5 of Chapter IV, the lifetime of this level in ^{26}Al is used to determine the stopping parameters for ^{26}Al ions in Xe gas. The results of that section are reviewed here. At a Xe gas pressure of 0.519 atm and for an initial ion recoil velocity and energy of $\beta(0) = 0.00728$ and E = 640 keV, the observed DSAM factor F is F = 0.41 ± 0.03. The measured F value and the initial velocity above lead to a value $f_e(Z_1, \overline{v}/v_o) = 0.68$ from Table I. The measured F value is then used to determine the values of f_e(gas) necessary to reproduce the known lifetime of $\tau = 1.82 \pm 0.04$ ns when f_n takes on the values $f_n = 1.0, 0.8$ and 0.6. Experimentally, it is observed that the derived lifetime is too short, and that the electronic and/or nuclear stopping power must be reduced to obtain longer lifetimes. For example, when $f_n = 0.8$, then f_e(gas) = 0.50 ± 0.15 is necessary to obtain the correct lifetime. However, this whole analysis is based on the assumption that the electronic

stopping cross section varies as the square root of the energy, or
in the LSS dimensionless notation,

$$-(d\epsilon/d\rho)_e = f_e k \epsilon^{1/2} \, .$$

In order to investigate the effect on the calculated DSAM factor F of
a linear dependence of $(d\epsilon/d\rho)_e$ on ϵ, the DSAM factor F has
been recomputed using an electronic stopping power of the form

$$-(d\epsilon/d\rho)_e = k'\epsilon^{1.05} \qquad k' = 0.152$$

where k' has been extracted from the measured electronic stopping
cross section data for ^{27}Al ions in Xe.

Before giving the results of that full numerical calculation,
it might be appropriate to consider the approximation in which
nuclear stopping and scattering are neglected; that is, we consider
the approximation in which only the electronic energy loss is impor-
tant. In Figure 53 is shown a graph of the electronic stopping cross
section S_e as a function of ion energy for ^{27}Al in Xe for three
different functional dependences. Curve (a) is a graph of the experi-
mentally measured S_e for ^{27}Al in Xe gas and is given by Equation 30
above. This functional dependence has been verified experimentally
only in the energy range $800 < E < 2200$ keV, but has been extended
to zero energy for the purposes of this discussion. Curve (b) is a
graph of the LS theoretical prediction ($f_e = 1$) as given by Equation 29.
As in Figure 52, the two curves intersect at about 800 keV ion
energy. Curve (c) is the LS prediction scaled down by a factor
$f_e = f_e(Z_1, \bar{v}/v_o) = 0.68$. The initial energy for the ^{26}Al ions in the

)oppler-shift-attenuation measurement is 640 keV and is also indi-
ated on the figure. Consider now the expected DSAM factor F for
he decay of the 418-keV level of ^{26}Al when the rate of electronic
energy loss is described by curves (a) and (b). At all energies below
;00 keV, the rate of electronic energy loss for curve (a) is less
han that for curve (b), and therefore the ^{26}Al ion velocity at any
inite time t is greater for curve (a) than for curve (b). The ^{26}Al
lecay γ rays will be produced at a higher mean velocity for curve
a), and for a given level lifetime, the DSAM factor F will be
;reater for curve (a) than for curve (b). Conversely, a given
measured F value leads to a longer lifetime for an electronic
energy loss described by curve (a) than for that described by curve
b), and thus leads to better agreement with the known lifetime.
This qualitative result is verified by an exact calculation. However,
the rate of electronic energy loss used in the analysis of the ^{26}Al
lifetime data is not curve (b), where $f_e = 1$, but rather is curve (c),
with $f_e = f_e(Z_1, \overline{v}/v_o) = 0.68$, which takes into account the velocity-
dependent oscillations of S_e with Z_1. In this case, it is not obvious
whether curve (a) or curve (c) leads to a greater lifetime τ for a
given value of F, since curve (c) lies partly above and partly below
curve (a) for different values of the ion energy. This qualitative
ambiguity is enhanced by the fact that in the actual energy-loss
process, nuclear stopping and scattering will tend to wash out any
difference produced between curves (a) and (c), particularly at
energies below 130 keV, where the nuclear stopping power (for
$f_n = 0.8$) equals the electronic stopping power of curve (c).

In order to include the effects of nuclear stopping and scattering as well as the experimentally measured dependence of S_e on energy for ^{27}Al in Xe, a computer program has been written (N. M. Denkin, 1972) to compute the Doppler-shift-attenuation factor F as a function of the nuclear lifetime τ for electronic and nuclear energy losses of the form

$$-(d\epsilon/d\rho)_e = k'\epsilon^{p'} \quad \text{for} \quad 0.01 < \epsilon < \epsilon_o$$

$$-(d\epsilon/d\rho)_n = m_1 \epsilon^{n_1} \quad \text{for} \quad 1.2 < \epsilon < \epsilon_o$$

$$-(d\epsilon/d\rho)_n = m_2 \epsilon^{n_2} \quad\quad 0.01 < \epsilon < 1.2$$

where k', m_1 and m_2 are arbitrary real numbers and where p', n_1 and n_2 are arbitrary positive or negative real numbers. This computer program includes the relations for $\overline{\cos\phi}$ due to nuclear scattering formulated by Blaugrund (1966). The results of calculations of F with this computer program agree with the results obtained with the computer program of Appendix A when the same stopping parameters are used in both. For the particular case under consideration, the constants m_1, m_2, n_1 and n_2 are chosen so as to agree with the LSS formulation of the nuclear stopping power with $f_n = 0.8$. That is, the constants are $m_1 = 0.32$, $n_1 = -0.50$, $m_2 = 0.304$ and $n_2 = 0$. Furthermore, p' is taken as $p' = 1.05$ as determined experimentally. The constant k' for ^{26}Al in Xe gas is $k' = 0.152$, taking into account the mass difference between ^{26}Al and ^{27}Al. This constant k' can be obtained by setting $(d\epsilon/d\rho)_e$(EXP) equal to $(d\epsilon/d\rho)_e$(LS) at an ion energy $E = 800$ keV, so that

$$k'\epsilon^{1.05} = k(LSS)\epsilon^{0.5} \quad \text{for} \quad E = 800 \text{ keV}.$$

For ^{27}Al ions in Xe at an energy $E = 800$ keV, the dimensionless energy is $\epsilon = 6.90$ and the constant $k(LSS)$ is $k(LSS) = 0.424$. The conversion factor for ^{27}Al to ^{26}Al is 1.04. Using the constants defined above, the Doppler-shift-attenuation computer program of Denkin (1972) has been used to obtain the lifetime of the 418-keV level of ^{26}Al from the measured DSAM factor $F = 0.41 \pm 0.03$. This result has been compared with the result obtained employing the analysis of Chapter IV using the computer program of Appendix A with $f_n = 0.8$ and with $f_e = f_e(Z_1, \overline{v}/v_o) = 0.68$ (i.e., f_e(gas) = 1). The value of k for this case is $k = 0.302$. The lifetime obtained with an electronic stopping power of the form $-(d\epsilon/d\rho)_e = 0.152 \, \epsilon^{1.05}$ is $\tau(418) = 1.33 \pm 0.16$ ns, while the lifetime obtained with the method of analysis adopted in Chapter IV, leading to an electronic stopping power of the form $-(d\epsilon/d\rho)_e = 0.302 \, \epsilon^{0.50}$, is $\tau(418) = 1.36 \pm 0.16$ ns. The result of the numerical calculation of F as a function of τ is given for both cases in Figure 54. From this figure, it can be seen that the two curves lie nearly on top of one another; the greatest deviation occurs for short lifetimes. This is the anticipated result, since for short lifetimes, the electronic stopping power is dominant for this case. For both forms of the electronic stopping power, the derived lifetime is smaller than the known lifetime ($\tau(418) = 1.82 \pm 0.04$ ns), thus requiring a reduction of the electronic and/or nuclear stopping power, as was carried out in Chapter IV. It thus appears that the analysis adopted in Chapter IV

is still valid even though for this case the actual dependence of the electronic energy loss on ion energy is different from that assumed.

REFERENCES

F. Ajzenberg-Selove, 1971, Nucl. Phys. A166, 1.

T. K. Alexander and K. W. Allen, 1965, Can. J. Phys. 43, 1563.

R. J. Ascuitto, D. A. Bell and J. P. Davidson, 1968, Phys. Rev. 176, 1323.

R. E. Azuma, L. W. Oleksiuk, J. D. Prentice and P. Taras, 1966, Phys. Rev. Lett. 17, 659.

R. E. Azuma, N. Anyas-Weiss and A. M. Charlesworth, 1968, Nucl. Phys. A109, 577.

F. G. Bailey and D. C. Choudhury, 1970, Nucl. Phys. A144, 628.

G. C. Ball, W. G. Davies, J. S. Forster, A. N. James and D. Ward, 1972, to be published.

T. T. Bardin, J. A. Becker, R. E. McDonald and A. D. W. Jones, 1970, Phys. Rev. C 2, 2283.

R. D. Barton, J. S. Wadden, A. L. Carter and H. L. Pai, 1971, Can. J. Phys. 49, 971.

R. Bass and R. Wechsung, 1970, Phys. Letters 32B, 602.

J. A. Becker, L. F. Chase, Jr., D. B. Fossan and R. E. McDonald, 1966, Phys. Rev. 146, 761.

J. A. Becker and E. K. Warburton, 1971, Phys. Rev. Letters 26, 143.

R. A. I. Bell, J. L'Ecuyer, R. D. Gill, B. C. Robertson, I. S. Towner and H. J. Rose, 1969, Nucl. Phys. A133, 337.

I. Bergström and B. Domeij, 1966, Nucl. Inst. and Meth. 43, 146.

M. Bini, P. G. Bizzeti, A. M. Bizzeti-Sona, A. Cambi, M. Mandó and P. R. Maurenzig, 1971, Nuovo Cimento 4A, 45.

G. A. Bissinger, P. A. Quin and P. R. Chagnon, 1968, Nucl. Phys. A115, 33.

G. A. Bissinger, P. A. Quin and P. R. Chagnon, 1969, Nucl. Phys. A132, 529.

A. E. Blaugrund, 1966, Nucl. Phys. 88, 501.

A. E. Blaugrund, A. Fisher and A. Schwarzschild, 1968, Nucl. Phys. $\underline{A107}$, 411.

J. F. Boulter and W. V. Prestwich, 1970, Can. J. Phys. $\underline{48}$, 868.

M. C. Bouten, J. P. Elliott and J. A. Pullen, 1967, Nucl. Phys. $\underline{A97}$, 113.

F. Brandolini, J. Benuzzi-Martins, R. A. Ricci and C. Signorini, 1969, Lett. Nuovo Cimento $\underline{2}$, 600.

F. Brandolini and C. Signorini, 1969, Phys. Letters $\underline{30B}$, 342.

F. Brandolini, C. Signorini and P. Kusstatscher, 1971, Nucl. Inst. and Meth. $\underline{91}$, 341.

J. W. Champlin, A. J. Howard and J. W. Olness, 1971, Nucl. Phys. $\underline{A164}$, 307.

D. M. Clement and E. Baranger, 1968, Nucl. Phys. $\underline{A108}$, 27.

CRC Handbook of Chemistry and Physics, 1968, (The Chemical Rubber Co., Cleveland, Ohio, 1968) 49th ed., B-188.

J. E. Cummings and D. J. Donahue, 1970, Nucl. Phys. $\underline{A142}$, 609.

W. M. Currie, 1969, Nucl. Inst. and Meth. $\underline{73}$, 173.

J. A. Davies and G. A. Sims, 1961, Can. J. Chem. $\underline{39}$, 601.

N. M. Denkin, 1972, private communication.

A. de-Shalit, Nuclear Structure and Electromagnetic Interactions, ed. N. MacDonald (Oliver and Boyd, Edinburgh, 1965) p. 1.

S. Devons, G. Manning and D. St. P. Bunbury, 1955, Proc. Phys. Soc. (London) $\underline{A68}$, 18.

S. Devons, 1960, Nuclear Spectroscopy Part A, edited by F. Ajzenberg-Selove (Academic Press, New York), 512.

A.E.L. Dieperink and P. J. Brussaard, 1968, Nucl. Phys. $\underline{A106}$, 177.

A.E.L. Dieperink, H. P. Leenhouts and P. J. Brussaard, 1968, Nucl. Phys. $\underline{A116}$, 556.

A.E.L. Dieperink and P. J. Brussaard, 1969a, Nucl. Phys. $\underline{A128}$, 34.

A.E.L. Dieperink and P.W.M. Glaudemans, 1969b, Phys. Letters 28B, 531.

D. J. Donahue and R. L. Hershberger, 1971, Phys. Rev. C 4, 1693.

D. D. Duncan, K. H. Buerger, R. L. Place and B. D. Kern, 1969, Phys. Rev. 185, 1515.

P. M. Endt and C. Van der Leun, 1967, Nuc. Phys. A105, 1.

G.A.P. Engelbertink and P.W.M. Glaudemans, 1969, Nucl. Phys. A123, 225.

G.A.P. Engelbertink, K. W. Jones, J. W. Olness and E. K. Warburton, 1970, Phys. Letters 33B, 353.

R. Engmann, E. Ehrmann, F. Brandolini and C. Signorini, 1971, Nucl. Phys. A162, 295.

L. Eriksson, J. A. Davies and P. Jespersgaard, 1967, Phys. Rev. 161, 219.

F. C. Erné, 1966, Nucl. Phys. 84, 91.

D. Evers and W. Stocker, 1970, Phys. Letters 33B, 559.

B. Fastrup, P. Hvelplund and C. A. Sautter, 1966, Kgl. Danske Videnskab. Selskab, Mat. - Fys. Medd. 35, No. 10.

B. Fastrup, A. Borup and P. Hvelplund, 1968, Can. J. Phys. 46, 489.

R. M. Freeman and A. Gallmann, 1970, Nucl. Phys. A156, 305.

P.W.M. Glaudemans, G. Wiechers and P. J. Brussaard, 1964a, Nucl. Phys. 56, 529.

P.W.M. Glaudemans, G. Wiechers and P. J. Brussaard, 1964b, Nucl. Phys. 56, 548.

P.W.M. Glaudemans, P. J. Brussaard and B. H. Wildenthal, 1967, Nucl. Phys. A102, 593.

P.W.M. Glaudemans, A.E.L. Dieperink, R. J. Keddy and P. M. Endt, 1969, Phys. Letters 28B, 645.

P.W.M. Glaudemans, P. M. Endt and A.E.L. Dieperink, 1971, Ann. Phys. (N.Y.) 63, 134.

S. Goldstein and I. Talmi, 1956, Phys. Rev. 102, 589.

D. R. Goosman and R. W. Kavanagh, 1967, Phys. Letters 24B, 507.

S. A. Goudsmit and J. L. Saunderson, 1940a, Phys. Rev. 57, 24.

S. A. Goudsmit and J. L. Saunderson, 1940b, Phys. Rev. 58, 36.

F. Haas, B. Heusch, G. Frick, A. Gallmann and D. E. Alburger, 1970, Nucl. Phys. A156, 385.

G. I. Harris and A. K. Hyder, Jr., 1966, Phys. Letters 22, 159.

G. I. Harris, 1969, in Proceedings of the International Conference on Properties of Nuclear States, Montreal, Canada, 1969, edited by M. Harvey et al. (Presses de l'Université de Montréal, Canada, 1969).

G. I. Harris, A. K. Hyder, Jr. and J. Walinga, 1969, Phys. Rev. 187, 1413.

G. I. Harris and J. J. Perrizo, 1970, Phys. Rev. C 2, 1347.

H. Hasper and P. B. Smith, 1971, in a private communication quoted by Engmann et al. (1971).

O. Häusser, T. K. Alexander and C. Broude, 1968, Can. J. Phys. 46, 1035.

N. Hazewindus, W. Lourens, A. Scheepmaker and A. H. Wapstra, 1963, Physica 29, 681.

B. W. Hooten, O. Häusser, F. Ingebretsen and T. K. Alexander, 1970, Can. J. Phys. 48, 1259.

P. Hvelplund and B. Fastrup, 1968, Phys. Rev. 165, 408.

P. Hvelplund, 1971, Kgl. Danske Videnskab. Selskab, Mat. - Fys. Medd. 38, No. 4.

F. Ingebretsen, T. K. Alexander, O. Häusser and D. Pelte, 1969, Can. J. Phys. 47, 1295.

A. N. James, P. R. Alderson, D. C. Bailey, P. E. Carr, J. L. Durell, M. W. Greene and J. F. Sharpey-Schafer, 1971, Nucl. Phys. A172, 401.

J. Jänecke, 1963, Nucl. Phys. 48, 129.

R. W. Kavanagh, 1967, Bull. Am. Phys. Soc. 12, 913.

R. W. Kavanagh, J. C. Merdinger and N. Schulz, 1970, Nucl. Phys. A146, 410.

E. F. Kennedy, D. H. Youngblood and A. E. Blaugrund, 1967,
    Phys. Rev. 158, 897.

B. D. Kern and P. D. Bond, 1972, Nucl. Phys. A181, 403.

D. Kohler and H. H. Hilton, 1958, Phys. Rev. 110, 1094.

A. Lachaine and B. Hird, 1970, Can. J. Phys. 48, 2336.

J. Leon and N. H. Steiger-Shafrir, 1971, Can. J. Phys. 49, 1004.

H. W. Lewis, 1950, Phys. Rev. 78, 526.

J. Lindhard and M. Scharff, 1961, Phys. Rev. 124, 128.

J. Lindhard, M. Scharff and H. E. Schiøtt, 1963, Kgl. Danske
    Videnskab. Selskab, Mat. - Fys. Medd. 33, No. 14.

J. Lindhard, V. Nielsen and M. Scharff, 1968, Kgl. Danske
    Videnskab. Selskab, Mat. - Fys. Medd. 36, No. 10.

J. Lindskog, D. M. Gordon and R. W. Kavanagh, 1972, Nucl. Phys.,
    to be published.

A. E. Litherland, M.J.L. Yates, B. M. Hinds and D. Eccleshall,
    1963, Nucl. Phys. 44, 220.

J. R. Macdonald, J. H. Ormrod and H. E. Duckworth, 1966,
    Z. Naturforsch, 21a, 130.

S. Maripuu, 1969, Nucl. Phys. A123, 357.

S. Maripuu and G. A. Hokken, 1970, Nucl. Phys. A141, 481.

M. Marmor, S. Cochavi, S. H. Henson and D. B. Fossan, 1969,
    Bull. Am. Phys. Soc. 14, 628.

R. A. Mendelson, Jr. and R. T. Carpenter, 1968, Phys. Rev. 165,
    1214.

J. C. Merdinger, 1969, Ph.D. Thesis, University of Strasbourg,
    France.

J. C. Merdinger, 1972, private communication.

F. R. Metzger, 1959, Progr. Nucl. Phys. 7, 53.

R. J. Nickles, 1969, Nucl. Phys. A134, 308.

L. C. Northcliffe and R. F. Schilling, 1970, Nuclear Data Tables
    A7, 233.

J. M. O'Dell, R. W. Krone and F. W. Prosser, Jr., 1966,
    Nucl. Phys. 82, 574.

J. H. Ormrod and H. E. Duckworth, 1963, Can. J. Phys. 41, 1424.

J. H. Ormrod, J. R. Macdonald and H. E. Duckworth, 1965,
    Can. J. Phys. 43, 275.

J. H. Ormrod, 1968, Can. J. Phys. 46, 497.

S. P. Pandya, 1956, Phys. Rev. 103, 956.

S. M. Perez, 1969, Nucl. Phys. A136, 599.

J. Picard and A. G. De Pinho, 1966, Nuovo Cimento 41B, 239.

R. E. Pixley and A. R. Poletti, 1969, Bull. Am. Phys. Soc. 14,
    125.

A. M. Poskanzer, 1963, Phys. Rev. 129, 385.

D. Powers and W. Whaling, 1962, Phys. Rev. 126, 61.

F. W. Prosser, Jr. and G. I. Harris, 1971, Phys. Rev. C 4, 1611.

C. E. Ragan, III, C. E. Moss, R. V. Poore, N. R. Roberson,
    G. E. Mitchell and D. R. Tilley, 1969, Phys. Rev. 188,
    1806.

C. E. Ragan, III, C. E. Moss, C. R. Gould, N. R. Roberson,
    G. E. Mitchell and D. R. Tilley, 1970, Phys. Rev. C 2,
    557.

C. E. Ragan, III, G. E. Mitchell, D. R. Tilley, C. R. Gould and
    N. R. Roberson, 1971, Phys. Rev. C 3, 2076.

W. L. Randolph, Jr., R. R. Borchers, R. Michaelson, D. W. Haag
    and W. Ribbe, 1971, Phys. Rev. Letters 27, 603.

A. Z. Schwarzschild and E. K. Warburton, 1968, Ann. Rev. Nucl.
    Sci. 18, 265.

R. E. Segel, N. G. Puttaswamy, N. Williams, G. H. Wedberg and
    G. B. Beard, 1970, Bull. Am. Phys. Soc. 15, 600.

R. E. Segel, G. H. Wedberg, G. B. Beard, N. G. Puttaswamy and
    N. Williams, 1970, Phys. Rev. Letters 25, 1352.

L. S. Senhouse, Jr., 1964, Ph.D. Thesis, California Institute of
    Technology.

J. F. Sharpey-Schafer, P. R. Alderson, D. C. Bailey, J. L. Durrell, M. W. Greene and A. N. James, 1971, Nucl. Phys. A167, 602.

S. J. Skorka, J. Hertel and T. W. Retz-Schmidt, 1966, Nucl. Data A2, 347.

F. Tabakin, 1964, Ann. Phys. (N.Y.) 30, 51.

P. Taras, 1966, Can. J. Phys. 44, 1563.

P. Taras, L. W. Oleksiuk, R. E. Azuma and J. D. Prentice, 1967, Phys. Rev. 164, 1386.

P. Taras and J. Matas, 1970, Can. J. Phys. 48, 603.

Ya. A. Teplova, V. S. Nikolaev, I. S. Dmitriev and L. N. Fateeva, 1962, J. Exptl. Theoret. Phys. (U.S.S.R.) 42, 44.

J. Thirion and V. L. Telegdi, 1953, Phys. Rev. 92, 1253, and the references cited therein.

P. J. Twin, W. C. Olsen and D. M. Sheppard, 1970, Nucl. Phys. A143, 481.

G. van Middelkoop and G.A.P. Engelbertink, 1969, Nucl. Phys. A138, 601.

C. W. Vermette, W. C. Olsen, D. A. Hutcheon and D. H. Sykes, 1968, Nucl. Phys. A111, 39.

E. K. Warburton, D. E. Alburger and D. H. Wilkinson, 1963, Phys. Rev. 129, 2180.

E. K. Warburton, J. W. Olness, K. W. Jones, C. Chasman, R. A. Ristinen and D. H. Wilkinson, 1966, Phys. Rev. 148, 1072.

E. K. Warburton, 1967, Nuclear Research with Low Energy Accelerators, edited by J. B. Marion and D. M. Van Patter (Academic Press, New York), 43.

E. K. Warburton, J. W. Olness and A. R. Poletti, 1967, Phys. Rev. 160, 938.

E. K. Warburton and J. Weneser, 1969, in Isospin in Nuclear Physics, edited by D. H. Wilkinson (North-Holland Publishing Company, Amsterdam, 1969), 173.

P. Wasielewski and F. B. Malik, 1971, Nucl. Phys. A160, 113.

D. D. Watson and F. D. Lee, 1967, Phys. Letters 25B, 472.

D. D. Watson, J. C. Manthuruthil and F. D. Lee, 1967, Phys. Rev.
164, 1399.

R. Wechsung, W. Strassheim and R. Bass, 1971, Nucl. Phys.
A170, 557.

W. Whaling, 1958, Handbuch der Physik 34, 193; and also
D. Demirlioglu and W. Whaling, private communication.

G. Wiechers and P. J. Brussaard, 1965, Nucl. Phys. 73, 604.

W. J. Wiesehahn, 1971a, Can. J. Phys. 49, 2396.

W. J. Wiesehahn, 1971b, Can. J. Phys. 49, 2415.

B. H. Wildenthal, J. B. McGrory, E. C. Halbert and
P. W. M. Glaudemans, 1968a, Phys. Letters 26B, 692.

B. H. Wildenthal, J. B. McGrory, E. C. Halbert and
P. W. M. Glaudemans, 1968b, Phys. Letters 27B, 611.

B. H. Wildenthal, E. C. Halbert, J. B. McGrory and T. T. S. Kuo,
1970, Phys. Letters 32B, 339.

B. H. Wildenthal, E. C. Halbert, J. B. McGrory and T. T. S. Kuo,
1971a, Phys. Rev. C 4, 1266.

B. H. Wildenthal, J. B. McGrory, E. C. Halbert and H. D. Graber,
1971b, Phys. Rev. C 4, 1708.

TABLE I

Values of $f_e(Z_1, \overline{v(t)}/v_o)$ Versus Projectile Atomic Number Z_1 and Mean Velocity $\overline{v(t)}/v_o$ [a]

			$\overline{v(t)}/v_o$			
Z_1	0.2	0.4	0.6	0.8	1.0	1.2
1	1.28	1.11	-	-	-	-
2	1.40	1.27	-	-	-	-
3	1.04	0.95	-	-	-	-
4	1.15	1.11	-	-	-	-
5	1.40	1.34	-	-	-	-
6	1.56	1.42	1.34	1.27	1.22	1.19
7	1.63	1.50	1.33	1.26	1.21	1.17
8	1.50	1.35	1.25	1.19	1.15	1.11
9	1.30	1.21	1.08	1.06	1.04	1.02
10	1.03	0.99	0.95	0.96	0.98	1.06
11	0.82	0.80	0.85	0.91	0.99	1.06
12	0.73	0.73	0.83	0.90	0.96	1.00
13	0.66	0.68	0.94	1.00	1.04	1.08
14	0.80	0.86	0.99	1.04	1.08	1.12
15	0.89	1.00	1.11	1.15	1.18	1.20
16	1.14	1.17	1.18	1.18	1.19	1.19
17	1.22	1.29	1.20	1.19	1.18	1.17
18	1.25	1.34	1.30	1.24	1.20	1.16
19	1.26	1.30	1.27	1.23	1.20	1.18
20	-	-	1.22	1.20	1.18	1.16

a   The data for $\overline{v(t)}/v_o$ = 0.2 and 0.4 are taken from Ormrod and Duckworth (1963) and from Ormrod et al. (1965), while the data for $\overline{v(t)}/v_o$ = 0.6, 0.8, 1.0 and 1.2 are taken from Fastrup et al. (1966), and from Hvelplund and Fastrup (1968).

(See page 52.)

TABLE II

The Observed DSAM Factor F Versus Beam Current I for ^{26}Al in Xe

Determination of the ^{26}Al Recoil Velocity

Kinematics		Recoil Velocity $\beta(0) \times 10^3$	Adopted $\beta(0) \times 10^3$
Bombarding Energy	= 6.10 MeV		
Beam Energy at Target Layer	= 4.85 ± 0.10 MeV		
Reaction Threshold (Lab)	= 3.97 MeV	7.38 ± 0.12	
Maximum ^{26}Al Kinematic Angle	= 11.6°		
Recoil Energy Loss in Target	= 57 ± 11 keV		
Calculated Recoil Energy	= 663 ± 20 keV		7.28 ± 0.22
γ-ray Energy			
Observed Full Doppler Shift	= 2.87 ± 0.08 keV		
Corrected Full Shift	= 3.00 ± 0.09 keV	7.18 ± 0.22	

TABLE II (continued)

Measured DSAM Factor F Versus Beam Current I

Case 1: Xe Pressure = 0.52 atm, $\beta(0)$ = 0.00728

I (nA)	F
100 ± 5	0.41 ± 0.03
70 ± 5	0.39 ± 0.02
18 ± 2	0.34 ± 0.02

Case 2: Xe Pressure = 0.40 atm, $\beta(0)$ = 0.0061

I (nA)	F
125 ± 5	0.42 ± 0.02
100 ± 5	0.40 ± 0.02
80 ± 5	0.38 ± 0.02
60 ± 5	0.34 ± 0.02
40 ± 5	0.35 ± 0.02

TABLE III

The Observed DSAM Factor F Versus Beam Current I for ^{33}S in Xe

Determination of the ^{33}S Recoil Velocity

Kinematics		Recoil Velocity $\beta(0) \times 10^3$	Adopted $\beta(0) \times 10^3$
Bombarding Energy	= 9.70 MeV		
Beam Energy at Target Layer	= 7.60 ± 0.20 MeV		
Reaction Threshold (Lab)	= 7.30 MeV	6.51 ± 0.18	
Maximum ^{33}S Kinematic Angle	= 5.5°		
Recoil Energy Loss in Target	= 226 ± 22 keV		
Calculated Recoil Energy	= 652 ± 37 keV		6.35 ± 0.21
γ-ray Energy			
Observed Full Doppler Shift	= 18.38 ± 0.60 keV		
Corrected Full Shift	= 18.65 ± 0.61 keV	6.35 ± 0.21	

TABLE III (continued)

Measured DSAM Factor F Versus Beam Current I

Xe Pressure = 13.6 atm, $\beta(0) = 0.00635$

I (nA)	F
130 ± 10	0.43 ± 0.04
100 ± 10	0.44 ± 0.03
75 ± 5	0.38 ± 0.04
50 ± 5	0.36 ± 0.07
20 ± 5	0.35 ± 0.04

TABLE IV

Stopping Parameters f_n, f_e(gas) for Xenon from ^{26}Al (418) Decay

Xe Pressure	= 0.519 atm
Initial ^{26}Al Velocity $\beta(0) \times 10^3$	= 7.28 ± 0.22
$f_e(Z_1, \overline{v}/v_o)$	= 0.68
Measured $\overline{F}$	= 0.41 ± 0.03

Stopping Parameters

f_n	f_e(gas)
1.0	0.29 ± 0.16
0.8	0.50 ± 0.15
0.6	0.77 ± 0.17

TABLE V

Stopping Parameters[a] f_n, f_e(gas) for Argon from ^{26}Al (418) Decay

f_n	Xe Pressure (atm)	$f_e(Z_1, \overline{v}/v_o)$	F	f_e(gas)	Adopted f_e(gas)
	0.340	0.97	0.70 ± 0.03	0.47 ± 0.12	
1.0	0.714	0.85	0.54 ± 0.02	0.38 ± 0.10	0.45 ± 0.06
	1.01	0.72	0.43 ± 0.02	0.49 ± 0.09	
	0.340	0.97	0.70 ± 0.03	0.56 ± 0.11	
0.8	0.714	0.85	0.54 ± 0.02	0.48 ± 0.09	0.56 ± 0.06
	1.01	0.72	0.43 ± 0.02	0.63 ± 0.09	
	0.340	0.97	0.70 ± 0.03	0.68 ± 0.13	
0.6	0.714	0.85	0.54 ± 0.02	0.62 ± 0.10	0.70 ± 0.06
	1.01	0.72	0.43 ± 0.02	0.80 ± 0.10	

a   Calculated with an initial ^{26}Al velocity $\beta(0) \times 10^3 = 7.23 \pm 0.25$.

(See page 64.)

TABLE VI

Stopping Parameters[a] f_n, f_e(gas) for Helium from ^{26}Al (418) Decay

f_n	Xe Pressure (atm)	$f_e(Z_1, \bar{v}/v_o)$	F	f_e(gas)	Adopted f_e(gas)
1.0	3.74	0.74	0.54 ± 0.02	0.40 ± 0.07	
	5.44	0.68	0.41 ± 0.02	0.51 ± 0.07	0.46 ± 0.05
0.8	3.74	0.74	0.54 ± 0.02	0.51 ± 0.08	
	5.44	0.68	0.41 ± 0.02	0.61 ± 0.08	0.56 ± 0.06
0.6	3.74	0.74	0.54 ± 0.02	0.62 ± 0.07	
	5.44	0.68	0.41 ± 0.02	0.73 ± 0.08	0.67 ± 0.05

a   Calculated with initial ^{26}Al velocity $\beta(0) \times 10^3 = 6.11 \pm 0.21$.

(See page 65.)

TABLE VII

Experimental Details for the ^{16}O 6131-keV Level Lifetime

Determination of the ^{16}O Recoil Velocity from the Full Doppler Shift

Observed Full Doppler Shift	= 73.3 ± 0.4 keV
Corrected Full Shift	= 74.0 ± 0.4 keV
Observed Recoil Velocity $\beta(0) \times 10^2$	= 1.21 ± 0.01

Experimental Lifetime for the 6131-keV Level of ^{16}O

Xe Pressure (atm)	$\overline{F}$	$f_e(Z_1, \overline{v}/v_o)$	f_n	f_e(gas)	τ (ps)	Adopted τ (ps)[a]
			1.0	0.29 ± 0.16	37 ± 8	
21.1	0.59 ± 0.02	1.15	0.8	0.50 ± 0.15	30 ± 6	29 ± 5
			0.6	0.77 ± 0.17	25 ± 5	

a   Weighted average of the three results. The error has not been reduced since the three values are not independent.

(See page 69.)

TABLE VIII
Experimental Details for the ^{37}Ar 1611-keV Level Lifetime Measurement

Determination of the ^{37}Ar Recoil Velocity

Kinematics		Recoil Velocity $\beta(0) \times 10^3$	Adopted Velocity $\beta(0) \times 10^3$
Bombarding Energy	= 9.40 MeV		
Beam Energy at Target Layer	= 8.40 ± 0.08 Mev		
Reaction Threshold (Lab)	= 6.97 MeV	7.0 ± 0.1	
Maximum ^{37}Ar Kinematic Angle	= 11.5°		
Recoil Energy Loss in Target	= 56 ± 21 keV		
Calculated Recoil Energy	= 841 ± 22 keV		6.2 ± 0.1

γ-ray Energy

Observed Full Doppler Shift	= 9.75 ± 0.15 keV		
Corrected Full Shift	= 10.00 ± 0.15 keV	6.2 ± 0.1	

TABLE VIII (continued)

Experimental Lifetime for the 1611-keV Level of ^{37}Ar

Xe Pressure (atm)	$\overline{F}$	f_n	$f_e(\text{gas})$	$f_e(Z_1, \overline{v}/v_o)$	τ (ps)	Adopted τ (ps)[a]
		0.6	0.77 ± 0.17	1.34	8.1 ± 1.3	
0.108	0.30 ± 0.02	0.8	0.50 ± 0.15	1.34	8.2 ± 1.4	8.2 ± 1.3
		1.0	0.29 ± 0.16	1.34	8.4 ± 1.5	

a   Adopted lifetime is the weighted average of the three results; the error has not been reduced since these values are not independent.

(See page 71.)

TABLE IX

Experimental Details for the ^{30}P 709-keV Level Lifetime Measurement

Determination of the ^{30}P Recoil Velocity

Kinematics		Recoil Velocity $\beta(0) \times 10^3$	Adopted Velocity $\beta(0) \times 10^3$
Bombarding Energy	= 6.50 MeV		
Beam Energy at Target Layer	= 4.92 ± 0.14 MeV		
Reaction Threshold (Lab)	= 3.85 MeV		
Maximum ^{30}P Kinematic Angle	= 12.8°	6.39 ± 0.13	
Recoil Energy Loss in Target	= 75 ± 6 keV		
Calculated Recoil Energy	= 571 ± 22 keV		
			6.2 ± 0.2
γ-ray Energy			
Observed Full Doppler Shift	= 3.82 ± 0.04 keV		
Corrected Full Shift	= 4.21 ± 0.19 keV	6.0 ± 0.3	

TABLE IX (continued)

Experimental Lifetime for the 709-keV Level of ^{30}P

Xe Pressure (atm)	$\overline{F}$	$f_e(Z_1, \overline{v}/v_o)$	τ (ps)[a]	$\overline{\tau}$ (ps)	Adopted τ (ps)[b]
9.86 ± 0.03	0.51 ± 0.01	1.05	45.1 ± 5.2		
8.50 ± 0.03	0.57 ± 0.01	1.05	42.2 ± 4.8		
6.80 ± 0.03	0.62 ± 0.01	1.05	44.0 ± 4.9	43.4 ± 2.5	43 ± 6
3.40 ± 0.03	0.78 ± 0.01	1.11	42.4 ± 5.1		

a   Computed with $f_n = 0.8$, f_e (gas) = 0.50 ± 0.15.

b   Adopted lifetime includes a 12% uncertainty for the rate of energy loss assumed in the analysis.

(See page 76.)

TABLE X

Decay Properties of the 709-keV Level of ^{30}P

Experimental Decay Properties

Level Lifetime τ (ps)					
a	b	c	d	e	Adopted τ^f
43 ± 6	55 ± 7	22 ± 5	≥ 3.0	≥ 1.1	48 ± 5

Multipole Mixing Ratio $\delta(E2/M1)$			
g	h	i	Adopted $\delta(E2/M1)^j$
-0.48 ± 0.04	$-0.25 \begin{smallmatrix} +0.33 \\ -0.21 \end{smallmatrix}$	-0.22 ± 0.02	-0.22 ± 0.02
or	or	or	or
-2.0 ± 0.2	$-4.0 \begin{smallmatrix} +19 \\ -2.3 \end{smallmatrix}$	$-4.5 \begin{smallmatrix} +0.3 \\ -0.5 \end{smallmatrix}$	$-4.5 \begin{smallmatrix} +0.3 \\ -0.5 \end{smallmatrix}$

Transition Strengths	
$\lvert M(M1) \rvert^2$ (W.u.) $\times 10^3$	$\lvert M(E2) \rvert^2$ (W.u.)
1.77 ± 0.19	0.79 ± 0.16
or	or
$0.087 \begin{smallmatrix} +0.014 \\ -0.021 \end{smallmatrix}$	16.3 ± 1.7

TABLE X (continued)

Theoretical Transition Strengths and Mixing Ratios

	Wiechers and Brussaard (1965)		Wildenthal et al. (1971b)	
	k	ℓ	m	n
$\|M(M1)\|^2$ (W.u.)$\times 10^3$	45.0	14.4	1.0	5.6
$\|M(E2)\|^2$ (W.u.)	-	-	2.9	0.43
$\delta(E2/M1)$	-	-	-	-

	Glaudemans et al. (1971)			Wasielewski and Malik (1971)
	o	p	q	r
$\|M(M1)\|^2$ (W.u.)$\times 10^3$	1.0	10.0	1.0	3.5
$\|M(E2)\|^2$ (W.u.)	0.7	2.9	-	6.1
$\delta(E2/M1)$	-	-	-	-0.43

a Present work.
b Haas et al. (1970).
c Pixley and Poletti (1969).
d Kennedy et al. (1967).
e Lachaine and Hird (1970).
f Weighted average of a) and b).
g Harris and Hyder (1966).
h Vermette et al. (1968).
i Harris et al. (1969).
j Weighted average of h) and i).
k With single-particle g factors.
ℓ With effective g factors.
m Modified surface delta interaction with effective charges and single-particle g factors.
n Free-parameter surface delta interaction with effective charges and single-particle g factors.
o MSDI with single-particle g factors and charges.
p MSDI with effective g factors and charges.
q MSDI with effective matrix elements.
r Unified model with single-particle g factors and charges.

TABLE XI

Experimental Details for the ^{35}Cl 3163-keV Level Lifetime Measurement

Determination of the ^{35}Cl Recoil Velocity

Kinematics		Recoil Velocity $\beta(0) \times 10^3$	Adopted Velocity $\beta(0) \times 10^3$
Bombarding Energy	= 9.34 MeV		
Beam Energy at Target Layer	= 8.34 ± 0.08 MeV		
Reaction Threshold (Lab)	= 5.65 MeV	7.22 ± 0.06	
Maximum ^{35}Cl Kinematic Angle	= 15.8°		
Recoil Energy Loss in Target	= 119 ± 10 keV		
Calculated Recoil Energy	= 851 ± 14 keV		6.5 ± 0.1

γ-ray Energy

Observed Full Doppler Shift	= 20.0 ± 0.3 keV		
Corrected Full Shift	= 20.6 ± 0.3 keV	6.5 ± 0.1	

TABLE XI (continued)

Experimental Lifetime for the 3163-keV Level of ^{35}Cl

Xe Pressure (atm)	$\overline{F}$	τ (ps)[a]	$\overline{\tau}$ (ps)	Adopted τ (ps)[b]
5.44 ± 0.03	0.63 ± 0.01	55 ± 7		
			55 ± 5	55 ± 8
8.16 ± 0.07	0.52 ± 0.01	54 ± 7		

a   Computed with $f_n = 0.8$, $f_e(Z_1, \overline{v}/v_o) = 1.24$ and f_e (gas) = 0.50 ± 0.15.

b   Adopted lifetime includes a 12% uncertainty for the rate of energy loss assumed in the analysis.

(See page 85.)

TABLE XII

Experimental Decay Properties of the 7/2⁻ Level of ^{35}Cl at 3163 keV

Branching Ratios

Final Level[a]		Branching Ratios (%)									
Energy (keV)	J^π	b	c	d	e	f	g	h	i	j	Weighted Average
0	3/2+	84±7	90	95	79±5	92±2	90±3	90±2	94±6	90±1	90±1
1219	1/2+	<1						<1			<1
1763	5/2+	<1			<2	<1		<1	<0.3	0.30±0.04	0.30±0.04
2645	7/2+	16±3	10	5	21±5	8±2	10±3	10±2	6±2	8±1	8.7±0.7
2695	3/2+	<2				<0.5					<0.5
3003	5/2+	<10				<0.5				1.7±0.2	1.0±0.4

Mixing Ratios

Final Level	J^π	$\delta(\frac{L+1}{L})$	c	d	e	g	h	j	Weighted Average
0	3/2+	δ(E3/M2)	-0.16±0.01	-0.24±0.05	$-0.14^{+0.08}_{-0.07}$	-0.14±0.02	-0.25±0.04	-	-0.16±0.01
1763	5/2+	δ(M2/E1)	-	-	-	-	-	-0.44±0.12	-0.44±0.12

Lifetime (ps)

f	k	ℓ	m	Adopted Value[n]
60±7	55±8	140±40	37±4	58±5

a Level energies are from Prosser and Harris (1971) while level spins and parities are from Endt and Van der Leun (1967) and from Taras and Matas (1970).
b Hazewindus et al. (1963).
c Watson et al. (1967).
d Taras et al. (1967).
e Duncan et al. (1969).
f Ingebretsen, et al. (1969).
g Hooten et al. (1970).
h Taras and Matas (1970).
i Wiesehahn (1971a).
j Prosser and Harris (1971).
k Present work.
ℓ Azuma et al. (1968).
m Barton et al. (1971).
n Adopted value is the weighted average of the present work and that of Ingebretsen et al. (1969).

TABLE XIII

Transition Strengths for the Decay of the $7/2^-$ Level of ^{35}Cl at 3163 keV

E_i (keV)	E_f (keV)	J_i^π	J_f^π	δ	Experimental $\lvert M(E1)\rvert^2$	Experimental $\lvert M(M2)\rvert^2$	Experimental $\lvert M(E3)\rvert^2$	Theoretical[b] $\lvert M(M2)\rvert^2$
3163	0	$7/2^-$	$3/2^+$	-0.16 ± 0.01	–	0.20 ± 0.02	2.9 ± 0.4	1.52 [c] 3.00 [d]
3163	1219	$7/2^-$	$1/2^+$	NR[a]	–	–	<40	–
3163	1763	$7/2^-$	$5/2^+$	-0.44 ± 0.12	$(1.4\pm0.3)\times10^{-8}$	$(6.5\pm3.2)\times10^{-3}$	–	5.56×10^{-3} [e]
3163	2645	$7/2^-$	$7/2^+$	NR	$(9.8\pm1.2)\times10^{-6}$	–	–	–
3163	2695	$7/2^-$	$3/2^+$	NR	–	<16	–	–
3163	3003	$7/2^-$	$5/2^+$	NR	$(3.8\pm1.6)\times10^{-5}$	–	–	–

a   Mixing ratio not reported. Except as noted, the transitions are assumed to occur as the probable lowest multipole. Branching ratios are from Table X. The lifetime of the 3163-keV level ($\tau = 58\pm5$ ps) is the weighted average of the present work and that of Ingebretsen et al. (1969).

b. Taken from the work of Harris and Perrizo (1970) and Prosser and Harris (1971).

c   Obtained with a pure $1d^2_{3/2}1f_{7/2}$ configuration for the 3163-keV level.

d   Obtained with the wavefunctions of Maripuu (1969) and Maripuu and Hokken (1970).

e   Obtained with the derived wavefunction for the 3163-keV level.

(See page 88.)

TABLE XIV

Decay Properties of the $7/2^-$ Level of ^{33}S at 2934[a] keV

Lifetime (ps)

Experimental										Theoretical
b	c	d	e	f	g	h	i	j	Weighted Average [k]	ℓ
43 ± 7	40.5 ± 2.0	44 ± 4	36 ± 8	38 ± 11	> 1.4	> 4	> 7	> 10	41.0 ± 1.7	161

Experimental Branching Ratio (%)

Final State

E (keV)	J^π	n	o	h	Weighted Average
0	$3/2^+$	49 ± 3	50 ± 5	-	49.3 ± 2.6
1966[m]	$5/2^+$ [m]	51 ± 3	50 ± 5	-	50.7 ± 2.6
2313	$3/2^+$	< 2	-	< 2	< 2

Experimental Multipole Mixing Ratio

Final State

E (keV)	J^π	Multipole Type	n	o	Weighted Average [p]
0	$3/2^+$	E3/M2	0.09 ± 0.27 or $2.1 \leq \delta \leq \infty$	0.48 ± 0.09 or 1.64 ± 0.45	0.44 ± 0.09
1966	$5/2^+$	M2/E1	0.0 ± 0.1	0.08 ± 0.09	0.04 ± 0.07

(See page 93.)

TABLE XIV (continued)

Experimental Transition Strengths

Final State		Transition Strength (W.u.)[q]		
E (keV)	J^π	$\lvert M(E1) \rvert^2$	$\lvert M(M2) \rvert^2$	$\lvert M(E3) \rvert^2$
0	$3/2^+$	–	0.20 ± 0.02	28 ± 10
1966	$5/2^+$	$(1.29 \pm 0.09) \times 10^{-5}$	0.1 ± 0.4	
2313	$3/2^+$	–	$< 23^{[r]}$	–

a   Level energy is the weighted average of the present work and that of Ref. f.
b   Present work.
c   Ragan et al. (1970).
d   Brandolini et al. (1971).
e   Kavanagh et al. (1970).
f   Brandolini and Signorini (1969).
g   Cummings and Donahue (1970).
h   Ragan et al. (1969).
i   van Middelkoop and Engelbertink (1969).
j   Brandolini et al. (1969).
k   Weighted average of Ref. b - f.
ℓ   Harris (1969).
m   Level energy and parity from Bardin et al. (1970).
n   Becker et al. (1966).
o   O'Dell et al. (1966).
p   Larger value excluded as noted in text.
q   Weisskopf units (W.u.) as defined by Skorka et al. (1966).
r   Transition assumed to occur as lowest probable multipole.

TABLE XV

Experimental Details for the ^{38}K 451-keV Level Lifetime Measurement

Determination of the ^{38}K Recoil Velocity

Kinematics		Recoil Velocity $\beta(0) \times 10^3$	Adopted Velocity $\beta(0) \times 10^3$
Bombarding Energy	= 9.56 MeV		
Beam Energy at Target Layer	= 7.74 ± 0.15 MeV		
Reaction Threshold (Lab)	= 7.05 MeV	6.56 ± 0.10	
Maximum ^{38}K Kinematic Angle	= 8.2°		
Recoil Energy Loss in Target	= 28 ± 3 keV		
Calculated Recoil Energy	= 763 ± 20 keV		
			6.5 ± 0.3
γ-ray Energy (Ta backing)			
Observed Full Doppler Shift	= 1.59 ± 0.26 keV	5.8 ± 1.0	
Corrected Full Shift	= 1.89 ± 0.34 keV		
γ-ray Energy (C backing)			
Observed Full Doppler Shift	= 2.01 ± 0.08 keV	6.51 ± 0.33	
Corrected Full Shift	= 2.14 ± 0.11 keV		

TABLE XV (continued)

Experimental Lifetime for the 451-keV Level of ^{38}K

Xe Pressure (atm)	$\overline{F}$	f_n	f_e (gas)	$f_e(Z_1, \overline{v}/v_o)$	τ (ps)	Adopted τ (ps)[a]
		0.6	0.70 ± 0.06	1.25	141 ± 82	
13.6 ± 0.03	0.78 ± 0.11	0.8	0.56 ± 0.06	1.25	155 ± 89	155 ± 90
		1.0	0.45 ± 0.06	1.25	164 ± 89	

a   Adopted lifetime includes a 12% uncertainty for the rate of energy loss assumed in the analysis.

TABLE XVI

Transition Strengths for the Decay of the 1^+ Level of ^{38}K at 451 keV

Experimental Transition Strength

Final Level		Transition Strength[a] (W.u.)	
E (keV)	J^π	$10^3 \times |M(M1)|^2$	$|M(E2)|^2$
127	0^+	$5.8 \begin{smallmatrix} +8.0 \\ -2.1 \end{smallmatrix}$	-
0	3^+	-	< 0.9[b]

Theoretical Lifetimes and Transition Strengths

	Dieperink and Glaudemans (1969b)		Evers and Stocker (1970)			Wildenthal et al. (1971a)
	c	d	e	f	g	
Lifetime (ps)	110	120	12	23	63	-
$10^3 \times |M(M1)|^2$ (W.u.) $(451 \rightarrow 127)$	-	-	-	-	-	4.5
$|M(E2)|^2$ (W.u.) $\quad (451 \rightarrow 0)$	-	-	-	-	-	4.5

a   Calculated with lifetime from present work.
b   Assumes pure E2 transition.
c   Tabakin interaction.
d   MSDI interaction.
e   MSDI interaction.
f   MSDIT interaction.
g   MSDIT C interaction.

(See page 101.)

TABLE XVII

Experimental Details for the ^{26}Al 1760-keV Level Lifetime Measurement

Determination of the ^{26}Al Recoil Velocity

Kinematics		Recoil Velocity $\beta(0) \times 10^3$	Adopted Velocity $\beta(0) \times 10^3$
Bombarding Energy	= 6.06 MeV		
Reaction Threshold (Lab)	= 5.55 MeV		
Maximum ^{26}Al Kinematic Angle	= 7.9°	8.02 ± 0.11	
Recoil Energy Loss in Target	= 101 ± 19 keV		
Calculated Recoil Energy	= 781 ± 19 keV		
			7.1 ± 1.0
γ-ray Energy			
Observed Full Doppler Shift	= 9.06 ± 0.14 keV	7.06 ± 0.13	
Corrected Full Shift	= 9.49 ± 0.15 keV		

Experimental Lifetime[a] for the 1760-keV Level of ^{26}Al

$$F = 0.11 \pm 0.03 \qquad \tau(1760) = 5.0 \begin{smallmatrix} +2.2 \\ -1.4 \end{smallmatrix} \text{ ps}$$

a Computed with $f_n = 0.8 \pm 0.2$, $f_e(Z_1, \bar{v}/v_o) = 0.66$ and $D = 1.70 \begin{smallmatrix} +0.20 \\ -0.10 \end{smallmatrix} \text{ g/cm}^3$

(See page 105.)

TABLE XVIII

Decay Properties of the 2^+ Level of ^{26}Al at 1760 keV

Lifetime (ps)

a	b	c	Adopted[d]
$5.0 \, ^{+2.2}_{-1.4}$	6.5 ± 2.0	> 3.4	$5.8 \, ^{+1.5}_{-1.1}$

Branching Ratio to 418-keV Level (%)

c	e	Adopted
> 90	$100 \, ^{+0}_{-20}$	$100 \, ^{+0}_{-10}$

Electromagnetic Transition Strengths for Decay to the 418-keV Level (W.u.)

Experimental[f]		Theoretical[g]	
$10^3 \times \lvert M(M1) \rvert^2$	$\lvert M(E2) \rvert^2$	$10^3 \times \lvert M(M1) \rvert^2$	$\lvert M(E2) \rvert^2$
$2.3 \, ^{+0.5}_{-0.6}$	$7.1 \, ^{+1.5}_{-2.0}$	0.12	0.96

a Present work.
b Marmor et al. (1969).
c Häusser et al. (1968).
d Weighted average of a) and b).
e Bissinger et al. (1968).
f Transition strengths calculated for $\delta(E2/M1) = 0$ and ∞, respectively.
g Wasielewski and Malik (1971).

(See page 108.)

TABLE XIX

Experimental Details for the ^{40}K 800-keV and 890-keV Level Lifetime Measurements

Determination of the ^{40}K Recoil Velocity

Kinematics		Recoil Velocity $\beta(0) \times 10^3$	Adopted $\beta(0) \times 10^3$
Bombarding Energy	= 5.90 MeV		
Reaction Threshold (890-keV Level)	= 5.28 MeV		
Maximum ^{40}K Kinematic Angle	= 9.0°	5.0 ± 0.2	
Recoil Energy Loss in Target	= 117 ± 33 keV		
Calculated Recoil Energy	= 461 ± 33 keV		
γ-ray Energy (Day 1)			
Observed Full Doppler Shift (890)	= 3.74 ± 0.14 keV	4.4 ± 0.2	4.4 ± 0.2
Corrected Full Shift (890)	= 3.90 ± 0.15 keV		
γ-ray Energy (Day 2)			
Observed Full Doppler Shift (890)	= 4.54 ± 0.20 keV	5.2 ± 0.2	5.2 ± 0.2
Corrected Full Shift (890)	= 4.68 ± 0.21 keV		

TABLE XIX (Continued)

Experimental Lifetimes[a] for the 800-keV and 890-keV Levels of ^{40}K

Day 1   <u>Adopted Lifetimes[b]</u>

$\overline{F}$	τ

$F(800) = 0.60 \pm 0.03$ $\tau(800) = 0.26 \pm 0.05$ ps

$F(890) = 0.24 \pm 0.04$ $\tau(890) = 1.02 \begin{smallmatrix} +0.27 \\ -0.22 \end{smallmatrix}$ ps

Day 2 $\tau(800) = 0.35 \pm 0.07$ ps

$F(800) = 0.49 \pm 0.03$ $\tau(800) = 0.43 \pm 0.07$ ps $\tau(890) = 1.17 \pm 0.31$ ps

$F(890) = 0.13 \pm 0.05$ $\tau(890) = 2.34 \begin{smallmatrix} +1.62 \\ -0.75 \end{smallmatrix}$ ps

a   Computed with $f_n = 0.8 \pm 0.2$, $f_e(Z_1, \overline{v}/v_o) = 1.28$ and $D = 1.82 \pm 0.10$ g/cm^3.

b   Weighted average of the two runs, with a 10% uncertainty in the rate of energy loss for ^{40}K in carbon included in the final result.

(See page 112.)

TABLE XX

Decay Properties of the 2^- 800-keV and 5^- 890-keV Levels of ^{40}K

Lifetime (ps)

Level (keV)	Experimental						Theoretical Dieperink et al. (1968)		
	a	b	c	d	e	Adopted[f]	g	h	i
800	0.35±0.07	$0.33^{+0.10}_{-0.08}$	0.50±0.15	0.65±0.15	0.37±0.10	0.39±0.04	2.1	0.46	0.83
890	1.17±0.31	$0.91^{+0.55}_{-0.25}$	1.5 ±0.4	1.6 ±0.3	1.00±0.26	1.25±0.15	4	1.1	2.1

Branching Ratio (%)

Initial Level (keV)	Final Level (keV)	j	k	ℓ
800	30	100	100^{+0}_{-3}	100
	0	<5	-	<3
890	30	<5	-	<4
	0	100	-	100

Mixing Ratio δ(E2/M1)

	j	k
800 → 30	0.00 ± 0.03	0.00 ± 0.01
890 → 0	-0.11 ± 0.05	-

TABLE XX (Continued)

Electromagnetic Transition Strengths (W. u.)

	Experimental		Wechsung et al. (1971)		Becker and Warburton (1971)	
					m	n
Transition	$\lvert M(M1)\rvert^2$	$\lvert M(E2)\rvert^2$	$\lvert M(M1)\rvert^2$	$\lvert M(E2)\rvert^2$	$\lvert M(M1)\rvert^2$	$\lvert M(M1)\rvert^2$
$2^- \rightarrow 3^-$	0.18 ± 0.02	<0.1	0.15	-0.35	0.117	0.060
$5^- \rightarrow 4^-$	0.035 ± 0.004	$1.7^{+1.9}_{-1.2}$	0.073	0.8	0.055	0.018

a   Present work.

b   Merdinger (1969).

c   Bass and Wechsung (1970).

d   Segel et al. (1970).

e   James et al. (1971).

f   Weighted average of ref. a) - e).

g   Tabakin interaction.

h   Modified-surface-delta interaction in the random-phase approximation.

i   MSDI in the Tamm-Dancoff approximation.

j   Wechsung et al. (1971).

k   Twin et al. (1970).

ℓ   Freeman and Gallmann (1970).

(See page 114.)

m   With pure $1f_{7/2}1d_{3/2}^{-1}$ wavefunction.

n   With the wavefunctions of Perez (1969).

TABLE XXI

Electronic Stopping Cross Section S_e for ^{12}C in He

E (keV)	$S_e \cdot 10^{14}$ (ev-cm^2/atom)	Pressure (Torr)	$N\Delta R \cdot 10^{-18}$ (cm^{-2})	ΔE_0 (keV)	θ[a]
564 ± 22	3.29 ± 0.10	15.39 ± 0.05	4.48 ± 0.03	147.3 ± 4.4	55°
687 ± 25	3.49 ± 0.10	15.39 ± 0.05	4.48 ± 0.03	156.3 ± 4.4	55°
803 ± 31	3.87 ± 0.11	15.40 ± 0.05	4.49 ± 0.03	173.6 ± 4.8	55°
989 ± 32	4.38 ± 0.10	15.39 ± 0.05	4.48 ± 0.03	196.1 ± 4.3	55°
1072 ± 24	4.87 ± 0.11	15.39 ± 0.05	4.48 ± 0.03	218.3 ± 4.7	31°
1183 ± 38	4.56 ± 0.10	15.39 ± 0.05	4.48 ± 0.03	204.4 ± 4.3	55°
1359 ± 26	5.26 ± 0.10	15.39 ± 0.05	4.48 ± 0.03	235.5 ± 4.2	31°
1378 ± 44	4.78 ± 0.11	15.39 ± 0.05	4.48 ± 0.03	214.3 ± 4.7	55°
1559 ± 29	5.64 ± 0.15	11.42 ± 0.06	3.33 ± 0.03	187.8 ± 4.7	31°
1568 ± 49	5.11 ± 0.10	15.39 ± 0.05	4.48 ± 0.03	229.1 ± 4.2	55°
1766 ± 55	5.15 ± 0.10	15.39 ± 0.05	4.48 ± 0.03	230.5 ± 4.2	55°

a   The detector angle is θ.

TABLE XXII

Electronic Stopping Cross Section S_e for ^{12}C in Xe

E (keV)	$S_e \cdot 10^{13}$ (ev-cm^2/atom)	Pressure (Torr)	$N\Delta R \cdot 10^{-17}$ (cm^{-2})	ΔE_o (keV)	θ^a
680 ± 27.	3.09 ± 0.13	1.78 ± 0.05	5.19 ± 0.15	160.4 ± 4.8	55°
701 ± 25	2.85 ± 0.25	1.46 ± 0.12	4.25 ± 0.35	121.1 ± 4.0	55°
815 ± 30	3.38 ± 0.15	1.46 ± 0.05	4.25 ± 0.15	143.7 ± 3.9	55°
973 ± 33	3.63 ± 0.12	2.15 ± 0.05	6.26 ± 0.15	227.1 ± 4.8	55°
1171 ± 39	3.64 ± 0.36	2.15 ± 0.05	6.26 ± 0.15	228.1 ± 23.0	55°
1353 ± 45	4.20 ± 0.13	2.15 ± 0.05	6.26 ± 0.15	263.1 ± 5.0	55°
1539 ± 50	4.61 ± 0.14	2.15 ± 0.05	6.26 ± 0.15	288.3 ± 4.9	55°

a   The detector angle is θ.

(See page 128.)

TABLE XXIII

Electronic Stopping Cross Section S_e for ^{27}Al in He

E (keV)	$S_e \cdot 10^{14}$ (ev-cm^2/atom)	Pressure (Torr)	$N\Delta R \cdot 10^{-18}$ (cm^{-2})	ΔE_o (keV)	θ[a]
790 ± 18	2.10 ± 0.18	14.50 ± 0.05	4.22 ± 0.03	88.5 ± 7.6	31°
967 ± 19	2.59 ± 0.28	10.70 ± 0.05	3.12 ± 0.02	80.7 ± 8.8	31°
1290 ± 19	3.51 ± 0.29	10.70 ± 0.05	3.12 ± 0.02	109.4 ± 9.0	31°
1295 ± 19	3.34 ± 0.32	10.35 ± 0.05	3.02 ± 0.02	101.0 ± 9.7	31°
1619 ± 25	3.96 ± 0.46	10.70 ± 0.05	3.12 ± 0.02	123.7 ± 14.2	31°
1783 ± 27	4.14 ± 0.38	10.70 ± 0.05	3.12 ± 0.02	129.2 ± 11.8	31°
1969 ± 29	5.06 ± 0.21	10.70 ± 0.05	3.12 ± 0.02	158.0 ± 6.5	31°
2132 ± 31	5.24 ± 0.40	10.70 ± 0.05	3.12 ± 0.02	163.5 ± 12.5	31°
2317 ± 34	6.22 ± 0.36	10.70 ± 0.05	3.12 ± 0.02	194.2 ± 11.2	31°

a   The detector angle is θ.

(See page 128.)

TABLE XXIV

Electronic Stopping Cross Section S_e for ^{27}Al in Xe

E (keV)	$S_e \cdot 10^{13}$ (ev-cm^2 atom)	Pressure (Torr)	$N\Delta R \cdot 10^{-17}$ (cm^{-2})	ΔE_o (keV)	θ^a
797 ± 20	2.11 ± 0.16	1.25 ± 0.05	3.64 ± 0.15	76.8 ± 5.0	31°
808 ± 19	2.72 ± 0.40	0.71 ± 0.05	2.07 ± 0.15	56.3 ± 7.2	31°
895 ± 20	2.83 ± 0.52	1.25 ± 0.05	3.64 ± 0.15	103.1 ± 18.6	31°
897 ± 31	3.14 ± 0.26	2.15 ± 0.05	6.26 ± 0.15	196.3 ± 15.8	55°
974 ± 21	3.57 ± 0.36	1.25 ± 0.05	3.64 ± 0.15	130.1 ± 11.8	31°
1076 ± 36	3.05 ± 0.30	2.15 ± 0.05	6.26 ± 0.15	190.9 ± 18.5	55°
1076 ± 22	3.55 ± 0.36	1.25 ± 0.05	3.64 ± 0.15	129.1 ± 12.0	31°
1169 ± 21	3.94 ± 0.28	1.25 ± 0.05	3.64 ± 0.15	143.3 ± 8.5	31°
1173 ± 23	3.74 ± 0.43	1.25 ± 0.05	3.64 ± 0.15	136.0 ± 13.8	31°
1228 ± 45	3.79 ± 0.28	2.18 ± 0.05	6.35 ± 0.15	240.7 ± 16.6	55°
1259 ± 23	4.50 ± 0.34	1.25 ± 0.05	3.64 ± 0.15	163.7 ± 10.3	31°
1265 ± 22	4.21 ± 0.41	1.25 ± 0.05	3.64 ± 0.15	153.2 ± 13.6	31°
1360 ± 26	4.51 ± 0.84	1.25 ± 0.05	3.64 ± 0.15	164.2 ± 30.0	31°
1640 ± 27	5.59 ± 0.35	1.25 ± 0.05	3.64 ± 0.15	203.3 ± 9.7	31°
1651 ± 30	5.65 ± 0.74	1.25 ± 0.05	3.64 ± 0.15	205.8 ± 25.4	31°
2210 ± 34	6.01 ± 0.64	1.25 ± 0.05	3.64 ± 0.15	218.9 ± 21.4	31°

a   The detector angle is θ.

(See page 128.)

TABLE XXV

Values of the Exponent p and Coefficient K in the Relation[a] $S_e = K[E(keV)]^p$

Projectile	Stopping Gas	Experimental[b]			Theoretical[c]	
		K (10^{-15} ev-cm^2/atom)	p	Energy Interval (keV)	K (10^{-15} ev-cm^2/atom)	p
^{12}C	He	1.63	0.47	560 - 1770	1.66	0.5
^{12}C	Xe	12.5	0.49	680 - 1540	6.57	0.5
^{27}Al	He	0.033	0.97	790 - 2320	1.55	0.5
^{27}Al	Xe	0.23	1.05	800 - 2210	9.03	0.5

a For ^{12}C ions, the experimental data generally agree with this relation to within $\pm 5\%$; for ^{27}Al ions, the agreement is generally to within $\pm 10\%$.

b Present work.

c Lindhard and Scharff (1961).

(See page 128.)

Figure 1. The observed yield of γ rays with energies between 3.3 and 7.2 MeV as a function of the proton beam energy at the 698-keV resonance in the excitation function for the $^{29}Si(p,\gamma)^{30}P$ reaction. The γ rays were observed in a 12.7-cm by 10.2-cm NaI(Tl) detector placed at 90° from the beam. The solid line is hand drawn to guide the eye.

RELATIVE YIELD OF 3.3-7.2 MeV γ RAYS (10³ COUNTS)

E_p (keV)

7.2 keV
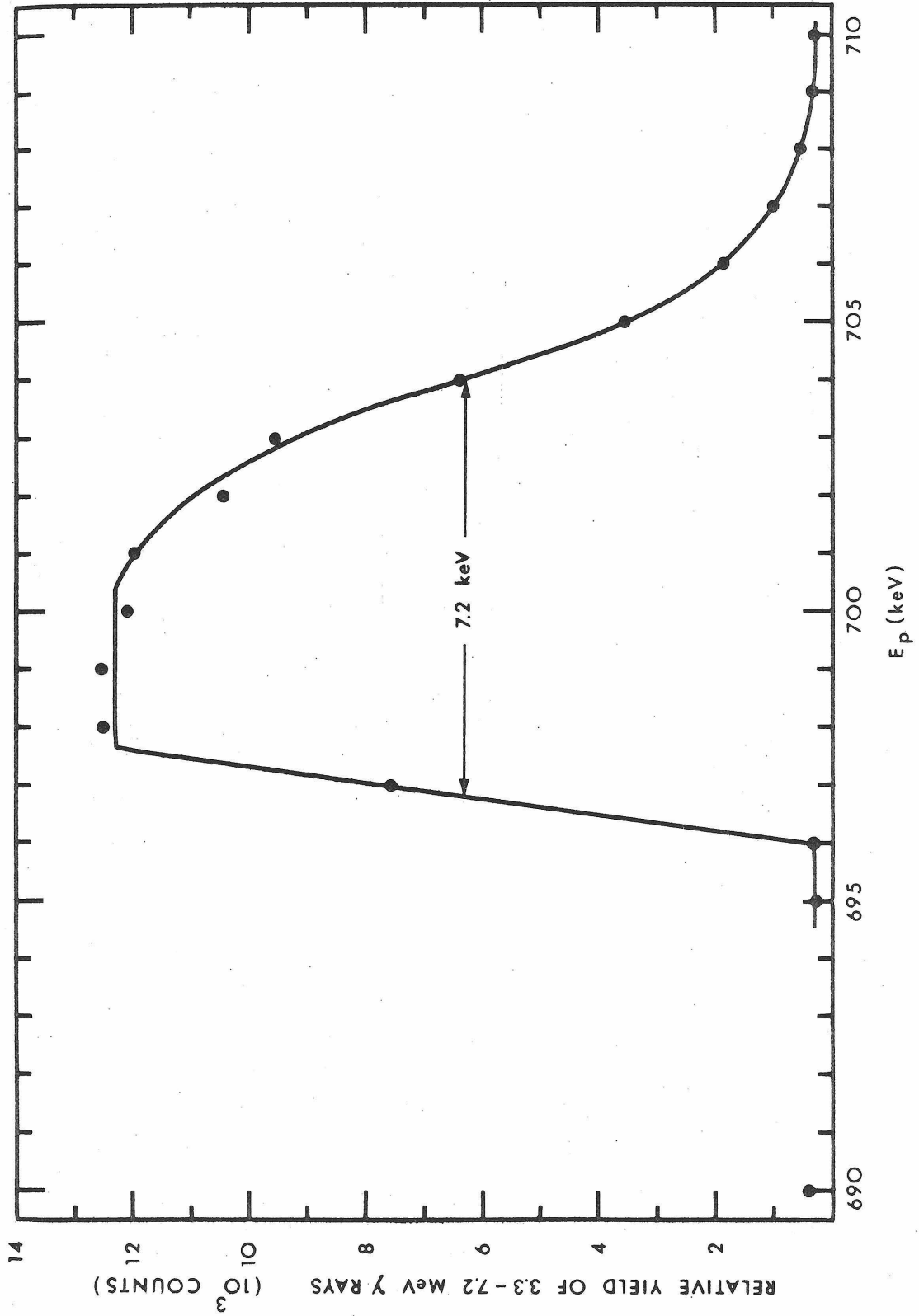
Figure 2. The target geometry for the recoil-distance lifetime measurements. The triangle downbeam from the target indicates the maximum kinematic recoil angle.

(See page 15.)

Ge (Li)

1 cm

0.56 mm WALL Sn

0.19 mm WALL Ta

TARGET

α BEAM
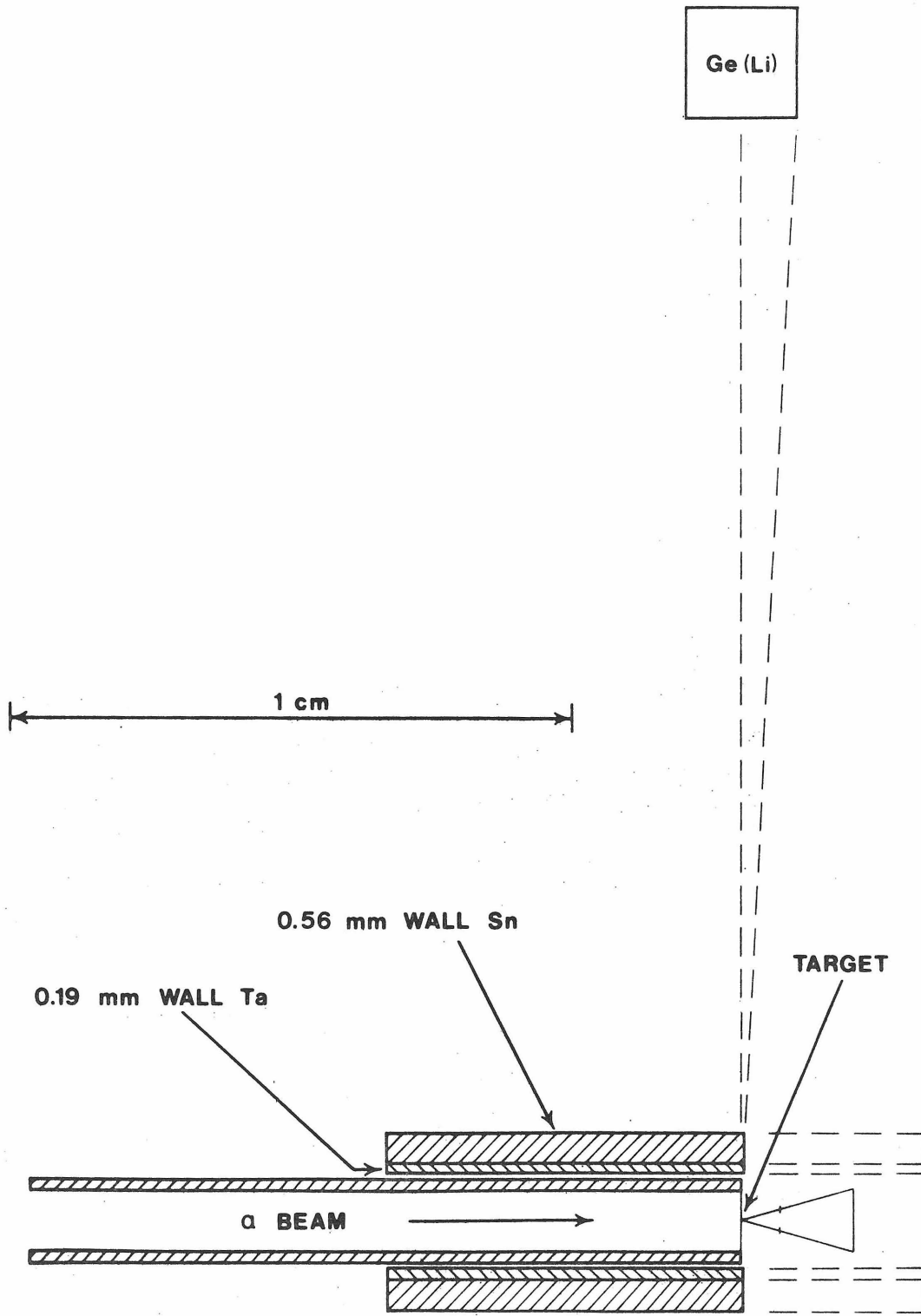
Figure 3. The complete recoil-distance apparatus.

(See page 15.)

TARGET

Ta/Sn ABSORBER

Ge(Li)

SUPPRESSOR

α BEAM

VIEWING PORT

BEAM STOP

1 cm
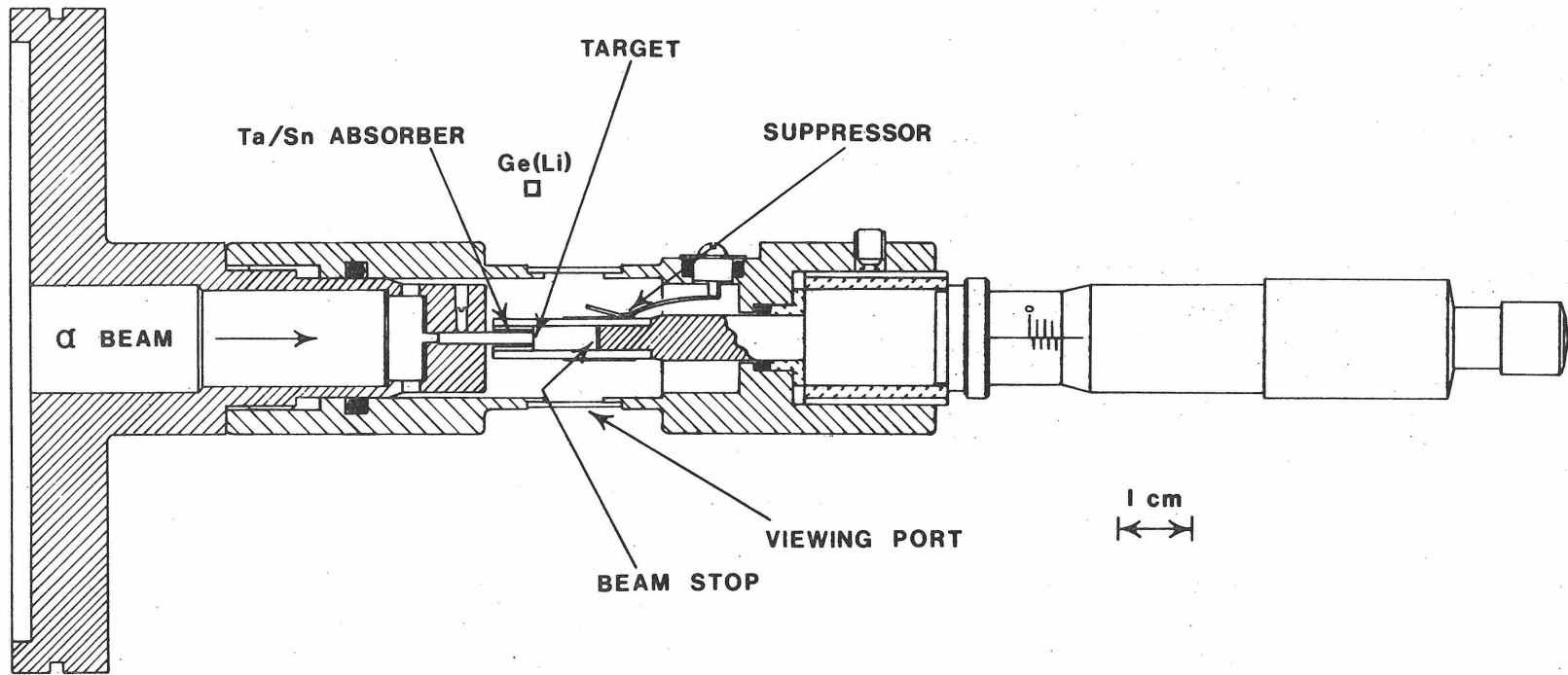
Figure 4. Two of the ^{32}P γ-ray spectra obtained in the Ge(Li)
detector for typical absorber positions. The
spectrum (a) illustrates the yield of 78-keV γ rays
when there is no attenuation by the absorber while
(b) illustrates the yield when the absorber has been
advanced to a position 1.6 mean lives downstream
from the target.

(See page 16.)
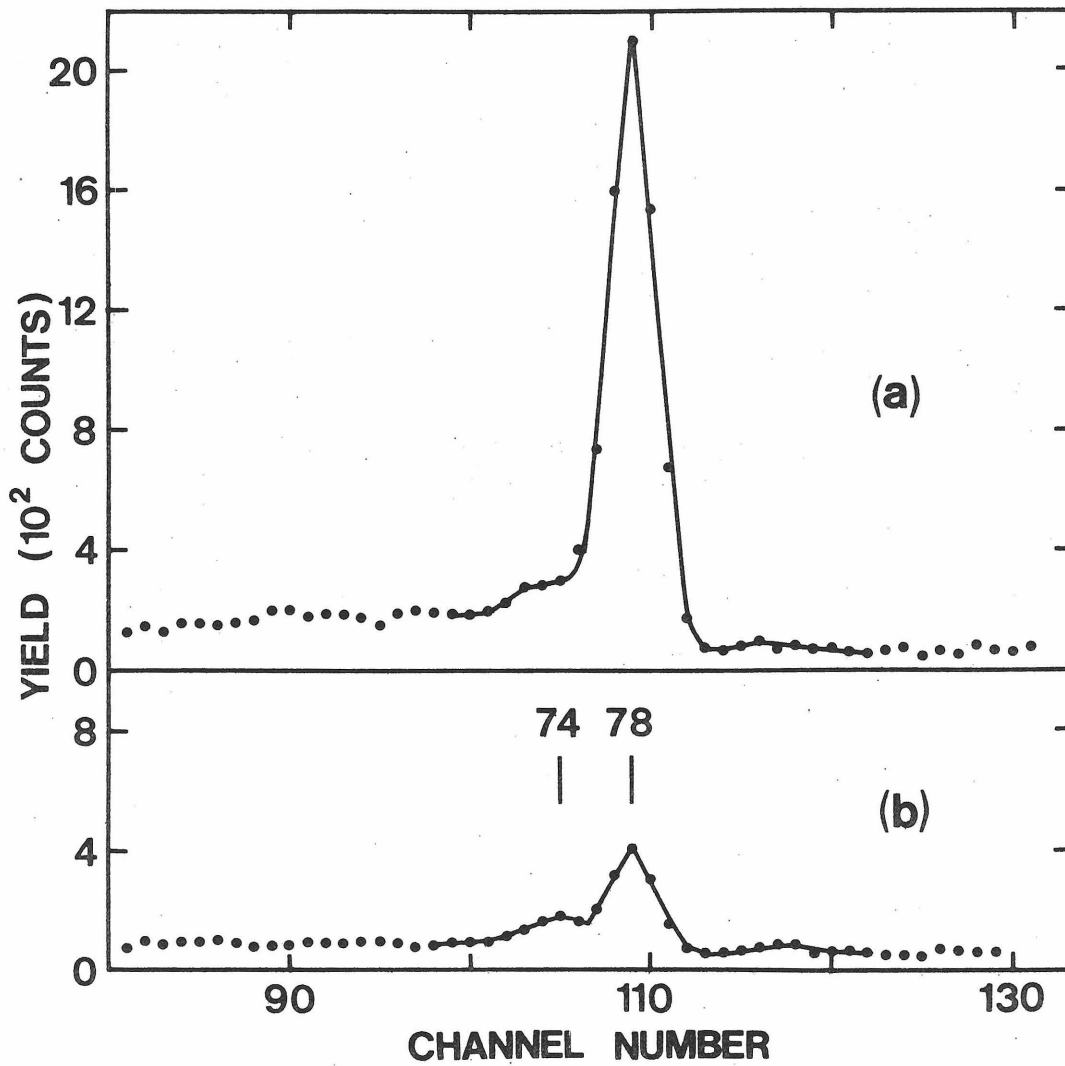
Figure 5. Relative yield of 78-keV γ rays from ^{32}P versus absorber position. The errors indicated are statistical errors only. The circular data points (b) denote the yield of 78-keV γ rays when the ^{32}P nuclei are permitted to recoil into vacuum, while the crosses (a) denote the yield when the recoils are stopped in a layer of copper. The resolution of the apparatus is found from the mean recoil distance in curve (a) to be 54 μm. The solid lines are least-squares fits to an exponential function.
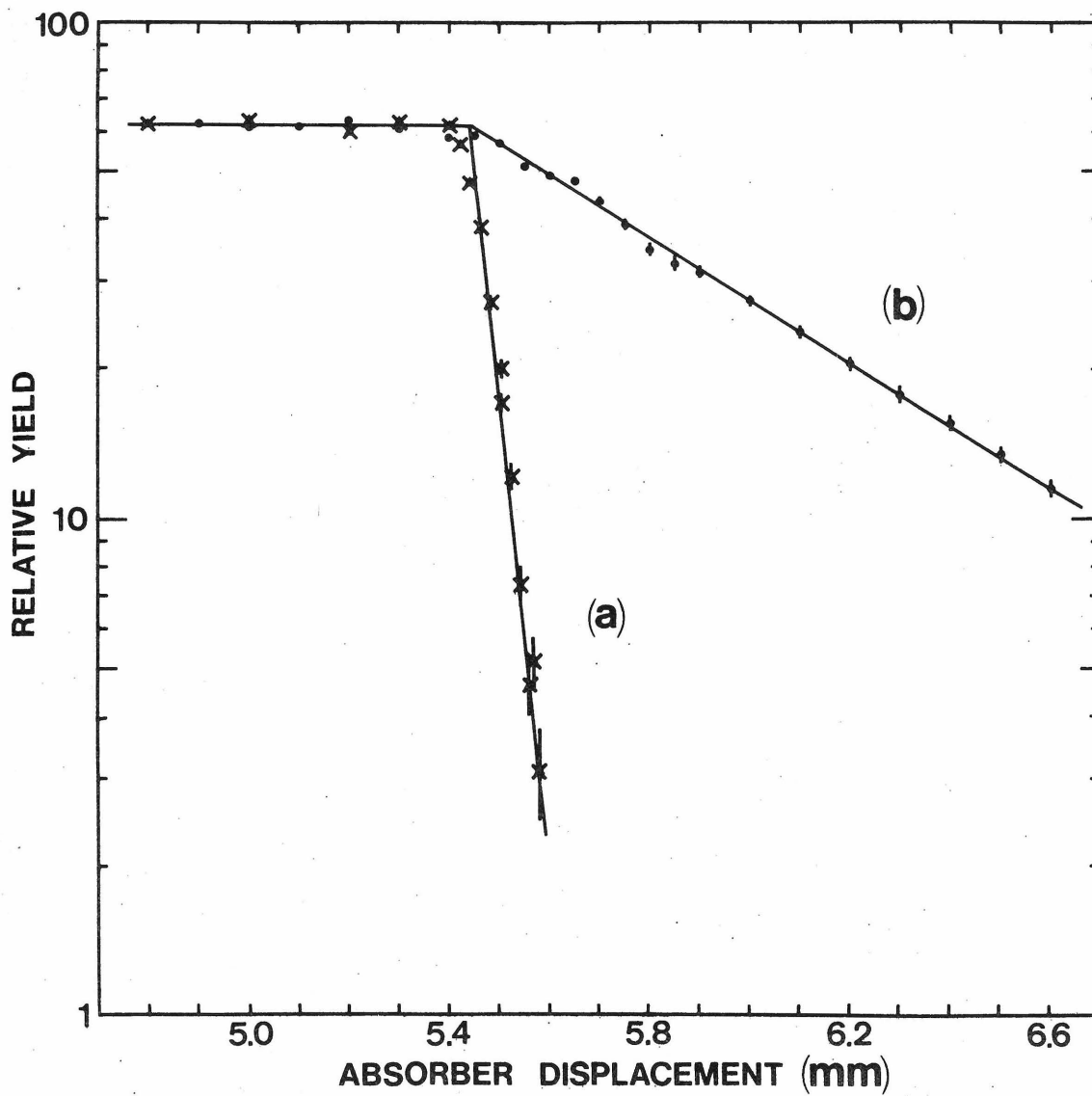
Figure 6. The angular distribution of protons populating the
78-keV level of ^{32}P by the ^{29}Si(^{4}He,p)^{32}P reaction.
The statistical errors are within the size of the
data points unless otherwise indicated. The smooth
curve shown is that used in deducing the mean
recoil velocity for the ^{32}P nuclei. The circular
and triangular data points indicate two separate
runs.
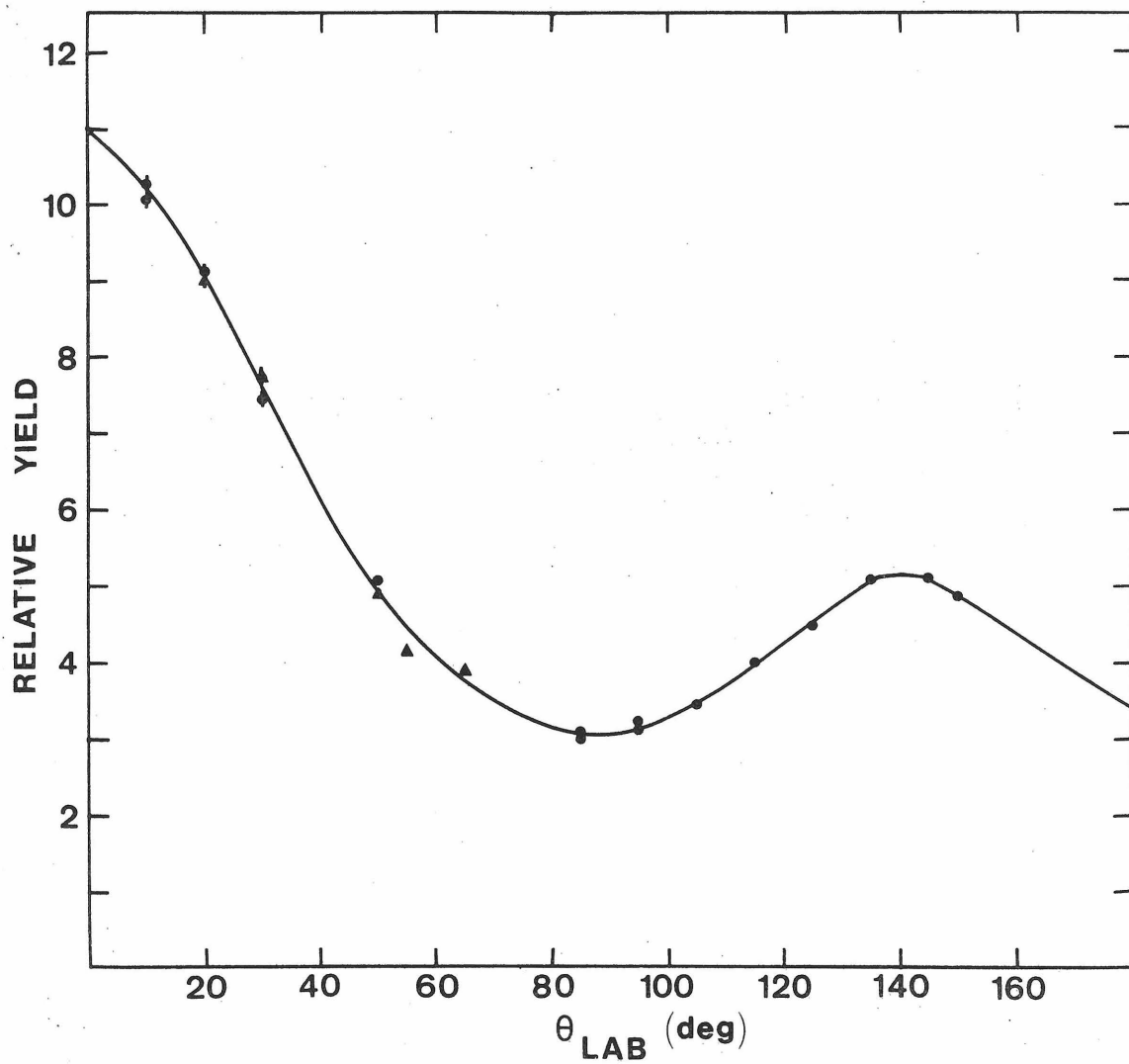
Figure 7. Schematic experimental arrangement for Doppler-

shift-attenuation lifetime measurements.

(See page 22.)
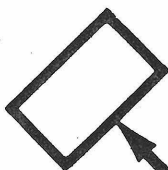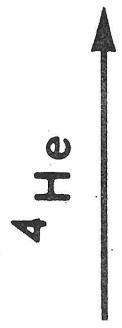
Figure 8. Plot of the DSAM factor F as a function of τ/α
for the approximation $F = \alpha/(\alpha + \tau)$. This relation
arises from the approximation that the rate of
energy loss is **proportional** to the ion velocity.

(See page 25.)

$$F = \frac{1}{1 + \tau/\alpha}$$
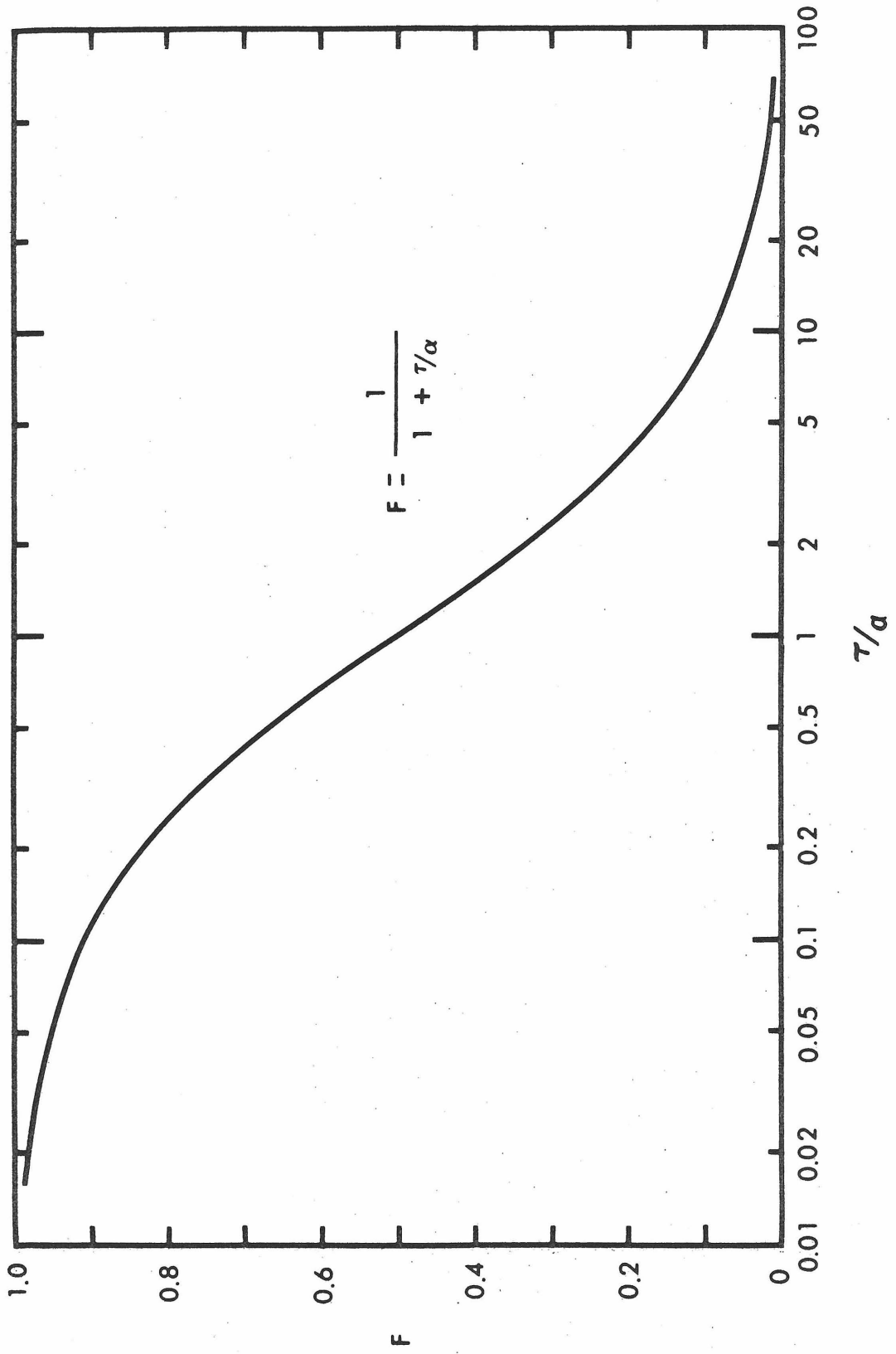
Figure 9. Experimental target arrangement employed when gases are used as the stopping medium.

(See page 28.)

SUPPRESSOR RING

Ta
BEAM CATCHER

VITON "O" RINGS

Ta LINER

FOIL

Ta LINER

Ta COLLIMATOR

TO GAS SUPPLY
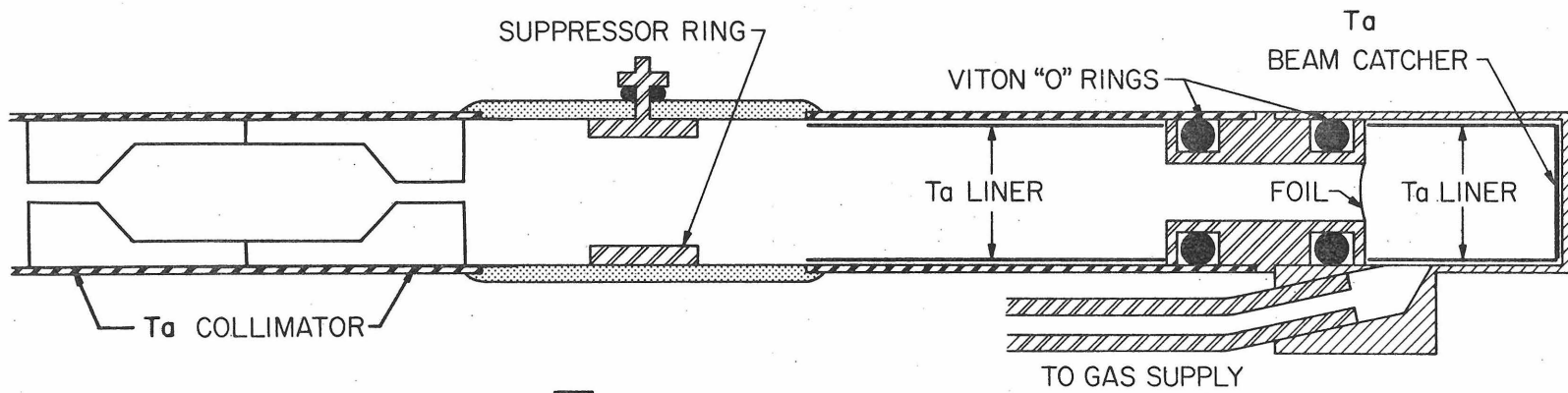
▨ STAINLESS STEEL

▨ KOVAR

▨ GLASS

▨ ALUMINUM

1 cm

Figure 10. Experimental arrangement employed when solids are used as the stopping medium.

(See page 29.)

TARGET ON CARBON FOIL

GLASS
TARGET CHAMBER

Ta
BEAM STOP

α BEAM

Ge(Li)
55 cm³

1 CM
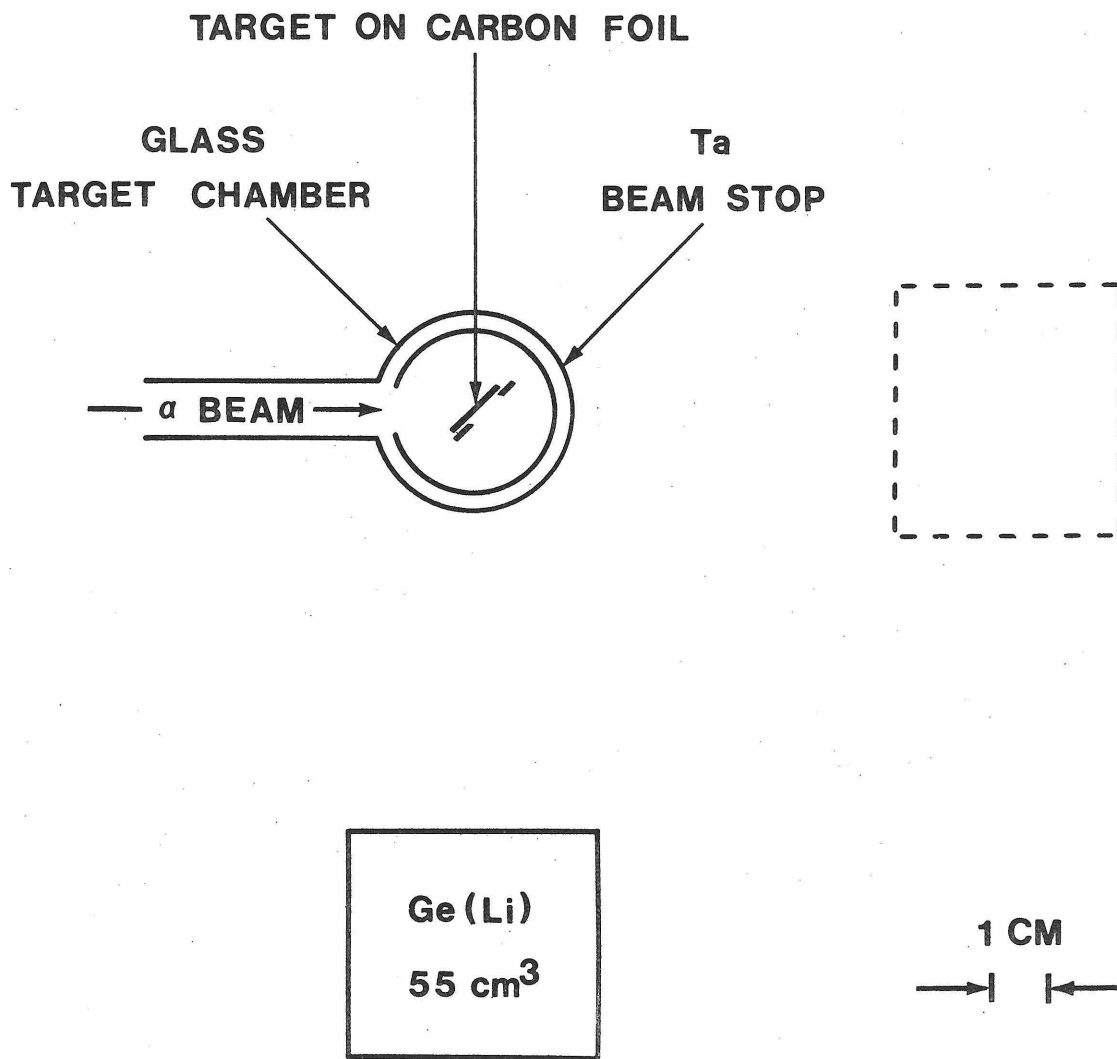
Figure 11. Electronic pulse-height analysis system employing digital spectrum stabilization, as used in the DSAM measurements.

(See page 30.)

DETECTOR

Ge(Li)

PREAMPLIFIER

ORTEC 118A

LINEAR AMPLIFIER

TENNELEC TC200

PULSE-HEIGHT ANALYZER

RIDL 34-27
OR
NUCLEAR DATA ND2200

γ

A

B

ZERO LEVEL CORRECTION

ADC
PULSE
TRAIN

ΔV_0

-2.1 KV

Ge(Li) BIAS SUPPLY

FLUKE 415B

ELECTRONIC
PULSER

GAIN STABILIZER

CI 1495

ZERO STABILIZER

CI 1496
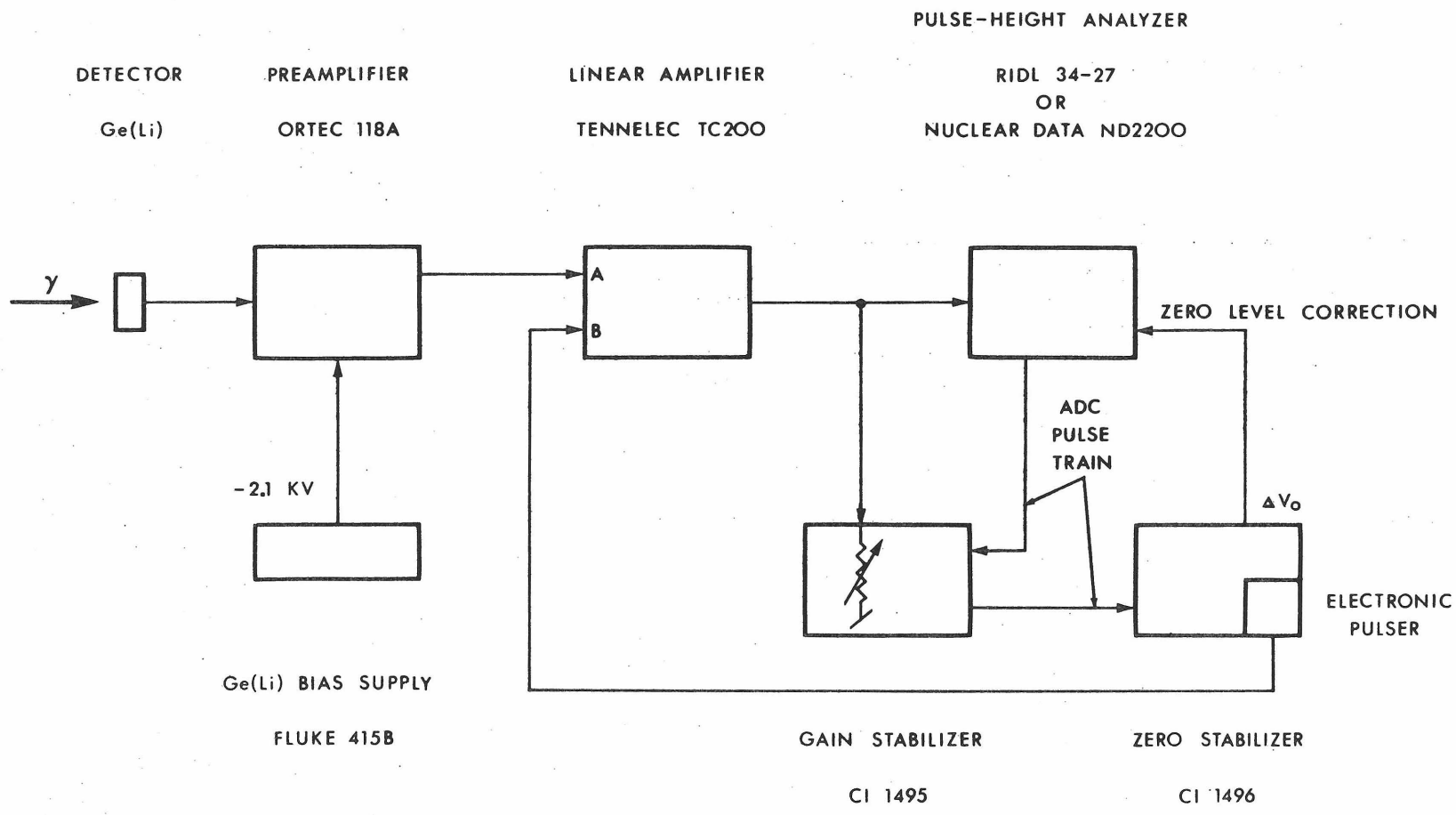
Figure 12. The measurement of the thickness of the ^{27}Al target used in the determination of the lifetime of the 1^+ level of ^{30}P at 709 keV. The figure shows the yield of elastically scattered 5-MeV ^{4}He particles as observed in the 61-cm-radius magnetic spectrometer. The horizontal axis gives the spectrometer NMR frequency. The triangular data points (b) show the yield of ^{4}He particles elastically scattered at 90° by a clean thick Pt backing, while the circular data points (a) give the yield when the ^{4}He particles pass through the ^{27}Al layer deposited on the Pt backing. The midpoint of curve (a) is 20.370 ± 0.002 MHz while the midpoint of curve (b) is 20.507 ± 0.002 MHz, leading to an energy difference of 64.0 ± 1.4 keV for the target turned at 45° to the beam and to the spectrometer. Including the uncertainty in the dE/dx tabulations, the derived target thickness is 36.5 ± 3.0 µg/cm^2 of ^{27}Al.
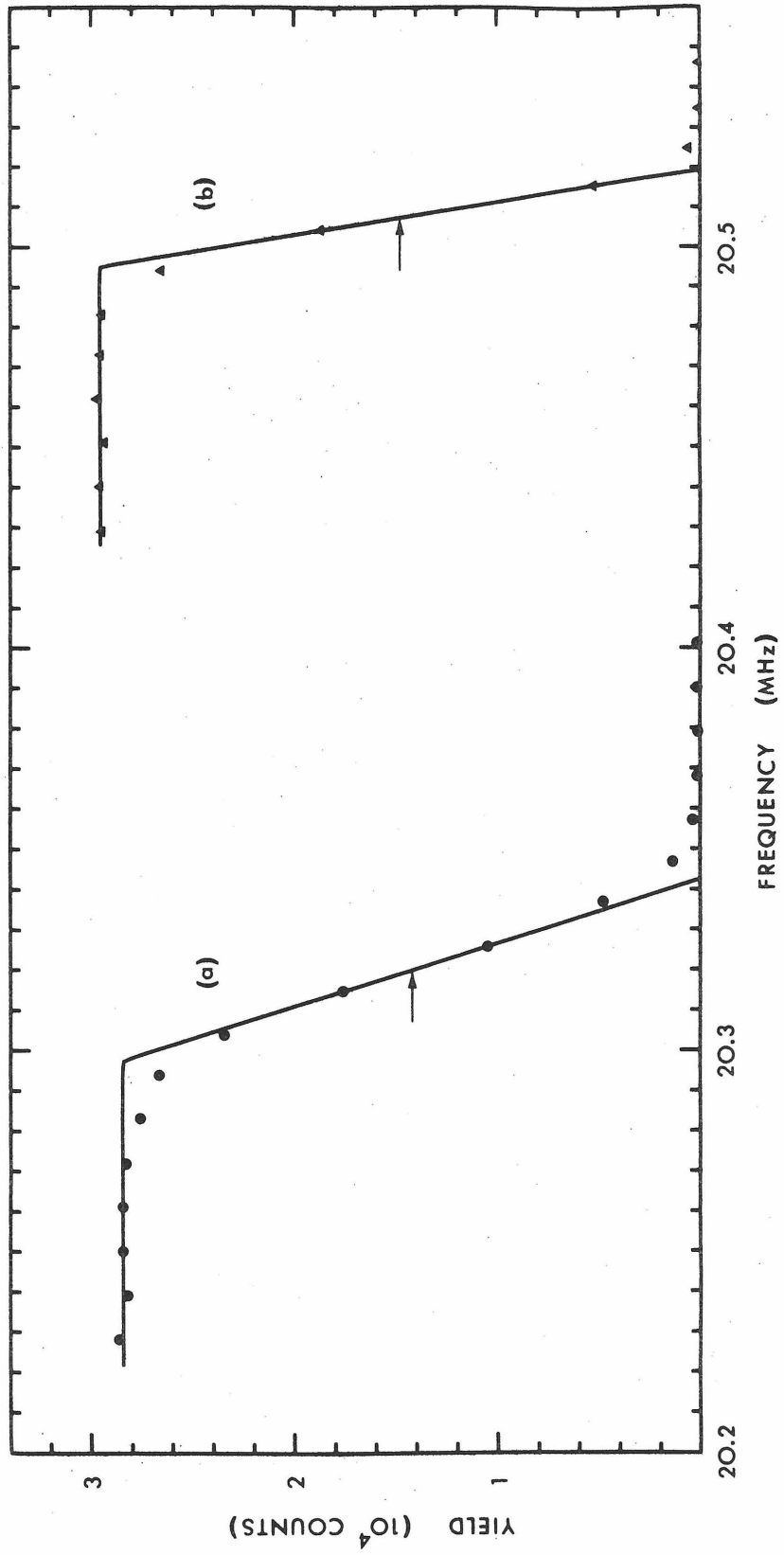
Figure 13. The nuclear $(d\epsilon/d\rho)_n$ and electronic $(d\epsilon/d\rho)_e$ energy loss in reduced units as a function of the energy ϵ. The analytic-function approximations to the numerical nuclear energy loss of the LSS theory mentioned on page 37 are shown. The electronic energy loss for four values of k as derived by the LS theory is also given.
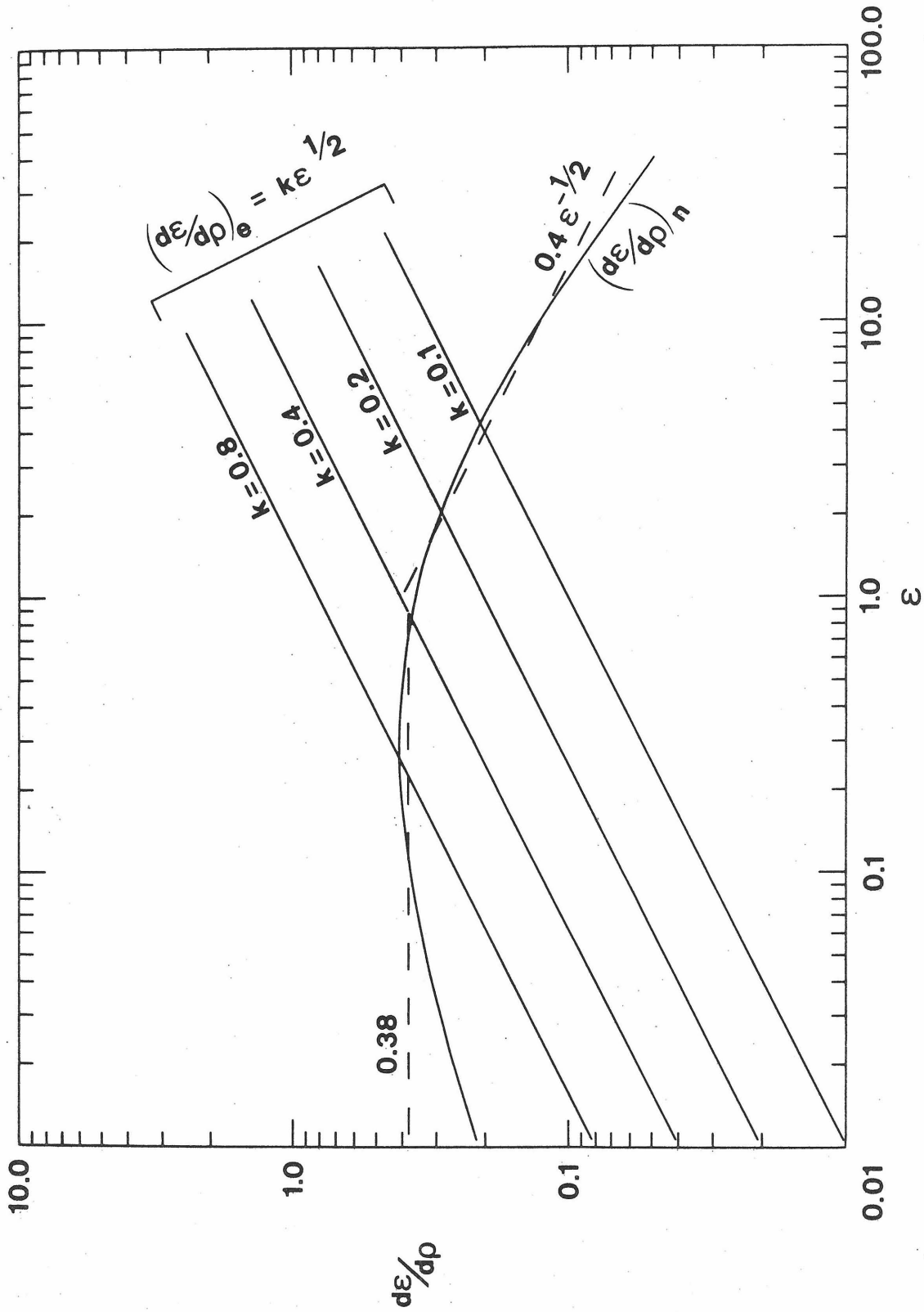
Figure 14. The electronic stopping cross section S_e for ions

with $Z_1 \leq 20$ at a constant ion velocity $v = 0.41 v_o$.

The data for N and Ar are from Ormrod (1968)

while the data for C are from Ormrod, Macdonald,

and Duckworth (1965). The solids curves labeled

$\xi = Z_1^{1/6}$ are the theoretical predictions of LS

theory. For ions in C, the solid curves labeled

$\xi = 1$ and $\xi = 2$ are the limits on ξ proposed by

LS theory. For ions in Ar, the curves labeled

$\xi = 0.7 Z_1^{1/6}$, $0.5 Z_1^{1/6}$, and $0.4 Z_1^{1/6}$ are the

theoretical predictions scaled down by factors of

0.7, 0.5, and 0.4 respectively.

$V = 0.41 V_O = 0.9\,mm/ns$

CARBON

$\xi = 2$

$\xi = Z_1^{1/6}$

$\xi = 1$

S_e (10^{-14} eV$-$cm^2/ATOM)

NITROGEN

$\xi = Z_1^{1/6}$

ARGON

$\xi = Z_1^{1/6}$

$\xi = 0.7 Z_1^{1/6}$
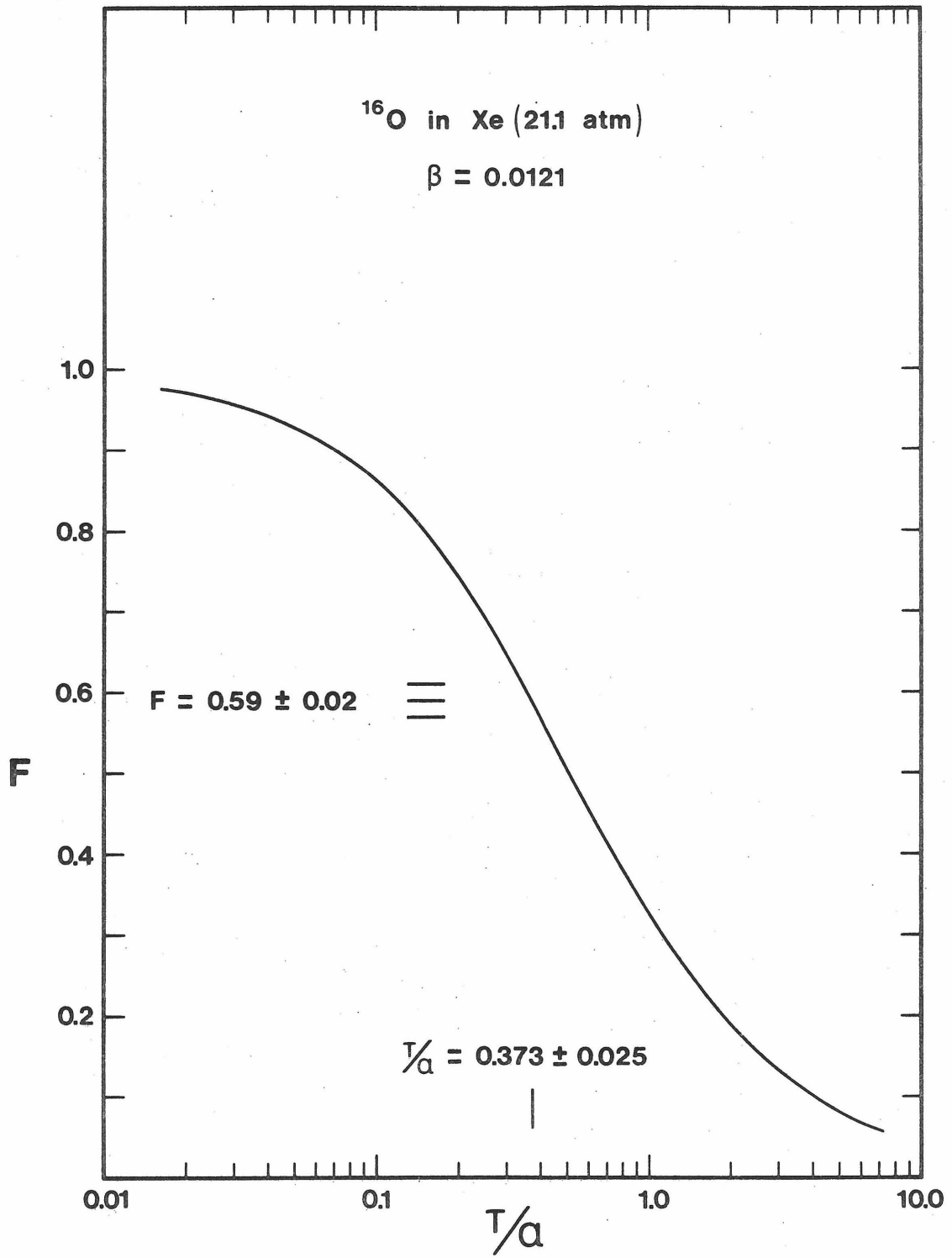
$\xi = 0.5 Z_1^{1/6}$

$\xi = 0.4 Z_1^{1/6}$

Z_1
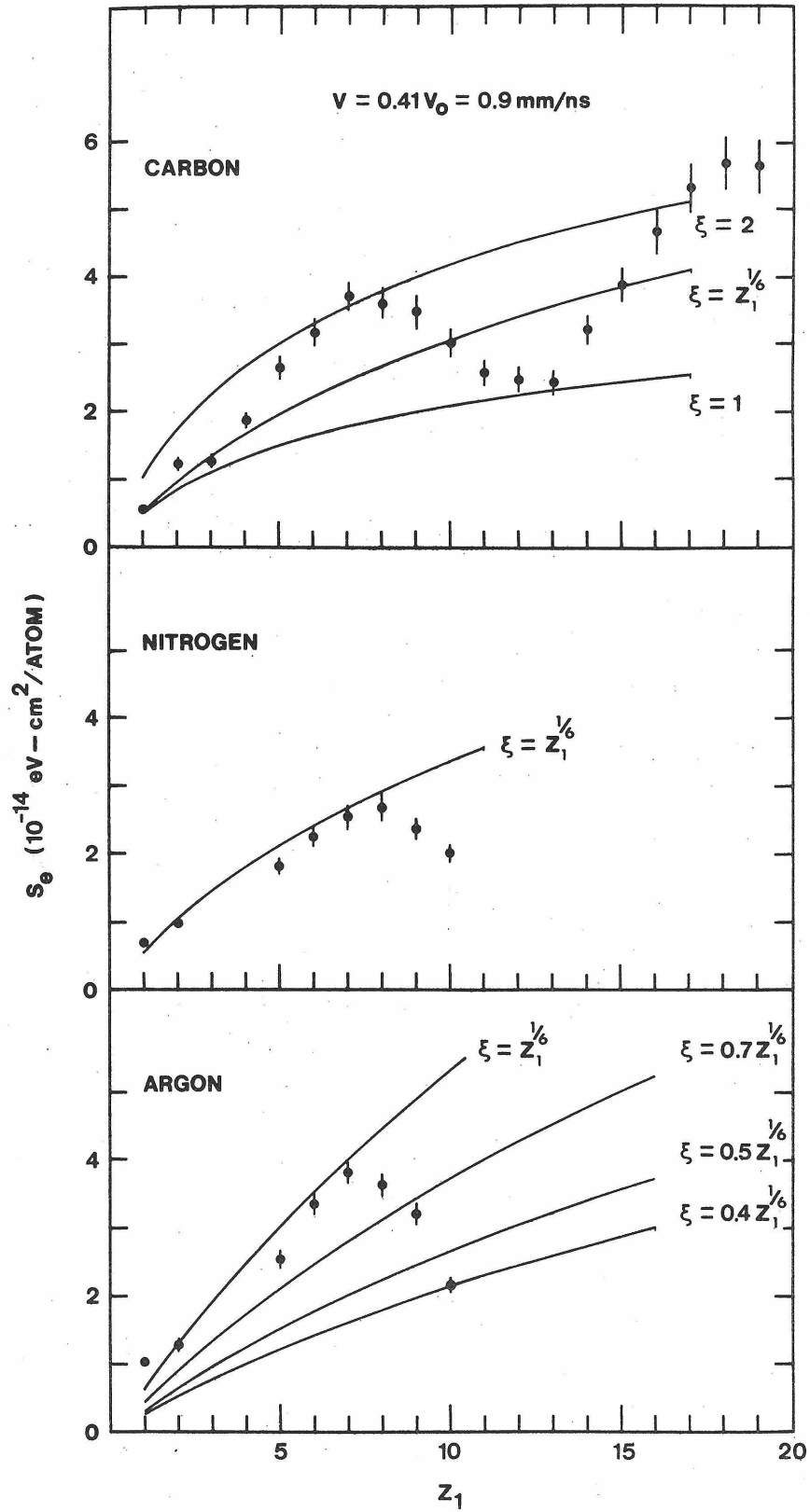
Figure 15. The relevant part of the level diagram for ^{26}Al.
This summary is that given by Endt and Van der Leun
(1967).

(See page 56.)

1.760 ——————●———— $2^+, 0$

1.059 ——————●———— $1^+, 0$

0.418 ——●—————— $3^+, 0$

0.229 ———————— $0^+, 1$

0 ———————— $5^+, 0$

^{26}Al

-2.964 ————————

$^{23}Na + \alpha - n$
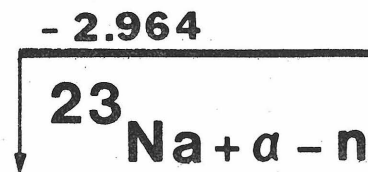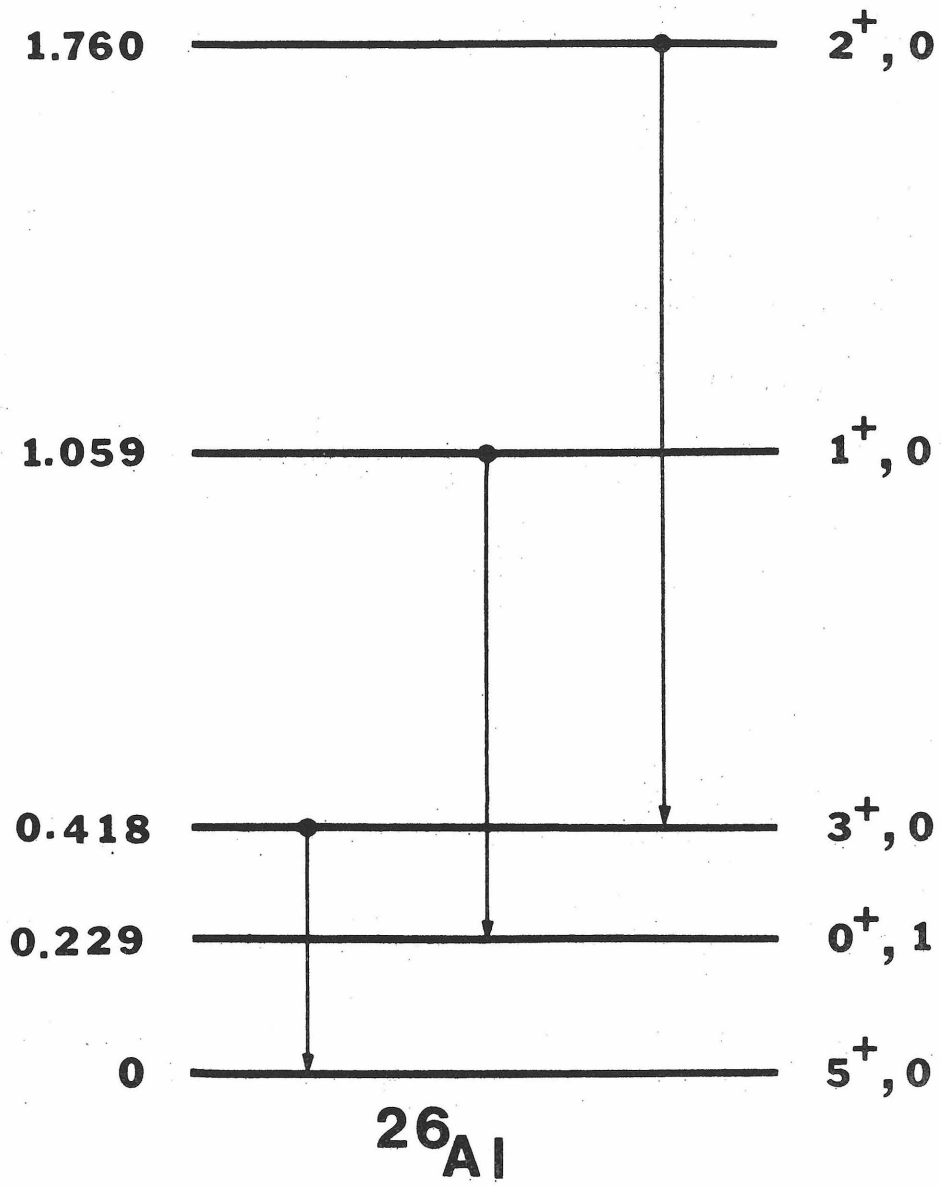
Figure 16. A portion of the γ-ray spectra obtained with the 6-cm^3 Ge(Li) detector resulting from the ^{23}Na(^{4}He,n)^{26}Al reaction. The γ ray at 418 keV arises from the decay of the 418-keV level of ^{26}Al while the 356-keV and 408-keV γ rays arise from Coulomb excitation of ^{194}Pt and ^{198}Pt isotopes in the Pt gas-retaining foil. The dispersion is 0.69 keV/ch. The beam current is maintained at 100 ± 5 nA and the Xe pressure is 0.52 atm. The notation × 5 indicates that these data have been multiplied by a factor of 5.
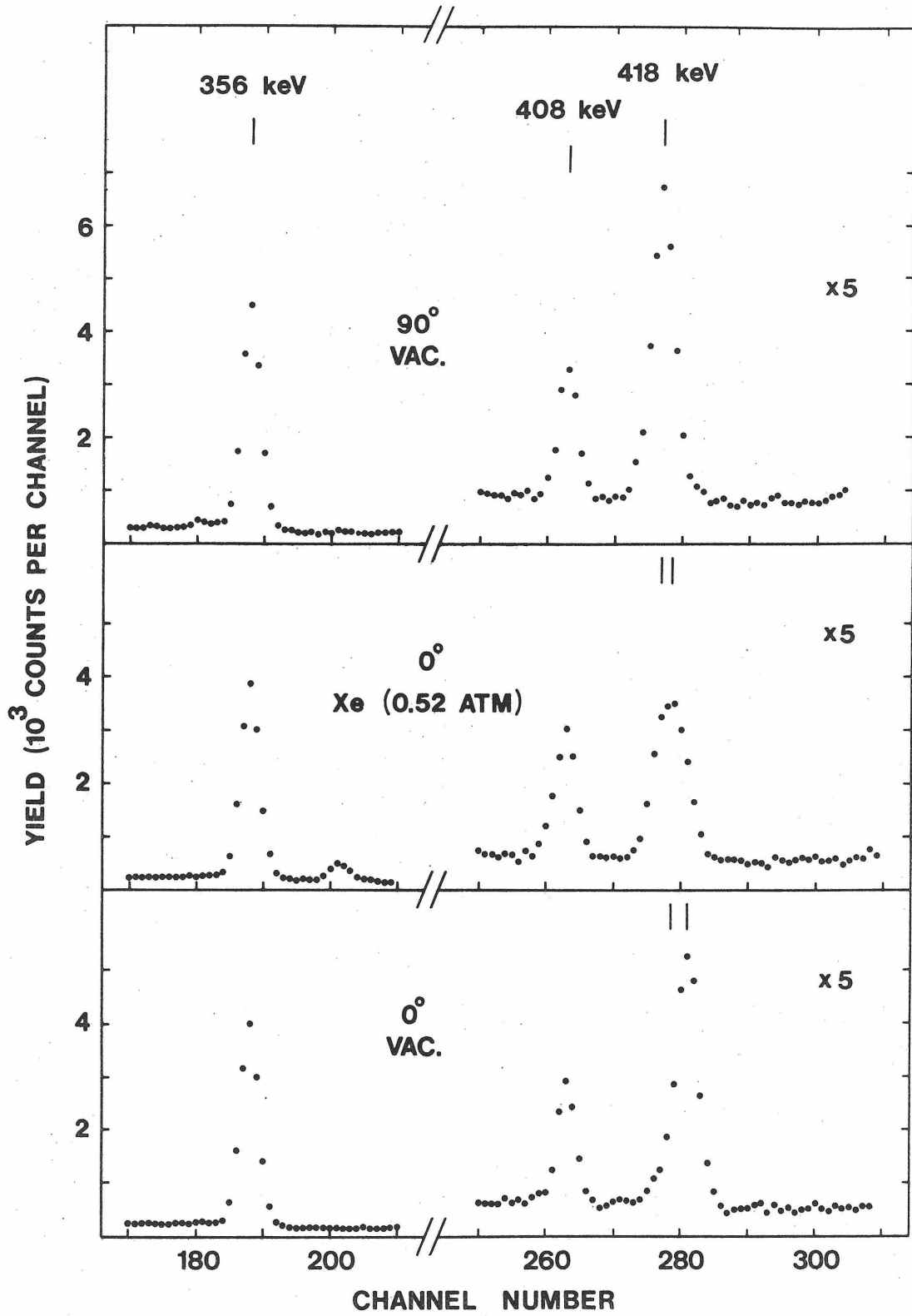
Figure 17. The observed DSAM factor F as a function of the beam current for ^{26}Al recoils slowing in Xe gas. The data of Fig. 17(a) are for ^{26}Al recoils with initial velocity $\beta(0) = (7.28 \pm 0.22) \times 10^{-3}$ slowing in Xe at a pressure of 0.52 atm, while the data of Fig. 17(b) are for recoils with initial velocity $\beta(0) = (6.1 \pm 0.3) \times 10^{-3}$ slowing in Xe at a pressure of 0.40 atm. The dashed straight lines are hand-drawn to guide the eye.

Figure 18. The relevant part of the level diagram for ^{33}S.

This summary is that given by Endt and Van der Leun

(1967).

(See page 58.)

^{33}S

$^{30}Si + \alpha - n$
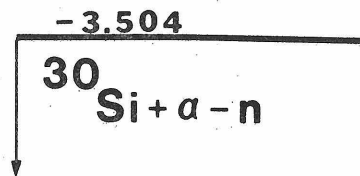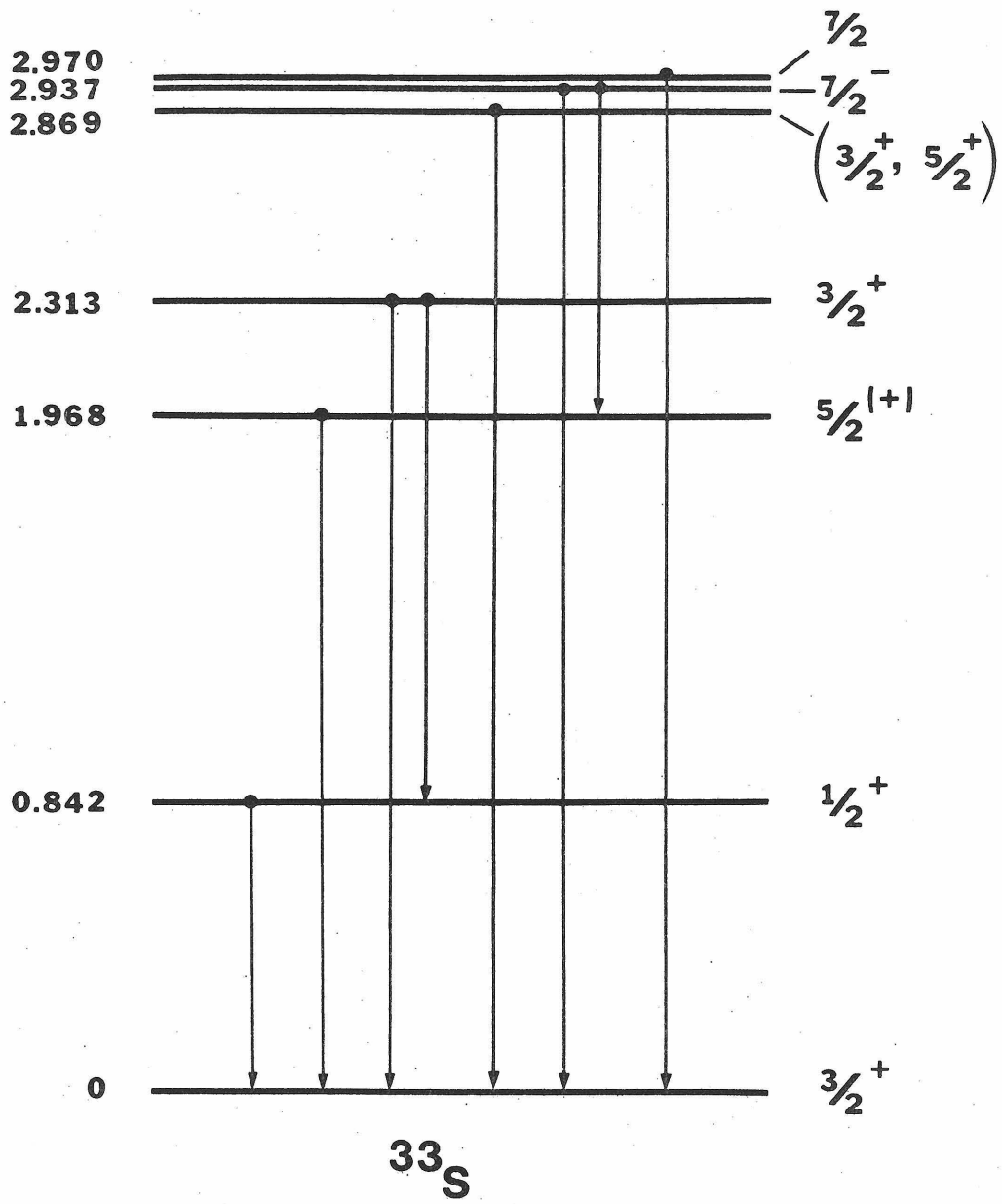
Figure 19.   A portion of the γ-ray spectra obtained with the
55-cm^3 Ge(Li) detector resulting from the
^{30}Si(^{4}He,n)^{33}S reaction.   The γ rays at 2970 keV,
2934 keV and 2869 keV arise from the decays to
the ground state of levels in ^{33}S with these energies.
The lines at 2615 keV and 511 keV arise from a
^{212}Pb (ThB) source placed near the target.   The
dispersion is 0.89 keV/ch.   The beam current is
maintained at 130 ± 10 nA and the Xe pressure is
13.6 atm.
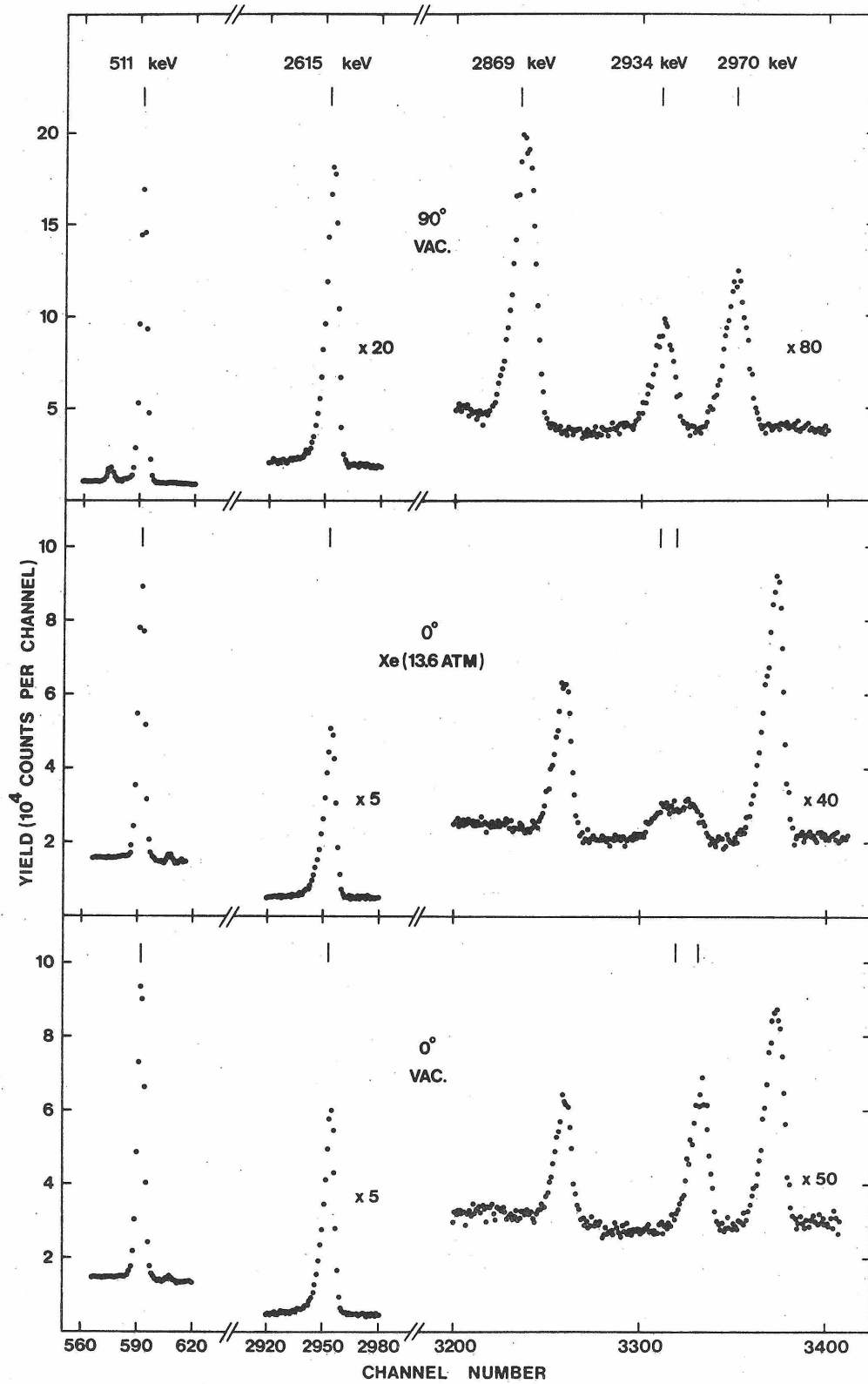
Figure 20. The observed DSAM factor F as a function of the beam current for ^{33}S recoils slowing in Xe gas at a pressure of 13.6 atm. The initial ion velocity was $\beta(0) = (6.35 \pm 0.21) \times 10^{-3}$. The dashed straight line is hand-drawn to guide the eye.

(See page 60.)
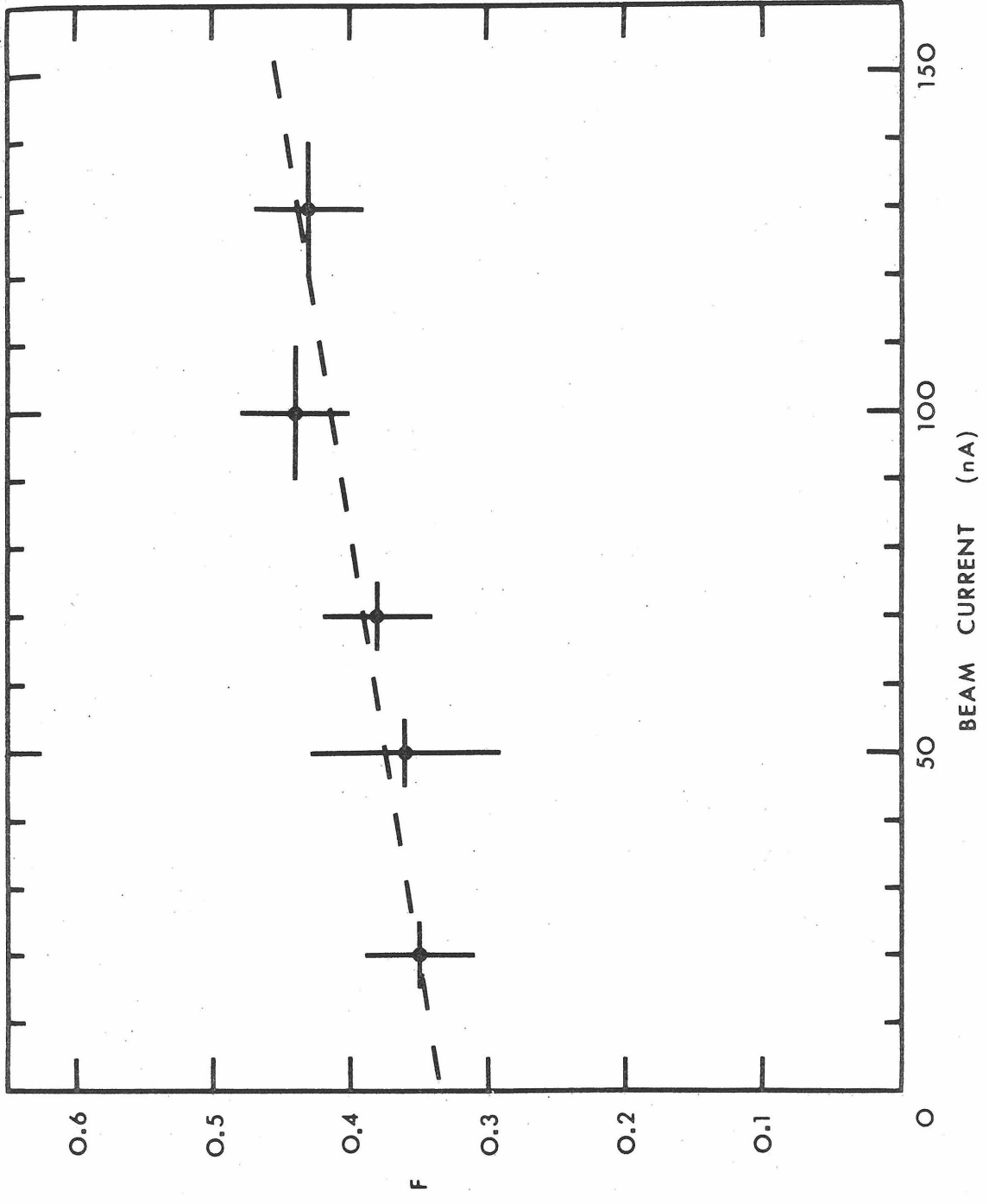
Figure 21. A plot of the calculated DSAM factor F as a function

of τ/α, along with the measured $F = 0.41 \pm 0.03$,

for the decay of the 418-keV level of ^{26}Al recoils

with initial velocity $\beta(0) = (7.28 \pm 0.22) \times 10^{-3}$

slowing in Xe gas at 0.52 atm pressure. Both

curves (a) and (b) include the electronic and nuclear

energy losses, as well as the effects of nuclear

scattering. Curve (a) is calculated for $f_e(gas) =$

0.50, $f_n = 0.8$, and $f_e(Z_1, \bar{v}/v_o) = 0.68$, leading to

an electronic slowing-down time of $\alpha = 5.82$ ns.

Curve (b) is calculated for the LSS theoretical

values $f_e(gas) = 1.0$ and $f_n = 1.0$, and corrected

for S_e oscillations with Z_1 using $f_e(Z_1, \bar{v}/v_o) =$

0.68; these lead to an electronic slowing-down time

of $\alpha = 2.92$ ns. Using the measured F value,

curve (b) leads to a lifetime of $\tau = 1.20 \pm 0.14$ ns,

while curve (a) leads to the correct value

$\tau = 1.81 \pm 0.23$ ns.

^{26}Al in Xe $\left(0.52 \text{ atm}\right)$

$\beta = 0.00728$

$F = 0.41 \pm 0.03$

(b)

(a)

F

T/a
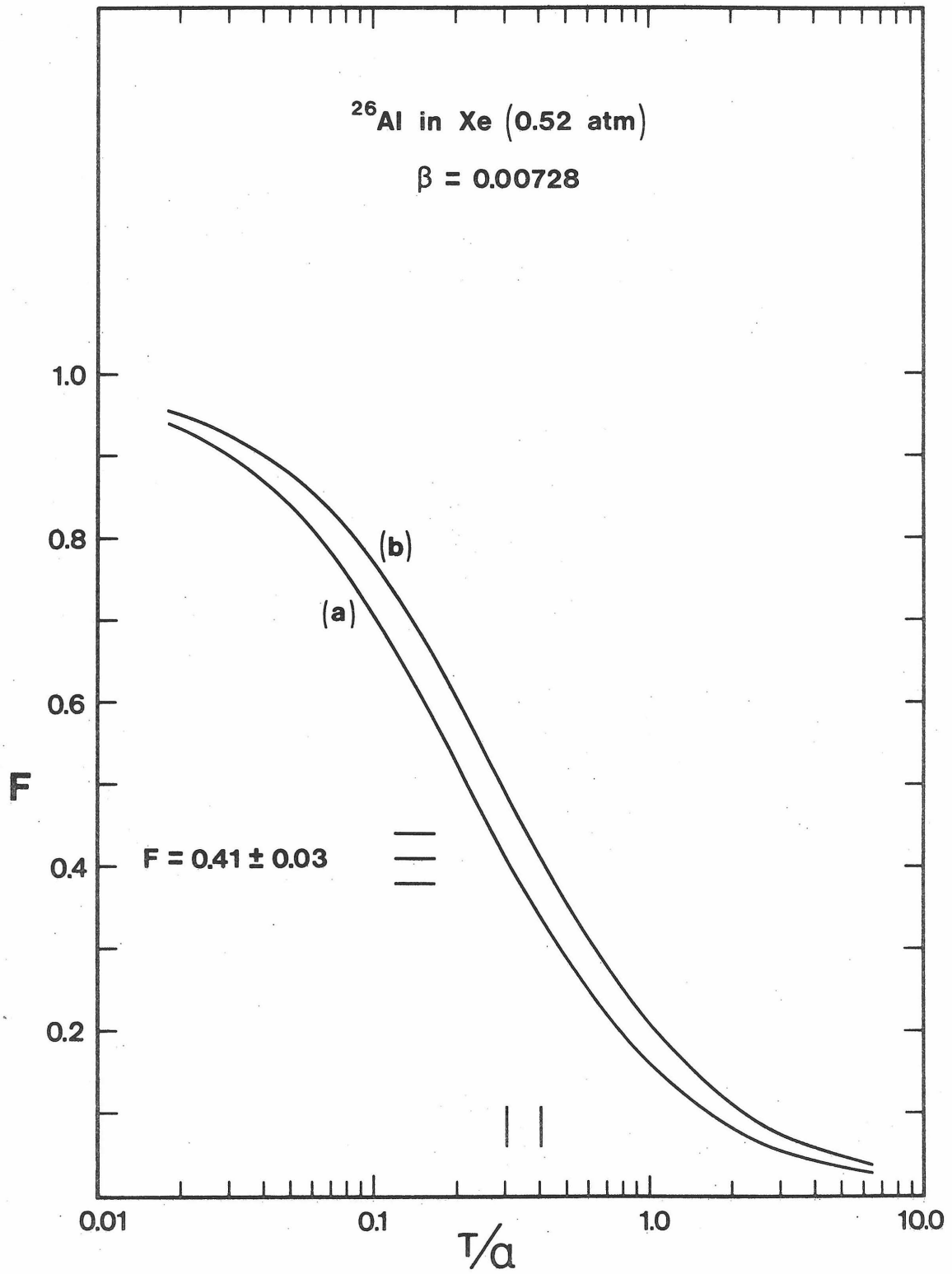
Figure 22. A portion of the γ-ray spectra obtained with the 55-cm^3 Ge(Li) detector resulting from the ^{23}Na(^{4}He,n)^{26}Al reaction. The γ ray at 418 keV arises from the decay of the 418-keV level of ^{26}Al, while the 279-keV and 408-keV γ rays arise from a ^{203}Hg source placed near the target and from Coulomb excitation of the ^{194}Pt isotope in the platinum gas-retaining foil. The dispersion is 0.69 keV/ch. The beam current was maintained at 100 ± 10 nA and the He pressure was 5.44 atm.
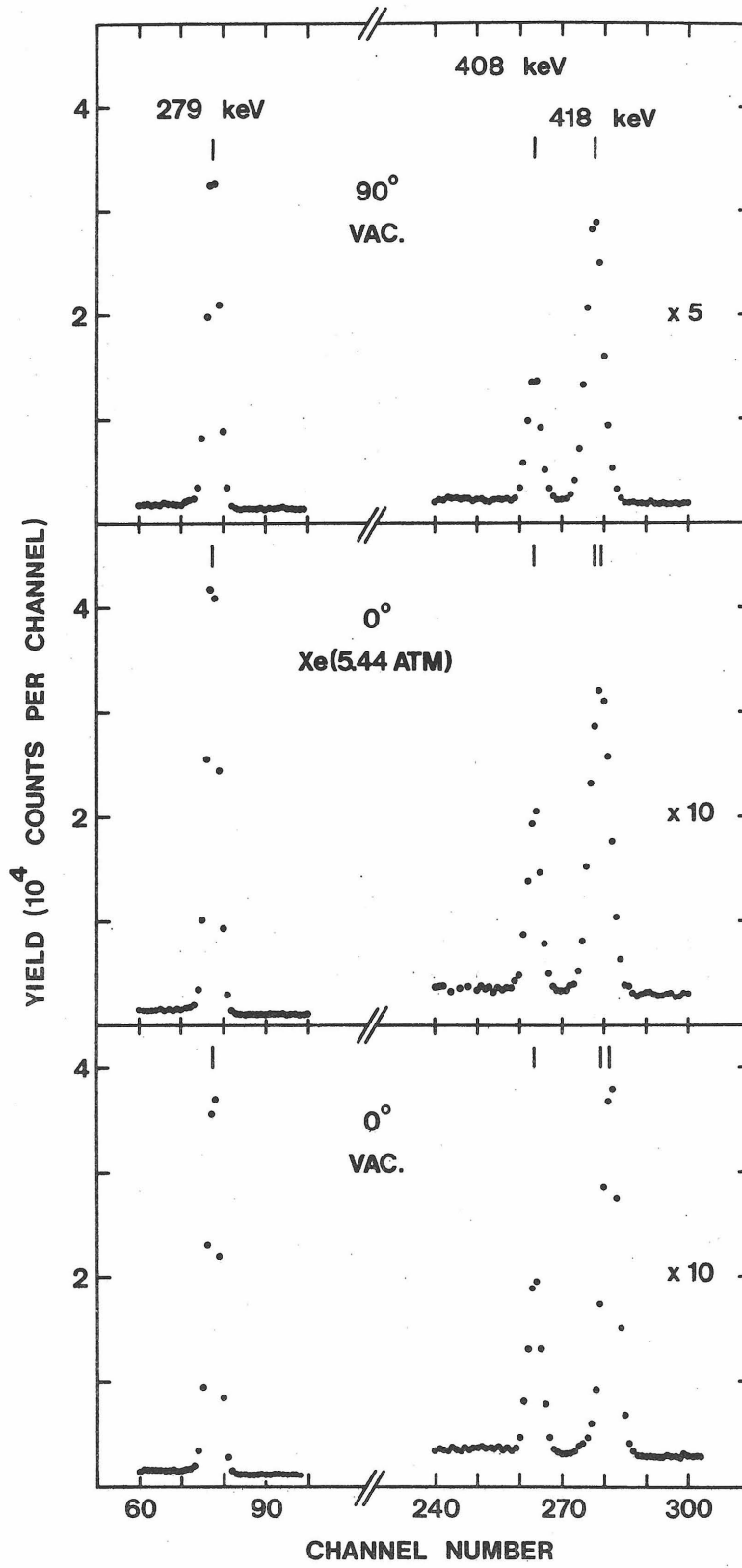
Figure 23. The relevant portion of the level diagram for ^{16}O. This summary is that given by Ajzenberg-Selove (1971).

(See page 66.)
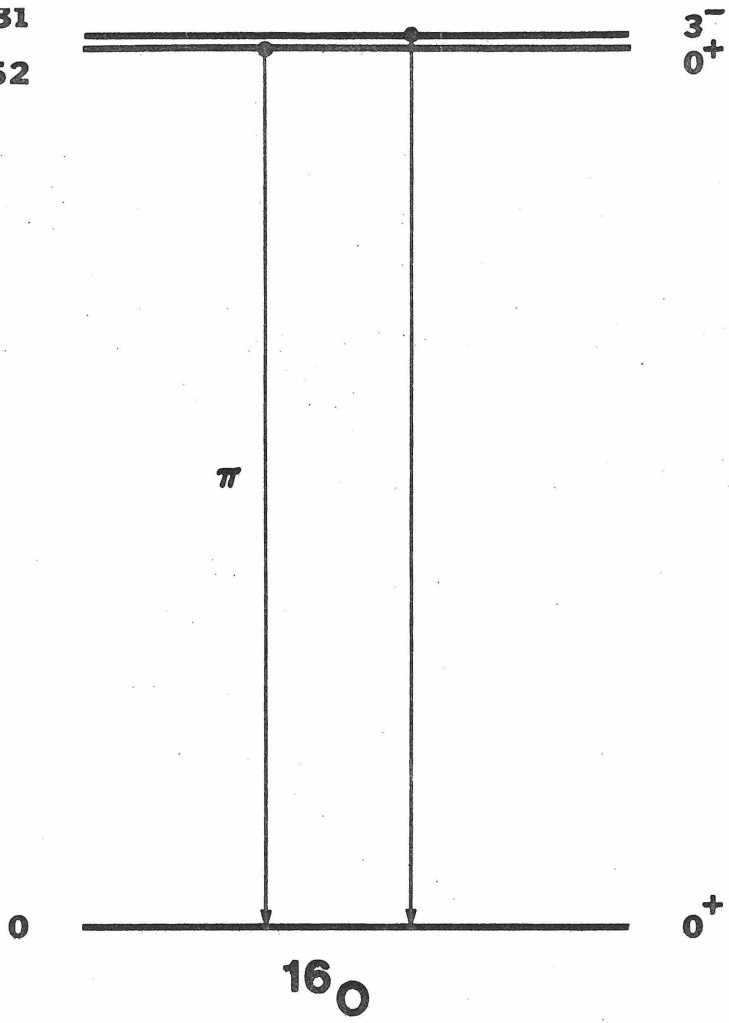
Figure 24.   A portion of the γ-ray spectra obtained with the
40-cm^3 Ge(Li) detector resulting from the
^{13}C(^{4}He,n)^{16}O reaction.   The line at 6131 keV is
the photopeak of the γ ray from the decay of the
6131-keV level to the ground state of ^{16}O, while
the lines at 6131 - 511 keV and at 6131 - 1022 keV
are the single-escape and double-escape lines,
respectively, produced by this γ ray.   The dis-
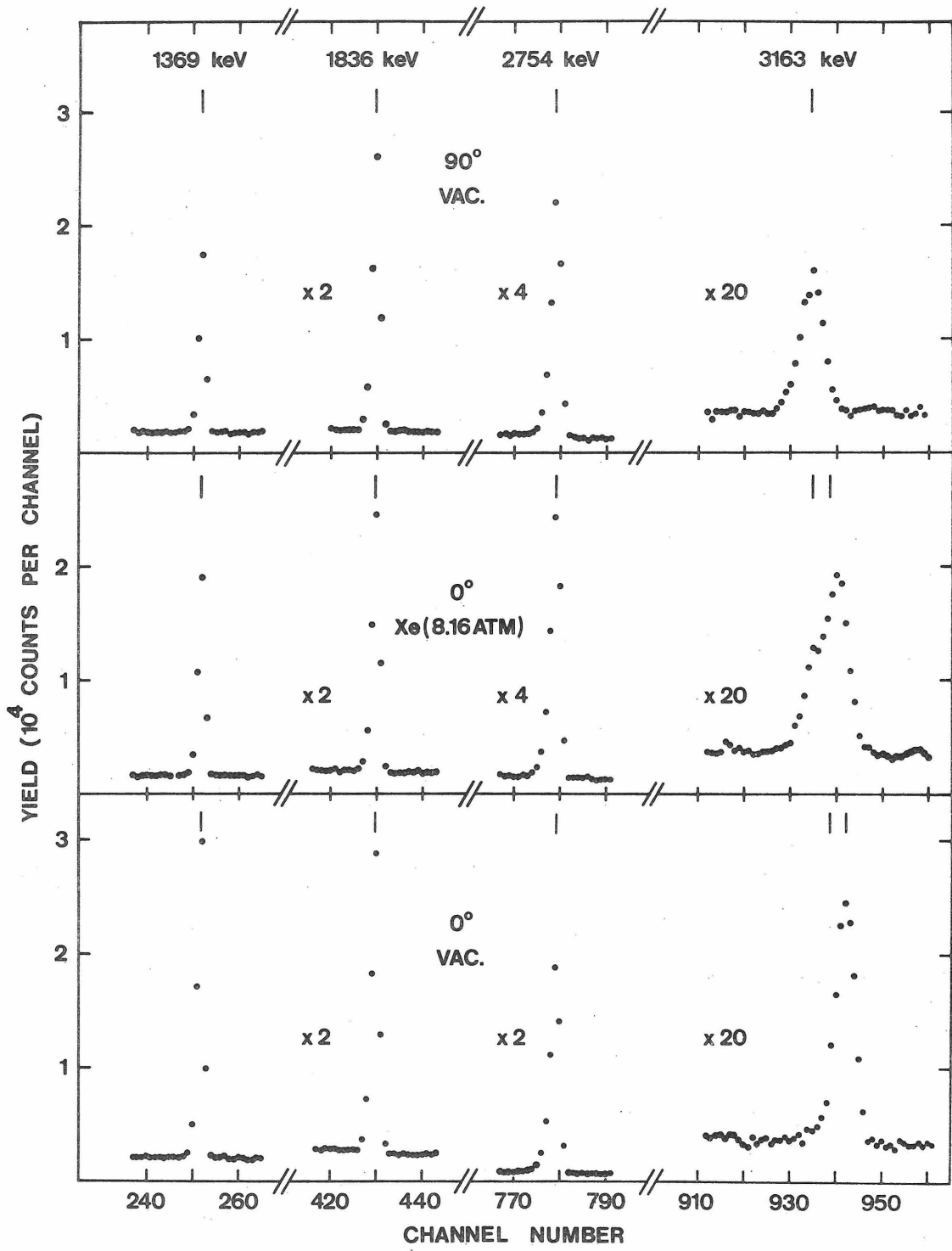persion is 8.63 keV/ch.
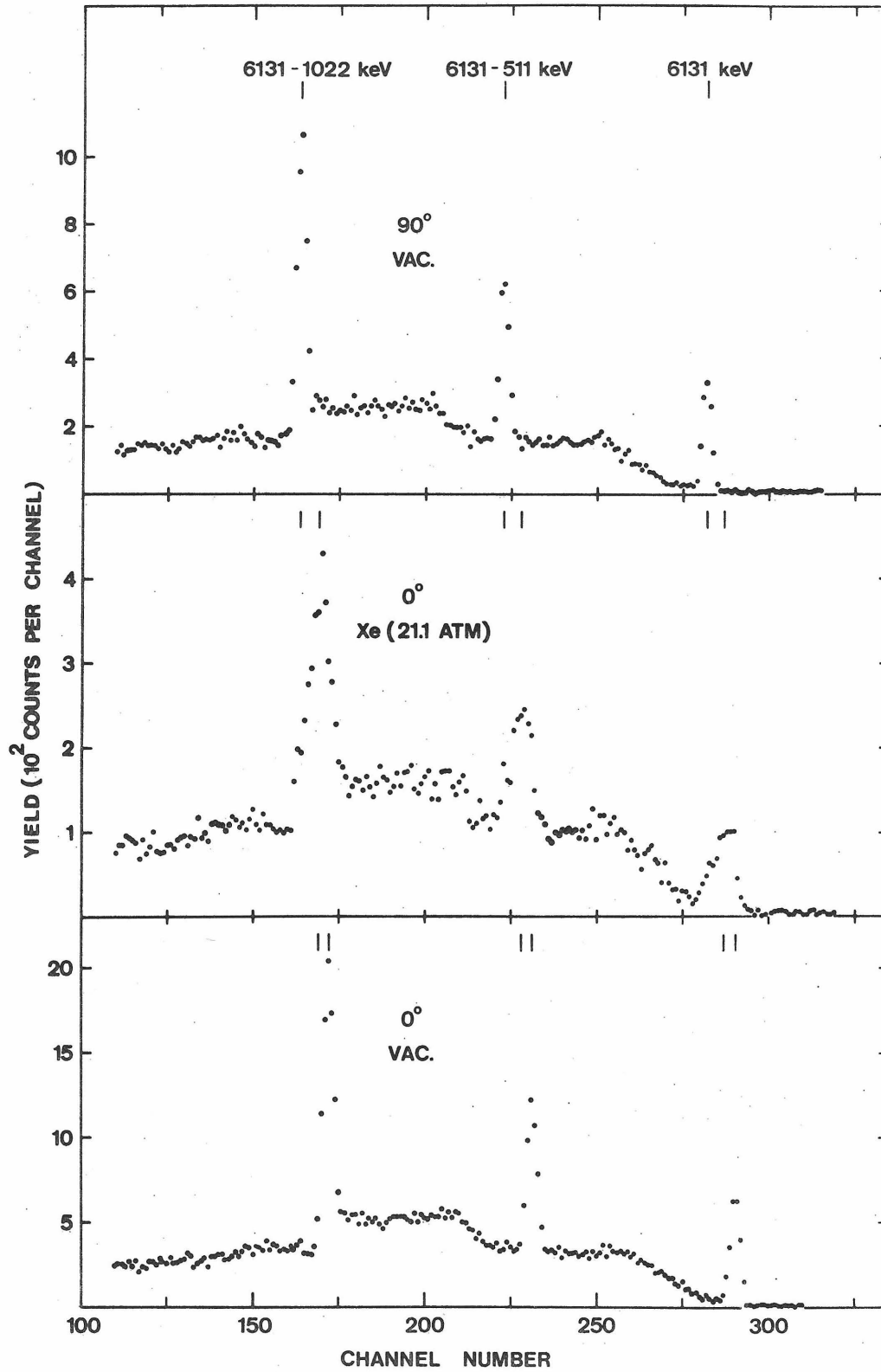
Figure 25. A plot of the calculated DSAM factor F as a

function of τ/α, along with the measured

$F = 0.59 \pm 0.02$, for the decay of the 6131-keV

level of ^{16}O recoils with initial velocity $\beta(0) =$

1.21×10^{-2} slowing in Xe gas at 21.1 atm pres-

sure. The curve is calculated with $f_n = 0.8$,

$f_e(Z_1, \bar{v}/v_0) = 1.15$ and $f_e(gas) = 0.50$, leading

to an electronic slowing-down time of $\alpha = 81.2$ ps

and a lifetime of $\tau = 30.3 \pm 2.2$ ps. Inclusion of

the uncertainty in $f_e(gas)$ leads to the uncertainty

($\pm$ 6 ps) quoted in Table VII for the case with

$f_n = 0.8$.

^{16}O in Xe (21.1 atm)

$\beta = 0.0121$

F = 0.59 ± 0.02

T/a = 0.373 ± 0.025

Figure 26. The relevant portion of the level diagram for ^{37}Ar.
This summary is that given by Endt and
Van der Leun (1967).

(See page 70.)
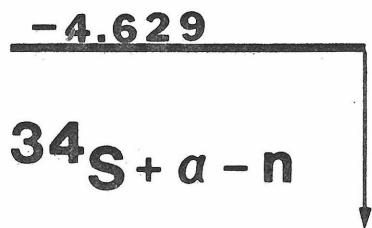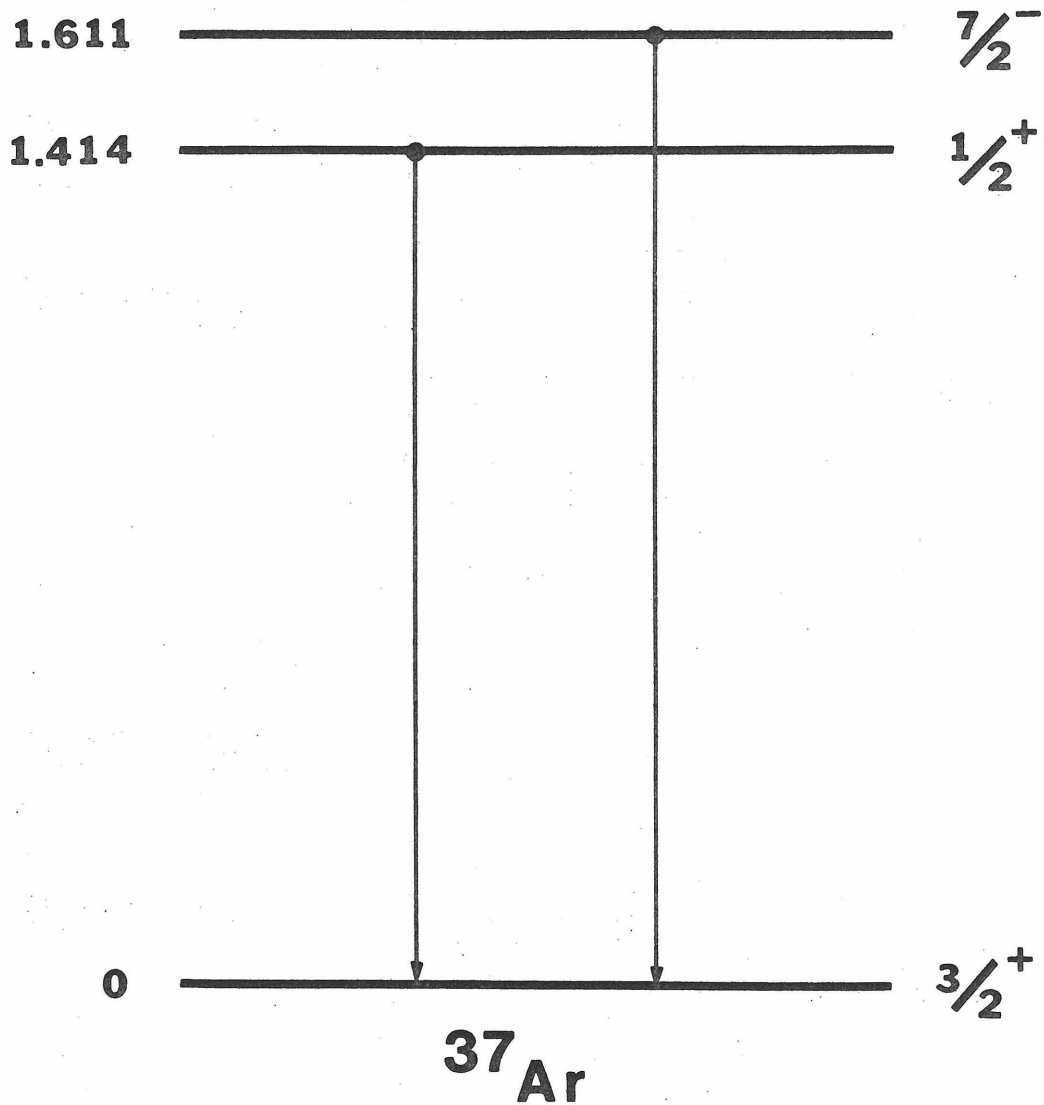
Figure 27.   A portion of the γ-ray spectra obtained with the

55-cm^3 Ge(Li) detector resulting from the

^{34}S(^{4}He,n)^{37}Ar reaction.   The γ ray at 1611 keV

arises from the decay of the 1611-keV level of

^{37}Ar, while the 1333-keV and 1173-keV lines

arise from a ^{60}Co source placed near the target.
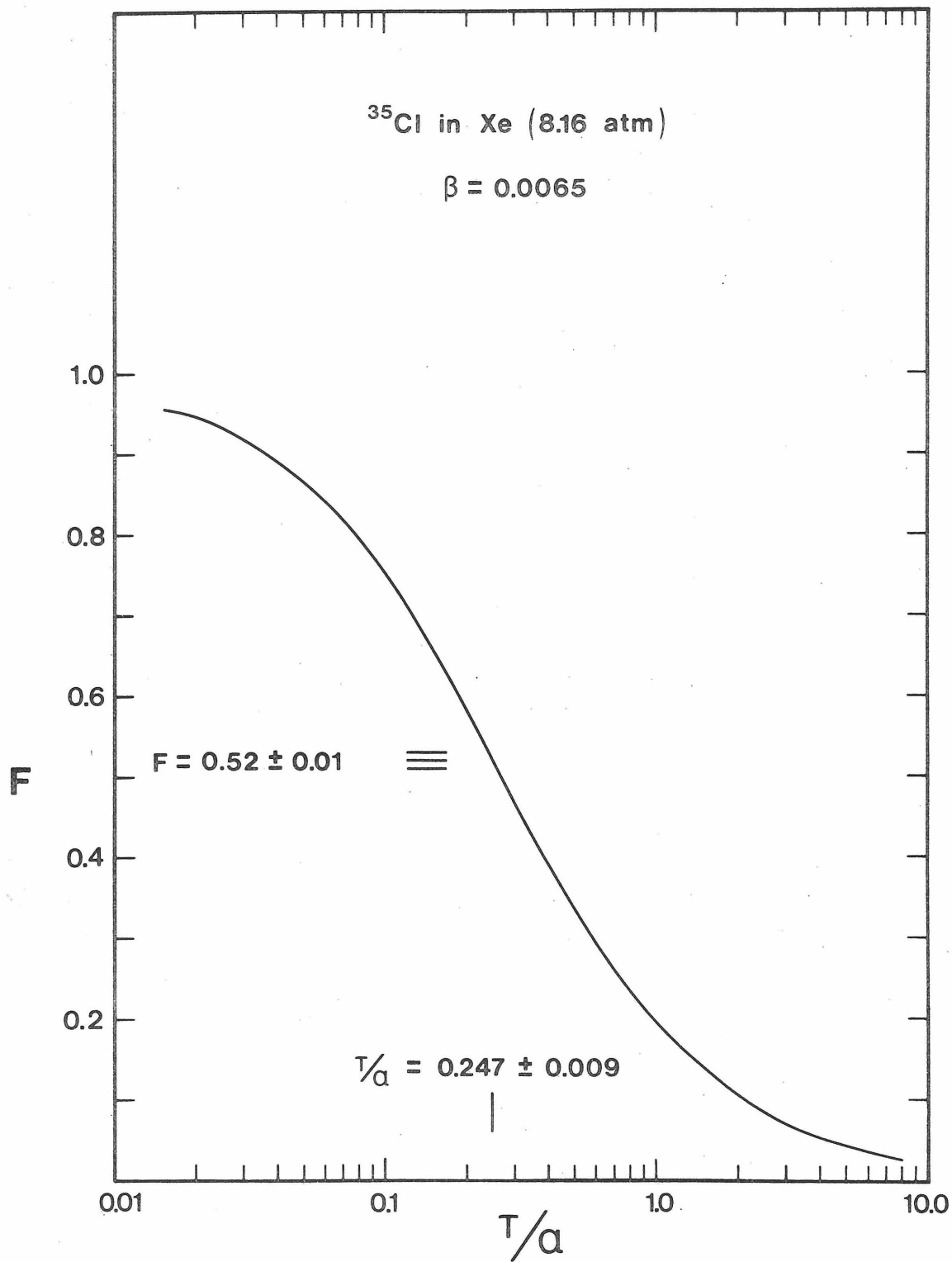
The dispersion is 1.49 keV/ch.
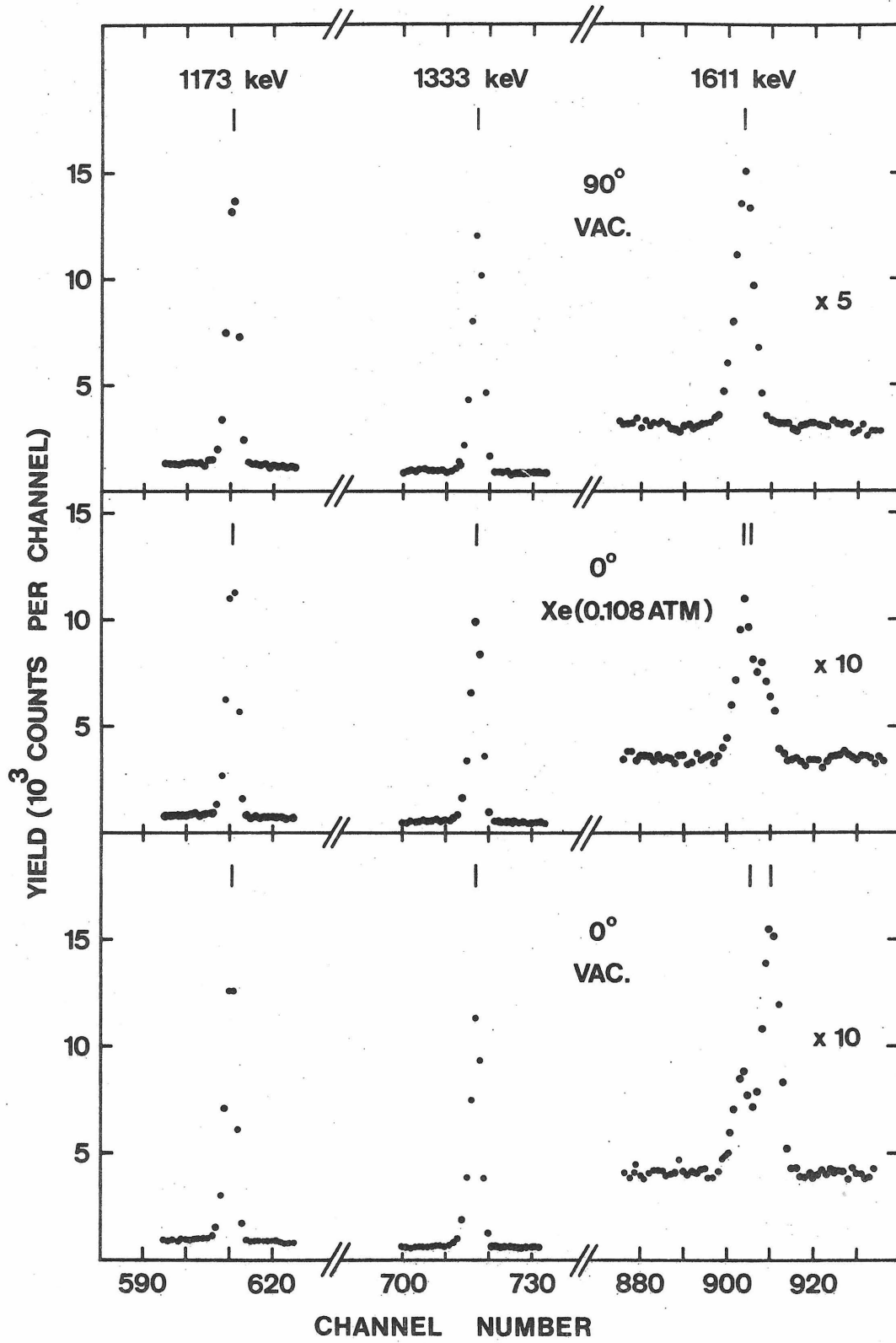
Figure 28. A plot of the calculated DSAM factor F as a

function of τ/α, along with the measured

$F = 0.30 \pm 0.02$, for the decay of the 1611-keV

level of ^{37}Ar recoils with initial velocity

$\beta(0) = 6.2 \times 10^{-3}$ slowing in Xe gas at 0.108 atm

pressure. The curve is calculated with $f_n = 0.8$,

$f_e(Z_1, \overline{v}/v_o) = 1.34$ and $f_e(\text{gas}) = 0.50$, leading to

an electronic slowing-down time of $\alpha = 15.2$ ns

and a lifetime of $\tau = 8.2 \pm 0.9$ ns. Inclusion of the

uncertainty in $f_e(\text{gas})$ leads to the uncertainty

(± 1.4 ns) quoted in Table VIII for the case with

$f_n = 0.8$.

^{37}Ar in Xe (0.108 atm)

$\beta = 0.0062$

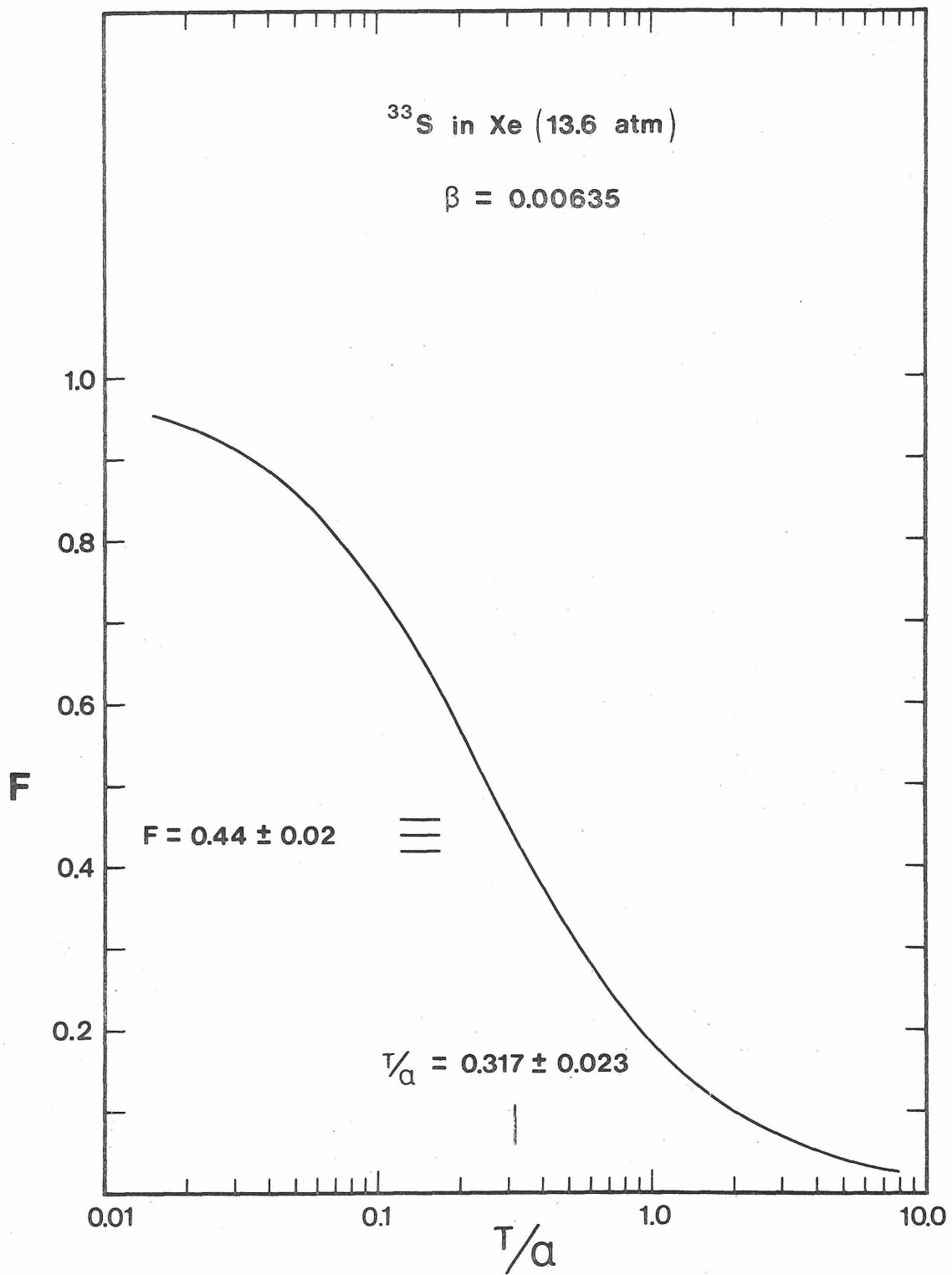F = 0.30 ± 0.02

$T/a = 0.54 \pm 0.06$
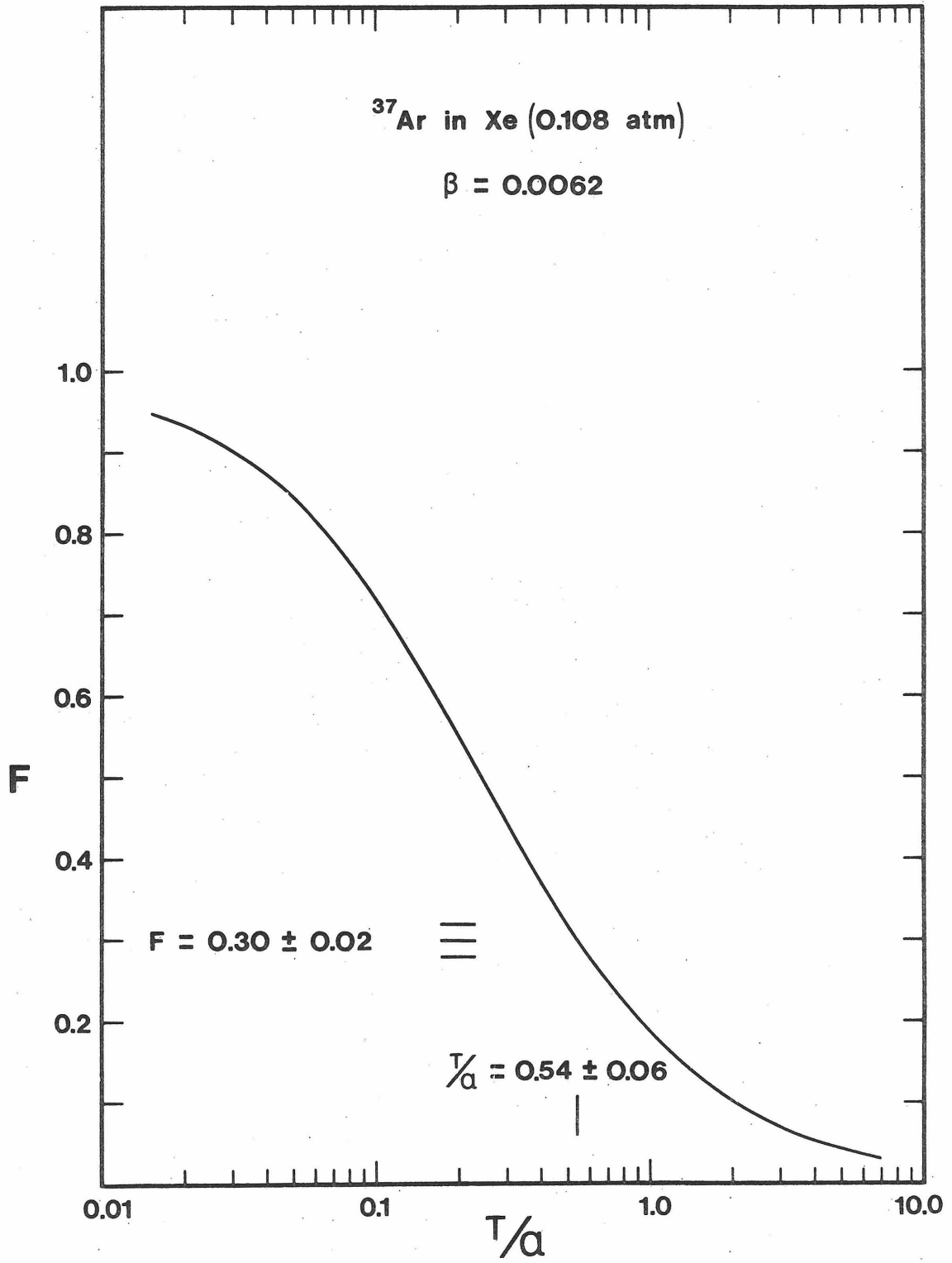
Figure 29. The relevant portion of the level diagram for ^{30}P.

This summary is that given by Endt and Van der Leun

(1967).

(See page 75.)
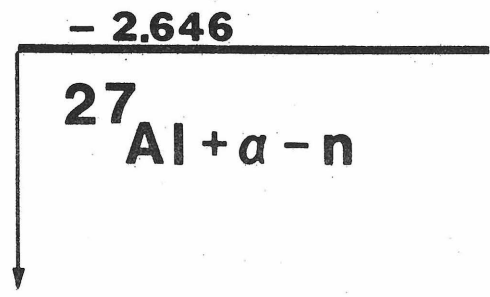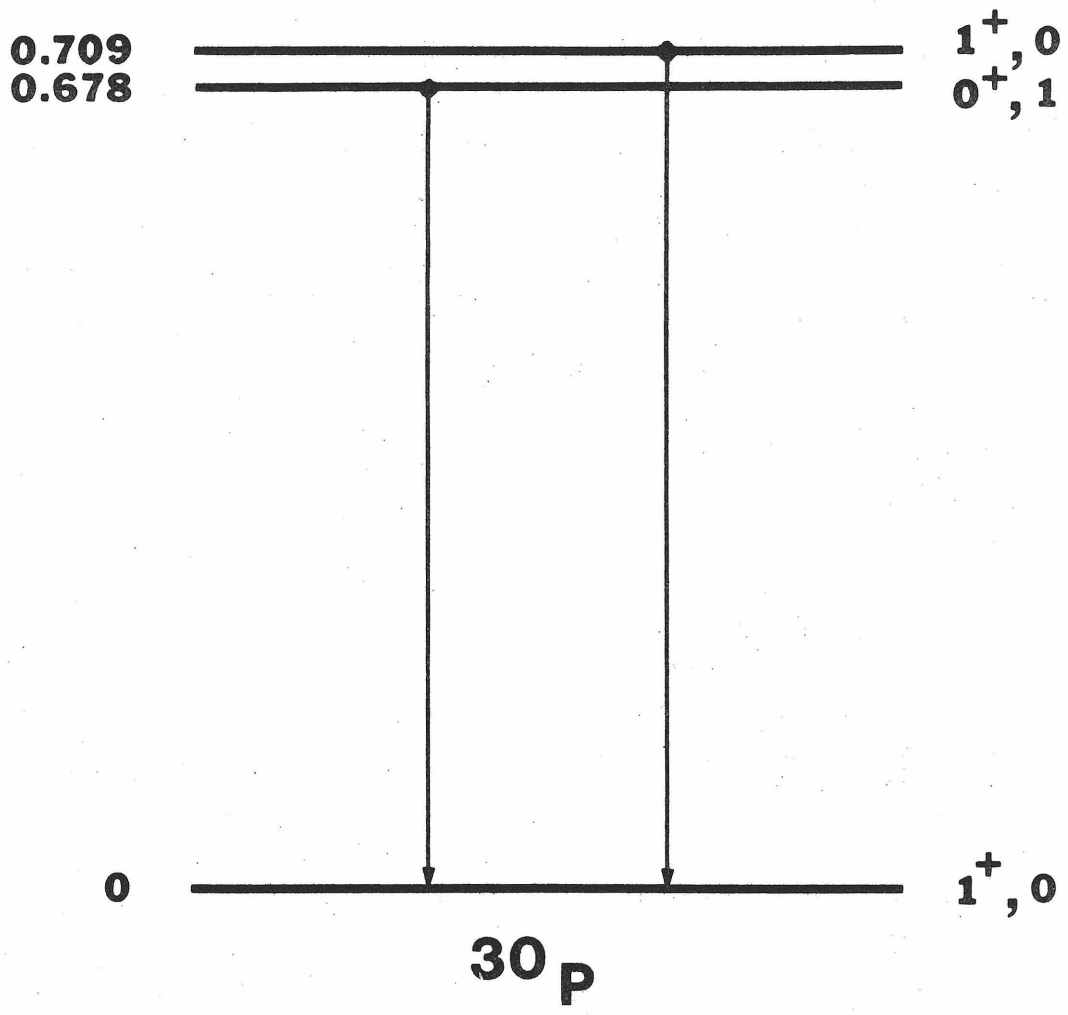
Figure 30.   A portion of the γ-ray spectra obtained in the
55-cm^3 Ge(Li) detector resulting from the
^{27}Al(^{4}He,n)^{30}P reaction.   The γ ray at 709 keV
arises from the decay of the 709-keV level of
^{30}P, while the 662-keV line arises from a ^{137}Cs
source placed near the target.   The dispersion
is 1.19 keV/ch.
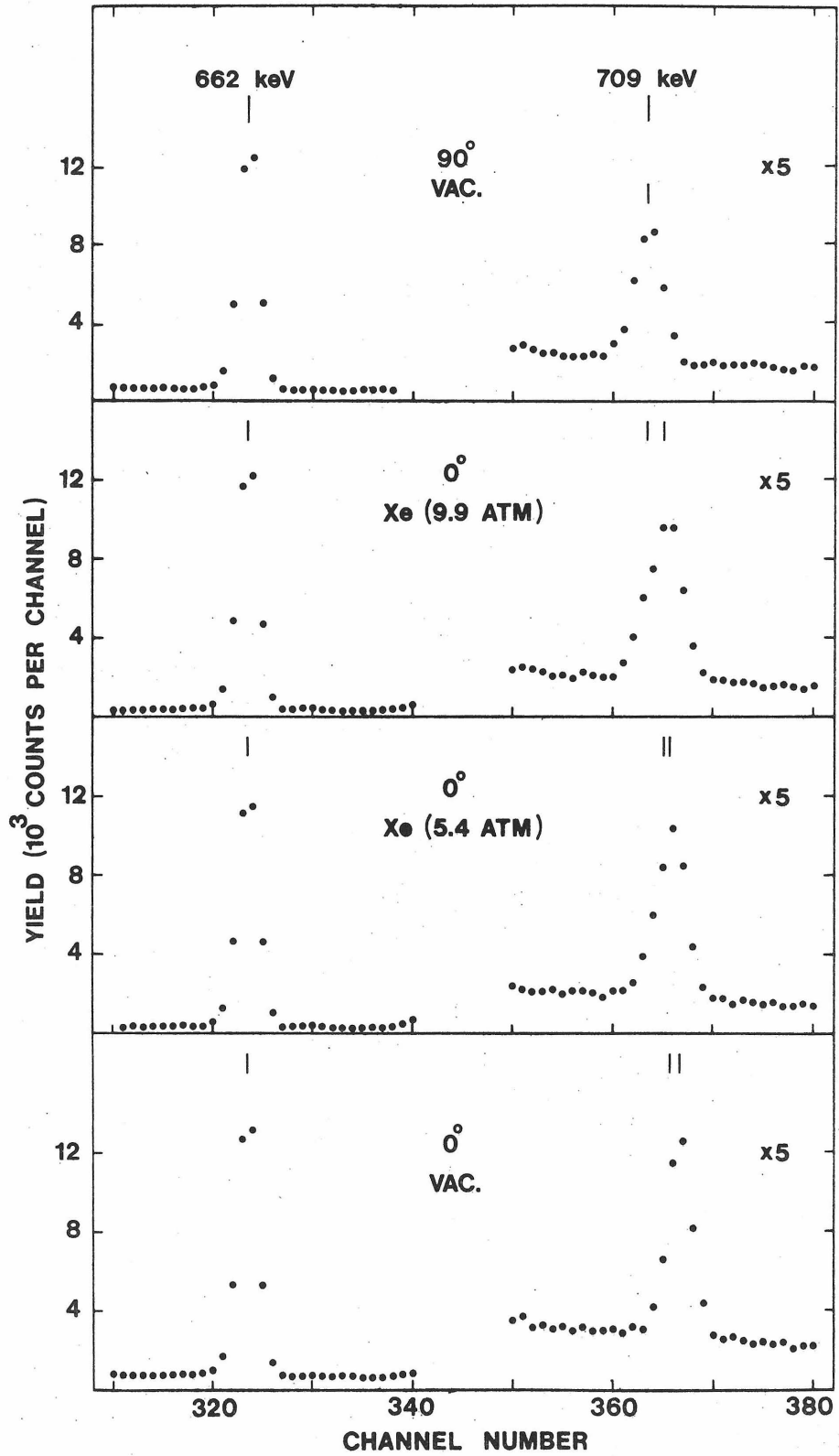
Figure 31. A plot of the calculated DSAM factor F as a

function of τ/α, along with the measured

$F = 0.51 \pm 0.01$, for the decay of the 709-keV

level of ^{30}P recoils with initial velocity

$\beta(0) = 6.2 \times 10^{-3}$ slowing in Xe gas at 9.86 atm

pressure. The curve is calculated with $f_n = 0.8$,

$f_e(Z_1, \overline{v}/v_o) = 1.05$, and $f_e(gas) = 0.50$, leading

to an electronic slowing-down time of $\alpha = 202$ ps

and a lifetime of $\tau = 45.1 \pm 1.6$ ps. Inclusion

of the uncertainty in $f_e(gas)$ leads to the uncer-

tainty (± 5.2 ps) quoted in Table IX.

^{30}P in Xe (9.86 atm)

$\beta = 0.0062$

F = 0.51 ± 0.01

$\tau/a = 0.223 \pm 0.008$
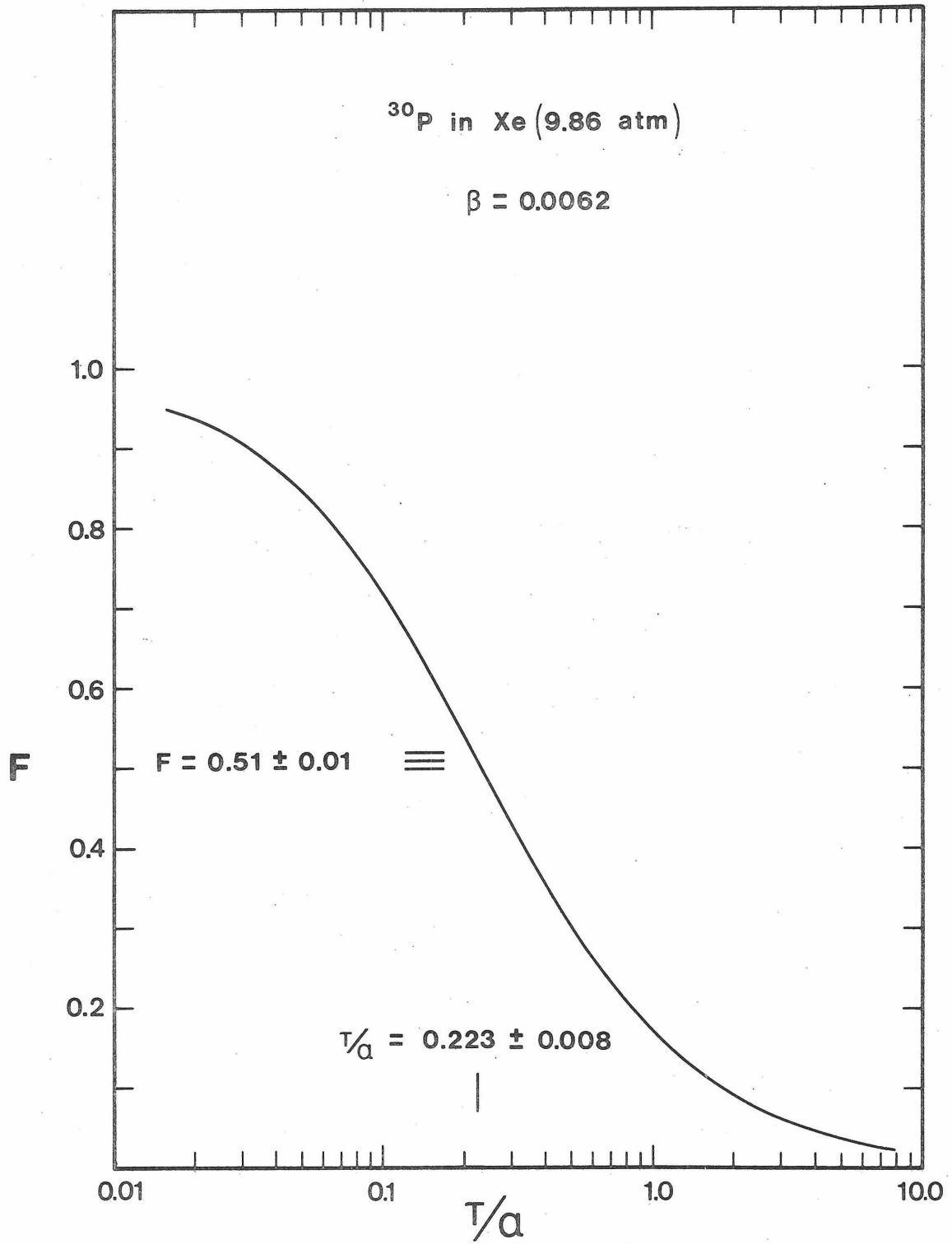
Table 32. The relevant portion of the level diagram for ^{35}Cl.
This summary is that given by Endt and Van der Leun
(1967).

(See page 83.)
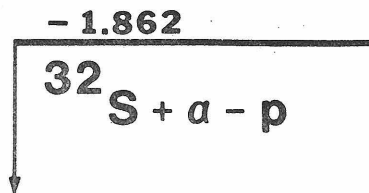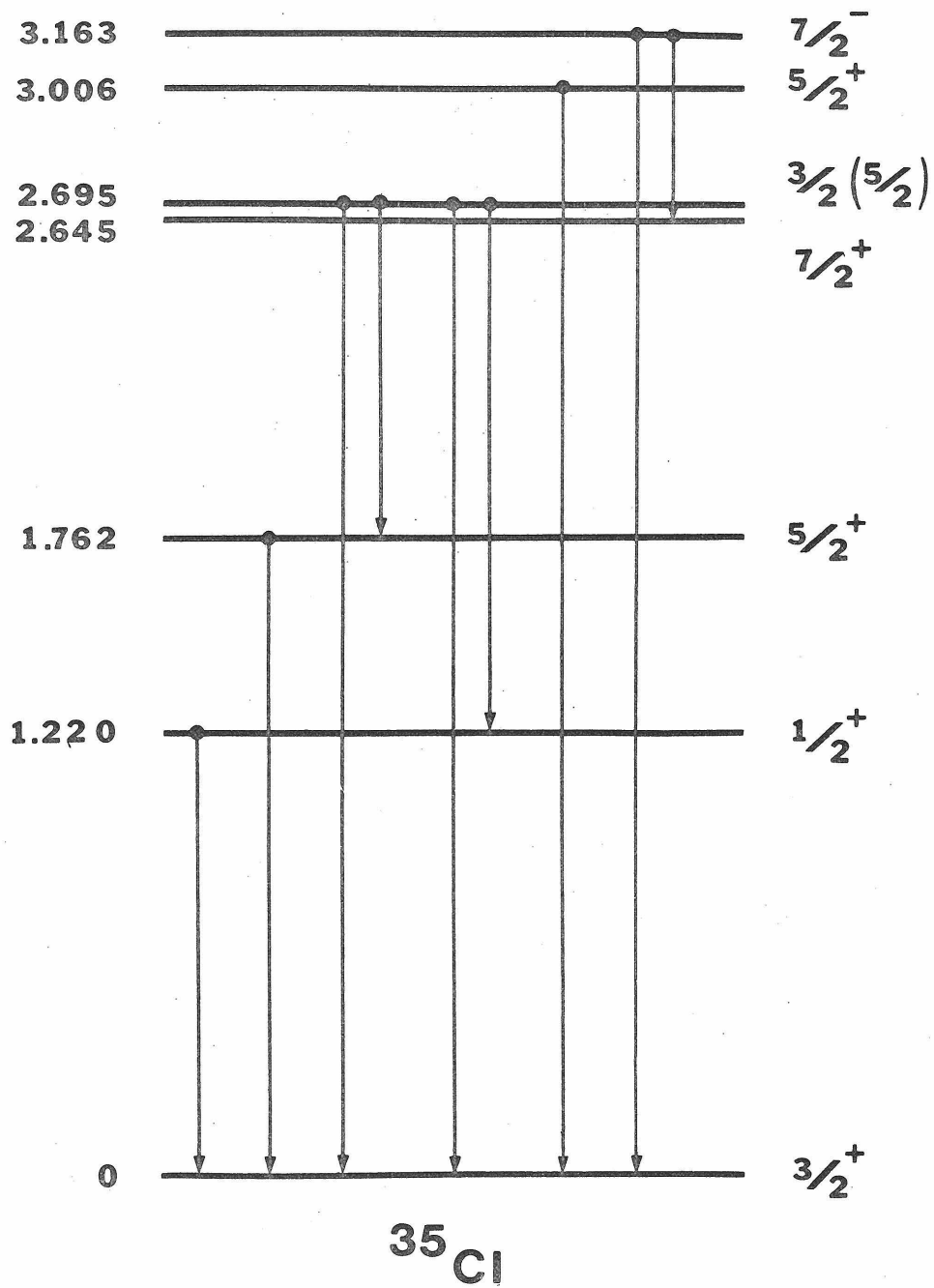
^{35}Cl

Figure 33. A portion of the γ-ray spectra obtained in the 55-cm^3 Ge(Li) detector resulting from the ^{32}S(^{4}He,p)^{35}Cl reaction. The γ ray at 3163 keV arises from the decay of the 3163-keV level of ^{35}Cl, while the 1369-keV, 1836-keV and 2754-keV lines arise from ^{88}Y and ^{24}Na sources placed near the target. The dispersion is 2.63 keV/ch.

(See page 86.)

Figure 34. A plot of the calculated DSAM factor F as a function of τ/α, along with the measured $F = 0.52 \pm 0.01$, for the decay of the 3163-keV level of ^{35}Cl recoils with initial velocity $\beta(0) = 6.5 \times 10^{-3}$ slowing in Xe gas at 8.16 atm pressure. The curve is calculated with $f_n = 0.8$, $f_e(Z_1, \bar{v}/v_o) = 1.24$, and $f_e(\text{gas}) = 0.50$, leading to an electronic slowing-down time of $\alpha = 217$ ps and a lifetime of $\tau = 53.7 \pm 1.9$ ps. Inclusion of the uncertainty in $f_e(\text{gas})$ leads to the uncertainty ($\pm$ 7 ps) quoted in Table XI.

(See page 87.)

^{35}Cl in Xe (8.16 atm)

$\beta = 0.0065$
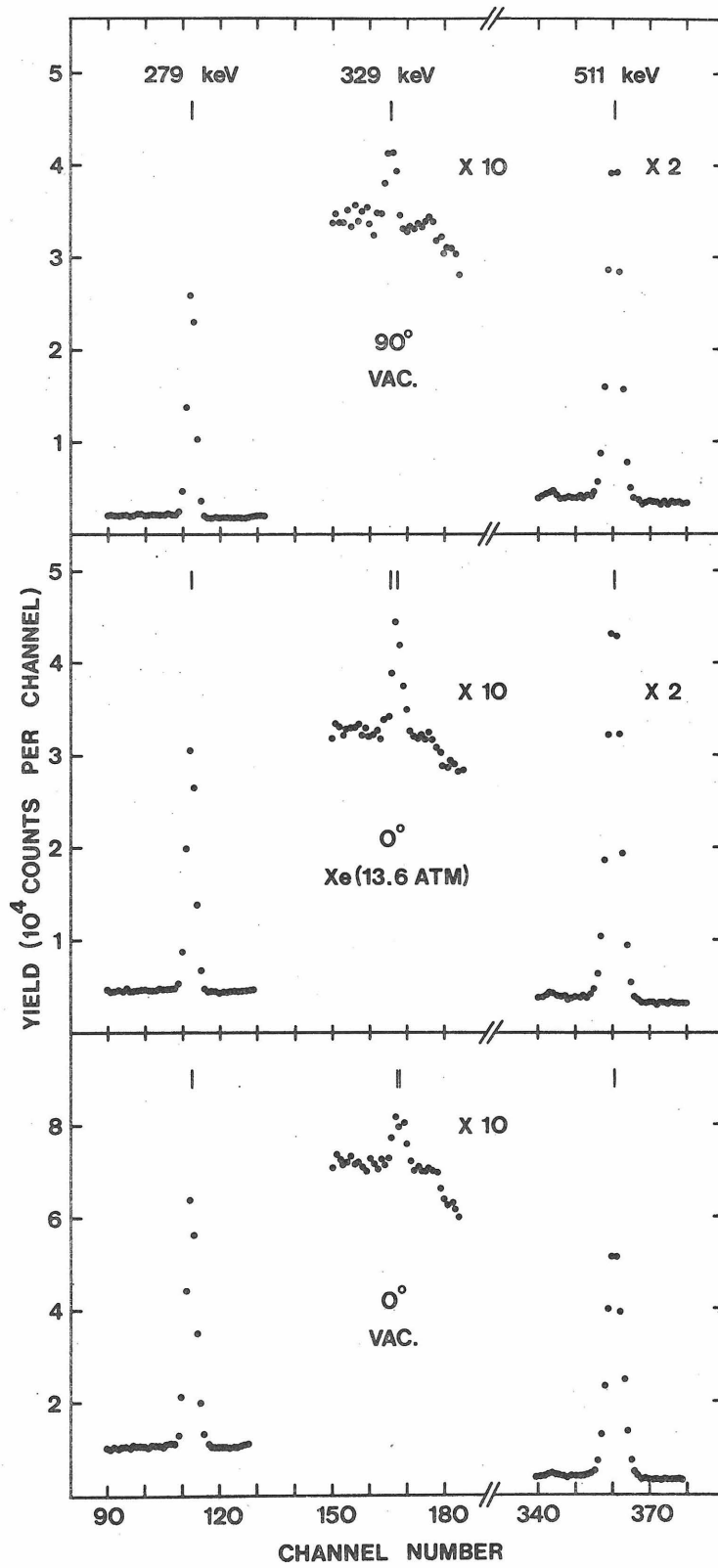
F = 0.52 ± 0.01

$^T/a = 0.247 \pm 0.009$

F

$^T/a$

Figure 35. A plot of the calculated DSAM factor F as a function
of τ/α, along with the measured $F = 0.44 \pm 0.02$,
for the decay of the 2934-keV level of ^{33}S recoils
with initial velocity $\beta(0) = 6.35 \times 10^{-3}$ slowing in
Xe gas at 13.6 atm pressure. The curve is calcu-
lated with $f_n = 0.8$, $f_e(Z_1, \bar{v}/v_o) = 1.17$, and
f_e(gas) $= 0.50$, leading to an electronic slowing-
down time of $\alpha = 137$ ps and a lifetime of
$\tau = 43.3 \pm 3.1$ ps. Inclusion of the uncertainty of
f_e(gas) and a 10% uncertainty in the rate of energy
loss assumed in the analysis leads to the uncer-
tainty (± 7 ps) quoted in the text.

^{33}S in Xe (13.6 atm)

$\beta = 0.00635$

F = 0.44 ± 0.02

T/a = 0.317 ± 0.023

Figure 36. The relevant portion of the level diagram for ^{38}K.

This summary is that given by Endt and

Van der Leun (1967).

(See page 96.)
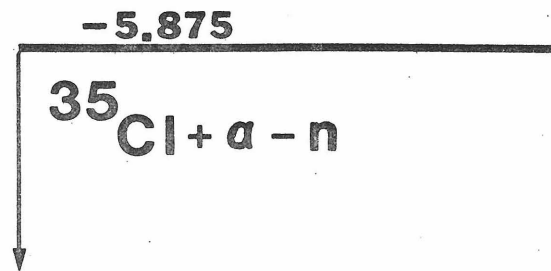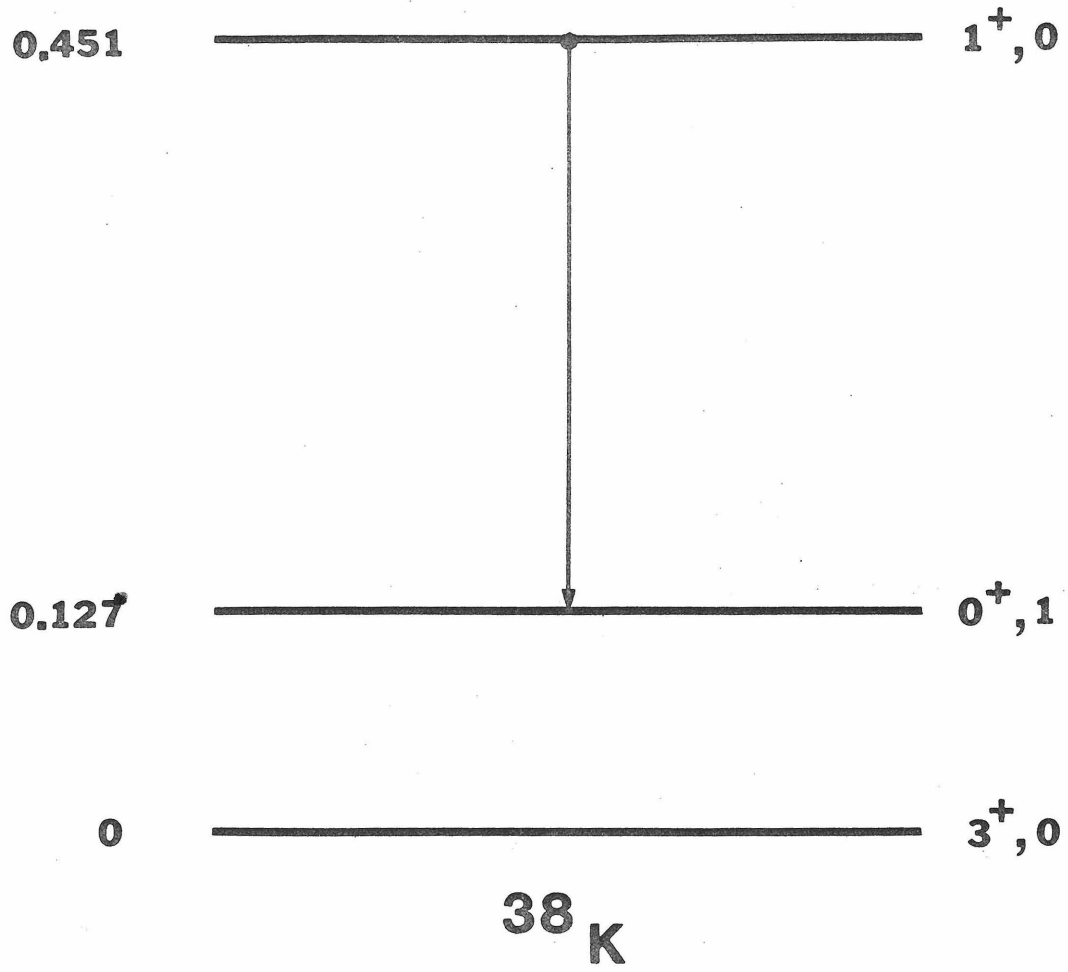
Figure 37. A portion of the γ-ray spectra obtained with the 55-cm^3 Ge(Li) detector resulting from the ^{35}Cl(^{4}He,n)^{38}K reaction. The γ ray at 329 keV arises from the decay of the 451-keV level of ^{38}K, while the 279-keV and 511-keV lines arise from a ^{203}Hg source placed near the target and from positron-annihilation radiation. The dispersion is 0.89 keV/ch. The target was 20 μg/cm^2 of Ba^{35}Cl$_2$ evaporated onto a 10 - μg/cm^2 carbon backing, and the spectra were obtained as the ^{38}K nuclei recoiled into vacuum.
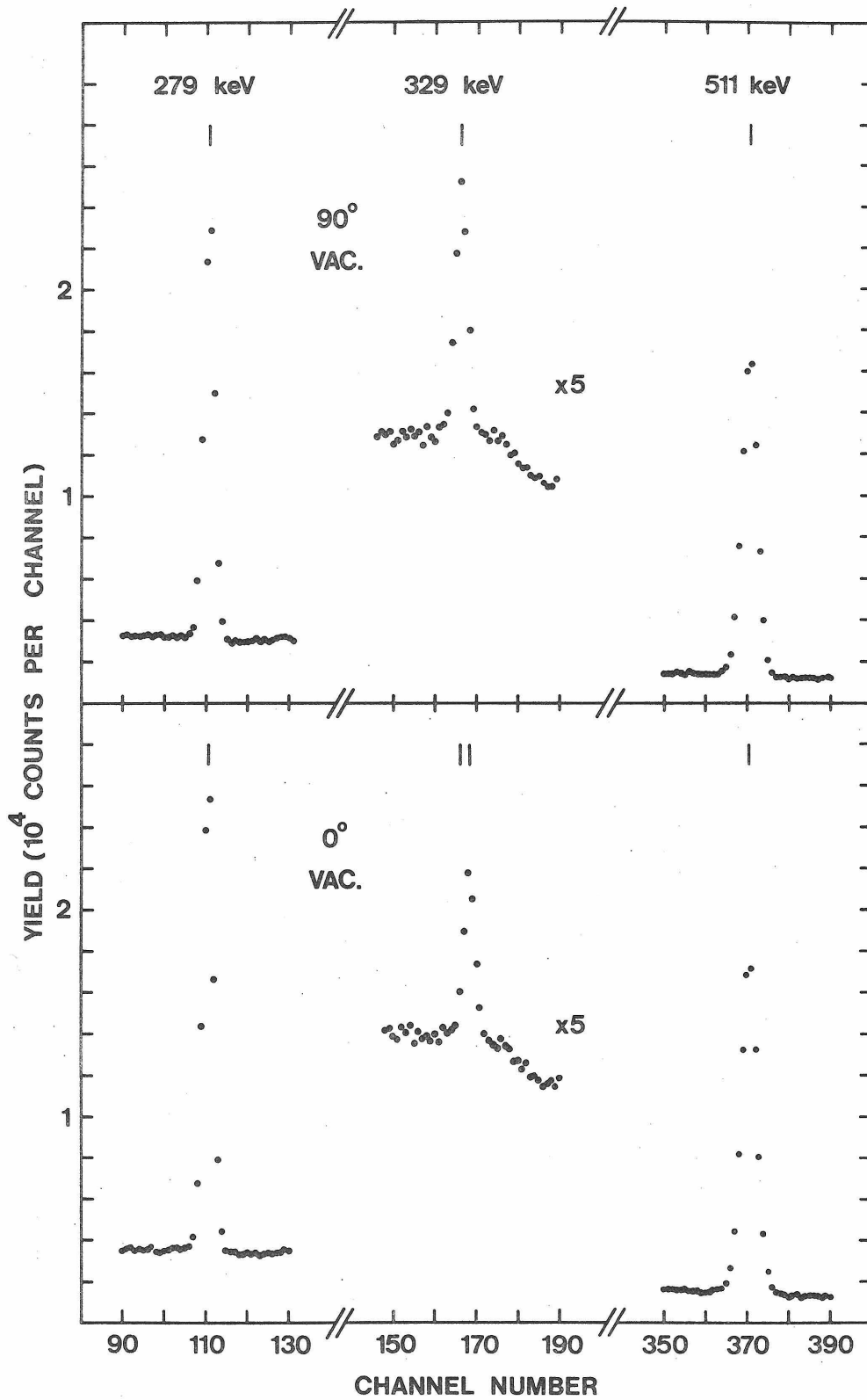
Figure 38. A portion of the γ-ray spectra obtained with the 55-cm^3 Ge(Li) detector resulting from the ^{35}Cl(^{4}He,n)^{38}K reaction. The γ ray at 329 keV arises from the decay of the 451-keV level of ^{38}K, while the 279-keV and 511-keV lines arise from a ^{203}Hg source placed near the target and from positron-annihilation radiation. The dispersion is 0.93 keV/ch. The target was 20 μg/cm^2 of Ba^{35}Cl$_2$ evaporated onto a 9.7-mg/cm^2 Ta foil, and the spectra were obtained with the detector at 0° and 90° from the beam direction as the ^{38}K nuclei recoiled into vacuum and into He gas at 13.6 atm pressure.

Figure 39. A plot of the calculated DSAM factor F as a

function of τ/α, along with the measured

$F = 0.78 \pm 0.11$, for the decay of the 451-keV

level of ^{38}K recoils with initial velocity

$\beta(0) = 6.5 \times 10^{-3}$ slowing in He gas at 13.6 atm

pressure. The curve is calculated with

$f_n = 0.8$, $f_e(Z_1, \overline{v}/v_0) = 1.25$, and $f_e(gas) = 0.56$,

leading to an electronic slowing-down time of

$\alpha = 798$ ps and a lifetime of $\tau = 155 \pm 89$ ps.

Inclusion of the uncertainties in the initial recoil

velocity and in the nuclear stopping parameter f_n

leads to the uncertainty quoted in the text.

^{38}K in He (13.6 atm)

$\beta = 0.0065$

$F = 0.78 \pm 0.11$

$T/a = 0.195 \begin{smallmatrix} +0.118 \\ -0.105 \end{smallmatrix}$
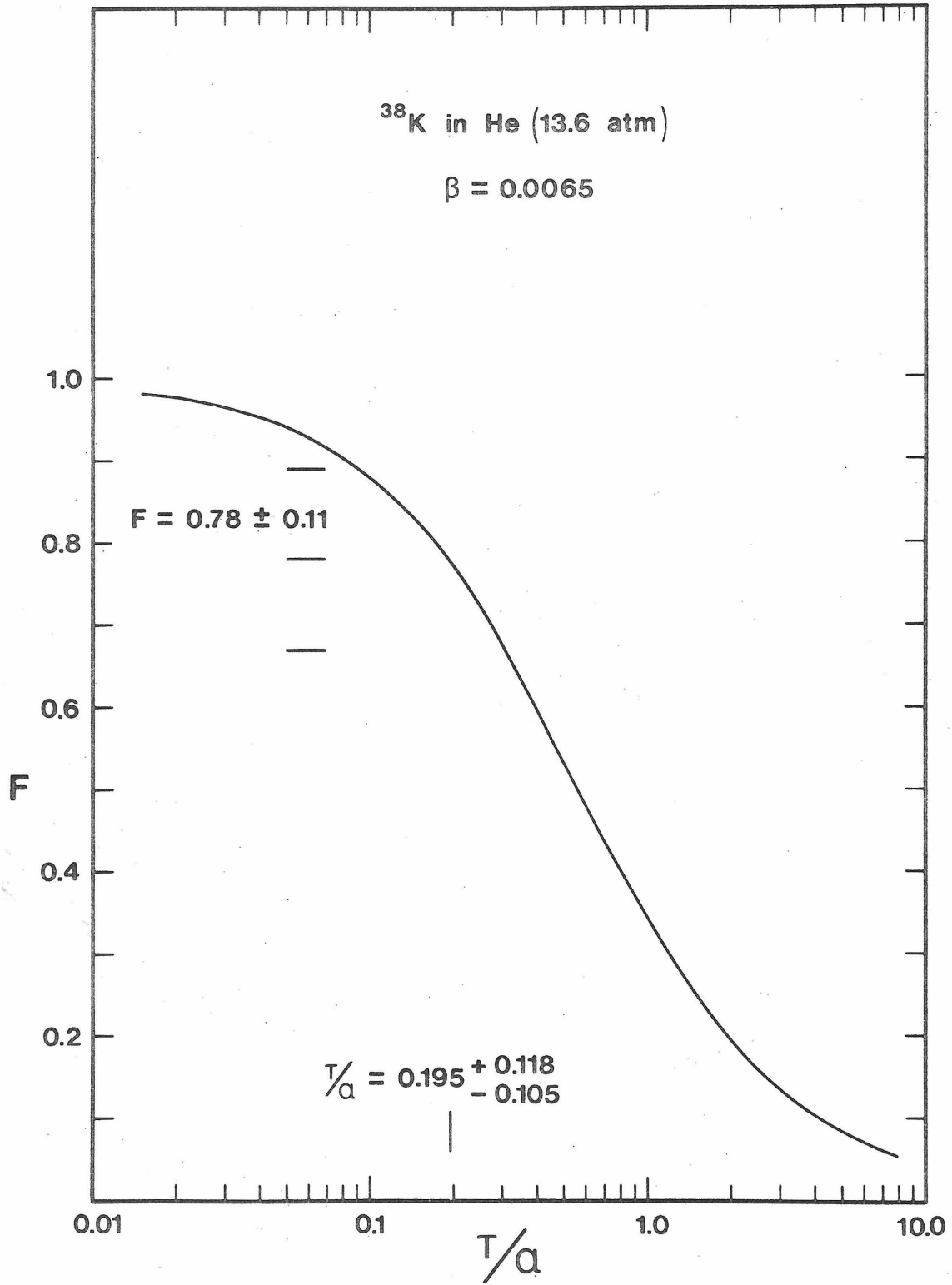
Figure 40. A portion of the γ-ray spectra obtained in the
55-cm^3 Ge(Li) detector resulting from the
^{23}Na(^{4}He,n)^{26}Al reaction. The γ ray at 1341 keV
arises from the decay of the 1760-keV level of ^{26}Al,
while the 1275-keV and 835-keV lines arise from
^{22}Na and ^{54}Mn calibration sources placed near
the target. The dispersion is 1.54 keV/ch.
Figures 40a and 40c were obtained for ^{26}Al nuclei
recoiling into vacuum, while Figure 40b was ob-
tained with the ^{26}Al recoiling into the thick carbon
block.
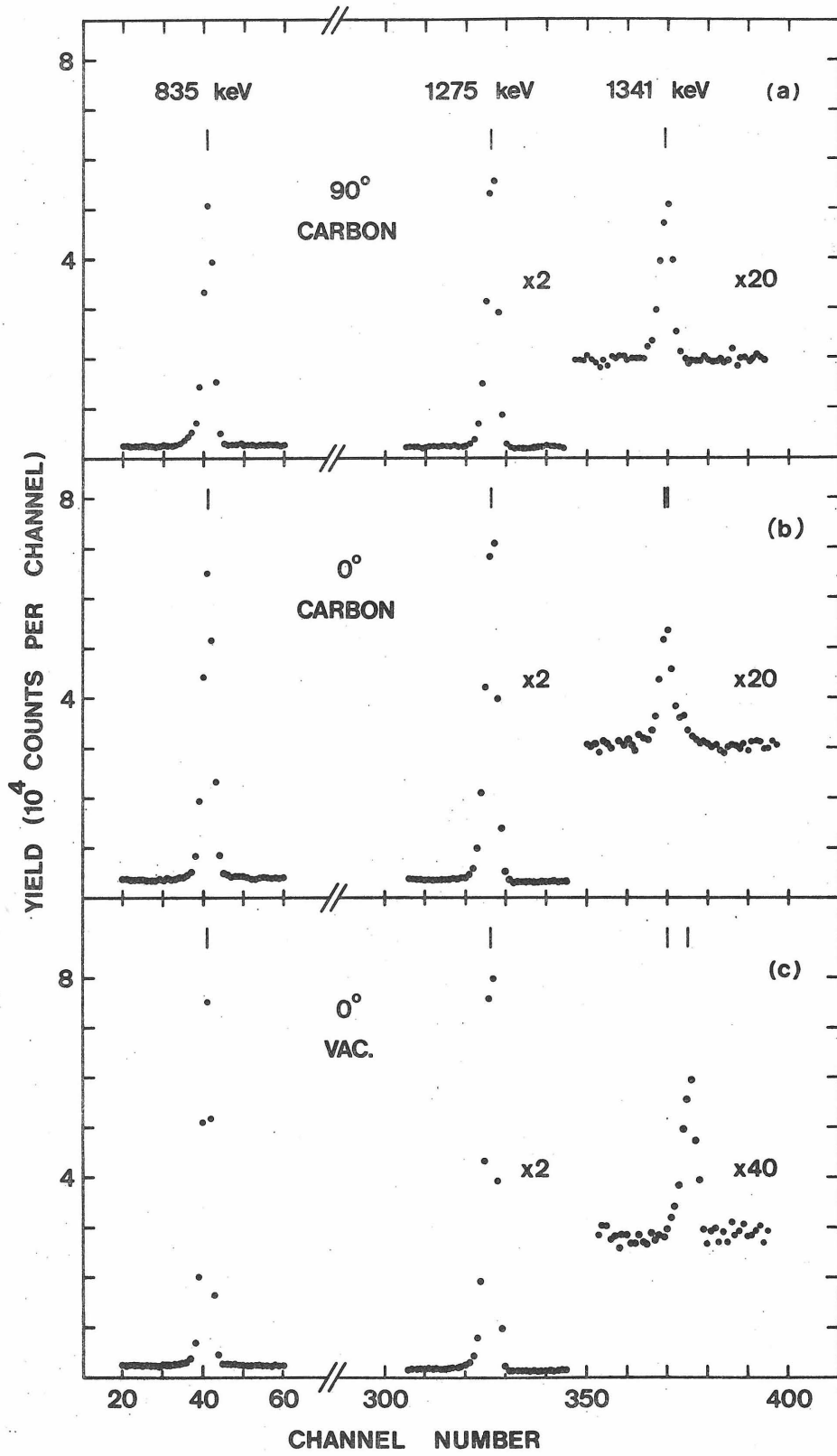
Figure 41. A plot of the calculated DSAM factor F as a
function of τ/α, along with the measured
$F = 0.11 \pm 0.03$, for the decay of the 1760-keV
level of ^{26}Al recoils with initial velocity
$\beta(0) = 7.1 \times 10^{-3}$ slowing in carbon with density
$D = 1.70$ g/cm^3. The curve is calculated with
$f_n = 0.8$ and $f_e(Z_1, \overline{v}/v_o) = 0.66$, leading to an
electronic slowing-down time of $\alpha = 1.21$ ps
and a lifetime of $\tau = 5.0 \, ^{+2.1}_{-1.1}$ ps. With the
uncertainties in density and recoil velocity as
mentioned in the text added in quadrature, the
lifetime becomes $\tau = 5.0 \, ^{+2.2}_{-1.4}$ ps.
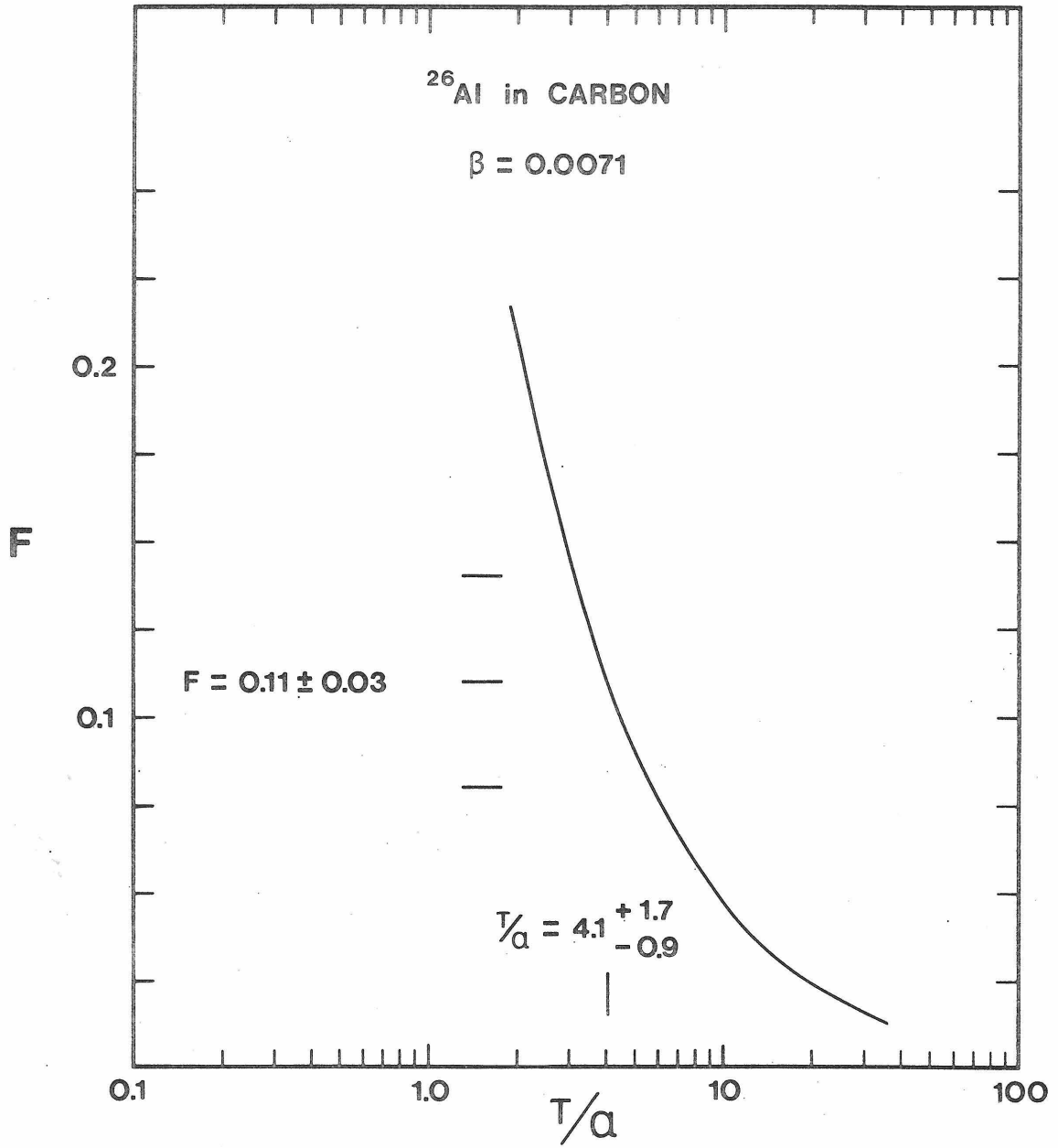
Figure 42. The relevant portion of the level diagram for ^{40}K.

This summary is that given by Endt and

Van der Leun (1967).

(See page 110.)
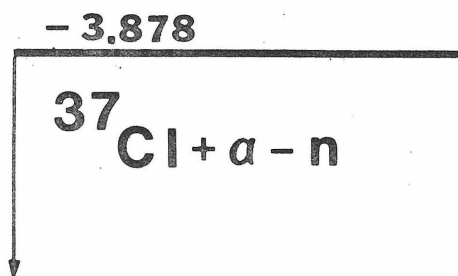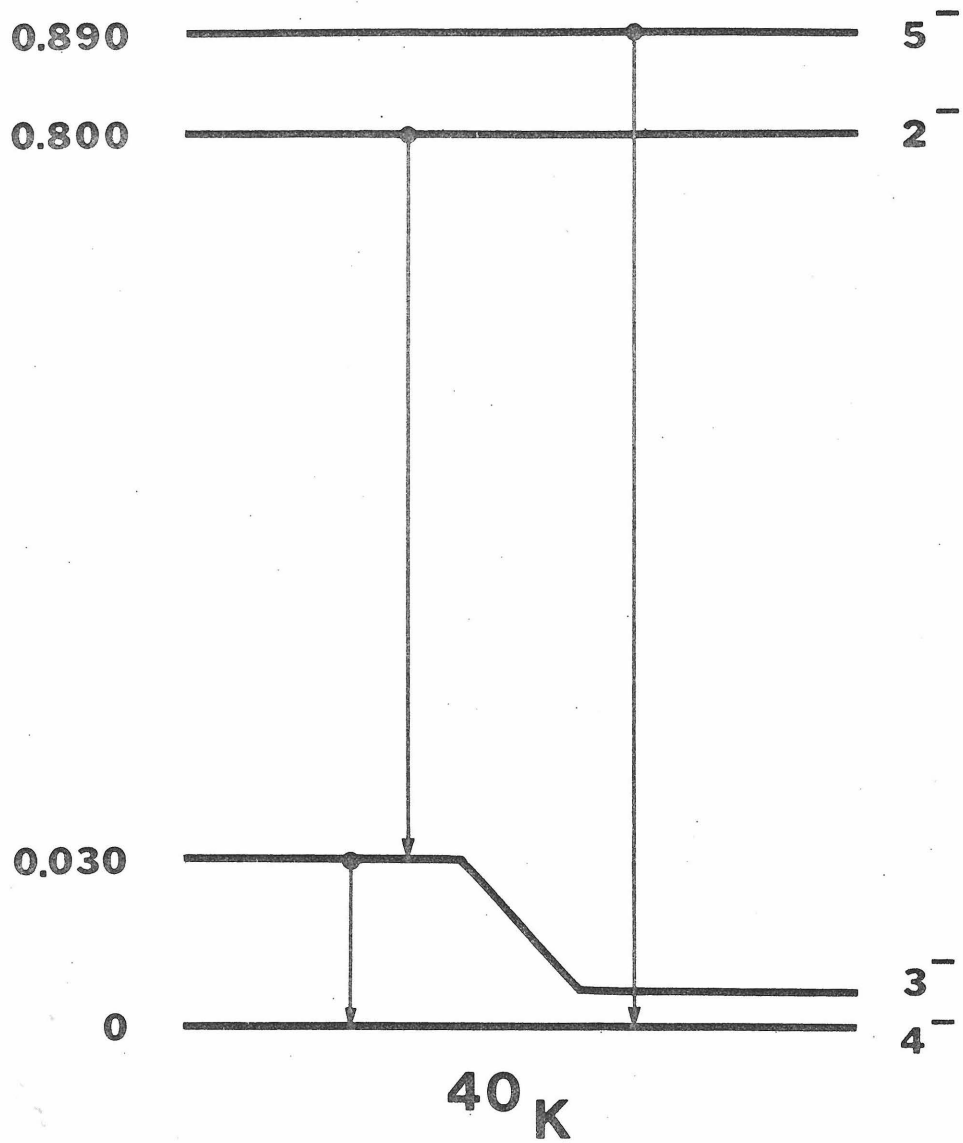
Figure 43. A portion of the γ-ray spectra obtained with the 55-cm^3 Ge(Li) detector resulting from the ^{37}Cl(^{4}He,n)^{40}K reaction. The γ rays at 770-keV and 890-keV arise from the decays of the 800-keV and 890-keV levels of ^{40}K, respectively, while the 662-keV line arises from a ^{137}Cs source placed near the target. The dispersion is 0.89 keV/ch. The target was 38 ± 10 μg/cm^2 Na^{37}Cl evaporated onto a 180 μg/cm^2 carbon backing, and the spectra were obtained as the nuclei recoiled into vacuum and into the backing.
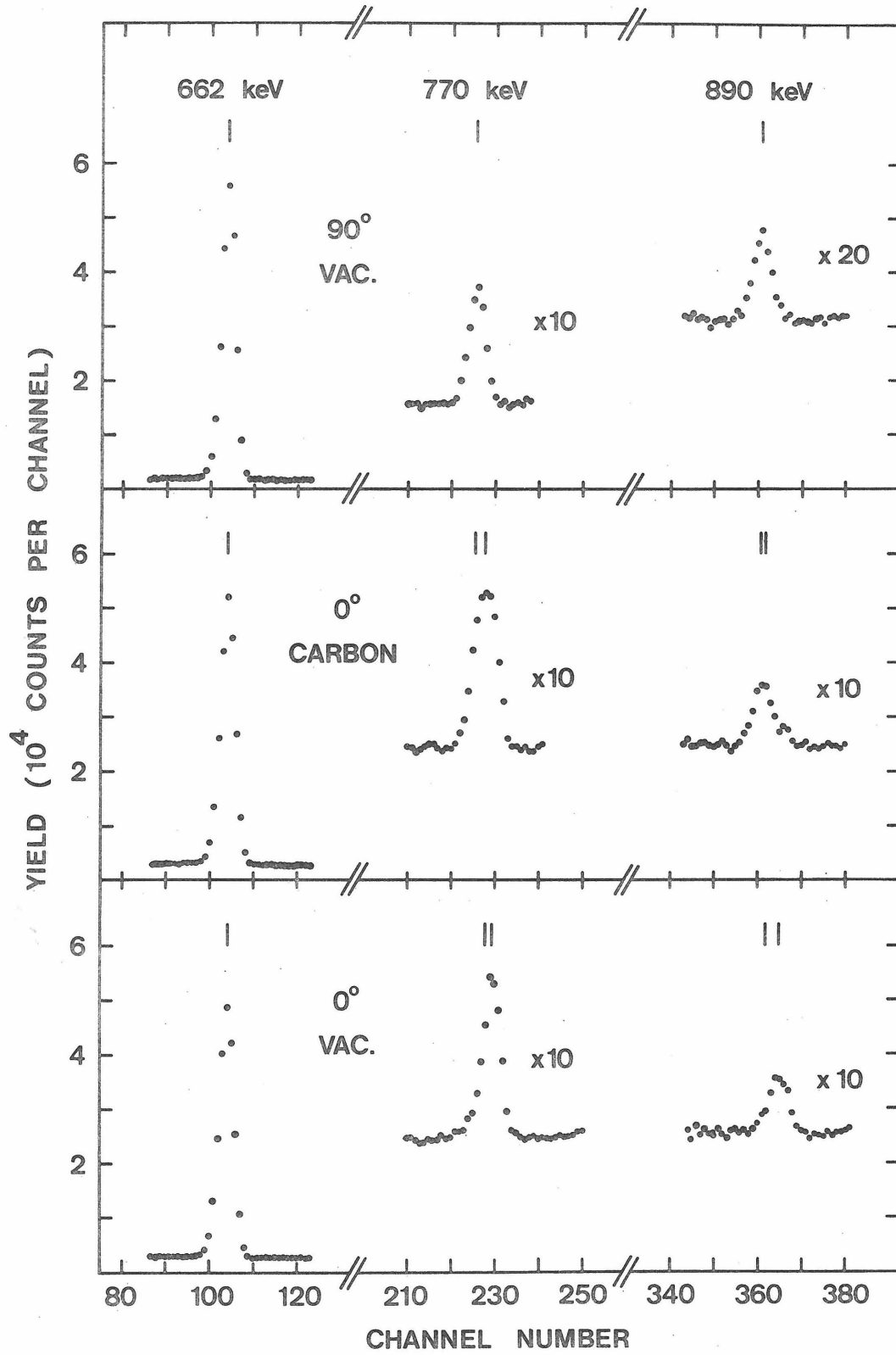
Figure 44. A plot of the calculated DSAM factor F as a
function of τ/α, along with the measured F
values, for the decay of the 800-keV and 890-keV
levels of ^{40}K recoils with initial velocity
$\beta(0) = 4.4 \times 10^{-3}$ slowing in carbon with a density
$D = 1.82$ g/cm^3. The curve is calculated with
$f_n = 0.8$ and $f_e(Z_1, \bar{v}/v_o) = 1.28$, leading to an
electronic slowing-down time of $\alpha = 0.743$ ps.

(See page 113.)

^{40}K in CARBON

$\beta = 0.0044$

F = 0.60 ± 0.03

$T/\alpha = 0.345 \pm 0.040$

F = 0.24 ± 0.04

$T/\alpha = 1.37 \,^{+\,0.32}_{-\,0.24}$

F

T/α
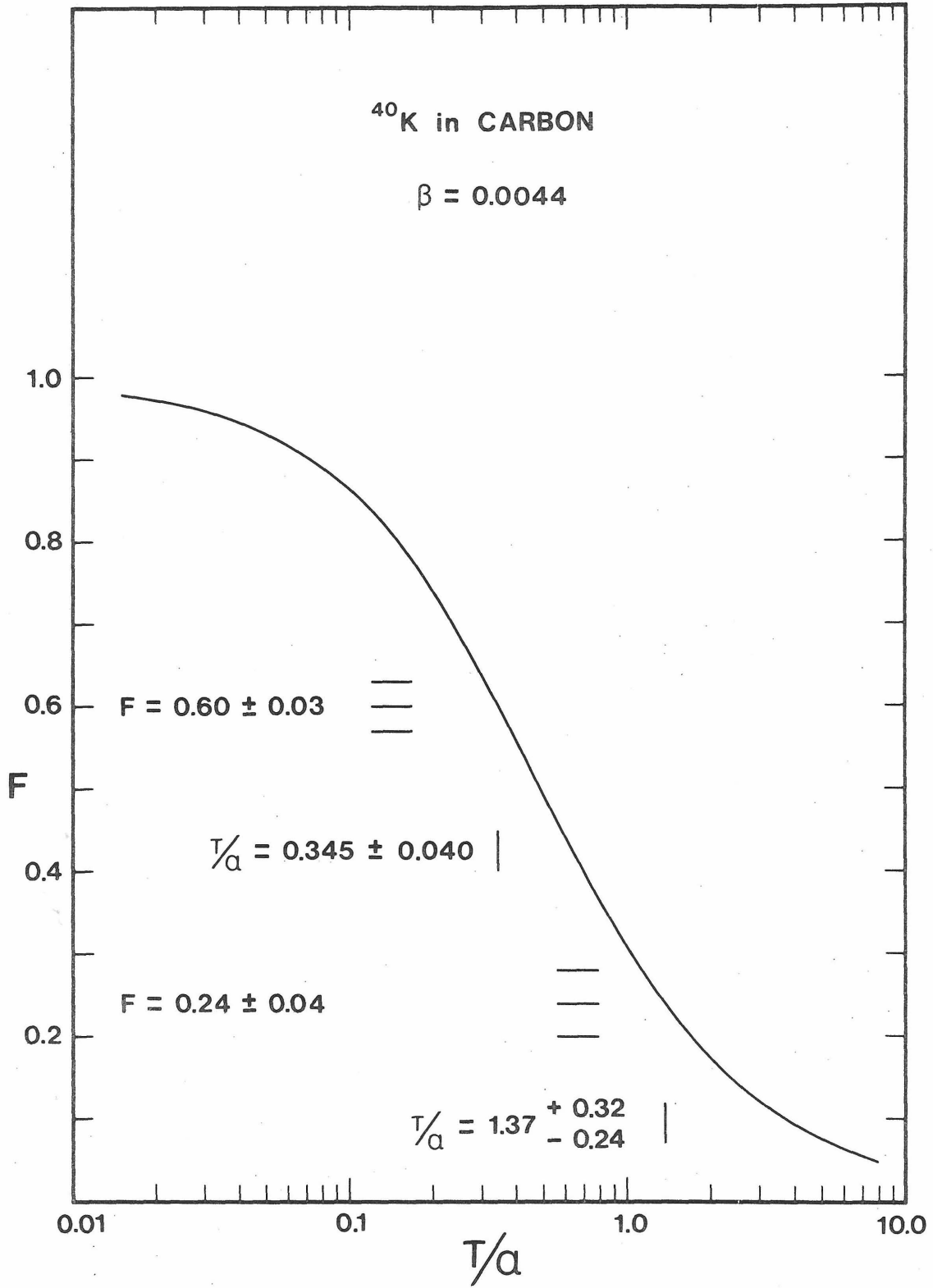
Figure 45. The experimental apparatus used for the measure-
ments of electronic stopping cross section for ^{12}C
and ^{27}Al in He and Xe. The detector-collimator
assembly is constructed asymmetrically to allow
small detector angles without intercepting the beam.

TARGET CHAMBER

TARGET

SUPPRESSOR

FARADAY CUP

⊢←10 cm→⊣

α BEAM

BEAM
COLLIMATOR

DETECTOR
COLLIMATOR

Si DETECTOR

Ni ENTRANCE FOIL
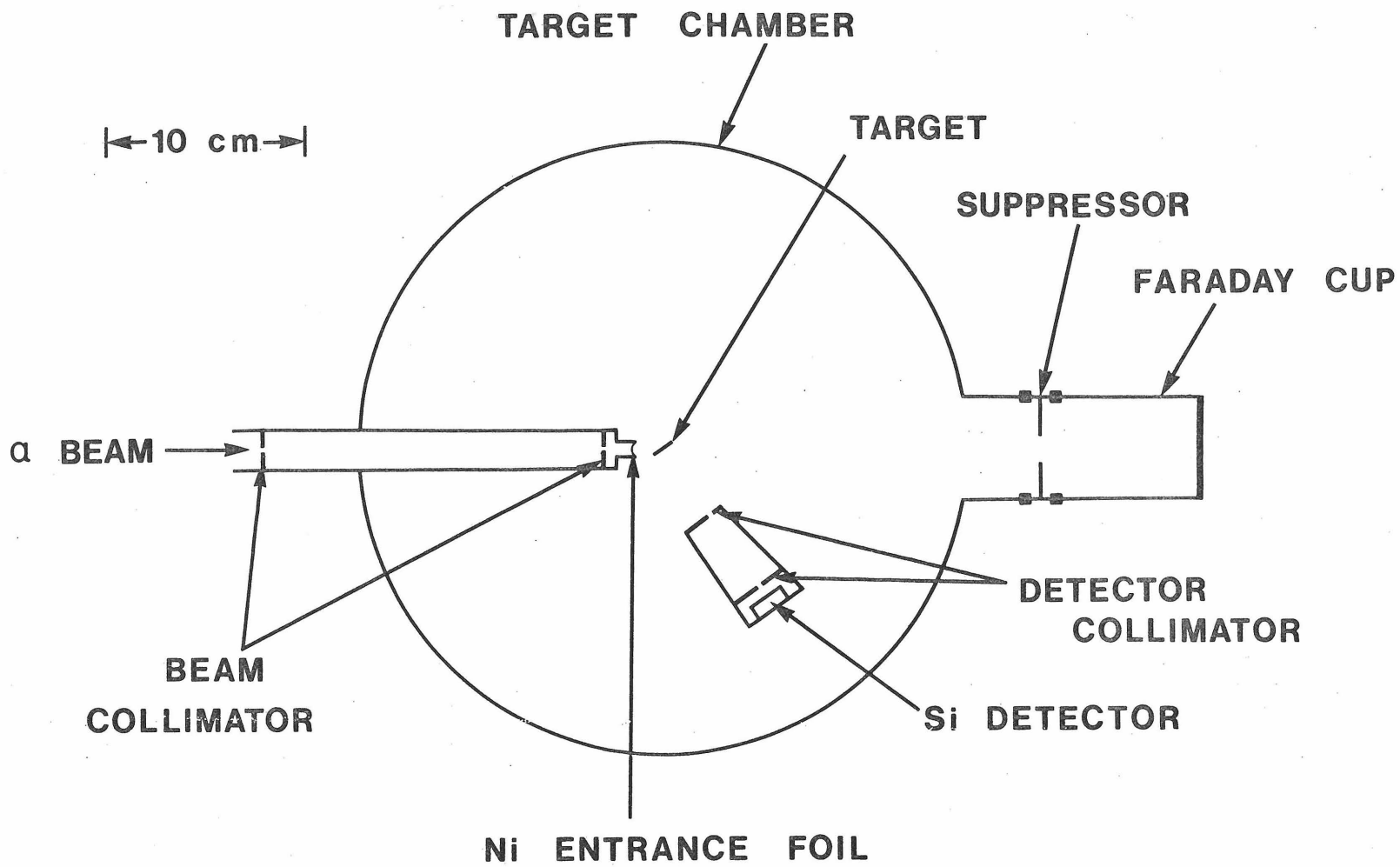
Figure 46. The yield of elastically scattered 5-MeV ^{4}He
particles as observed in the 61-cm-radius magnetic
spectrometer and used to measure target thick-
nesses. The horizontal axis gives the spectrometer
NMR frequency. The triangular data points (b)
show the yield of ^{4}He particles elastically scattered
at 90° by a clean thick Ta backing, while the
circular data points (a) give the yield when the ^{4}He
particles pass through the Al target layer
deposited on the Ta backing. The midpoint of
curve (a) is 20.356 ± 0.003 MHz while the midpoint
of curve (b) is 20.438 ± 0.003 MHz, leading to an
energy difference of 38.2 ± 1.9 keV. The midpoints
of the curves are indicated by the + symbol. Includ-
ing the uncertainty in the dE/dx tabulations, the
derived target thickness is 22.2 ± 2.0 μg/cm^2 of Al.
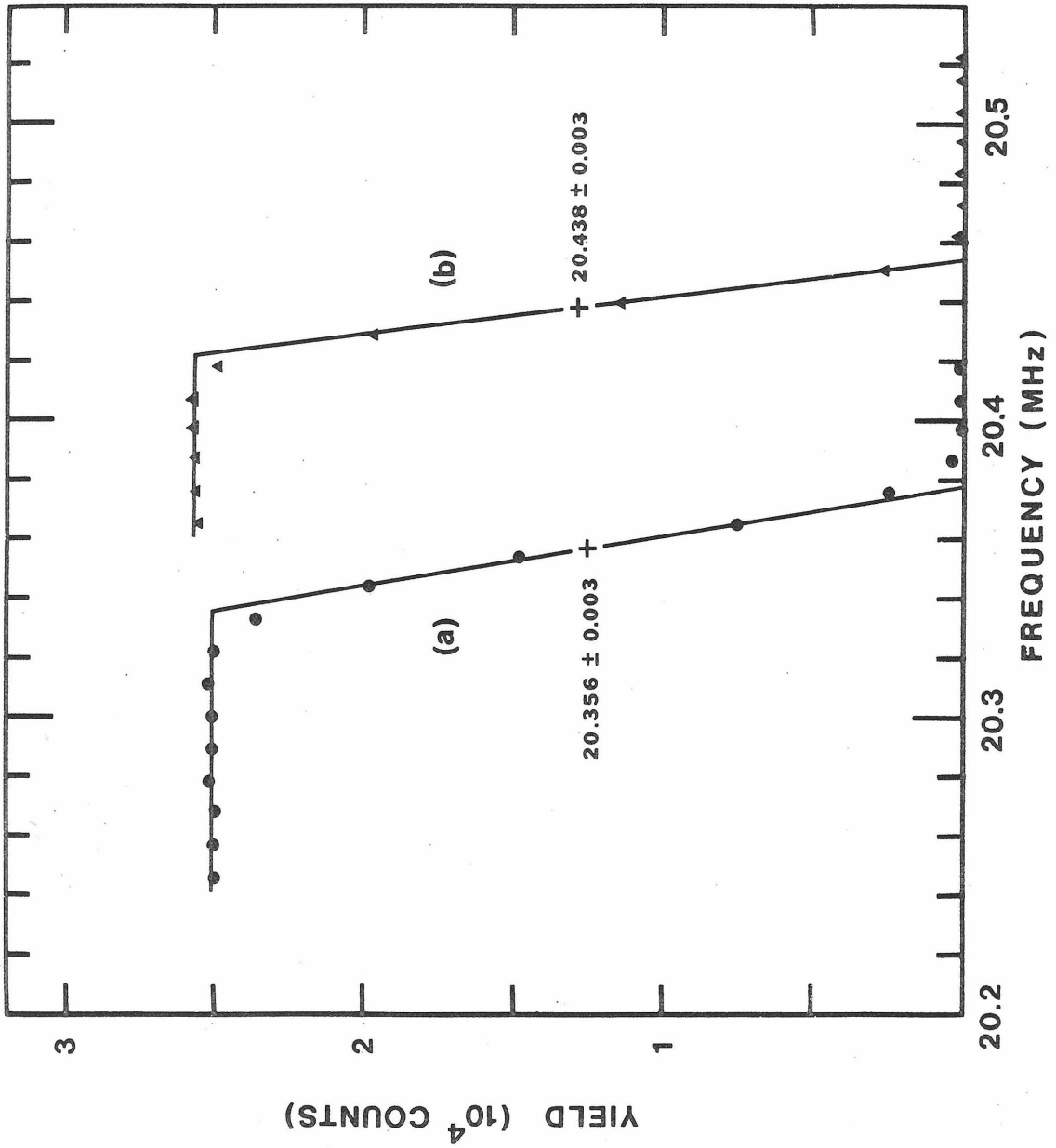
Figure 47. The yield of elastically-scattered C recoils at
the 4241 ± 25 keV resonance in the reaction
^{12}C(^{4}He,^{4}He)^{12}C used in measuring the thickness
of the Ni entrance foil. Curve (b) shows the yield
when the ^{4}He beam was directly incident upon the
14.4 μg/cm^2 carbon target, while curve (a) shows
the yield when the incident beam passed through the
Ni foil prior to striking the target. The peak of
curve (a) occurs at 4.480 ± 0.004 MeV while the peak
of curve (b) occurs at 4.262 ± 0.005 MeV, giving an
energy shift of 218 ± 6 keV. Including the uncertainty
in the dE/dx tabulations, this leads to a Ni thick-
ness of 468 ± 40 μg/cm^2, or 5260 ± 450 Å.
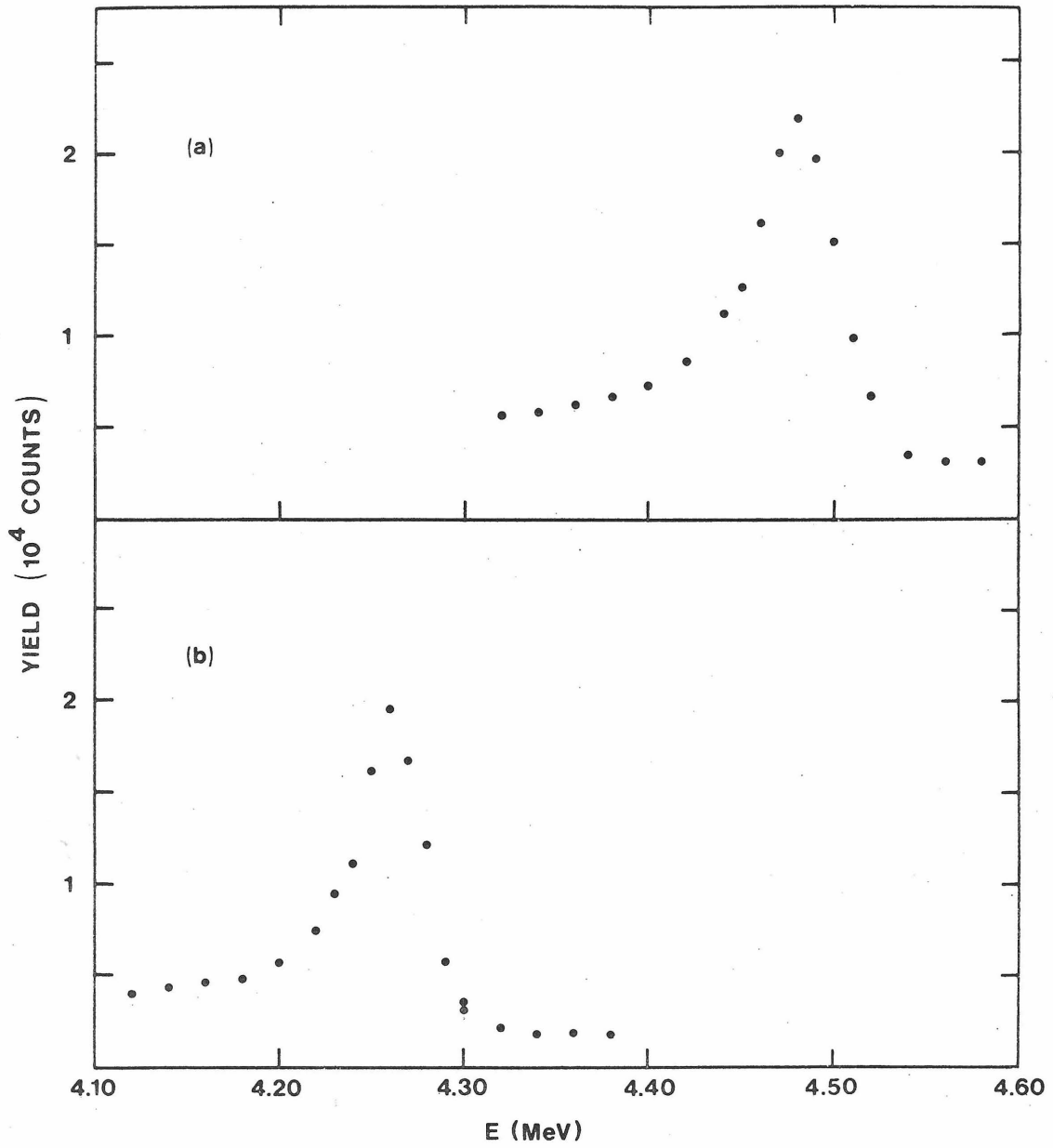
Figure 48. An example of the spectra obtained in the Si detector.
The peak is due to C recoils elastically scattered
out of a thin $(14.4 \,\mu g/cm^2)$ C foil into the detector
at 55°. Curves (a) and (c) are calibration runs taken
at two beam energies with a vacuum in the chamber,
while curve (b) was taken with the target chamber
filled with ^{4}He at a pressure of 15.40 Torr. The
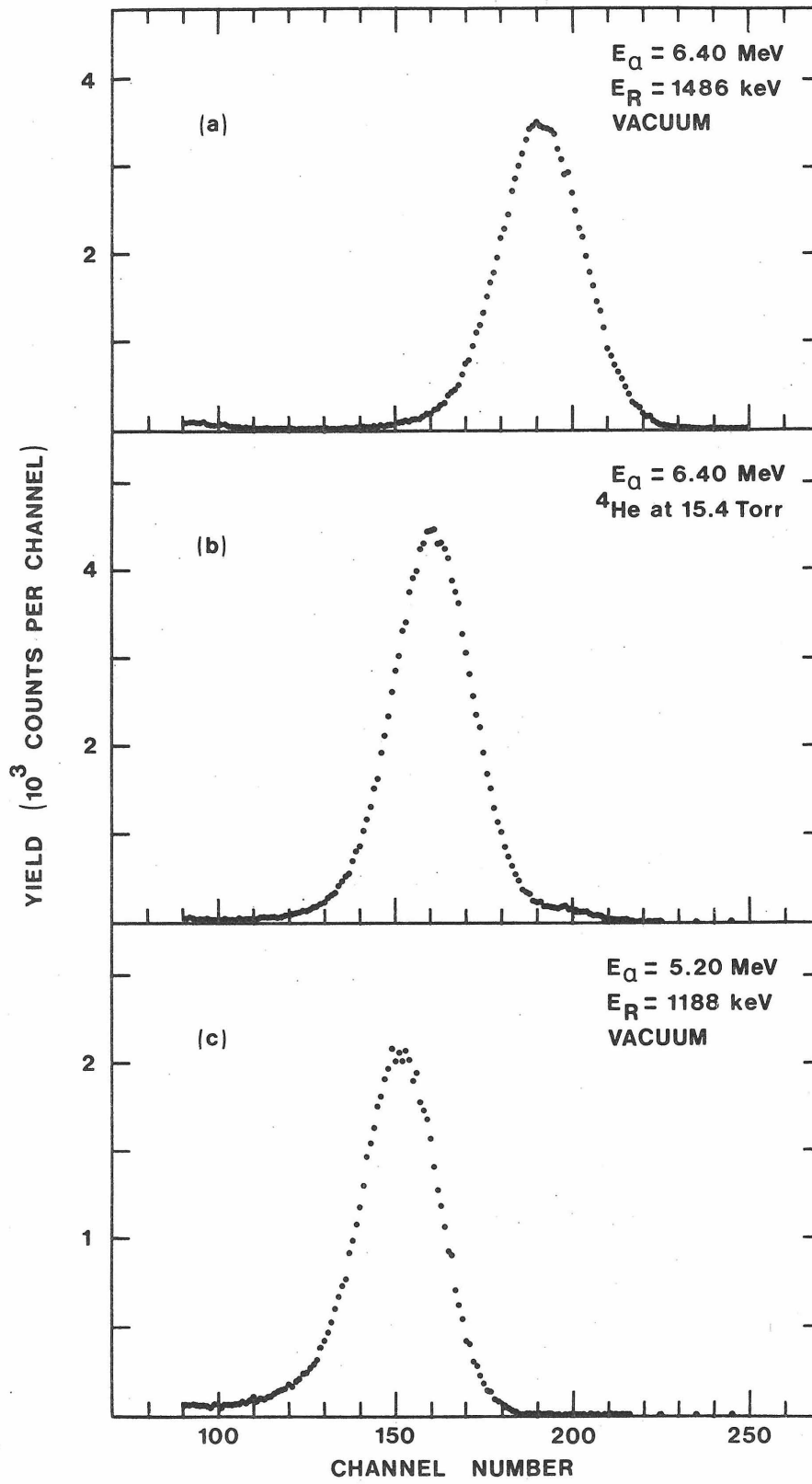energy loss ΔE_o for this set of data is 219 ± 2 keV.

(See page 126.)

Figure 49. An example of the spectra obtained in the Si

detector for Al ions with energies near the

lowest measured in these experiments. The peak

is due to Al recoils elastically scattered out of a

thin $(22.2 \pm 2.0 \ \mu g/cm^2)$ Al foil into the detector

at 55°. Curves (a) and (c) are calibration runs

taken at the two beam energies specified with a

vacuum in the chamber, while curve (b) was taken

with the target chamber filled with ^{4}He gas at a

pressure of 10.70 Torr. The energy loss for

this set of data is 88 ± 5 keV.
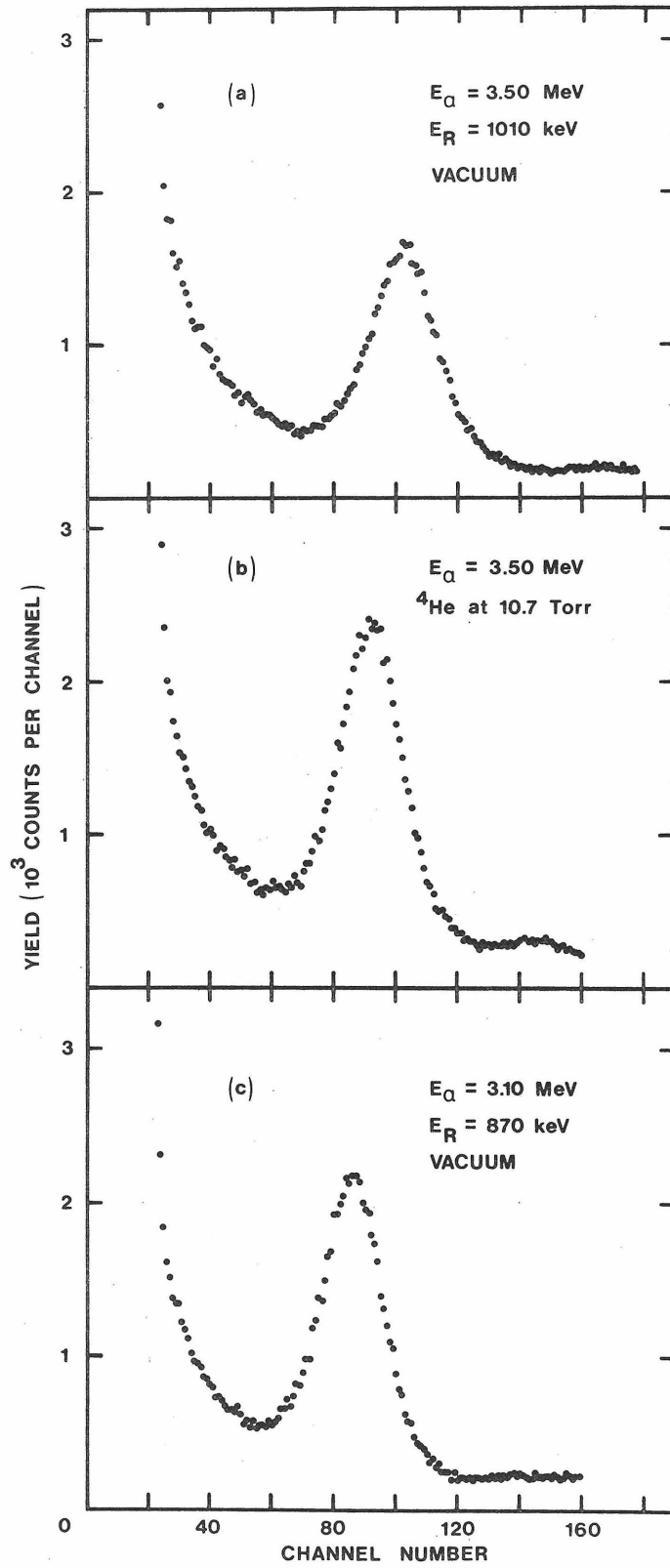
Figure 50. The electronic stopping cross section S_e for ^{12}C in He gas. The data of the present work are the circular data points, and the dashed line is a best fit to these data of the form $S_e = KE^p$ as given in Table XXV. The dot-dash line is of the form $S_e = 1.30 \times 10^{-15}[E(keV)]^{0.50}$ ev-cm^2/atom, quoted by Hvelplund (1971) as the best fit to his experimental results for C in He. The vertical bar associated with the dot-dash line indicates the 5% uncertainty quoted by that author for his result. The solid lines are the theoretical prediction of Lindhard and Scharff (1961) and the calculated result of Northcliffe and Schilling (1970).

Figure 51. The electronic stopping cross section S_e for ^{12}C in Xe gas. The data of the present work are the circular data points, and the dashed line is a best fit to these data of the form $S_e = KE^p$ as given in Table XXV. The solid lines are the theoretical prediction of Lindhard and Scharff (1961) and the calculated result of Northcliffe and Schilling (1970).
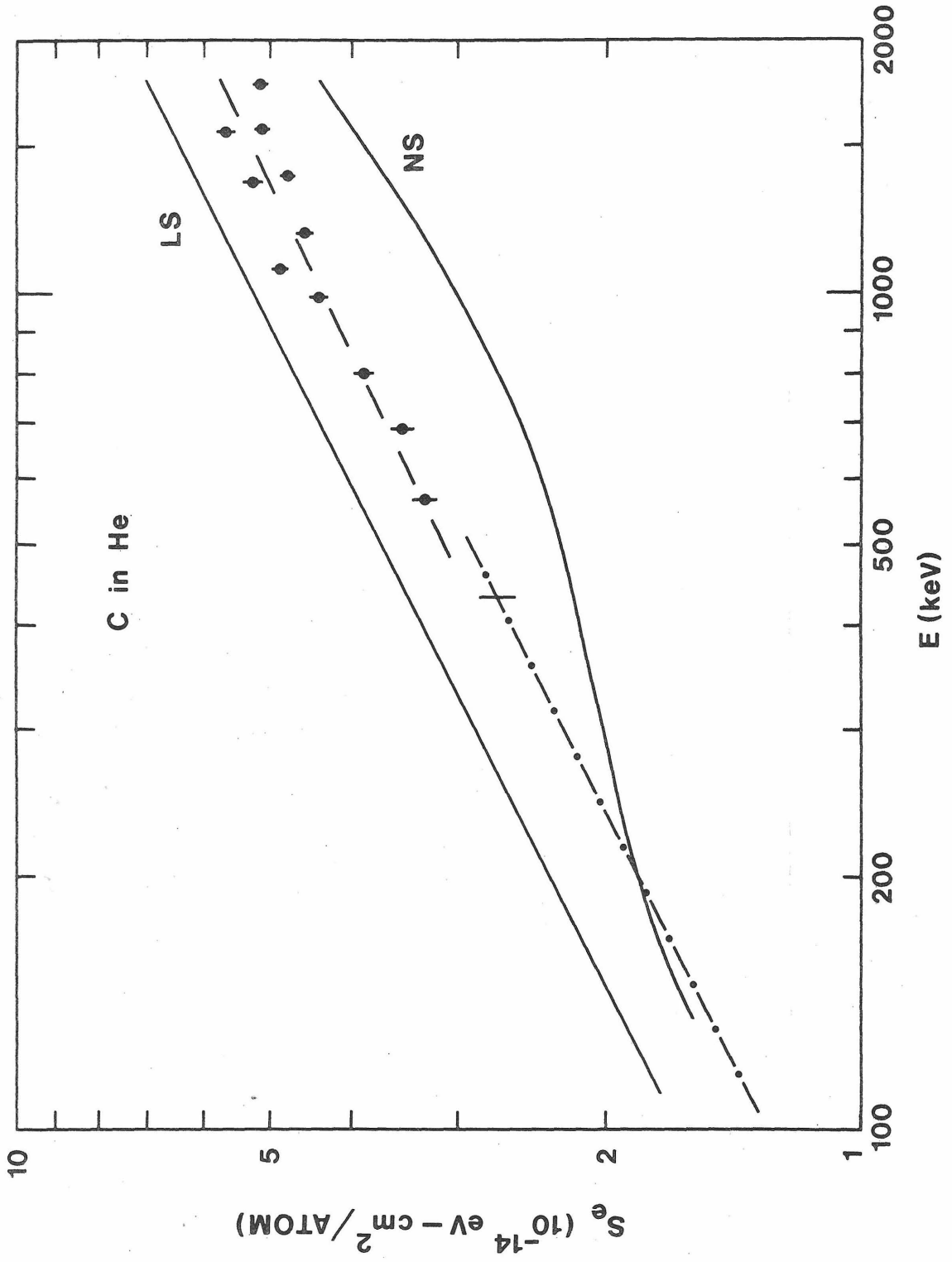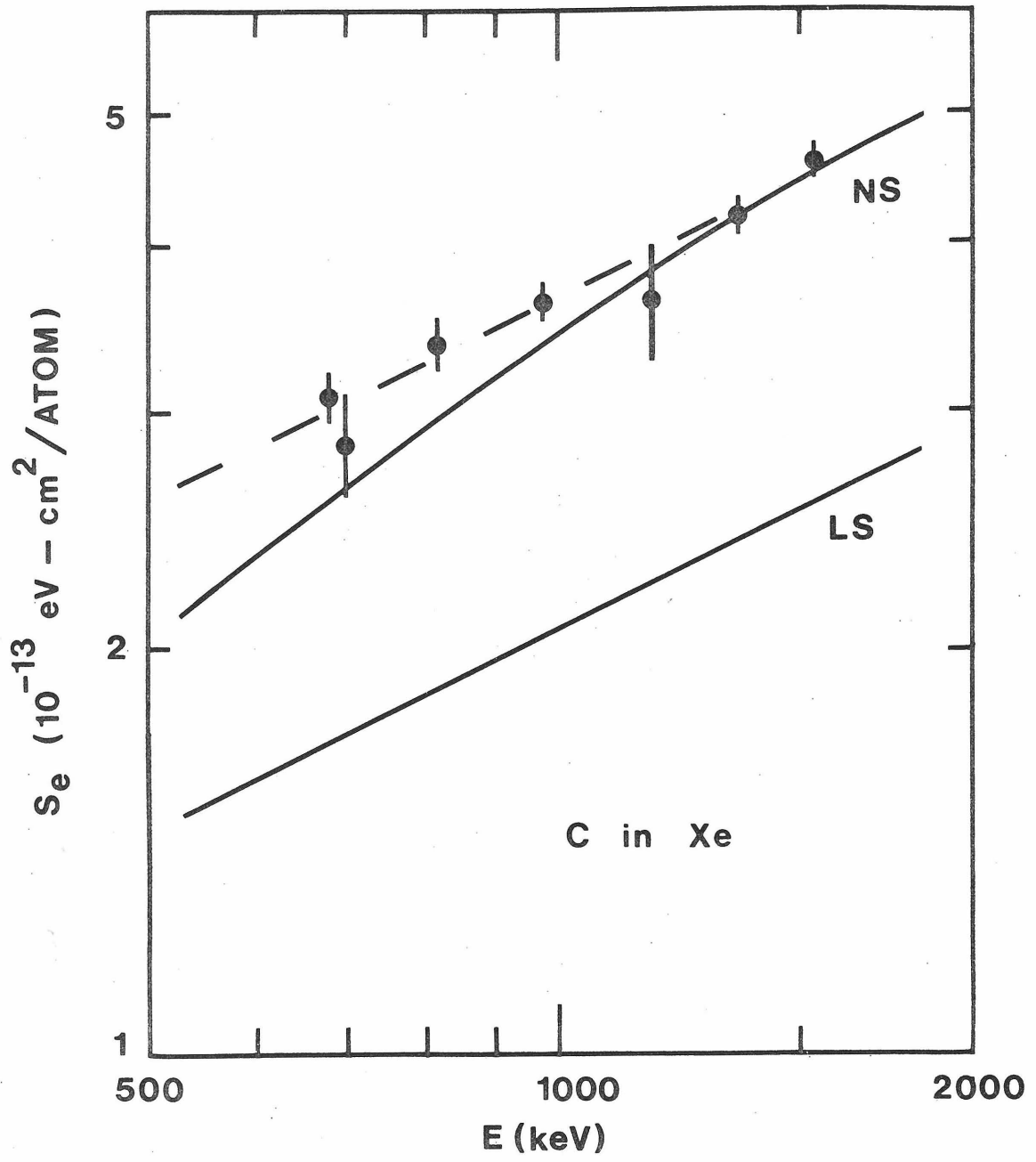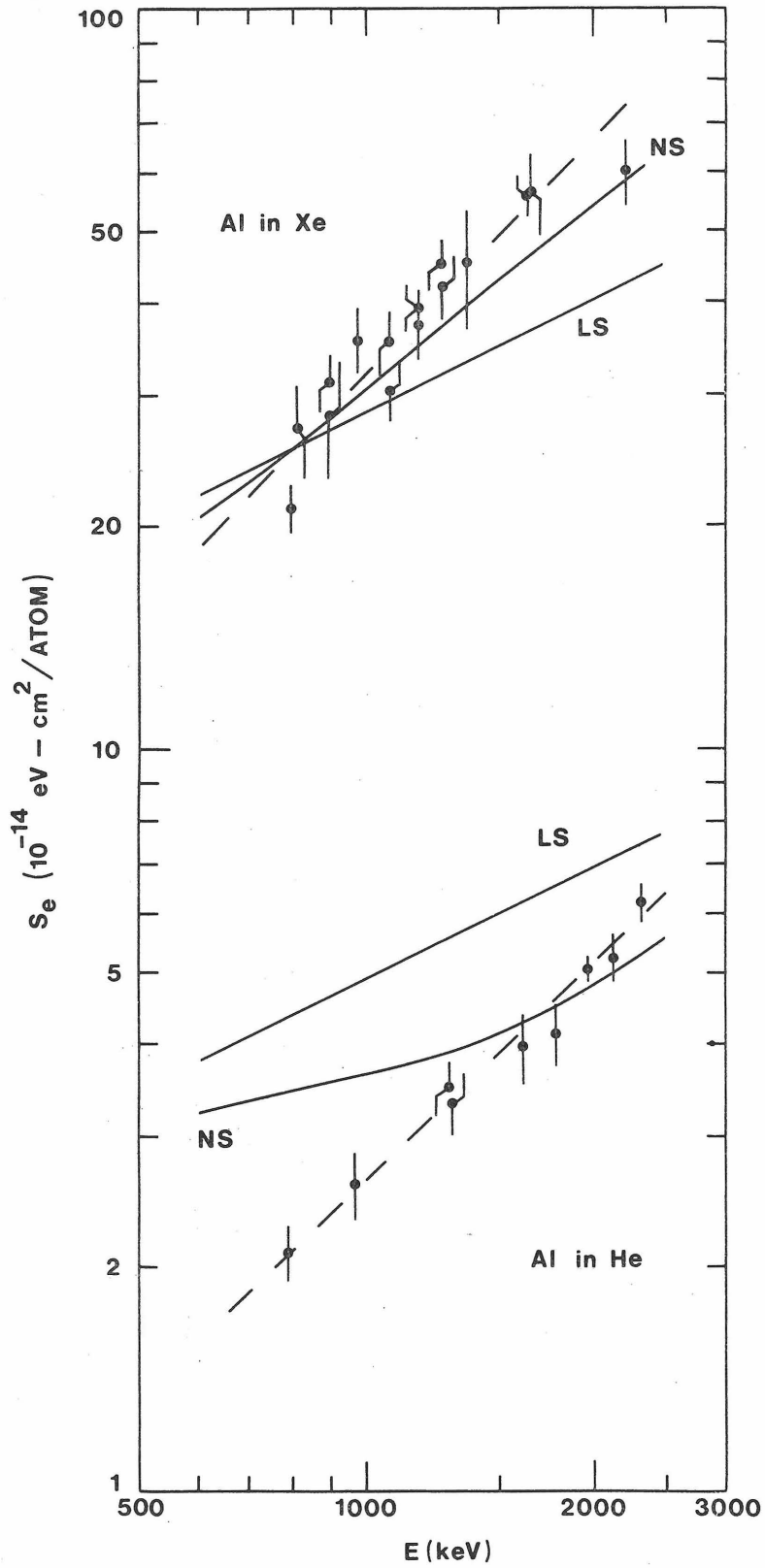
(See page 128.)

Figure 52. The electronic stopping cross section S_e for ^{27}Al in Xe and He. The data of the present work are the circular data points, and the dashed lines are best fits to the data of the form $S_e = KE^p$ as given in Table XXV. The solid lines are the theoretical predictions of Lindhard and Scharff (1961) and the calculated result of Northcliffe and Schilling (1970).

Figure 53. A graph of electronic stopping cross section S_e as a function of ion energy E for ^{27}Al in Xe. Curve (a) is the experimentally measured electronic stopping cross section S_e extrapolated to zero energy, while curve (b) is the Lindhard-Scharff (1961) theoretical prediction. Curve (c) is the Lindhard-Scharff prediction scaled down by the factor $f_e = 0.68$. The ^{26}Al lifetime measurements were performed with an initial Al energy of $E = 640$ keV.
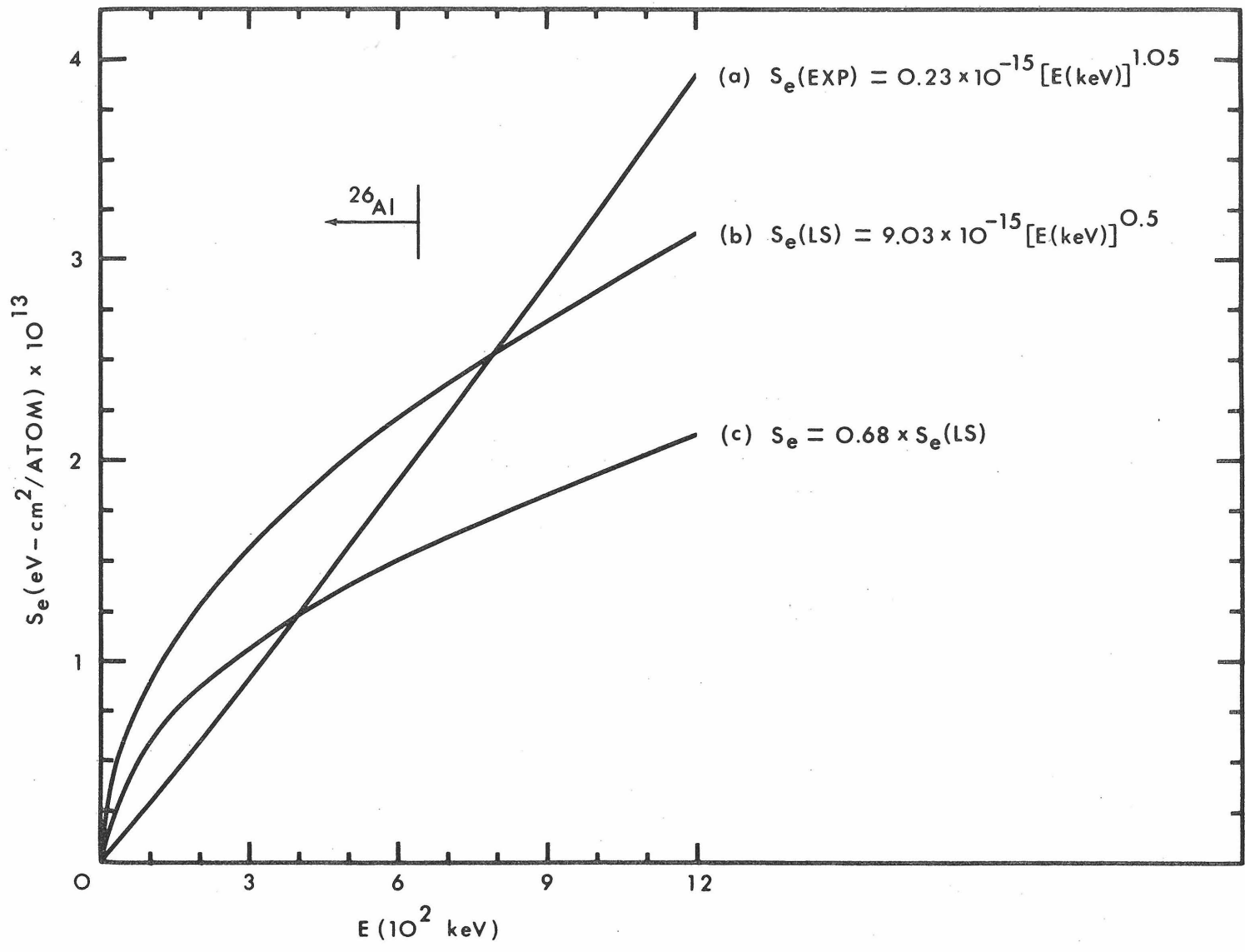
(a) $S_e(EXP) = 0.23 \times 10^{-15} [E(keV)]^{1.05}$

(b) $S_e(LS) = 9.03 \times 10^{-15} [E(keV)]^{0.5}$

(c) $S_e = 0.68 \times S_e(LS)$

^{26}Al

$S_e (eV-cm^2/ATOM) \times 10^{13}$

$E (10^2\ keV)$

Figure 54. The computed DSAM factor F as a function of nuclear level lifetime τ for ^{26}Al nuclei with an initial recoil velocity of $\beta = 0.00728$ slowing down in Xe gas. Curve (a) is computed using an electronic stopping power of the form $-(d\epsilon/d\rho)_e = 0.152 \, \epsilon^{1.05}$, while curve (c) is computed using an electronic stopping power of the form $-(d\epsilon/d\rho)_e = 0.302 \, \epsilon^{0.50}$. The measured DSAM factor F for this case is $F = 0.41 \pm 0.03$. Curve (a) leads to a lifetime $\tau(418) = 1.33 \pm 0.10$ ns, while curve (c) leads to a lifetime $\tau(418) = 1.36 \pm 0.16$ ns.